Ph.D. program in Computational and Applied Physics

Atomistic Study of Slip Transfer in BCC Metals

Doctoral thesis by:
Nikolai Kvashin

Thesis supervisors:
Dr. Napoleon Anento
Dr. Dmitry Terentyev

Departament of Civil & Environmental Engineering
Universitat Politècnica de Catalunya
Barcelona, July 2022

The work was carried out within the framework of a collaboration of UPC, SCK·CEN and M4F project.

This research was performed at:

UPC
Universitat Politècnica de Catalunya
Department of Civil & Environmental Engineering
08034 Barcelona, Spain

In collaboration with:

SCK·CEN
Belgian Nuclear Research Centre
Institute for Nuclear Materials Science
Boeretang 200,
2400 Mol, Belgium

The work was supported by:

M4F Project
Multiscale modeling for fusion and fission materials
Euratom research and training programme 2014–2018
Grant agreement No. 755039

Acknowledgements

This work has become a very important part of my life and I would like to express my gratitude to the people and organizations that have made it possible.

First of all, I would like to thank my advisor Dr. Napoleon Anento and Prof. Anna Serra for giving me the opportunity to do the research and complete the PhD thesis at Universitat Politècnica de Catalunya. I would like to thank them for the guidance, advice and support they provided during my entire stay in Barcelona. Their perseverance and expertise pointed me in the right direction and gave me the level of knowledge necessary to complete the study.

I also thank my co-supervisor Dr. Dmitry Terentyev for all the constructive suggestions, the opportunity to conduct resource-intensive simulations at the SCK·CEN facilities and his willingness to spend his time on expert clarifications (even late at night) during all the stages of the research.

I also acknowledge the M4F project (the Euratom research and training programme 2014-2018 under grant agreement No. 755039), that provided the funding for this PhD work.

Finally, I would like to thank my wife Ekaterina. Without her all of it would not be possible. Thank you for all your support and care during all these challenging years, for your love and faith that allowed me to finish the study.

Abstract

The mechanical properties of structural materials, which are naturally polycrystalline, is defined by a number of physical processes that take place at different time and space scales. On several of those processes, bulk dislocations and grain boundaries (GBs) play a relevant role. The plastic deformation in these materials is mainly due to the mobility of dislocations, therefore the interaction of these defects with other preexisting defects like GBs is a key factor to explain the evolution of the properties over the time.

It has been experimentally observed that degradation in the mechanical properties of the steels in service is connected with the formation of slip-bands. Propagation of slip-bands through grain boundaries increases material heterogeneity, leading to premature failure and detrimental loss of ductility. There are many possible types of GBs and the behavior of one specific GB interacting with dislocations cannot be anticipated and consequently must be analyzed individually. Macroscopically, these reactions are classified as absorption, transmission or reflection of dislocations. The relationship of these reactions with the GB structure as well as the external parameters (stress, temperature, etc.) is the objective of this research.

The aim of the work is to predict the result of slip bands interaction with GBs based on a multiscale modeling approach. This work presents of a report on the transferability of dislocations through GBs and the role played by the intrinsic defects at GBs. The main goal to achieve is a set of rules to describe the interaction between dislocations and GBs which can be used in larger scale models (OKMC, DD, FEM). The purpose is to improve the description of the microstructure evolution and subsequently, the predicted long-term evolution of the macroscopic properties of the materials of interest, namely ferritic/martensitic steels, which are widely used in nuclear industry for both fusion and fission applications. In order to investigate the mechanisms of the dislocation – GB interaction it is required to access the atomic level, for that reason it has been chosen the Molecular Dynamics modeling technique to carry out this research work.

CONTENTS

LIST OF FIGURES

LIST OF TABLES

LIST OF ABBREVIATIONS

bcc – Body centered cubic
GB – Grain boundary
GBD – Grain boundary dislocation
OKMC – Object Kinetic Monte Carlo method
DD – Discrete Dislocation continuum method
FEM – Finite Element method
TB – Twin boundary
DPU – Dislocation pileup
STGB – Symmetric tilt grain boundary
MD – Molecular Dynamics method
fcc – Face centered cubic
SCGBM – Shear-coupled grain boundary migration
Bv – Burgers vector
EDisc – Elementary disconnection
hcp – Hexagonal close-packed
EAM – Embedded-atom Method
DFT – Density functional theory
LAMMPS – Large-scale Atomic/Molecular Massively Parallel Simulator
OVITO – Open Visualization Tool
CRSS – Critical resolved shear stress
CSL – Coincident-site lattice
HS Disc – High-stepping disconnections
DP – Dichromatic pattern
TBD – Twin boundary dislocation
A – Absorption
R – Reflection
T – Transmission
TW – {112} twin formation
IF – Interfaces formation

GENERAL CONCEPTS

The purpose of the present research work is to investigate one of the mechanisms involved in the plastic deformation of metals and alloys, materials which are polycrystalline in nature, known as slip transfer. This mechanism involves the transmission of dislocations across grain boundaries and has been subject of interest, from the early stages of materials science, of many theoretical, experimental and more recently, simulation works. To achieve a better understanding of this phenomenon it is required an analysis of the role played by the key element: grain boundaries.

The study of grain boundaries represents a very specific and complex research field, because for each crystallographic structure many types of interfaces can be formed and there are several criteria to classify them. As the readers of this work are not expected to be experts in the field, we have considered useful to include a preliminary chapter containing a general description of a grain boundary including also the defects found on these interfaces, which have a decisive role on the interaction between grain boundaries and dislocations. The last Section in this chapter is devoted to explain the use of the dichromatic pattern to identify such defects in order to characterize the processes at the grain boundary.

Grain boundaries

In a general way, a grain boundary is a 2D defect separating two different regions of a material. The differences between regions can be related to the composition, crystallographic structure, thermodynamic phase or other features. In this work we are only considering a specific type of interface: the boundary between crystallites in a polycrystalline material. These crystallites are called grains, and the boundaries between them are grain boundaries, respectively. The sizes and orientations of the grains relative to each other significantly vary. Depending on the relative orientation, the arrangement of atoms at the boundaries changes. However, it is noteworthy that the area of disorder in the boundary structure is very narrow and is limited by several atomic planes in each grain. The way grain boundaries are distributed in a material contributes to the microstructure of this material. Many properties of the material, including macroscopic, are determined by its microstructure. Therefore, one of the important goals in material modeling is to understand the development, evolution of microstructures and their influence on the macroscopic characteristics of materials.

A grain boundary separates two regions with the same crystal structure, but different orientations. A detailed mathematical description is required in order to macroscopically characterize their complex structure. In the two-dimensional case four parameters are needed to mathematically define a grain boundary (Fig. 1), namely the angle ϕ, which describes the difference in orientation between neighboring crystals (orientation relationship), the angle ψ, which determines the spatial orientation of the grain boundary plane relative to one crystal (spatial orientation of the grain boundary) and components t_1, t_2 of the translation vector $\mathbf{t}$, which characterizes the displacement of two crystals relative to each other (translation vector). For the real three-dimensional case, eight parameters are already

required to uniquely identify the grain boundary, namely three parameters for the orientation ratio, for example, Euler angles ϕ_1, Φ, ϕ_2, two parameters for the spatial orientation of the grain boundary defined by the plane normal to the grain boundary $\mathbf{n}= (n_1, n_2, n_3)$ relative to one of the neighboring crystals (bearing in mind that $|\mathbf{n}|= 1$) and, finally, the three components of the translation vector $\mathbf{t} = (t_1, t_2, t_3)$. Grain boundary properties, in particular energy and mobility, depend on these eight parameters. Five of them can be varied from the outside, that is, the orientation relationship and the spatial orientation of the grain boundary. Since the total energy tends to be minimal, the relative displacement of the adjacent grains fixes the translation vector.

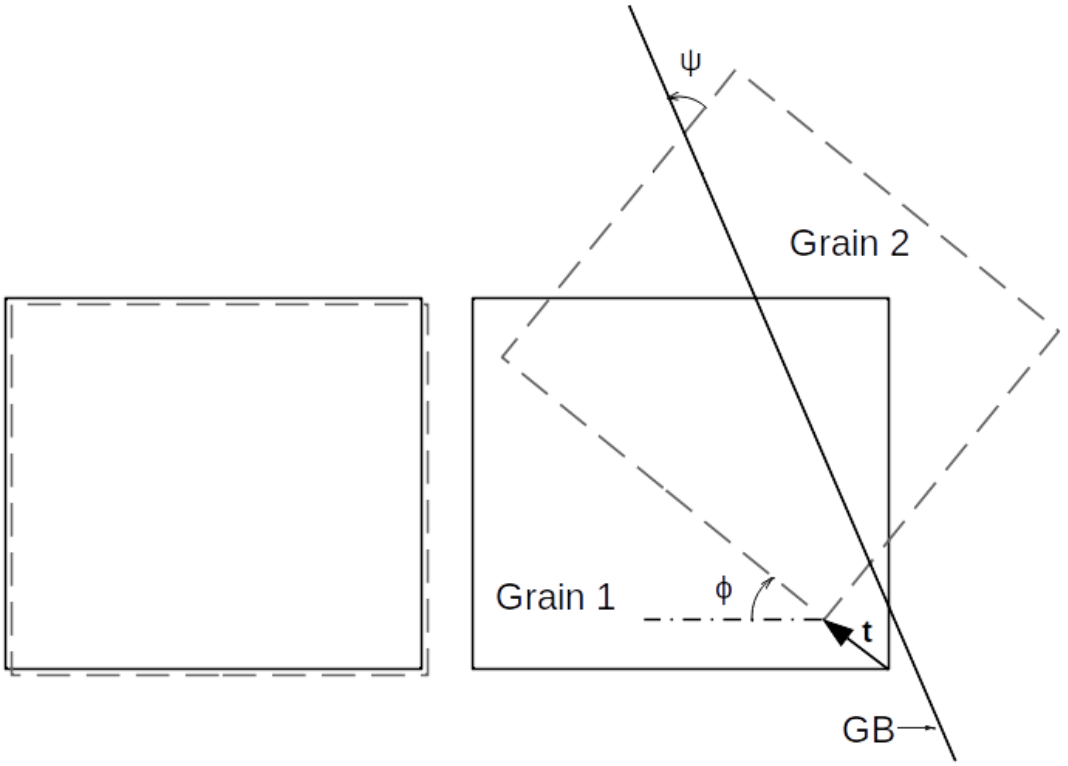

Figure 1: Parameters necessary to define a two-dimensional GB: angles ϕ and ψ and translation vector $\mathbf{t}$.

The orientation relationship between the crystal lattices of two grains is a transformation, when applied to one of the crystals, the orientation of their crystal lattices coincides. If the crystals have a common origin, the transformation is a rotation, since the relative positions of the axes coincide. One of the variants of the description is the use of Euler angles, but it is easier to describe the grain boundary in terms of the tilt axis and the misorientation angle. In order to reveal the dependence of the properties on the angle of rotation, it is necessary to keep the orientation of the grain boundary plane constant. If this plane is perpendicular to the tilt axis, then the interface is called twist boundary (Fig.2a). In this case, the choice of the grain boundary plane does not depend on the angle of rotation. On the other hand, if the axis of rotation is parallel to the plane of the grain boundary, such type of boundary is called tilt boundary. Since there are an infinite number of possible planes parallel to a given direction, there are an infinite number of tilt boundaries for a given tilt angle. If the crystallographic orientations of the grains at the boundary are mirror reflections of each other, such interface is called symmetric tilt boundary (Fig.2c). All other tilt boundaries refer to as asymmetric boundaries (Fig.2b). Neighboring crystals on the symmetric tilt boundary have equivalent Miller indices for grain boundary planes. By definition, the normal to the grain boundary plane is perpendicular to the tilt insertion axis, however, when the rotation angle changes, it is impossible to keep the Miller indices constant for the boundary plane. For at least one of the grains, the indices change corresponding to an asymmetric tilt boundary.

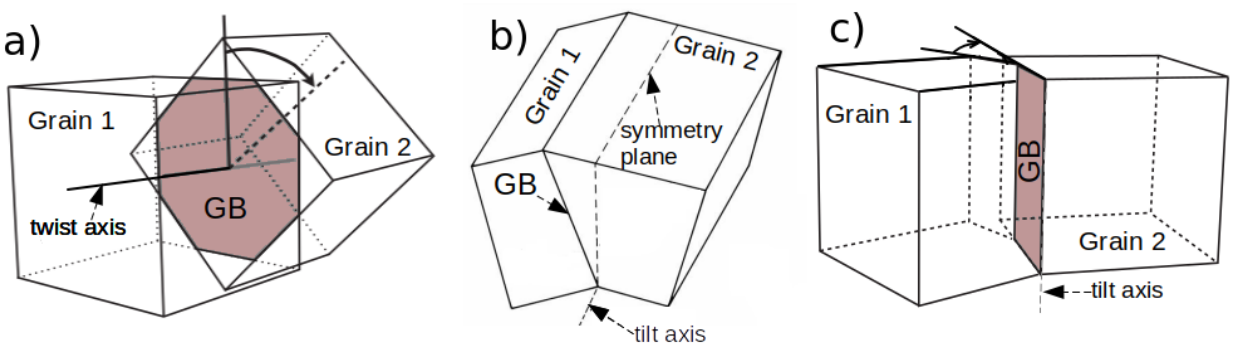

Figure 2: Relative orientation of grain boundaries and rotation axes for different types of grain boundaries. a) Twist boundary; b) asymmetrical tilt boundary; c) symmetrical tilt boundary.

Symmetric tilt boundaries are usually characterized by a misorientation angle between grains. Low-angle boundaries with a misorientation angle, typically assumed to be less than 15 degrees, can be described as a set of dislocations. High-angle grain boundaries are more complex structures and may consist of structural elements depending on the mutual orientation of the grains and the grain boundary plane.

Since the bonds of atoms belonging to the grain boundaries change in comparison with the atoms of an ideal crystal, the boundaries contribute additional positive free energy to the system. The Reed-Shockley equation allows us to describe the energy of low-angle boundaries represented by a set of dislocations:

$$\gamma_s = \gamma_0 \theta (A - ln\theta), \tag{1}$$

where $\theta = b/h$ is the misorientation angle, b is the modulus of the Burgers vector of the dislocations at the grain boundary, and h is the distance between these dislocations. The initial energy value is expressed as $\gamma_0 = \mu b/(4\pi(1-\nu))$, where μ is the shear modulus and ν is the Poisson's ratio; and $A = 1 + ln(b/2\pi r)$ where r is the size of the dislocation core.

There is no single equation to describe the energy of high-angle boundaries, since their structure is not explicitly expressed in a single way. The change in the energy of such grain boundaries is periodic with the changes of the misorientation angle, since when one grain rotates relative to another, eventually the grains will be oriented the same as in the initial position. It is also worth noticing the existence of special boundaries with low grain boundary energies. In such boundaries, the grains are oriented in such a way that a special ordered structure is formed.

Low-angle twist boundaries can also be represented by a simple set of dislocations. If we arrange two sets of parallel screw dislocations in a plane, the result is a twist in the boundary plane. The grain on one side of the interface is rotated by the twist angle relative to the grain on the other side. The twist axis is perpendicular to the plane of the boundary.

In general, large-angle grain boundaries can be represented simply by bringing together two crystals misoriented by an angle of the boundary relative to each other. While regular relaxed sections may be present on the interface, reducing its disorder, in general, the large-angle grain boundary is disordered, there are usually empty spaces and open channels. Such grain boundaries facilitate the diffusion of atoms in the solid state, and also have sites that allow dissolving substances and impurities that do not fit well into a bulk crystal, absorbing them as surfactants at the boundary.

However, there are some high-angle boundaries with a relative misorientation which provides a good geometric correspondence between the crystal orientations of neighboring grains. Such grain boundaries are called coincidence boundaries. In our study, we focus mainly on such grain boundaries.

The crystal has the lowest material energy without boundaries, therefore, due to the positive energy contribution of the grain boundaries, the polycrystalline material is metastable. When the material is heated, simultaneously with the evolution of the grains, the total area of the grain boundaries

decreases, therefore reducing the energy introduced by the grain boundaries. Thus, over time, the average grain size increases, that is, the grains grow.

The grain structure is usually characterized by its average size, defined as the average diameter of the grain. However, the grain size does not provide a complete description of its structure, since not only the grain size distribution is important, but also their shape. These grain structure parameters are difficult to quantify, since individual grain boundaries can affect the processes in the material in different ways.

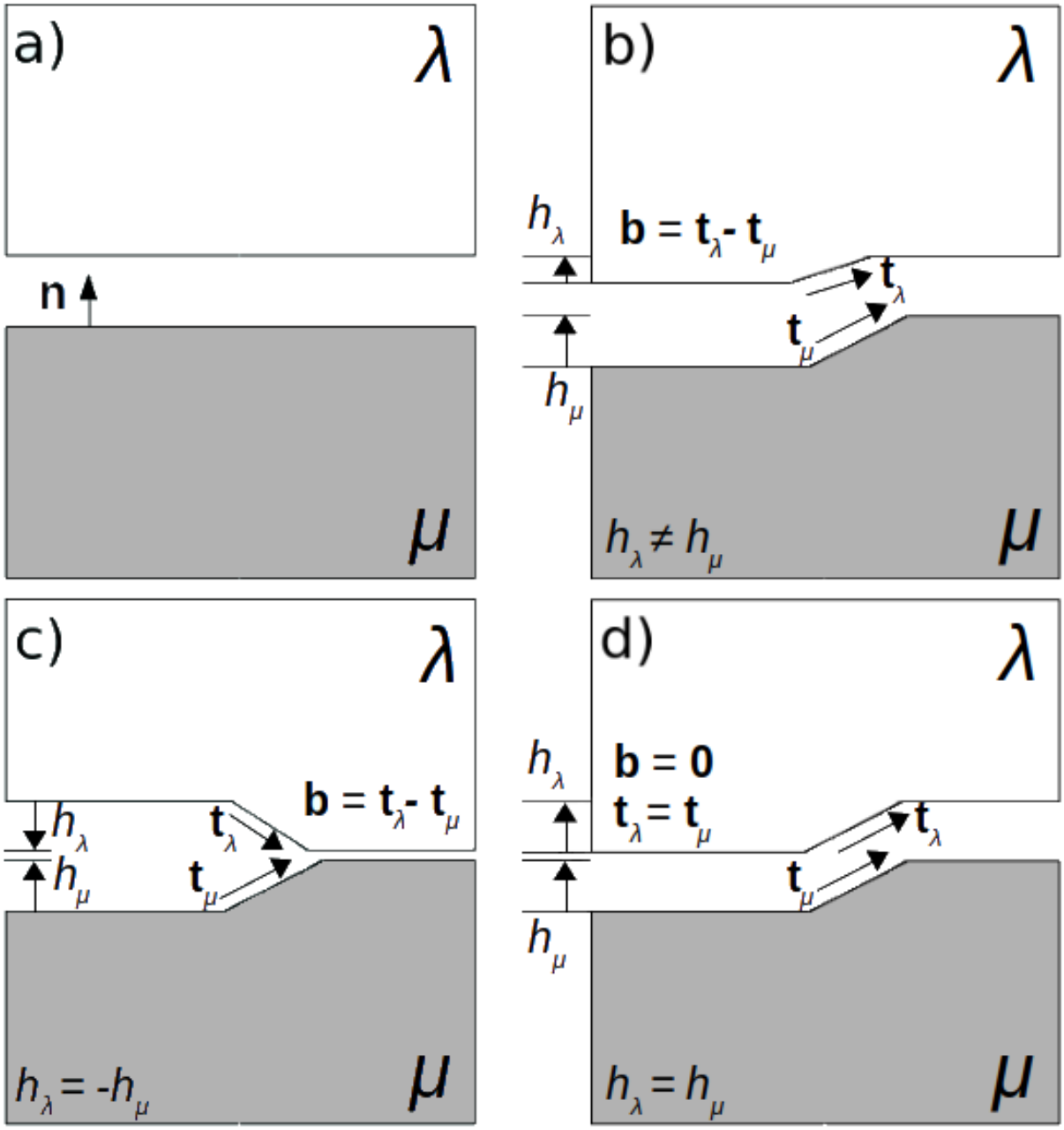

Figure 3: Formation of a bicrystal by joining the surfaces of the λ and μcrystals. a) Surfaces without steps, no interfacial defect. b) - d) Surfaces with steps. b) Grain boundary dislocation with a step and c) grain boundary dislocation without a step. d) A pure interfacial step without dislocation character. The interface structures are identical on both sides of the defect.

Grain boundary defects

Line defects appearing at grain boundaries are associated with the broken symmetries of two crystals forming the interface. Depending on the mutual conditions such defects may have both dislocation and step character. These defects play an important role in interfacial processes, contributing to the coherency of the boundaries For instance, they may be associated with transformations of one crystal at the expense of another, such as twinning or martensitic transformations. At the simplest consideration, the defect representing a step with dislocation character transforms the atoms of one crystal into sites of the other together with its motion along the interface. A brief description of the defects associated with grain boundaries is given below in this Section.

The topological properties of interfacial defects that appear during the formation of grain boundaries, such as the Burgers vector $\mathbf{b}$ or the step height h, are determined by the mutual orientation of crystals, specifically by the broken symmetries between them.

If the translation or point group symmetry is broken, an interfacial dislocation is formed. In Fig. 3 two crystals designated λ and μ (white and black) are shown. If a bicrystal is obtained by merging the upper plane of the crystal surface μ with the lower plane of the crystal surface λ along the normal vector n without the presence of steps on the crystal planes, as shown in Fig. 3a, the result is a defect-free grain boundary.

If there is a step on the surface dividing the interface into two surfaces identical in structure, then this step is associated with the symmetry of the crystal. In the simplest case, shown by steps on surfaces in Fig. 3b-d, the step is characterized by the translation vector $\mathbf{t}$ of the lattice. The height of this step is expressed as $h = \mathbf{n} \cdot \mathbf{t}$, and can have both positive and negative sign. If the steps on both surfaces have different heights and are not parallel ($\mathbf{t}_\lambda \neq \mathbf{t}_\mu$, $h_\lambda \neq h_\mu$)), when they are joined together without removing atoms and without gaps, a bicrystal is formed, the material of which is distorted near the resulting step, forming a linear defect (Fig. 3b). Thus, we obtain a dislocation with a Burgers vector that has the same interfaces on both sides:

$$\mathbf{b} = \mathbf{t}_\lambda - \mathbf{t}_\mu \tag{2}$$

Grain boundary defects with dislocation character, i.e., non-zero value of the Burgers vector $\mathbf{b}$, as well as stepping the interface are called disconnections. Since these defects have dislocation character they may move under an applied shear strain, leading to a transformation of the grain boundary. Among such disconnections we distinguish elementary disconnections with low step and short Burgers vector parallel to the interface. These elementary disconnections are of special interest, since they are responsible for shear-coupled grain boundary migration.

If the height of the steps on adjacent surfaces are the same, and their sign is opposite, as shown in Fig. 3c, the resulting grain boundary contains a dislocation that does not step the interface. Finally, if adjacent crystals have a common symmetry, i.e., $\mathbf{t}_\lambda = \mathbf{t}_\mu$, the resulting interface will have a clean step without dislocation character (Fig. 3d).

There are also so-called misfit dislocations that appear during the growth of the grains at the interfaces with different lattice parameters as a result of strain accommodation. If strain is applied to such bicrystal until their lattice parameters are equal, a coherent interface is formed with additional strain energy due to the initial lattice difference. This energy might be relieved by introducing a crystal dislocation on the interface (with $\mathbf{b} = \mathbf{t}_\lambda$ or $\mathbf{t}_\mu$).

Dichromatic pattern

If we plot an overlap of the two lattices of a bicrystal ensuring that atoms on the interface are common to both, then we will observe how these lattices interpenetrate each other. Combining the lattice point of each lattice by translation, we can get a dichromatic pattern. In this case, the grain boundary plane belongs to both crystals in the superposition. Such a pattern is an effective tool for characterization of all possible Burgers vectors of interfacial defects. Thus, any lattice site of the coinciding plane can be taken as the coordination origin for the displacement vectors of both crystals $\mathbf{t}_\lambda$ and $\mathbf{t}_\mu$. Consequently, any Burgers vector of grain boundary dislocation can be represented as an arrow on a dichromatic pattern going from black sites to white ones (Fig. 4b). This is a general condition for the Burgers vector of grain boundary dislocations, where translation symmetry is broken and the interface structure is identical on both sides of the defect.

A circuit map can be used to describe the topological characteristics of interfacial defects at grain boundaries. A closed circuit around the object to be identified is first created between crystallographically equivalent λ sites, and then μ sites crossing the interface in two equivalent places (Fig.4a). Then the resulting circuit can be transferred to the dichromatic pattern, preserving the values of jumps between crystals on the interface (Fig. 4b). The presence of a closure failure on the dichromatic pattern allows us to identify the direction and the length of the Burgers vector of the defect.

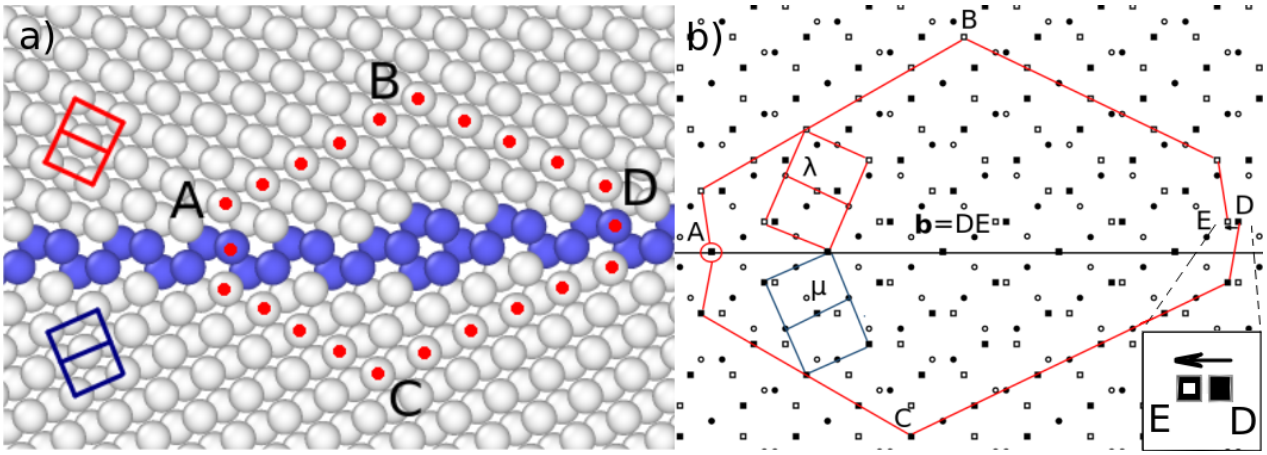

Figure 4: a) Burgers circuit drawn around the interfacial defect. b) Circuit from a) mapped onto the dichromatic pattern, showing that the analyzed defect has a Burgers vector **DE**, corresponding to an elementary disconnection.

CHAPTER 1

INTRODUCTION

This work is framed into the European project M4F that investigates the deformation mechanisms in ferritic steels going from atomistic up to continuum scale. The dynamic of dislocations is a key element in microstructure evolution of irradiated materials as it is behind the changes of macroscopic properties. One of the elements affecting the motion of dislocations are the Grain Boundaries (GB). The GB – dislocation interaction is very relevant because it not only alters the dynamics of the dislocations but it can also modify the GB itself changing the size and shape of the grains.

In real structural materials such as ferritic steels or other iron-based materials, grain boundaries present a variety of structures. Degradation of mechanical properties of materials is often observed along with formation of slip-bands – regions where dislocation glide occurs. Their propagation through grain boundaries lead to failures and harmful loss of ductility. Some experiments, however, indicate that certain GBs transmit slip-bands, while some absorb and repel them. That is why it is important to understand the role of GB atomic structure in the interaction between GB and dislocations.

1.1 Overview

Mechanical response of polycrystalline metals and alloys is defined by a number of physical processes such as motion of dislocations, creation and growth of twins, displacement of interfaces, such as grain boundaries and twin boundaries (TB) [1, 2], dislocation – dislocation interaction and interaction of the gliding dislocations with GBs [3]. The dynamics of these defects implies their mutual interactions that, in turn, determine the macroscopic properties of polycrystals under applied thermal and/or mechanical treatment. While the initiation of plastic deformation is controlled by the motion of dislocations, the sustainability and capacity of microscopically homogeneous deformation is defined by the propagation of slip through grains [1, 4], their interactions inside the grain with other defects [5] and the slip-twin interactions [6–12].

Structural materials for high-demand or extreme applications (e.g., space, high pressure, fast deformation, harsh nuclear environment) are required to exhibit high strength and ductility at the same time, which is challenging. BCC metals are often used as a basis because of the high strength and acceptable cost. Under quasi-static and moderate-speed dynamic loads, the plastic deformation is controlled by the activation of screw dislocations, interaction of dislocations with themselves and dislocation pileups with grain boundaries and eventually the grain boundary slip as the ambient temperature is sufficiently high. However, under high speed or shock-compressed deformation (the case of accidents or transients regimes) the formation of twins coexists with the regular dislocation multiplication [13]. Understanding of the mechanisms of the fast deformation has important consequences for practical applications such as the development of impact-resistant armors as well as fundamental relevance e.g., investigations on the state of matter during planetary collisions in space [14, 15].

GB strengthening or the Hall-Petch strengthening mechanism [16, 17] is based on the observation

that GBs impede dislocation movement and that the number of dislocations within a grain have an effect on how easily dislocations can traverse grain boundaries and travel from one grain to another. Indeed, the multiplication of dislocations leads to the formation of pileups whose propagation is controlled by the grain boundaries. This is why the knowledge of the grain morphology and substructure is important information usually supplied as one of the main characteristics of the structural material. Experiments involving nano-twinned pure copper show that the presence of nanometer-thickness nano-twins offers an exceptional combination of strength and ductility [18, 19], suggesting that specific GBs may improve not only strength but ductility as well. Kapp et al. [20, 21] have found that grain coarsening in cyclically deformed Ni is distinctively amplified in regions of shear localization, strengthening the concept of deformation driven boundary migration. To rationalize these results, the interaction of dislocation pileup (DPU) - inevitable upon severe plastic deformation - with several symmetric tilt grain boundaries (STGB) in copper, aluminum and nickel was studied [22–28].

The above noted works, employed direct atomistic simulations by Molecular Dynamics (MD) which provided rich details on local structural transitions occurring as the DPU impinges on the GB interface, and helped to extend the Lee-Robertson-Birnbaum criteria by accounting for local stress-field at the GB due to the pileup [22]. A practical implementation of MD was realized via a hybrid atomistic/discrete-dislocation model. With such an approach, MD was applied to study the possible events such as absorption of the head dislocation, reflection, transmission or the total absorption of the pileup. However, the above mentioned studies are essentially limited to investigation of face centered cubic (fcc) metals, while body centered cubic (bcc) metals represent an important segment of structural materials widely applied in transport, medicine and energy sectors.

The sustainability of the macroscopic deformation is defined by both, the propagation of dislocation - mediated slip through grains, ruled by the interaction of dislocations with the GB [1, 29, 30], and the activation of atomic processes that are intrinsic to the GB. Those processes are the creation of GB dislocations that favor the shear-coupled GB migration (SCGBM) [31, 32], nucleation of dislocations [33, 34] and the nucleation of twins [34–36]. This complex scenario of plastic deformation is firstly dependent on the atomic structure of the GB. Thus, a dislocation can be absorbed, transmitted or reflected when interacting with a GB and the interaction may leave some residual products at the GB that can either help or impede the displacement of the GB.

There are two main crystallographic restrictions for these reactions, i.e., the conservation of Burgers vector (Bv) and the set of possible interfacial defects. The former, links the Bv of the entrant dislocation with the GB dislocations (GBD) produced during the interaction; the latter, described by the theory of interfacial defects [37, 38], establishes that the Bv of a GBD is the difference of broken symmetries of the crystals that form the GB (λ = upper and μ = lower, hereafter). An efficient tool for the characterization of all possible Bv of GBDs is the dichromatic pattern formed by the superposition of the lattice sites of both crystals, λ and μ, with the plane of the GB in common [39]. Thus, any lattice site of the coincident plane may be taken as the origin of both $\mathbf{t}_\lambda$ and $\mathbf{t}_\mu$, therefore the Bvs are represented by arrows that connects the sites of the two crystals. Any admissible GBD, which Bv is depicted with an arrow in the dichromatic pattern, can be easily identified as it is related to the difference of broken symmetries of the two crystals forming the bicrystal ($\mathbf{b} = \mathbf{t}_\lambda - \mathbf{t}_\mu$) [37, 38, 40, 41]. The height of the step associated to the disconnection is $h = \mathbf{n} \cdot (\mathbf{t}_\lambda + \mathbf{t}_\mu)/2$ where $\mathbf{n}$ is the normal to the GB plane. Following the notation introduced in [42] we refer to all dislocations as $\mathbf{b}_{n/m}$, being n and m the number of planes of λ and μ along $\mathbf{t}_\lambda$ and $\mathbf{t}_\mu$, respectively. The crystal dislocations residing solely in one of the crystals, for instance the λ crystal, are denoted by $\mathbf{b}_{n/0}$. In the reactions involving dislocations, n and m are conserved separately.

1.2 Grain boundaries under plastic deformation. Shear-coupled GB migration

GB migration under stress is an important plastic deformation mechanism that has been studied both, experimentally and by computer simulation [31, 32, 43–55]. The migration occurs by the glide of disconnections along the GB. Disconnections are GBD that in addition have step character [31, 32, 49–55]. Among the variety of disconnections, we define as EDisc the glissile ones that have a Bv parallel to the interfaces [51]. They are responsible for the SCGBM [31, 40, 49, 51, 56–59]. Thus, the effectiveness of the accommodation of plastic deformation depends on the creation of disconnections, its glissile character and the interaction of these disconnections with other defects located on the GB. EDisc can be created, either directly as dipoles at the GB or by defects at the GB acting as sources of them. For these sources to be efficient, they must move together with the GB. Whether the process is conservative or not, depends on the crystallography of both, the GB and the source of disconnections. The most efficient process that leads to a shear-coupled GB migration is conservative, i.e., no atomic diffusion is needed; moreover, the process must be sustained by the continuous creation of disconnections.

A well-known example is the SCGBM of the $(10\bar{1}2)$ twin boundary that occurs in all hcp metals [32, 53]. In the fcc metals, Combe et al. [54] studied a new GB migration mechanism through the nucleation of a mobile disconnection from the sessile one in the (410) tilt GB. Bristowe and Crocker [55] suggested in 1977 the heterogeneous creation of disconnections in a pioneering study of twin boundary dislocations (referred as twinning dislocations) in the {211} twin boundary in bcc metals. More recently, Gumbsch and collaborators [60, 61] studied the interaction of $\frac{1}{2}(111)$ dislocations with the {112} tilt GBs in bcc tungsten. They reported transmission or absorption, depending on the character of the dislocation, but it was not found a source of disconnections that would facilitate the continuous GB migration. Finally, Jiang et al. [62] have presented experimental evidence using in situ high resolution transmission electron microscopy, of the growth of deformation twins in bcc tantalum and niobium. To analyze the growth mechanism, they performed MD simulations but only a particular case was presented where a dislocation with Bv parallel to the interface has to interact with a disconnection of screw orientation for the growth to occur.

SCGBM is a very efficient mechanism for the accommodation of plastic deformation [56, 63]. For this to occur it is necessary that EDisc are created at the GB in a continuous way either as dipoles in the pristine GB or be produced by a source of disconnections that should move together with the GB. During the motion of these disconnections along the GB they may encounter obstacles, such as segregated impurities or clusters of point defects, and they interact with other intrinsic defects of the GB, namely other GBDs. While the interaction with impurities and clusters may increase the critical resolved shear stress but does not change its characteristics [64], the interaction with other GBDs may result in a new sessile GBD. If so, this reaction may effectively inhibit the disconnection mobility or initiate a more complex process, for example, the nucleation of a twin. The latter reactions are linked to the Bv of the reacting defects and, consequently, directly related to the atomic structure of the GB. For some GBs, the reaction of the EDisc with a sessile GBD (with or without step) is mediated by a climb-compensated mechanism [65], which allows both, the glide of the EDisc and the motion of the GBD following the GB [53, 57, 66]. These constraints would justify that SCGBM is produced in specific GBs and there is a limited number of deformation twins for each crystal structure.

There is extensive experimental evidence of SCGBM in hcp [32] and fcc [31, 49, 54, 67–71] metals since it produces the growth of deformation twins [2], which are abundant in these crystal structures. SCGBM has been less reported in bcc metals despite the fact that this mechanism occurs in this crystal structure and it is crucial for the understanding of the growth of twins both {332} and, especially, its conjugate {112} [57].

1.3 Grain boundaries – dislocation interactions. Deformation accommodation

It is known that the interaction of a slip system with a GB is specific to each GB. It depends mainly on two factors: (i) the atomic configuration of the GB and the orientation of the Bv of the dislocations and (ii) the local stress in the interaction region. Let us have a look in detail each of these factors below.

(i) There is a variety of possible processes undergone by the dislocation at the GB. The possible reactions of the dislocation present a gradation of complexity, ranging from the transmission with a small resistance keeping the same Bv [72] up to the full absorption by the GB [56, 57]. In the other intermediate situations, the dislocation is partially transmitted leaving a residual defect at the GB, necessary to account for Bv conservation [73]. In partial (total) absorption of the dislocation by the GB, the dislocation is partially (totally) transformed into GBD. The GBDs could favor either the SCGBM or the nucleation of other defects such as twins [74–76] and dislocations [33]; this behavior occurs in GBs of the most common crystallographic structures in metals, i.e., bcc, fcc and hcp [33, 59, 74–79].

(ii) The influence of the local shear stress is evidenced by comparing the interaction of a single dislocation with the interaction of a pileup of dislocations since, for the latter the local shear stress at the interaction region is dominated by the incoming dislocations. Experimental approaches on the dislocation – -individual grain boundary interactions have evidenced the specificity of each interaction. Recently, Weaver et al. [80] reported the first bcc bicrystal pillar compression testing conducted on a Tantalum bicrystal to investigate the slip transmission across three high-angle GBs. They evidenced the different behavior of each boundary to stress-strain response and slip transmissibility.

The reaction at the GB may depend on whether there is only one crystal dislocation interacting with the GB or a pileup of crystal dislocations. The crystallographic analysis of the interaction with a single dislocation supplies a list of possible reactions but an atomic simulation is needed to discern which of them occur and which processes are feasible in the presence of other dislocations.

Considering all GBs simulated, three different types of reactions were observed, such as: absorption, transmission and reflection. The type of reaction varies from one GB to another but all of them begins by the initial absorption of the first dislocation from the pileup. Along with the reactions, several line defects associated with the GB were observed, namely GBD. Among the GBD, the ones that step the interface are named disconnections. For convenience, we follow the nomenclature: (1) EDisc is a mobile disconnection with Burgers vector parallel to the GB plane that glides along the interface; (2) other sessile disconnections are called GBD with core riser or simply “risers” if the dislocation character is implicit [81]. An EDisc glides under an applied stress due to its dislocation nature. This glide is accompanied by GB migration due to the step of the boundary associated with the disconnection. Thus, the motion of glissile disconnections produces two effects, on the one hand - it accommodates plastic deformation and, on the other hand - the motion of the step transforms one part of bi-crystal into another part (i.e., displacement of the GB interface in the normal direction) [51].

The initial absorption of the crystal dislocation can be divided into two groups: (1) Absorption and split into an EDisc and a sessile GBD that does not step the interface (Fig. 1.1a); (2) Absorption and split into several EDiscs and into a sessile grain boundary dislocation that steps the interface, i.e., GBD with core riser (Fig. 1.1b). The reactions of the next incoming dislocation of the pileup that follow the first absorption depend on the GB type. It can be either a full absorption with or without changes of GBD’s Bv (Fig. 1.1a,b), or transmission/reflection (Fig. 1.1c,d). The formation of dipoles of elementary disconnections occurs either at the GBD, acting as a source of disconnections, or at stress concentrations on the interface far from the GBD.

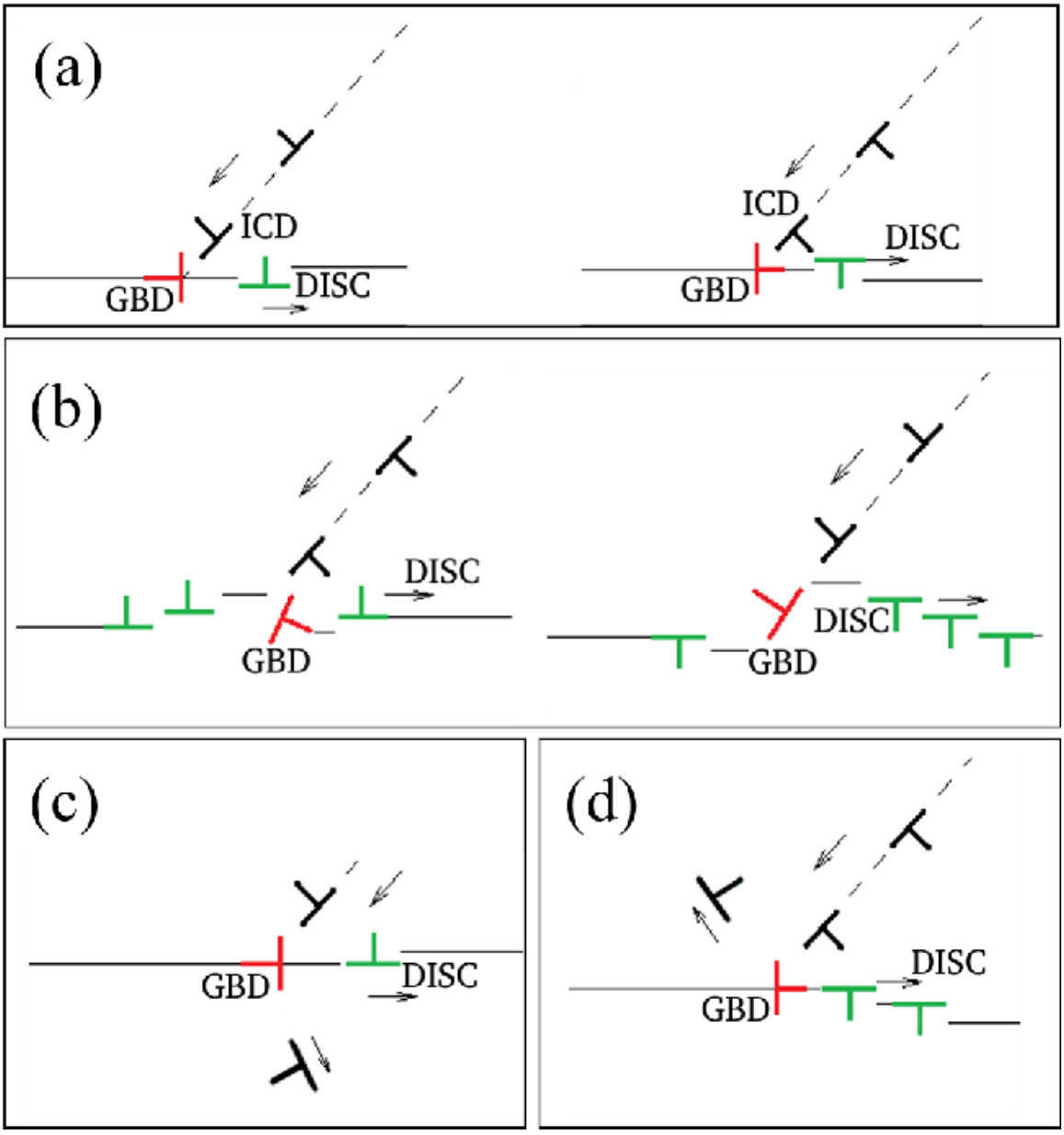

Figure 1.1: Schematics of the dislocation reactions at the GB: a) & b) Absorption of the pileup dislocation (black) and split into sessile GBD (red) and several EDisc (green) that step the interface several planes in both grains; Transmission (c) and reflection (d) with emission of EDiscs. The arrows indicate the sense of motion.

1.4 Objectives and research outline

The main purpose of the present PhD research work is to investigate the role of GB atomic structure in the GB – slip band interaction to be able to provide a set of interaction rules which can be easily transferable to models dealing with higher time and space scale, e.g., dislocation dynamics or finite element method. The model material is bcc iron as it is the basis for ferritic steels studied in the frame of the M4F project. For some GBs the effect of the material on the interaction processes and outcomes has also been analyzed. For that reason, two other materials sharing the same bcc structure have been chosen, namely chromium (Cr) and tungsten (W).

We focus mainly in the atomistic scale, which is the suitable scale to analyze properly this kind of interaction. The planned simulations allow us to understand how the conditions of temperature, strain rate and types of GB and dislocations affect the interaction. Finally, we summarize the results in a set of interaction rules which will be able to be used in higher scales of time and space.

As stated before, the GB – dislocation interaction is sensitive to the conditions present in the material: temperature, type of dislocation, strain rate and type of GB. Obviously, there is a large number of combinations of these conditions, so our first step has been to constraint these conditions to a reasonable range of cases, feasible within the duration of the project and representative of the conditions of operation for real materials.

The framework of the work is as follows:

1. Grain Boundaries: Symmetric tilt GB with $\langle 110 \rangle$ tilt axis;
2. GB type: high angle and low misorientation angle;
3. Dislocation type: edge and mixed dislocations;
4. Temperature range: from 150 K (below room temperature) up to 900 K;
5. Stress and strain rate: range of values corresponding to a different applied stress increments and different number of dislocations in the pileup.

For each GB considered an analysis of the results has been performed, being the output a description of the dependence on temperature and stress applied of the reaction type. The results obtained are used as an input for the second phase of work, that includes the extension of the simulation box to 3D simulations to study interaction of gliding disconnections with voids, He bubbles or Cr precipitates on the interface.

GBs act as sinks for mobile defects, such as point defects and their clusters under irradiation [4, 82–84]. In irradiated metals, the interaction between a GB and such defects may happen either thanks to the glide of a mobile cluster towards the GB or because a mobile GB encounters defects along its migration. Part of the defects formed as a result of the irradiation process may keep positions where they are formed, while the other may be displaced over time to interact with other defects. The mechanical properties of materials are strongly affected by the evolving microstructure. Thus, it is of great importance to study the interaction between such defects and GBs. More precise consideration of the GB — irradiation defects interaction is possible by atomistic simulations. The $\{112\}$ tilt GB in bcc metals experiencing SCGBM shows the highest mobility among the GBs studied. It is also worth studying the interactions between the EDiscs of the $\{112\}$ GB and the segregated at the GB irradiation defects.

CHAPTER 2

METHOD

The emergence of inexpensive and fast computers and the universal availability of software for various tasks have become the main reasons for the active development of computer modeling and simulations. Nowadays one can study the material response at the atomic level using a variety of developed modeling methods.

The present chapter describes the technical details of the methodology used in the present work to model the interaction between the defects and behavior of the studied GBs. Mainly two different modeling techniques have been employed to carry out the studies presented here, on one hand Molecular Dynamics (MD) and in the other hand a Discrete Dislocation continuum method which are described in the Sections 2.1 and 2.2, respectively. Section 2.1 presents MD method characteristics, as well as the main concepts of the method. Section 2.2 describes the main ideas behind the continuum method for describing dislocation and adaptations of the method to the present study. In order to apply the aforementioned methods for the different GBs considered it has been necessary to adapt the simulation setup to the specificities of each interface. Section 2.3 presents a summary of information on all the simulation setups employed along with technical details of the simulations.

2.1 Molecular Dynamics simulations

The MD method is the most used in modeling and simulations in materials research, as it provides information about the structure and dynamics of a material at atomic scales. The main idea of the method is the calculation of forces acting on atoms and the solving of Newton's equations to determine their motion.

This modeling technique was one of the first computer methods used in studies of the properties of materials, specifically with the work on the properties of liquids in the 1950s [85, 86]. As for the properties of solids, it is required a description of the energies and forces acting between the atoms of the material. The energies can be calculated using a model of interaction between atoms, which are usually based on simple functional forms reflecting the different types of bonds observed in solids.

2.1.1 Interatomic potentials

An accurate treatment of the problem of the interaction between atoms requires the use of quantum mechanics modeling which is computationally very expensive and the maximum number of atoms is very low. These limitations prevent the use of this modeling technique to study the phenomena of interest for the present work. The way to overcome these limitations is by using interatomic potentials, which describe approximately these interactions. Calculations based on them are approximations of the materials that are described. However, the use of atomic potentials, despite the lower accuracy,

makes it possible to model systems from a large number of atoms over long time intervals than for more accurate methods based on quantum mechanics.

Given two atoms i and j located in r_i and r_j the interaction energy is defined as the difference between the energy of a pair of atoms $E(i+j)$ and the energies of individual atoms $E(i)$ and $E(j)$: $\phi_{ij}(r_i, r_j) = E(i+j) - E(i) - E(j)$. If the distance between the atoms $r_{ij} = |r_i - r_j|$ is small enough, then the atoms should repel each other in order to avoid collapse. For large distances, there must be an attractive force between atoms, otherwise solids and liquids would not be formed at normal pressure. The short-range interaction can be represented as: $\phi_{sr}(r) = Ae^{-\alpha r}$.

Since metals in solid state consist of nuclei surrounded by electrons that are freely distributed over the volume of the solid, simple pair interactions do not allow us to accurately describe the bonds and properties of metals. In this regard, other types of potentials have been developed that describe the background electronic distribution in metals.

Pair potentials do not take into account the energy associated with freely distributed electrons in the description of the metals potential energy. The energy of this electron gas depends on the average electron density. Therefore, the addition of this electron density function to the sum of the paired terms may be justified for the description of metals. Considering the electron density as a function of the volume of the system V, we have:

$$U = \frac{1}{2}\sum_{i=1}^{N}\sum_{j=1}^{N}\phi(r_{ij}) + U_{eg}(V), \tag{2.1}$$

where $U_{eg}(V)$ is the volume-dependent potential [87].

Bulk modulus and other volume-dependent properties of metals are well reproduced with this model for the interactions, but has no advantages over simple paired potentials in describing other important properties of materials, especially energies of defects such as grain boundaries, surfaces, dislocation loops, etc. If the system volume does not change, $U_{eg}(V)$ does not contribute much, since it describes the energy of the electron gas. In the vicinity of defects, the electron density differs substantially from the ideal value, therefore a new model accounting for these changes is needed to correctly describe the properties of such defects.

The main bonding properties of atoms in metals can be well described by an empirical relation, the so-called Universal Binding Curve (Rose et al. [88]). This is an empirical approximation of real data, from which it is possible to approximately determine the total energy of a metallic solid.

$$U_{UBC} = -E_{sub}(1 + a^*)e^{-a^*}, \tag{2.2}$$

where E_{sub} is the absolute value of sublimation energy at zero pressure and temperature (i.e., cohesive energy), while a^* is the deviation from the equilibrium lattice constant:

$$a^* = \left(\frac{a}{a_0} - 1\right) / \left(\frac{E_{sub}}{9B\nu}\right)^{1/2}, \tag{2.3}$$

where B is the equilibrium volume module ($B = V(\partial^2 U/\partial V^2)_{NT}$); ν is the equilibrium volume per atom; a and a_0 are lattice constants for the studied material and the material in equilibrium, respectively.

Since the electron density affects the atoms positions, in order to correctly describe the properties of defects in the material, it is necessary to add the local electron density function to the pair potentials sum. To this day, there have been developed many interatomic potentials for pure metals and alloys using this approximation which is called the Embedded-atom Method (EAM) [89]. The general expression for an EAM potential is:

$$U = \sum_i F_i\left[\sum_{i\neq j} f_{ij}(r_{ij})\right] + \frac{1}{2}\sum_{i=1}^{N}\sum_{j=1}^{N}\phi(r_{ij}), \tag{2.4}$$

where f is a function of the interatomic distance, which is an electron density approximation; ϕ is the pair potential, with the members with $i = j$ excluded.

The exact form of these functions depends on the model used, each coming from different approximations and having different functional forms [89].

F is the functions sum depending on the local atoms positions. It is nonlinear; therefore it cannot be written as the sum of paired potentials, hence it describes the real interaction of many bodies. Despite the fact that the shape of various EAM potentials is based on theoretical aspects of bonding in metals, most of them are developed empirically with the approximation of parameters performed by comparing calculated with experimental properties of materials.

For the present task of modeling the interaction between dislocations and GBs in three different bcc metals the following set of EAM potentials has been used. The interatomic interactions in iron were modeled by using the potential by G. Ackland et al., fitted to reproduce properties of dislocation lines obtained from density functional theory (DFT) [90]. The accuracy of the potential in the study of $\langle 110 \rangle$ tilt GBs was checked in [91]. In chromium, the potential derived by G. Bonny et al., fitted to thermodynamic and point-defect properties obtained from DFT calculations and experiments has been used [92]. As for tungsten, the potential developed by M.C. Marinica et al. has been chosen [93]. The potential is fitted to a mixed database, containing various experimentally measured properties of tungsten and ab initio formation energies of defects. For all the materials studied the lattice parameters at different temperatures were obtained using the interpolation method, taking into account the linear dependence of the lattice constant on pressure.

2.1.2 Molecular dynamics method

As it was mentioned above this work has been carried out in the MD scope. Previously developed and implemented in the open source of the LAMMPS package MD algorithm has been chosen [94]. The basic version of the algorithm is implemented for the classical description of a closed system of particles in a state of thermodynamic equilibrium.

The used algorithm is designed to describe closed systems corresponding to a microcanonical statistical ensemble, where the number of particles, volume and total energy of the system remain unchanged. At non-zero temperatures, the thermalization procedure consisting in assigning to atoms velocities corresponding to desired temperature was used.

As for the boundary conditions, two different types have been used in the simulation setups, fixed and periodic. For the former, the atoms located in the boundaries of the simulation box are forced to be immobile. While when using the latter all the atoms are placed in a box, which is in mind translated to infinity in Cartesian directions, filling the space completely.

In this case, the "minimum image" criterion can be used: among all possible images of atom j, the nearest one is selected, and the rest are removed from consideration. Indeed, only the nearest atom can take part in the interaction. These conditions significantly simplify the modeling programs within the MD. Of course, it is necessary to keep in mind that the size of the box is at least twice the radius of the potential action along all directions for which periodic boundary conditions are defined.

To integrate Newton's equations of motion, the Verlet velocity method with a constant time step is used [95, 96]. The Verlet method directly solves the second-order equations:

$$m_i \ddot{\mathbf{r}}_\mathbf{i} = \mathbf{f}_\mathbf{i}, \tag{2.5}$$

where m_i is the mass of i-th atom; f_i is the force acting on this atom.

This method is based on the analysis of the following parameters: the positions of the atoms $\mathbf{r}(t)$, their accelerations $\mathbf{a}(t)$ and positions in the previous step $\mathbf{r}(t - \delta t)$. Atomic positions at a subsequent moment of time have the form:

$$\mathbf{r}(t + \delta t) = 2\mathbf{r}(t) - \mathbf{r}(t - \delta t) + \delta t^2 \mathbf{a}(t) \tag{2.6}$$

This formula does not explicitly include the atomic velocities. This is possible thanks to the summation of the equations obtained by decomposing $\mathbf{r}(t)$ into a Taylor series:

$$\begin{aligned} \mathbf{r}(t+\delta t) &= \mathbf{r}(t) + \delta t\mathbf{v} + \frac{1}{2}\delta t^2\mathbf{a}(t) + \dots \\ \mathbf{r}(t-\delta t) &= \mathbf{r}(t) - \delta t\mathbf{v} + \frac{1}{2}\delta t^2\mathbf{a}(t) + \dots \end{aligned} \tag{2.7}$$

There is no need to calculate particle trajectories for velocities, however they are important for estimating the kinetic energy of atoms (and, accordingly, the total energy). The atomic velocities can be found according to:

$$\mathbf{v}(t) = \frac{\mathbf{r}(t+\delta t) - \mathbf{r}(t-\delta t)}{2\delta t} \tag{2.8}$$

$\mathbf{v}(t)$ can be calculated only when the atomic coordinates at the subsequent time step are known. A feature of the Verlet algorithm is the use of central differences: in Eq. (2.6), $\mathbf{r}(t+\delta t)$ and $\mathbf{r}(t-\delta t)$ are symmetric with respect to zero, which makes the algorithm reversible in time.

There is an algorithm equivalent to the Verlet method – the Velocity Verlet method [97, 98]. It accumulates simultaneous values of atomic coordinates, velocities and accelerations, which minimizes rounding errors. According to the method, velocities and coordinates of atoms are calculated as:

$$\begin{aligned} \mathbf{r}(t+\delta t) &= \mathbf{r}(t) + \delta t\mathbf{v} + \frac{1}{2}\delta t^2\mathbf{a}(t) \\ \mathbf{v}(t+\delta t) &= \mathbf{v}(t) + \frac{1}{2}\delta t[\mathbf{a}(t) + \mathbf{a}(t+\delta t)] \end{aligned} \tag{2.9}$$

To perform calculations using this algorithm the atomic coordinates $\mathbf{r}$, velocities $\mathbf{v}$ and accelerations $\mathbf{a}$ need to be recorded. First, using Eq. (2.9), the new coordinates of the atoms at $(t+\delta t)$ time are calculated, as well as the velocities according to the equation:

$$\mathbf{v}(t+\frac{1}{2}\delta t) = \mathbf{v}(t) + \frac{1}{2}\delta t\mathbf{a}(t) \tag{2.10}$$

Then the forces acting on the atoms are calculated, as well as the accelerations at $(t+\delta t)$ time, and as a result the velocity equals to:

$$\mathbf{v}(t+\delta t) = \mathbf{v}(t+\frac{1}{2}\delta t) + \frac{1}{2}\delta t\mathbf{a}(t+\delta t) \tag{2.11}$$

Now the value of kinetic energy at time $(t+\delta t)$ can be calculated. The potential energy at the same point of time can be calculated in the next cycle.

The initial value of the time step corresponds to the time interval that the fastest atom needs to travel a distance of $0.02a_0$ (where a_0 is the lattice constant). A combined algorithm was also used in the work, it includes the linked cells and Verlet spheres algorithms to efficiently search for the nearest neighboring atoms [96]. With this approach the calculation time is directly proportional to the number of atoms of the model crystal, while the original Verlet method gives a quadratic dependence.

The key question in MD simulations is whether the algorithm used to integrate the equations of motion is accurate enough numerically. For standard MD algorithms, it is possible to control its accuracy by checking the fulfillment of the energy conservation law. Due to the fact that the equations of motion are not integrated precisely, the total energy will not be constant. In the best case, simulations using standard MD methods will give E values that will fluctuate around an average value. The fluctuations amplitude of the total energy should be less than the fluctuations amplitudes of the potential and kinetic energies. Calculations with $(E_{max} - E_{min})/\langle E\rangle \sim 10^{-4}$, where E_{max} and E_{min} are the maximum and minimum energy values during the simulation, and $\langle E\rangle$ is the average value of the total energy [96].

A key factor to control the accuracy of the MD algorithm is the time step δt. The time step must be small enough in order to accurately integrate the equations of motion. The time scale is

chosen based on the fastest movement in the system, oftentimes this is the shortest oscillation period. In a solid, this is of the order of picoseconds or less. The number of steps required for the correct integration of the equations during the oscillation period depends on the method used. For the Verlet algorithm, it is of the order of 50 steps to obtain sufficient accuracy. Therefore, the time step has the order of 10^{-15} - 10^{-14} seconds.

As soon as the studied material is defined, and the interatomic potential suitable for this material is developed and implemented within the MD code framework, it is necessary to determine the question of the study and choose the initial conditions. The system should be large enough to cover the main structures that are modeled. If the thermodynamic characteristics are to be calculated, the number of atoms should be large enough to reduce the size-dependent errors contribution. To model defects, other criteria must be taken into account, such as reducing elastic effects at the boundaries, for example.

Once the number of atoms, volume and shape of the simulation box are defined, it is necessary to set the initial positions and velocities for each particle of the system. The choice of initial conditions is very important from the point of view of the conservation energy law, since the energy given at the very beginning of the simulation is preserved throughout the simulation. For example, if two atoms are located too close to each other, their interaction energy is high, therefore, the potential energy of the entire system is high, as well as the total energy. Since the temperature is proportional to the average kinetic energy of the atoms, a poor choice of initial positions and velocities may affect the modeling of the desired thermodynamic conditions.

As it happens with any algorithm, MD calculation can be described as a set of steps. These steps do not depend on the studied system. At calculations always begin with a time interval when the system is not in equilibrium, therefore, there is a drift of the average values of the calculated quantities. As soon as the system reaches equilibrium, the averages acquire a physical meaning. Standard steps in MD modeling include:

1. Setting atoms positions $\{\mathbf{r}\}$ and momenta $\{\mathbf{p}\}$;
2. Calculation of the initial kinetic energy K, potential energy U, total energy $E = K + U$ and other quantities as well as the forces acting on each atom $\mathbf{F_i}$;
3. For the number of steps that bring the system into equilibrium, n_{equil}:
   (a) Solve the equations of motion for $\{\mathbf{r_i}(t+\delta t)\}$ and linear momenta $\{\mathbf{p_i}(t+\delta t)\}$ based on the values and forces at time t;
   (b) Calculate kinetic energy K, potential energy U, $E = K+U$ and forces acting on each atom $\mathbf{F_i}$;
   (c) Check values indicating the non-equilibrium state of the system for drift;
   (d) When the system is in equilibrium, resume the calculation.
4. For the number of steps n:
   (a) Solve the equations of motion for $\{\mathbf{r_i}(t+\delta t)\}$ and momenta $\{\mathbf{p_i}(t+\delta t)\}$ based on the values and forces at time t;
   (b) Calculate kinetic energy K, potential energy U, $E = K+U$ and forces acting on each atom $\mathbf{F_i}$;
   (c) Accumulate the statistics on the necessary quantities for averaging;
5. Data analysis: averaging, corrections, etc.

Considering the theoretical aspects listed above, it is possible to proceed directly to modeling the GBs. In this work, processes were simulated at different temperatures, loads, interaction with different numbers of dislocations were studied as well as the effect of the presence of irradiation defects in the crystal.

2.2 Coupled to continuum method

The time and space scales of the phenomena involved in the interaction between GBs and defects make Molecular Dynamics the most appropriate tool to investigate them. In order to study larger scale events, such as crack growth, chemical embrittlement, fatigue, dislocation pileups at grain boundaries etc., direct atomistic simulations are not always possible. The change in the physical properties of the materials can only be predicted accurately by using multiscale modeling: physical phenomena occurring at different scales are modeled separately, and the behavior of the system on a smaller scale provides the input data for the research on a larger scale.

In our study discrete dislocation (DD) techniques are useful to determine the behavior of dislocation pileups. In this approach, elastically determined fields define the motion of dislocations that are considered as continuous formations. This allows to accurately model the long-range interactions between defects, while small-scale phenomena and short-range interactions are described by a set of basic rules.

For the particular case of the interaction between a GB and a pileup of dislocations, the combination of these two methods is required. DD is used to model the behavior of the pileup of dislocations in external stress field, while MD is used to study in an accurate way the interactions between the defects at the atomic scale in presence of such field. A hybrid approach is applied that couples atomistic and discrete dislocations techniques. This method divides the physical problem into spatial regions that are modeled either with an atomistic or continuum approach. The combined use of both methods improves these techniques allowing the movement of the continuum dislocations and their interaction with each other and with the atoms in the atomistically defined region through the elastic field [99].

The main idea of the new method is that the parts of the material within the interaction region and its vicinity require a description with the atomistic representation, but at a distance far enough from these regions the processes are described well by using the elasticity and plasticity theories. The motion and interactions of continuum dislocations are well-defined and described by elastic continuum fields, similarly to the DD model approach. There is a wide range of phenomena that can be addressed by the formalism of the coupling model, such as nanoindentation, grain boundary sliding, fracture, void nucleation and slip transfer through grain boundaries.

The coupled method consists of four main components: (i) the atomistically modeled region; (ii) the continuum region of DD model; (iii) the connection between these regions and (iv) the methods of identification and transmission of dislocations between these two regions. The first two components are well-developed methods in terms of Molecular Dynamics and discrete dislocation formalisms. The coupling of the two regions is described in the following subsections.

2.2.1 Atomistic and continuum domains connection

Fig. 2.1 is a diagram of a general boundary value problem that needs to be solved. The material is exposed to a given load $\mathbf{T} = \mathbf{T}_0$ at the boundary $\delta\Omega_T$ and displacement $\mathbf{u} = \mathbf{u}_0$ at $\delta\Omega_u$. The body can be divided into two regions: atomistic Ω_A and continuum Ω_C. They are bounded by the interface $\delta\Omega_I$, defined by a line of atoms – the upper row of atoms in Fig. 2.1. This interface is not necessarily straight. Since the load of $\mathbf{T}$ on $\delta\Omega_A$ is discrete, it represents the forces $\mathbf{f}_A$ acting on individual atoms. In the material under consideration, there are N dislocations in the continuum region, for each i-th dislocation, the Burgers vector $\mathbf{b}_i$ and the position $\mathbf{d}_i$ are given. For each material point in the continuum, as well as for each atom in the atomistic domain, the initial position $\mathbf{X}$ in an ideal defect-free material is given. When a load is applied, these points and atoms experience a displacement $\mathbf{u}$, leading to a new configuration $\mathbf{x} = \mathbf{X} + \mathbf{u}$. It is necessary to solve the boundary problem based on the given equilibrium stress σ, strain ϵ, displacement fields $\mathbf{u}$, the position of discrete dislocations $\mathbf{d}_i$, as well as for the equilibrium position of atoms when applying certain boundary conditions.

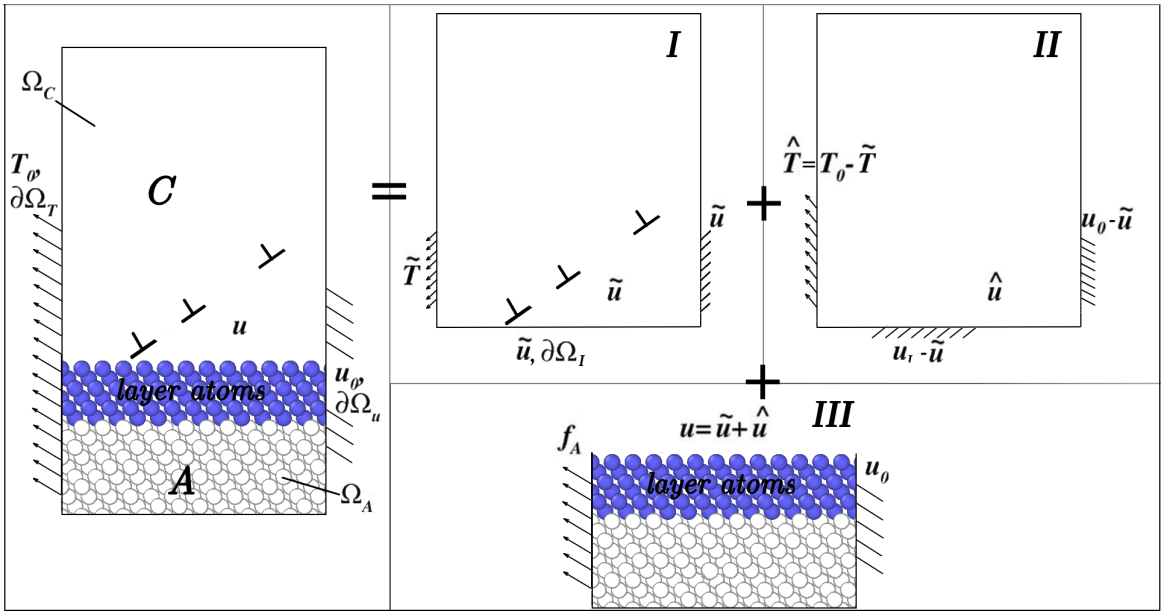

Figure 2.1: Scheme showing the sub-problems of coupling atomistic and discrete dislocation regions. Continuum region couples to the atomistic region by the interface atoms displacements - $\mathbf{u}_I$, while atoms couple to the continuum by the layer atoms. Fields defined in the continuum region control the displacements of the layer atoms.

For the convenience of distinguishing the quantities associated with the interface, the material points of the continuum and the atoms in the atomistic domain, the indices I, C and A, respectively, will be used henceforth. The atomistic domain can contain various defects in any quantity, including grain boundaries, vacancies, voids, interstitial atoms, as well as dislocations and dislocation loops. The atoms themselves with their positions $\mathbf{r}_A$ and $\mathbf{r}_I$ are the degrees of freedom in the domain. The main assumption is that near the interface between the regions, the behavior of atoms obeys the description in the framework of a linear elastic response, which is used for the continuum region description. The only nonlinear effect able to pass through the interface is the dislocation core. The atoms of the interface $\mathbf{r}_I$ are also interface nodes with $\mathbf{U}_I$ displacements for the continuum. This is necessary within the framework of continuum discretization, which must correspond to an atomistic lattice at the interface.

Special attention needs to be paid to the exact coupling between the two regions on the interface $\delta\Omega_I$. Due to the approximation of interatomic potentials, the action of which extends beyond the nearest neighbor, the atomic region is non-local. At the same time, the continuum is local, since the stresses at one point are completely determined by the deformation at that point. With the abrupt beginning of the material description by the finite element method in the continuum region, as well as the abrupt end of the atomistic region along the atomic plane, when creating the interface between the atomistic and continuum regions, incorrect surface energy appears, as well as non-physical reconstructions of the interface, due to the incorrect coordination number of the interface atoms.

In order to provide the correct number of neighbors for real atoms at and near the interface, a thin layer of atoms is introduced that overlaps with the continuum region. This layer of atoms is shown in Fig. 2.1, where the positions of the atoms are defined as $\mathbf{r}_l$. The thickness of the atomic layer should be greater than the cutoff radius of the interatomic potential, and also large enough so that the real atoms of the atomistic region keep the coordination number after the dislocations pass through the interface, which creates steps at the interface. The deformation of the continuum completely determines the positions of the atoms $\mathbf{r}_l$ of this layer, since they belong to the continuum region. The positions of the atoms in the layer are determined by the interpolation of nodal displacements obtained from the continuum solution of finite elements into the positions of the crystal lattice of the reference layer atoms located inside each finite element. The positions of the layer atoms in this case are instantly fixed from the point of view of the atoms in the atomistic domain and the atoms of the interface. Here

the basic assumption used is that the displacement field $\mathbf{u}$ in the continuum well approximates the real displacement field of atoms.

The total free energy of the atomistic domain should include its interaction with the layer atoms. The EAM potential defines the energy of an individual i-th atom as E_i, therefore, the functional of the total free energy of the atomistic domain has the form:

$$E^A = \sum_{i \in (A,I,l)} E_i(\mathbf{r}_A, \mathbf{r}_I, \mathbf{r}_l) - \mathbf{f}_A \mathbf{u}_A, \tag{2.12}$$

where $\mathbf{u}_A$ are the displacements of atoms. The atoms of the layer are included in the summations, despite the fact that they are not degrees of freedom. Taking the partial derivatives of the energy E^A with respect to the coordinates in the atomistic domain (A) and interface region (I), one can obtain the total forces acting on the atoms:

$$\mathbf{f} = -\nabla E^A(\mathbf{r}_A, \mathbf{r}_I). \tag{2.13}$$

The force calculated for the atoms near the interface and located on it is the real physical force produced by the local environment of the atoms. Partial derivatives of the free energy over the atoms of the layer are not included in the calculation, since they include non-physical surface effects. The atomic positions of the layer are determined by the displacements of the elements of the continuum region, as mentioned above.

In the general case, the functional of the total free energy of the continuum domain is expressed as the sum over the energies E_μ of the μ finite elements and the terms of the boundary work in the form:

$$E^C = \sum_{\mu} E_\mu(\mathbf{U}_I, \mathbf{U}_C, \mathbf{d}_i) - \int_{\delta\Omega_T} \mathbf{T}_0 \mathbf{u} dA. \tag{2.14}$$

As can be seen, the energy depends on the displacements $\mathbf{U}_I$ of the interface nodes, the displacements of the nodes of the discretized continuum $\mathbf{U}_C$ described below, and the positions of the dislocations $\mathbf{d}_i$. With respect to the atomistic domain and continuum coupling, it is important that the interface nodes are not degrees of freedom, but rather are determined from the current positions of the atoms via $\mathbf{U}_I = \mathbf{r}_I - \mathbf{R}_I$, where $\mathbf{R}_I$ is the initial position of the atom. In other words, the atoms of the interface move within the framework of the atomistic description, at the same time, from the point of view of the continuum, the atoms of the interface are fixed nodes with specified $\mathbf{U}_I$ displacements.

In this formulation, the interface atoms and the layer atoms serve the following important purposes. First, the atoms of the layer guarantee the preservation of the coordination number for atoms near the interface. Secondly, the layer atoms pass to the atomistic region the information about deformation in the continuum region and, similarly, the atoms of the interface transmit the information about deformation in the atomistic region to the continuum region. Since the atoms are not local, the layer region must have a finite thickness in order to transmit the deformation of the continuum to the atoms. On the other hand, since the finite element continuum is local, a finite number of interface atoms is necessary to transfer the atomistic deformation to the continuum region.

2.2.2 Continuum region containing discrete dislocations

Now we define the energy functional E^C of the continuum region with discrete dislocations. At any given time, the dislocations are located in positions $\mathbf{d}_i$, and the boundary problem for the continuum region is determined by the boundary conditions at $\delta\Omega_C$ and fixed displacements $\mathbf{U}_I$ along $\delta\Omega_I$, obtained thanks to the known positions of the atoms of the interface $\mathbf{r}_I$, which provides coherence between the atomistic and the continuum regions. Therefore, for a certain set of atomic displacements $\mathbf{U}_I$, the continuum problem is a correct, fully defined boundary value problem for discrete dislocations. The approach to solving this problem is very similar to the standard discrete dislocation method described in [100], as follows.

The elastic continuum problem, in turn, is divided into two related problems I and II, as shown in Fig. 2.1. Problem I is responsible for discrete dislocations located in an infinite homogeneous elastic material. By summing the known elastic fields generated by all dislocations located in $\mathbf{d}_i$ in the continuum, we obtain a solution for the total stress, strain and displacement in problem I, respectively:

$$\tilde{\sigma} = \sum_{i}^{N} \tilde{\sigma}^i, \quad \tilde{\epsilon} = \sum_{i}^{N} \tilde{\epsilon}^i, \quad \tilde{\mathbf{u}} = \sum_{i}^{N} \tilde{\mathbf{u}}^i, \tag{2.15}$$

where $\tilde{\sigma}^i$, $\tilde{\epsilon}^i$ and $\tilde{\mathbf{u}}^i$ are linear elastic solutions for the fields of each i-th dislocation in an infinite medium. The fields defined in problem I do not fully satisfy the boundary conditions, since the superposition leads to loads $\tilde{\mathbf{T}}$ along the surfaces $\delta\Omega_T$ and additional displacements $\mathbf{u} = \tilde{\mathbf{u}}$ along $\delta\Omega_u$ and $\delta\Omega_I$. To satisfy the real boundary conditions, a corrective problem II is introduced, with the superposition of its fields with the fields obtained from problem I, the desired $\mathbf{T}_0$, $\mathbf{u}_I$ and $\mathbf{u}_0$ can be obtained. Thus, problem II is the boundary problem of a linear elastic body without dislocations, to which the corrective effects $\hat{\mathbf{T}} = \mathbf{T}_0 - \tilde{\mathbf{T}}$ (on $\delta\Omega_T$) and the displacements $\hat{\mathbf{u}} = \mathbf{u}_0 - \tilde{\mathbf{u}}$ (on $\delta\Omega_u$) and $\hat{\mathbf{u}} = \mathbf{u}_I - \tilde{\mathbf{u}}$ (on $\delta\Omega_I$) are applied. Since all singularities and discontinuities associated with the presence of dislocations belong to the fields identified with the symbol $\sim$ and are included completely in problem I, the fields of problem II (marked with the symbol $\wedge$) are smooth and, therefore, can be obtained using the finite element method for a given geometry and load. Then the fields of the continuum domain are the sum of the fields from problems I and II:

$$\mathbf{u} = \tilde{\mathbf{u}} + \hat{\mathbf{u}}, \quad \sigma = \tilde{\sigma} + \hat{\sigma}, \quad \epsilon = \tilde{\epsilon} + \hat{\epsilon}, \tag{2.16}$$

which satisfies the boundary conditions imposed on the continuum region by the construction of the problem and equilibrium configurations from a linear elastic superposition.

This approach uses a completely anisotropic linear elastic composite relation for problem II, which leads to the correspondence of the continuum elasticity constants to the constants of the atomic domain. However, for the fields $\sim$ from problem I describing discrete dislocations (identified with $\sim$), analytical fields from the isotropic theory of elasticity with Voigt-averaged elastic constants are used [3]. Consequently, the composite relations for the continuum domain have the form:

$$\tilde{\sigma}_{ij} = 2\mu\tilde{\epsilon}_{ij} + \lambda\tilde{\epsilon}_{kk}\delta_{ij} \tag{2.17}$$

$$\hat{\sigma}_{ij} = c_{ijkl}\hat{\epsilon}_{ij}, \tag{2.18}$$

where μ and λ are Voigt-averaged elastic constants derived from a completely anisotropic stiffness tensor c_{ijkl}. A completely anisotropic solution is obtained in the special case without discrete dislocations, but small deviations are introduced due to the $\sim$ fields defined in the presence of dislocations.

Then the free energy functional E^C of the continuum region, taking into account the given above decomposition, has the form:

$$E^C = \frac{1}{2}\int_{\Omega_C} (\tilde{\sigma} + \hat{\sigma})/(\tilde{\epsilon} + \hat{\epsilon})dV - \int_{\delta\Omega_T} \mathbf{T}_0(\tilde{\mathbf{u}} + \hat{\mathbf{u}})dA \tag{2.19}$$

After additional manipulations, including discretization in a finite element implementation, the introduction of the function of Airy stresses for individual dislocations, the application of the principle of virtual work, etc., the energy functional can be written as:

$$E^C = \frac{1}{2}(\hat{\mathbf{u}}_C \cdot \mathbf{C}_{CC} \cdot \hat{\mathbf{u}}_C + \hat{\mathbf{u}}_I \cdot \mathbf{C}_{II} \cdot \hat{\mathbf{u}}_I) + \hat{\mathbf{u}}_C \cdot \mathbf{C}_{CI} \cdot \hat{\mathbf{u}}_I - \mathbf{t}_0 \cdot (\tilde{\mathbf{u}}_C + \hat{\mathbf{u}}_C) + \tilde{\mathbf{t}}_C \cdot \hat{\mathbf{u}}_C + \Delta, \tag{2.20}$$

where C_{ij} are the stiffness matrices obtained from the discretization of the continuum by the finite

element method, Δ is a term containing additional nonessential for our task elements. Then the equilibrium fields (denoted with $\wedge$), are obtained by minimizing equation (2.20) with respect to the degrees of freedom $\hat{\mathbf{u}}_C$, i.e.:

$$\frac{\partial E^C}{\partial \hat{\mathbf{u}}_C} = 0 = \mathbf{C}_{CC} \cdot \hat{\mathbf{u}}_C + \mathbf{C}_{CI} \cdot \hat{\mathbf{u}}_I - \hat{\mathbf{t}}_C \tag{2.21}$$

Solutions for an unbounded $\hat{\mathbf{u}}_C$ can be explicitly obtained in terms of the $\hat{\mathbf{u}}_C$ bounded on the boundary of the $\delta\Omega_C$ and degrees of freedom of the interface $\hat{\mathbf{u}}_I$ as

$$\hat{\mathbf{u}}_C = \mathbf{C}_{CC}^{-1}(\hat{\mathbf{t}}_C - \mathbf{C}_{CI} \cdot \hat{\mathbf{u}}_I) \tag{2.22}$$

Substituting the solution for $\hat{\mathbf{u}}_C$ from equation (2.22) into equation (2.20), it is obtained a reduced energy functional for the continuum region, where the only degrees of freedom remain the positions of discrete dislocations $\mathbf{d}_i$ from the Δ term. This energy functional of the continuum is further used to obtain forces acting on discrete dislocations.

2.2.3 Equilibrium state

The formalism of the coupled atomistic and continuum domains includes two energy functionals, as described above. They depend on various degrees of freedom, such as positions of atoms and discrete dislocations, which need to be brought into equilibrium after each increment of the external load. The minimum configuration can be achieved by searching for a point in the configuration space where the forces applied to the degrees of freedom will be zero. These forces can be obtained as partial derivatives of the energy functionals of the atomistic continuum regions with respect to the dislocation positions, then the force acting on the i-th dislocation is the Peach-Koehler (P-K) force given as:

$$\mathbf{p}_i = -\frac{\partial E_C}{\partial \mathbf{d}_i} \tag{2.23}$$

By limiting the movement of dislocations to their glide planes, i.e., excluding climbs and cross-slips, Eq. (2.23) can be replaced by:

$$p_i = -\frac{\partial E_C}{\partial s_i} = (\mathbf{m}_i)^T \left(\hat{\sigma} + \sum_{i \neq j}^{N} \tilde{\sigma}_j \right) \mathbf{b}_i, \tag{2.24}$$

where s_i is the position of the dislocation on its glide plane, $\mathbf{m}_i$ is the normal to the glide plane, and $\mathbf{b}_i$ is the Burgers vector. Van der Giessen and Needleman obtained this expression for the P-K forces along certain glide planes, and also showed that these forces can be directly obtained from the stress fields calculated in problems I and II [100].

When searching for an equilibrium configuration, the coordinates of atoms and the positions of dislocations are updated simultaneously. Taking into account the update of the positions of the interface atoms and dislocations in the continuum, it is possible to calculate the updated positions of the layer atoms and continuum displacements. P-K forces p_i acting on dislocations, as well as forces $\mathbf{f}_A$ acting on atoms, are calculated and transmitted to subsequent modeling steps, where the positions of atoms and discrete dislocations are updated along the search direction for the minimum forces. This force-based coupling makes it possible to significantly bring the interface to nonlinear atomistic behavior, without making a strong negative impact on the results obtained in modeling.

2.2.4 Detection and passing of dislocations

Dislocations generated in the continuum region or created in the atomistic region are subjected to forces provoking their movement from the continuum region to the atomistic region and vice versa. Thanks to the seamless nature of the interface between the two areas for elastic deformations, dislocations located even at a short distance do not experience the effects of the interface. If a dislocation from

the atomistic region, i.e., having a real atomistic core structure, approaches the interface, secondary spurious forces are created. The elastic continuum region is not able to correctly accommodate the shear deformations associated with the Burgers vector of dislocations. A fully elastic response that resists the deformation appears at the boundary, then, within the true atomistic consideration, the nonlinear response leads to softening of the material and continued glide of dislocations. Therefore, it is necessary to detect dislocations approaching the interface and artificially move them through it. In addition, when moving the dislocation from the atomistic region to the continuum region, the atomic structure of the core must be removed from the corresponding region and introduced into the continuum region accordingly. With the movement in the opposite direction, the process is similar and completely reversible.

It is necessary to capture dislocations before reaching the interface in the atomic domain. As a first step, it is possible to define the detection area as a thin strip at a short distance from the interface. This area is used only to track changes in the kinematics of the process and does not contribute to the calculation of energies or forces in the atomic region. Next, it is necessary to set a kinematic criterion that will uniquely detect a slip in the elements of the region and accurately determine the relationship of this slip with dislocations. Each individual dislocation must be accurately identified, since, firstly, during the simulation, many dislocations may pass through a specific detection area, and it may be necessary to isolate slip associated with each dislocation. Secondly, the displacements of atoms in the nodes of the detection elements also include displacements associated with elastic deformation, body displacement and rotation, which must be filtered out. Taking into account the given strict requirements, it is necessary to introduce the following key components: (i) the deformation relates and is referred back to the initial configuration of the ideal crystal, (ii) a certain measurement of slip must be invariant with respect to the rotation of the solid or lattice translation, and (iii) all slip-related activity is monitored to control only the deformation associated with the new slip.

As soon as the dislocation has been detected, it is necessary to transfer it to the adjacent region. The transfer involves an appropriate change in the displacements of all atoms and nodes in such a way that the atomistic dislocation core is removed while maintaining the sliding displacements during the transmission from the atomistic region to the continuum and, similarly, during the transmission back. The procedure of transition from the continuum to the atomistic domain, needed to be solved, is implemented as follows. As soon as the P-K force acting on the dislocation pushes it close enough to the interface to cross it, the process is identified geometrically. Then the dislocation is introduced into the atomistic region, directly into the detection region using the displacement field of the virtual dislocation dipole. The discrete dislocation is stored as an "image" in order to avoid additional influence of continuum fields on the atomistic domain. It should be noted that the core structure of the dislocation introduced into the atomistic region is not correct initially, but is quickly restored within the subsequent relaxation.

The ability to transfer back and forth dislocations between two regions can lead to random oscillations of defects at the boundary during relaxation. This may slow down convergence at some steps, but does not lead to convergence errors. At the same time, the equilibrium position of the dislocation is on or near the interface.

2.3 Simulation setup

The step prior to any simulation is the preparation of the atomistic domain that undergoes the described above procedures. The initial simulation box consists of a bcc bicrystal with an initially coherent symmetric tilt GB in the middle. The principal axes x, y and z of the upper crystal (λ) are oriented along the GB axis, the tilt axis and the axis perpendicular to the interface, respectively, while for the lower crystal (μ) the orientation of the axes is mirror reflected. Approximate dimensions of the cell size are in range from 700 × 16 × 500 Å to 950 × 18 × 700 Å along the corresponding directions with a total number of atoms ranging from ∼ 600000 up to ∼ 700000. In order to investigate the possible mechanisms involving disconnections on the SCGBM, different setups have been employed: (i) the GB interacting with a single dislocation and (ii) the GB interacting with a DPU.

(i). By using Atomsk software [101] we introduce a single $\frac{1}{2}\langle 111\rangle$ dislocation on the upper crystal of the simulation box. For edge dislocations the glide planes are of {112} type, while for mixed dislocations are {110} type. For a given glide plane inclination, we consider, in turn, two dislocations with opposite sense of their Bv, i.e., pointing away from the interface and pointing towards it. An incremental shear strain is applied in order to move the dislocation to initiate the interaction with the interface. Periodic boundary conditions were imposed on the tilt axis and the axis along the GB, with fixed boundaries in the direction perpendicular to the interface.

(ii). Interactions between grain boundaries and dislocation pileups were modeled using the hybrid model described above, combining atomistic and continuum approaches (shown schematically on Fig. 2.2. This approach uses separate continuum and atomistic modeling, which define mutual boundary conditions. The positions of continuum dislocations in pileups are determined as a function of the shear stress applied externally, and the positions of any dislocation in the atomistic region are fixed in certain positions. The continuum approach is used to determine atomistic displacements for each increment of the applied stress, which are then applied to the external atomic region represented as a layer of atoms, simulating an increase in stress. This model has already proved its efficiency in fcc metals [26].

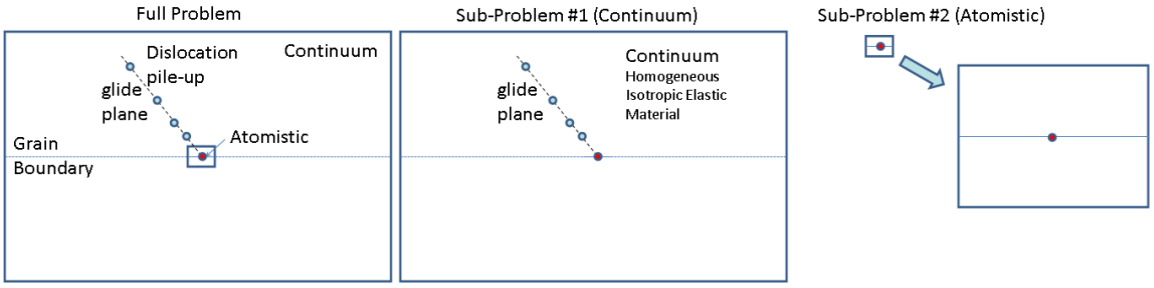

Figure 2.2: Schematic description of the algorithm used to model the interaction between a GB and a dislocation pileup. The full problem is divided into two sub-problems: #1 Continuum - solved by DD method, and #2 Atomistic - solved by MD method.

With respect to the loading conditions, the following parameters were fixed during the whole set of simulations: the number of dislocations in the pileup (15 units), the increment of the externally applied stress ($\Delta\sigma_{app}$ = 100 MPa) and the maximum value of the externally applied stress ($\sigma_{app,max}$ = 5.5 GPa). In this model periodic boundary conditions were imposed only along the tilt axis while along the other two directions were used fixed boundaries.

The bicrystals were relaxed using the conjugate gradient method [102] and then atomic displacements were applied to all the atoms of the simulation cell, corresponding to an initial applied stress. The crystal was relaxed again and thermalized for 20 ps to achieve a desired initial temperature. A fixed integration MD time step of 1 fs was used for all runs. The simulation temperature ranged from 150 K up to 900 K, thus enhancing or reducing the role played by thermal activation.

In all the simulations with both setups, the stress state of the system is recorded after each increment of strain and the open visualization tool OVITO [103] is used for visualization and analysis

of the atomic configuration. The peculiarities in simulations steps and setups used for modeling different GBs are provided in Table 2.1. This table presents the sizes of the simulation boxes, the direction vectors along the axes in the λ crystal and the approximate number of atoms simulated.

Table 2.1: Different GBs simulations features. l_i is the length of the simulation box along the corresponding direction in lattice constants, X, Y and Z are the orientation vectors for the corresponding axes of the λ crystal, N is the number of atoms in the simulation.

GB	l_x (a_0)	l_y (a_0)	l_z (a_0)	X	Y	Z	N
{112}	277.1	5.66	195.9	$[1\bar{1}1]$	[110]	$[\bar{1}12]$	$\sim 6 \times 10^5$
{332}	265.3	5.66	187.6	$[1\bar{1}\bar{3}]$	[110]	$[3\bar{3}2]$	$\sim 6 \times 10^5$
{111}	293.9	5.66	207.8	$[1\bar{1}\bar{2}]$	[110]	$[1\bar{1}1]$	$\sim 7 \times 10^5$
{116}	348.7	5.66	246.6	$[3\bar{3}1]$	[110]	$[\bar{1}16]$	$\sim 9 \times 10^5$

Finally, to assess the local evolution of stress state in the regions of interest at the GB – dislocation interactions, we have allocated several groups of atoms to record the forces and displacements during the simulation runs. These groups of atoms are placed in positions where they can provide relevant information on the reactions with the interface. They are indicated in Fig. 2.3: group "1" is chosen along the glide plane of the initial DPU; group"2" is at the initial reaction site; groups "3" and "4" are placed along the GB plane in order to analyze the glide of mobile disconnections; groups "5", "6" and "7" are chosen along the glide planes of possible transmitted or reflected dislocations. In order to determine accurately these glide planes, several ad hoc preliminary simulations are required. The most relevant group to study the interactions we are interested in is #2 (shown in detail on the inset of Fig. 2.3).

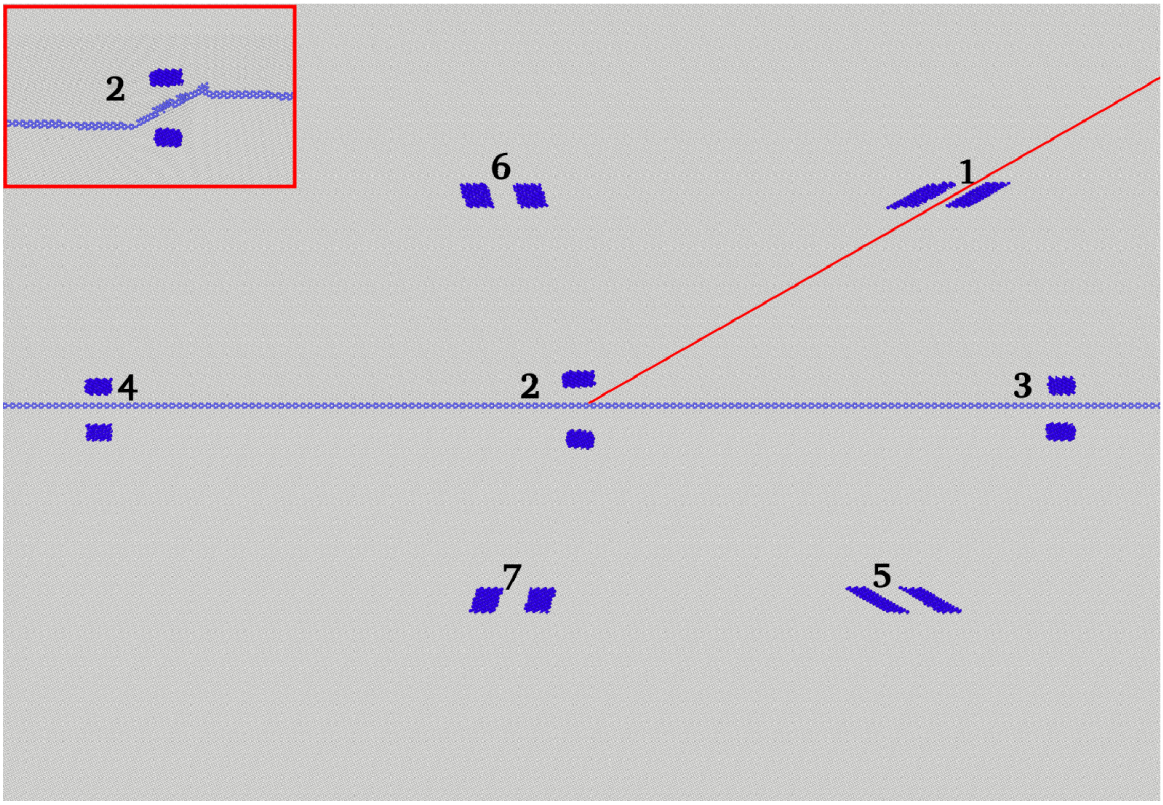

Figure 2.3: Snapshot of MD simulation of a {332} GB with marked selected groups of atoms. Each group is a pair of regions lying below and above glide planes. See text for details. The inset shows an example of reaction with group #2 around it.

CHAPTER 3

GRAIN BOUNDARY DISLOCATIONS AT THE ⟨110⟩ TILT GRAIN BOUNDARIES

Among the many possible interfaces present in metals, tilt GBs are of special interest because they are frequently observed in experimental measurements [104, 105], suggesting that they are energetically favored over other families of GBs. In the present work we focus on four symmetric tilt GBs with a ⟨110⟩ tilt axis, which have been chosen to represent cases of special interest on the plasticity of bcc metals. The first two GBs considered are the $\Sigma3\{112\}\langle110\rangle$ and the $\Sigma11\{332\}\langle110\rangle$; both are the coherent boundary of the conjugate twin modes found in bcc materials, namely {112} and {332} twins [106–109]. Glissile disconnections are observed in both boundaries, although as we will detail below, the dynamic behavior of each interface is quite different. The third GB chosen is the $\Sigma3\{111\}\langle110\rangle$, which represents an extreme case: no EDisc were found. This feature has many consequences on the response of this GB under externally applied shear stress being the more relevant the inability to perform SCGBM. Finally, the fourth GB investigated is the $\Sigma19\{116\}\langle110\rangle$ which can be considered as an intermediate case: several disconnections are involved in the reactions from the GB – dislocation interaction and SCGBM is observed. This set of GBs covers a wide range of values for the misorientation angle and low Σ, allowing to consider different structural units and enabling to investigate in detail the role of GB atomic structure in the creation of glissile disconnections involved in the motion of the ⟨110⟩ tilt GBs.

Table 3.1: Summary of the properties of the EDisc involved in SCGBM for each GB. CRSS is the critical resolved shear stress for an EDisc in MPa.

GB	$\mathbf{b}_{n/m}$	Bv magnitude	EDisc height	CRSS (MPa)
{112}	$\mathbf{b}_{\pm1/\pm1}$	0.288 a_0	0.408 a_0	20
{332}	$\mathbf{b}_{\pm2/\pm2}$	0.302 a_0	0.426 a_0	550; 620
{116}	$\mathbf{b}_{\pm3/\pm3}$	0.229 a_0	0.487 a_0	4000; 4700
	$\mathbf{b}_{\pm5/\pm5}$	0.344 a_0	0.811 a_0	unstable
	$\mathbf{b}_{\pm8/\pm8}$	0.115 a_0	1.298 a_0	–
	$\mathbf{b}_{\pm11/\pm11}$	0.115 a_0	1.784 a_0	–

The SCGBM is carried out by production and glide of highly mobile EDisc. The EDisc can be produced in several ways: (i) by nucleation of a dipole in the pristine interface, when the local shear stress exceeds a threshold value specific for each GB; (ii) as an outcome of the interaction between the GB and crystal dislocations; (iii) generated by a GBD acting as a source of disconnections [57]. As the EDisc glide along the GB they can interact with other GBDs, affecting its motion. On a dichromatic

pattern in Fig. 3.1 there are marked all the EDisc observed for each GB studied. The properties of the EDisc in iron are summarized in Table 3.1. The value of a_0 at T = 0 K is 2.855 Å.

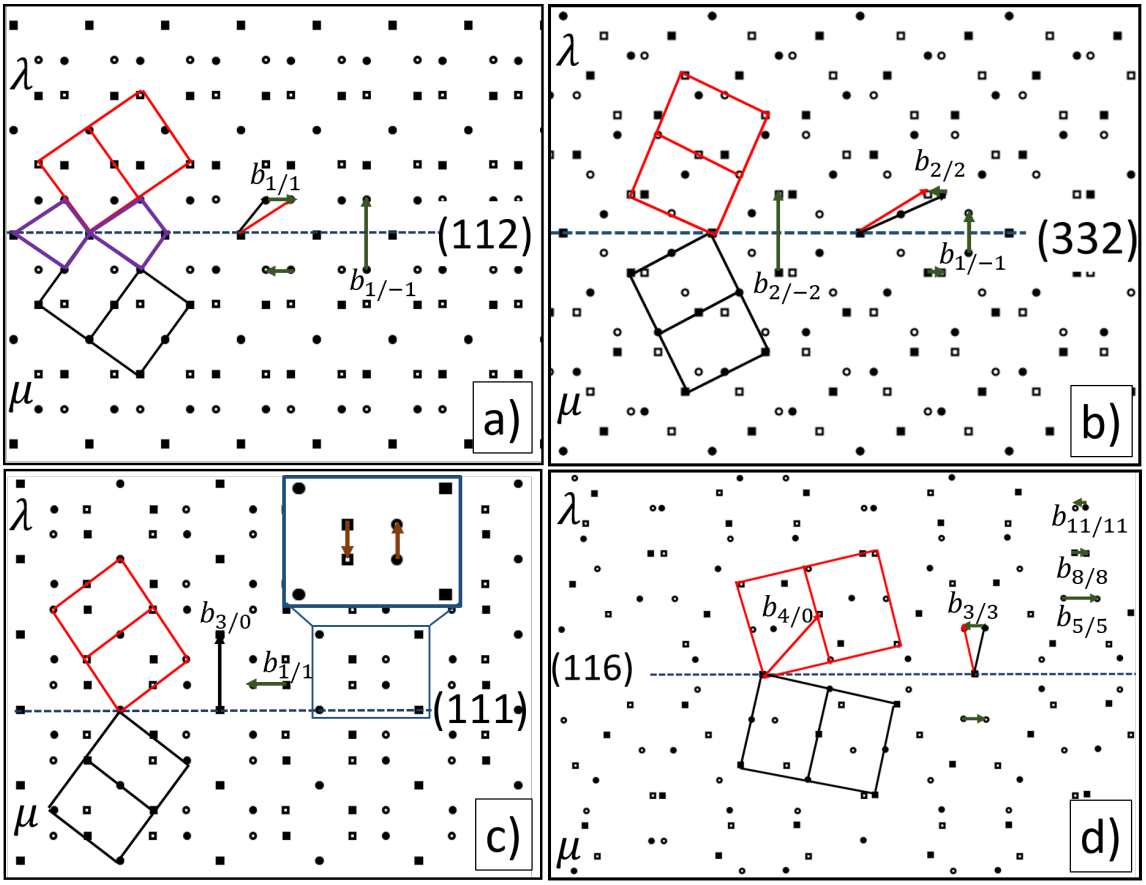

Figure 3.1: [110] projections of the dichromatic pattern for the ⟨110⟩ Symmetric tilt grain boundaries investigated including the GBDs involved in the reactions described.

This chapter presents Molecular Dynamics simulation study of the characteristic of the GBDs in {112} and {332} twin boundaries, their vicinal GBs, i.e., GBs obtained by increasing slightly its misorientation, and the {116} GB. The sources of disconnections and their interaction with the other GB dislocations are described together with their role in the shear-coupled GB migration. The absence of gliding disconnections in the {111} GB impedes the shear-coupled GB migration, but two pure shuffles inside the coincident site lattice unit facilitate the transformation of the {111} GB. In this chapter we summarize in Section 3.1 the main trends of the {112}, {332}, {111} and {116} GBs under an applied shear stress. We describe the properties of the GBs that are vicinal to the {112} and {332} GBs in Section 3.2. Finally in Section 3.3 we present the concluding remarks.

3.1 Main trends of {112}, {332}, {111} and {116} grain boundaries

3.1.1 {112} GB

The grain boundary $\Sigma3\{112\}\langle110\rangle$ presents several specific features endowing it with a relevant role on the plasticity mechanisms in bcc polycrystalline metals. As detailed before, it is the coherent boundary of the {112} twin, which has proven experimentally to effectively strengthen materials by impeding dislocation motion [12]. Another distinctive feature comes from the energetic analysis: ref. [82] shows that this interface has the lowest grain boundary energy among all the symmetric tilt GBs ($\sim 0.25\ J/m^2$ in α-Fe). The grain boundary population is shown to be inversely correlated with the grain boundary energy [104], which explains why the symmetric {112} GB is the most abundant GB in bcc-Fe. Finally, the interfacial structure of this GB is a repetition of a simple structural unit, marked in purple in Fig. 3.1a, presenting a slightly distorted perfect crystal coordination.

Fig. 3.2 shows a bicrystal with the orientation of the upper (λ) crystal indicated by the blue unit cell, where the axis a_1 and a_2 point inside the paper, and the disconnection dipoles created under shear stress.

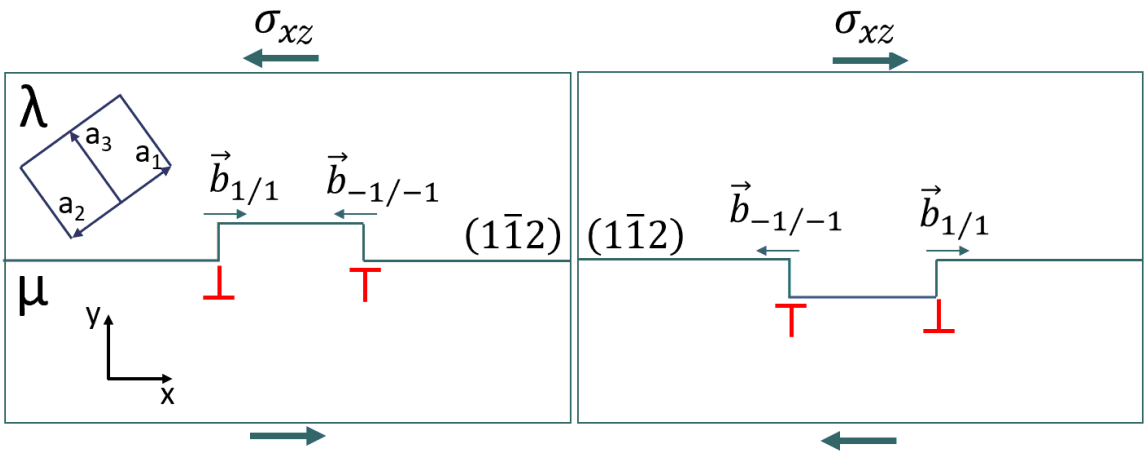

Figure 3.2: Schematic of the bicrystal showing the unit cell of the upper crystal (λ) and the disconnections dipoles created under applied shear stress.

The external shear stress parallel to the GB necessary to create a dipole $\{\mathbf{b}_{1/1};\ \mathbf{b}_{-1/-1}\}$ in the pristine {112} GB is about 2.8 GPa. The strain accommodation following the creation and glide of a disconnection dipole produces a drop about 0.2 GPa while the GB moves one plane upwards for $\sigma_{xy} < 0$ and downwards for $\sigma_{xy} > 0$, as shown in Fig. 3.2.

A GBD relevant for the {112} GB is the $\mathbf{b}_{1/-1}$ (shown in Fig 3.1a) which has its Bv perpendicular to the GB and does not step the GB ($h = 0$). The importance of this GBD is that it acts as a source of $\mathbf{b}_{1/1}$ EDisc (or the complementary $\mathbf{b}_{-1/-1}$), identified in Fig. 3.1a [57, 110]. This EDisc has a short Bv ($\sim 0.29\ a_0$), it steps the boundary only one plane ($h = 1$), which means that no shuffles are required during glide [111] and it shows a high mobility due to a very low resolved shear stress ($\sim$ 20 MPa [64]). The GBD $\mathbf{b}_{1/-1}$ acts as a source of pairs of disconnections of opposite sign created on each side of the GBD. This production process of EDisc can be sustained because the GBD moves together with the GB by a conservative climb [57]. The shear stress required to create a disconnection dipole in the pristine interface is around 2.8 GPa while for the source of disconnections the stress level required is lower, around 2 GPa. Both disconnection production mechanisms contribute to the SCGBM.

3.1.2 {332} GB

The second family of GBs investigated correspond to the {332} tilt GB. The GB energy for this interface lies in a local minimum on the GB energy - misorientation curve ($\sim 1.0\ J/m^2$ in Fe [112]). This GB shares many common features with the {112} GB: only one type of EDisc is observed ($\mathbf{b}_{2/2}$

or $\mathbf{b}_{-2/-2}$ in the corresponding dichromatic pattern of Fig. 3.1b), with a similar short Bv ($\sim$ 0.30 a_0) and step height ($\sim$ 0.43 a_0) but involving two {332} planes. However, the resolved shear stress is higher ($\sim$ 550 - 620 MPa [74]) due to the necessary shuffles of the atoms in the disconnection core.

Likewise, SCGBM is initiated when a EDisc dipole of $\mathbf{b}_{2/2}$ and $\mathbf{b}_{-2/-2}$ is created at the interface. The mechanisms are the same described above: formation in the pristine interface or produced by a source of disconnections (by the GBD denoted $\mathbf{b}_{2/-2}$), capable to move together with the GB (see Fig. 5 in ref. [74]).

In the pristine {332} GB dipole pairs of disconnections are created when the shear stress is $\sigma_{xz} =$ 1.45 GPa (at T = 0 K). Disconnections of opposite signs run in opposite directions under the shear stress and displace the GB by two planes per dipole, as shown in Fig. 3.3a. The resolved shear stresses to move the $\mathbf{b}_{\pm 2/\pm 2}$ EDiscs to the right is $|\sigma_{xz}| = 550$ MPa, whereas to move them to the left is $|\sigma_{xz}| = 620$ MPa.

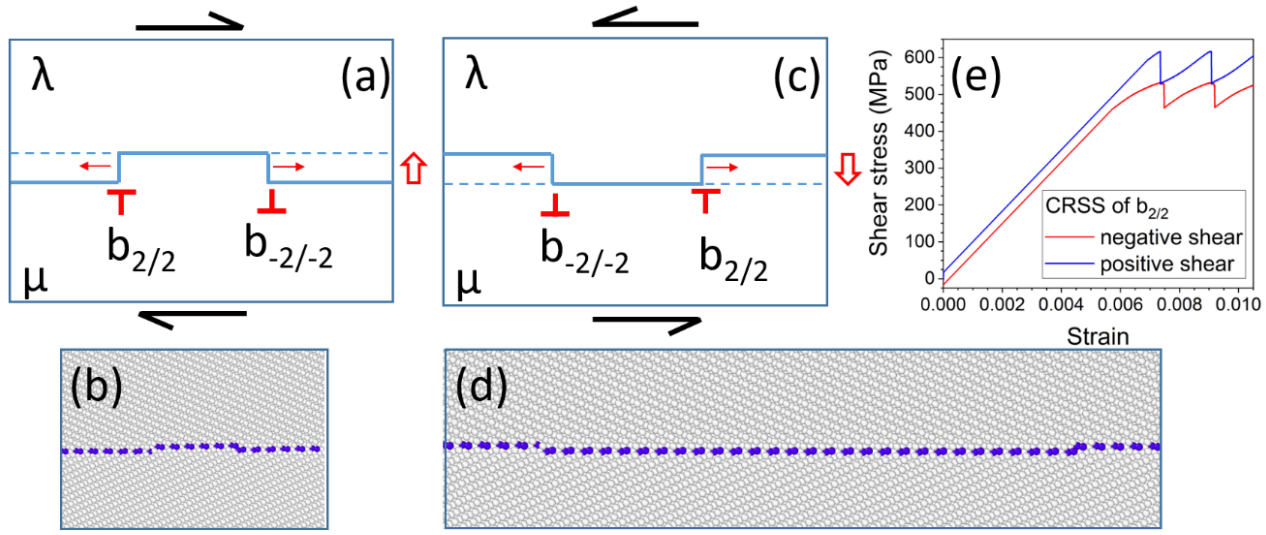

Figure 3.3: Dipole of disconnections gliding under an applied shear stress; the GB is displaced upwards (a, b) and downwards (c, d), as indicated by big red arrows. (e) Critical resolved shear stress (CRSS) of the $\mathbf{b}_{2/2}$ disconnection under a positive and negative shear stresses.

When the shear stress is positive (Fig. 3.3a,b), the GB is displaced upwards (transforms λ crystal into μ crystal); the process is reversible and the GB is displaced downwards when the shear stress is negative as shown schematically in Fig. 3.3c,d. The asymmetry of stresses favors the glide of EDisc that are moving to the right. This asymmetry may influence the displacement of the GB at low temperatures, especially if other GB defects are present.

3.1.3 {111} GB

The third GB considered has been the $\Sigma 3\{111\}\langle 110\rangle$ which is a symmetric tilt GB with a high-angle misorientation ($\theta = 109.53$ degrees) and a high GB energy ($\sim 1.3\ J/m^2$). The dichromatic pattern for this GB (Fig. 3.1c) shows that there is only one possible candidate of EDisc that could participate in the SCGBM, however neither this EDisc or a different one appears in the results.

In order to study the behavior of the interface in the absence of EDisc we investigated the shear response of the pristine {111} GB. Our simulations show that shear-coupled GB migration does not take place, as there is no production of EDisc. At 0 K we have observed the formation on the interface of pure steps without dislocation character. The steps are created by the shuffling of two atoms of the Coincident-site lattice (CSL) unit cell (inset in Fig. 3.1c) and an energy barrier for the process is 99 mJ/m^2 [113]. The process is initiated at around 9 GPa of shear stress accommodated in the system. Our results show that when a stress concentrator exists in the GB, the stress necessary to initiate transformations on the interface is lower.

The main conclusion from these observations is that stepping the interface is the preferential mechanism on this GB to accommodate plastic deformation. The comparison of the shear stress levels required to activate this mechanism (around 9 GPa) with the measured for the {112} GB (around 2.8 GPa) and the {332} GB (around 4.1 GPa) suggests that it is the least efficient of all.

3.1.4 {116} GB

The last GB considered has been the $\Sigma19\{116\}\langle110\rangle$ which is a symmetric tilt GB with a small-angle misorientation ($\theta = 26.53$ degrees) and a high GB energy ($\sim 1.2\ J/m^2$). The dichromatic pattern shows the potential candidates of EDisc for this GB (Fig. 3.1d). Based on the behavior observed in the previous GBs, the $\mathbf{b}_{\pm3/\pm3}$ looks as the most suitable candidate, as it is the one with smallest ($\mathbf{b}$, h) values (see Table 3.1), although its resolved shear stress (between 4 and 4.7 GPa) is remarkably higher than for $\mathbf{b}_{\pm1/\pm1}$ at the {112} ($\sim$ 20 MPa) and $\mathbf{b}_{\pm2/\pm2}$ at the {332} (between 550 and 620 MPa). Nonetheless, more types of glissile disconnection appear despite having larger Bv and/or higher step height (tagged as $\mathbf{b}_{\pm5/\pm5}$, $\mathbf{b}_{\pm8/\pm8}$ and $\mathbf{b}_{\pm11/\pm11}$ in Fig. 3.1d). But, at the same time, these high-stepping disconnections (HS Disc) are unstable and eventually split in pairs of $\mathbf{b}_{3/3}$ and $\mathbf{b}_{-3/-3}$. For this reason, the {116} GB can be considered as an intermediate case between the {112} and {332} GBs, where only one EDisc participates in SCGBM and the {111} GB where no EDisc are present, preventing the sustained migration of this interface.

In the case of the pristine interface, SCGBM starts when the shear stress is around 6.6 GPa, by inducing the creation of $\mathbf{b}_{3/3}$ and $\mathbf{b}_{-3/-3}$ pairs. The several reactions analyzed indicate that the HS Disc appearing in the reactions, although they show a very short lifetime, seem to play the role of facilitators, allowing a more efficient way to couple plastic deformations by creating new interfacial defects and EDisc capable to sustain SCGBM.

3.2 Grain boundaries vicinal to {112} and {332} interfaces

3.2.1 GBs vicinal to {112}

The boundaries vicinal to the low index {112} GB are formed by a {112} GB with a misorientation angle modified by a small increment. These GBs are high index boundaries and have higher energy formation. These GBs show a comparable accommodation as for low angle GBs, i.e., the increase of misorientation from the pristine {112} GB is accommodated by an array of $\mathbf{b}_{1/-1}$ GBDs, leaving segments of pristine {112} boundary between them, as shown in Fig. 3.4a. The distance between GBDs depends on the $\Delta\theta$ added to the misorientation angle $\theta = 70.53°$ of the {112} tilt GB, therefore there is a maximum $\Delta\theta$ corresponding to the minimum distance between GBDs that keeps the properties of the set of vicinal GBs. Table 3.2 presents the list of vicinal GBs studied. They are indicated by: the Miller indexes of the theoretical plane before relaxation; the increase of misorientation with respect to the {112} GB; the linear density of GBDs, i.e., number of GBD per unit length along the X direction; the GB energy (see Fig. 3.5). Under a shear stress, each GBD emits a dipole pair of EDisc (see Fig. 3.2) that glide up to their annihilation with the neighbor pair. Thanks to the compensated climb of GBDs, these vicinal GBs can perform efficiently SCGBM, with a shear stress level, which can be significantly lower than for the pristine interface.

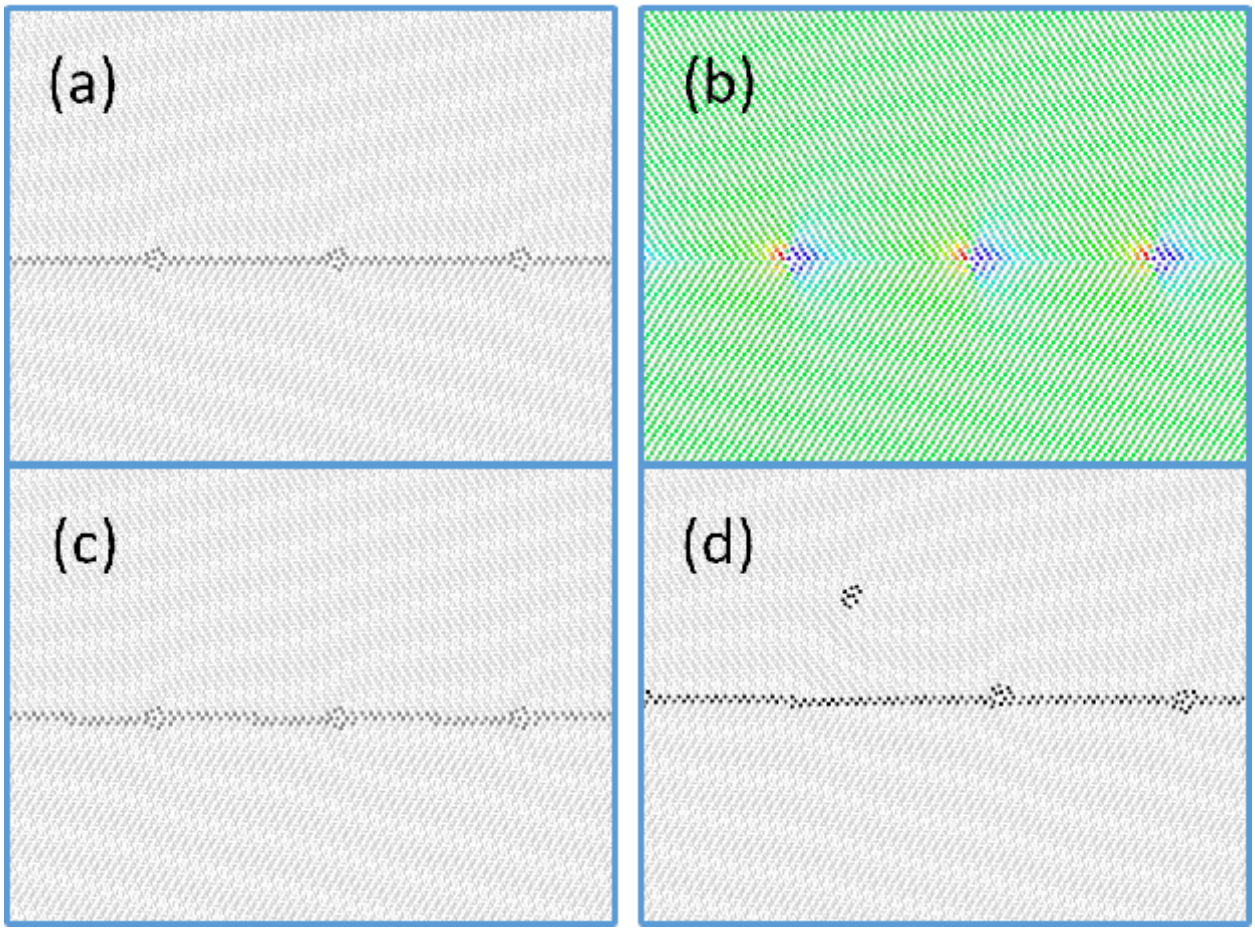

Figure 3.4: (19, 19, 40) GB vicinal to {112}. a) GB in equilibrium formed by GBDs and segments of {112} GB. b) Pressure map. c) GB under shear stress: disconnections are running towards the right from one GBD to the next. d) GB under a high strain rate: emission of a dislocation (see text for details).

Table 3.2: Parameters of the vicinal GBs to the {112} GB. GBs indicated by: the Miller indexes of the theoretical plane before relaxation. $\Delta\theta$ is the increase of misorientation with respect to the {112} GB; the linear density of GBDs is number of GBD per unit length along the X direction; the GB energy is plotted in Fig. 3.5.

GB plane	$\Delta\theta$ (degrees)	Linear density of GBD (nm^{-1})	GB energy (J/m^2)
(112)	0	0	0.245
Σ1681 (23, 23, 48)	-2.28	0.154	0.418
Σ1161 (19, 19, 40)	-2.74	0.205	0.433
Σ417 (8, 8, 17)	-3.22	0.242	0.451
Σ113 (4, 4, 9)	-6.22	0.466	0.499
Σ97 (5, 5, 12)	-9.51	0.711	0.570
Σ33 (2, 2, 5)	-11.53	0.862	0.595

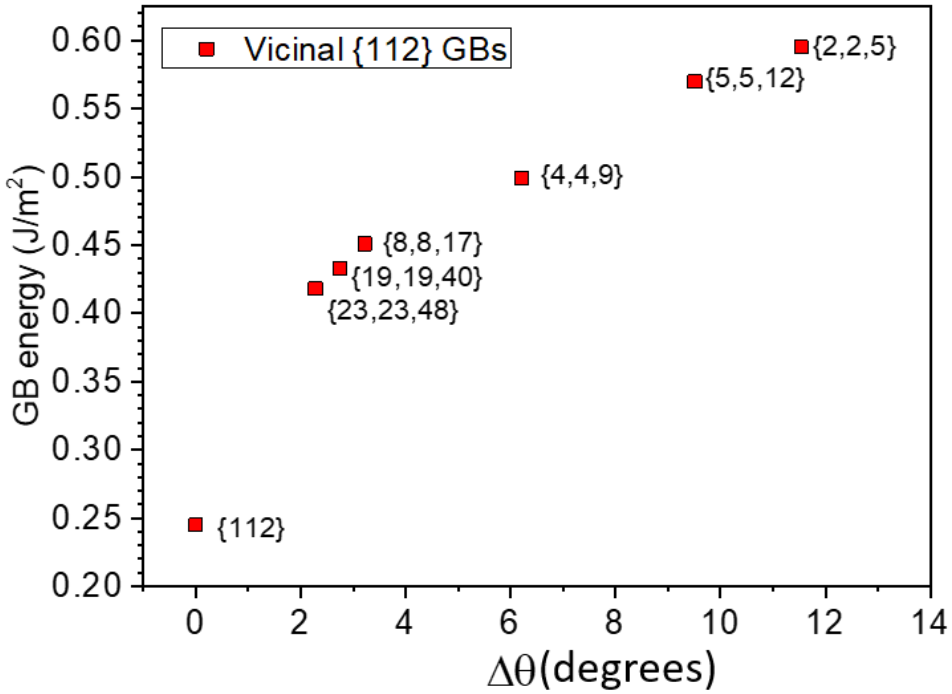

Figure 3.5: GB energy of the GBs vicinal to {112} as a function of increase of misorientation. The planes indicated with Miller indexes correspond to the GBs before relaxation into segments of {112} separated by GBDs.

In Fig. 3.4a we present the vicinal GB (19, 19, 40) corresponding to $\Delta\theta = -2.74°$. The distance between GBDs is $D = \frac{b_{1/-1}}{2sin\frac{\Delta\theta}{2}} = 20\frac{\sqrt{3}}{2}a_0$. Fig. 3.4b is a pressure map of the GB showing the regions of tension (blue) and compression (red) of the GBDs.

When the GB is under an applied shear stress, each of the GBDs acts as a source of dipoles of $\mathbf{b}_{1/1}$ disconnections and at each GBD the reaction occurs (see Fig. 3.4c) transforming the GBD into: $\mathbf{b}_{2/0} + \mathbf{b}_{-1/-1}$. The disconnection $\mathbf{b}_{-1/-1}$ runs towards the next $\mathbf{b}_{2/0}$ dislocation, that transforms back to $\mathbf{b}_{1/-1}$. As a result, the GB has moved two planes up and each GBD has moved along with the GB. All together is a conservative motion that occurs at a stress $\sigma_{xy} = 1.67$ GPa. The process reaches a steady state with drops of about 0.4 GPa for each displacement of the GB.

To check the efficiency of the mechanism under high strain rates we applied $\dot{\varepsilon} = 10^{10}s^{-1}$. We observed that some crystal dislocations may jump out the GB up to few lattice parameters (see Fig. 3.4d). At T = 0 K the process is unstable and they return to the GB (stable position), as it would happen with the dislocations that form a low angle GB, since the GB is the position of lowest energy for these GBDs.

The properties of the vicinal GBs described above are kept up to a distance between $\mathbf{b}_{1/-1}$ of about $5\frac{\sqrt{3}}{2}a_0$ that corresponds to $\Delta\theta = -11.536°$. In Fig. 3.6a we present the stress-strain curves for the vicinal GBs studied; the curve for the pristine {112} GB and the {112} GB after absorption of a crystal dislocation are included for comparison. We observe that the stress necessary to move any of the vicinal GBs under a shear-coupled migration up to $\Delta\theta = -6.22°$ is lower that the stress for the pristine GB. This is due to the presence of GBDs that act as sources of disconnections. For higher $\Delta\theta$ the number of GBDs demands a stress comparable to the pristine GB but the mechanism of creation of disconnection dipoles still applies.

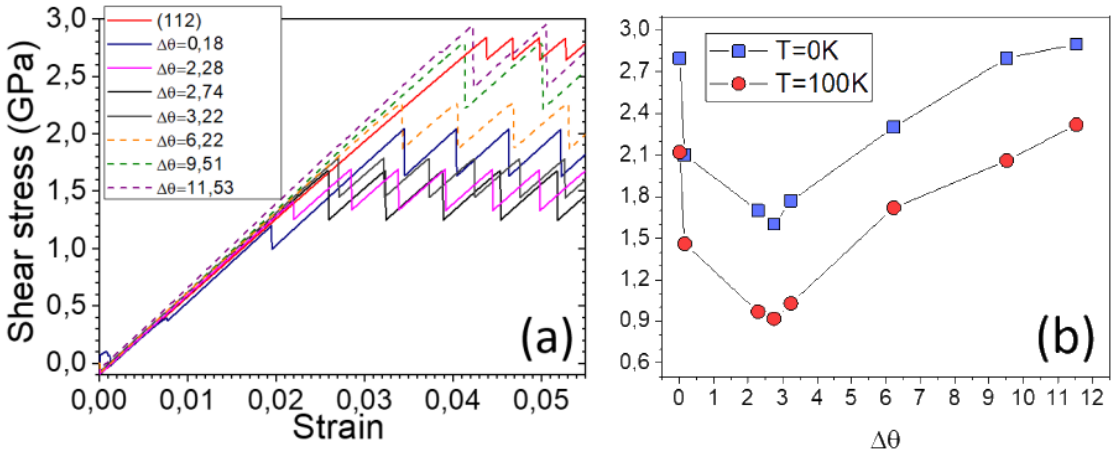

Figure 3.6: Shear stress applied to the {112} GB and its vicinal GBs. a) Strain-stress curves. b) Resolved shear stress versus increment of misorientation.

The critical resolved shear stress presented in Fig. 3.6b is decreasing for low increment of misorientation because there is an increase of sources of EDisc. The tendency is reversed when the distance between sources is small enough to have mutual interaction. As shown in Fig. 3.6b, the shear stress necessary to move the GB diminishes with temperature, but the dependency with the increase of misorientation angle is independent of the temperature, therefore the behavior is related to the distance between GBDs, namely the density of GBD that defines the vicinal GB. {112} GBs and the set of vicinal GBs show a high degree of simplicity: with only one type of EDisc the family of {112} tilt GBs is capable to perform efficiently SCGBM in a conservative way.

Thus, GBs vicinal to {112} GB can perform a shear-coupled GB migration more efficiently with lower stress in a fully conservative process. In Fig. 3.7 we present three examples of vicinal GBs. Fig. 3.7a&b present GBs with low and high GBD density, respectively. Fig. 3.7c&d capture two frames of the motion of a (5,5,12) GB under a strain rate of $\dot{\varepsilon} = 10^{10}s^{-1}$. There are two and four steps respectively corresponding to the disconnections running towards the right. In this case, the distribution of stresses is not uniform and not all sources are activated at the same time. Even in this extreme case, the process is fully conservative and the process at each GBD is as described above. This implies that the role of the $\mathbf{b}_{1/-1}$ GBD is important in the accommodation of plastic deformation of polycrystalline metals with bcc structure because it concerns the conservative growth of twins, the conservative displacement of {112} GBs and all its vicinal GBs.

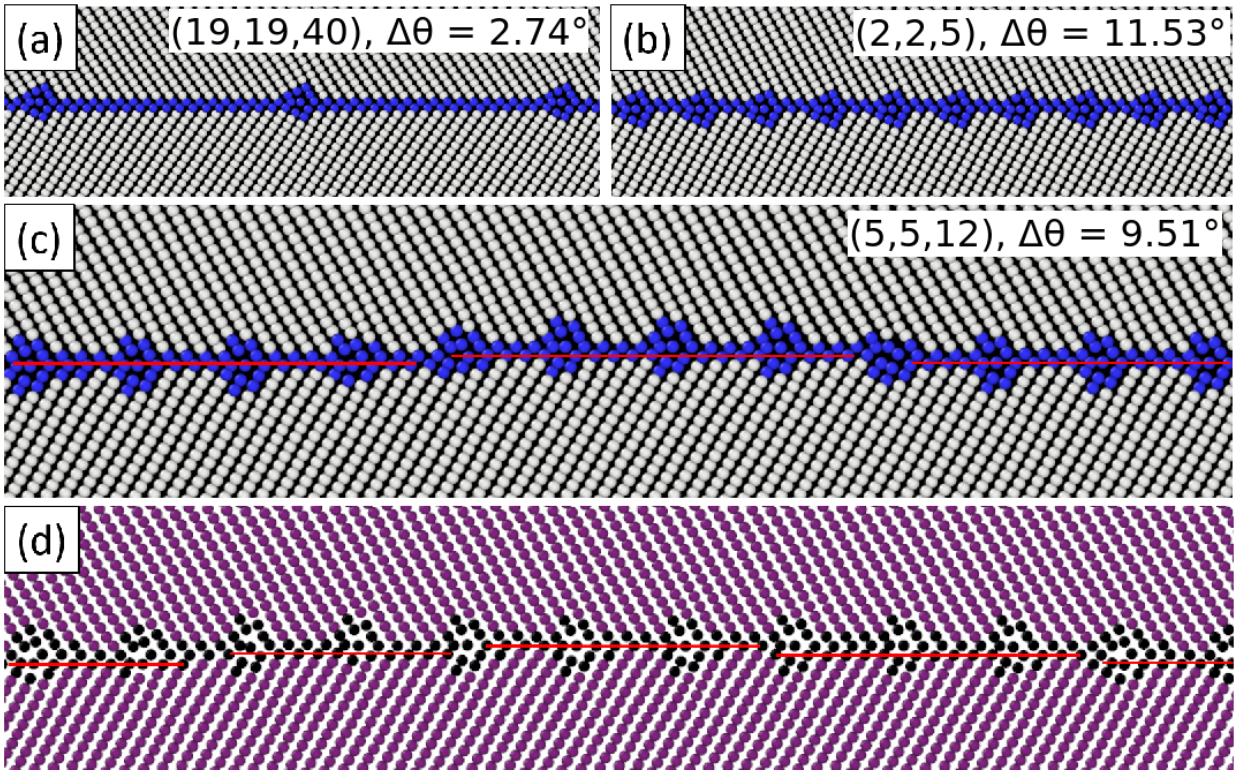

Figure 3.7: Vicinals to the {112} GB: a) (19,19,40) GB b) (2,2,5) GB c) & d) snapshots of (5,5,12) under high strain rate: inhomogeneous creation of disconnections.

3.2.2 GBs vicinal to {332}

The GBs vicinal to the {332} GB show an accommodation similar to the vicinals of {112}, with arrays of $\mathbf{b}_{1/-1}$ GBDs (shown in Fig. 3.1b) that accommodate the increment of misorientation. Fig. 3.8 show the family of possible vicinal GBs. However, there is a substantial difference: these GBDs are specific of the vicinal GBs, are not obtained as a result of the interaction with crystal dislocations, and they do not act as sources of EDisc. In fact, under shear stress, dipole pairs of EDisc are created in the segments of pristine {332} GB and run in the opposite directions towards the $\mathbf{b}_{1/-1}$ GBDs, as indicated in Fig. 3.9a.

Unlike the {112} vicinal, the migration mechanism of the {332} vicinal is temperature dependent: for T $<$ 50 K, the $\mathbf{b}_{1/-1}$ GBDs stop the glide of EDisc, leading to the formation of an array of {112} twins, as shown in Fig. 3.9b. For T $\geq$ 50 K the EDisc overcome the GBD and annihilate with the EDisc produced on the adjacent segments. Then, the GB is able to perform conservative migration as shown in Fig. 3.9d. The stress necessary for the migration diminishes with the temperature, as shown in Fig. 3.9c. Thus, for {332} tilt GBs and the set of vicinal GBs there are two different mechanisms to accommodate plastic deformation: either SCGBM or formation of {112} twins.

The results obtained for the twin modes underline the relevance of both, the production mechanisms of EDisc and the interaction of these EDisc with other GBDs present at the interface, which can activate alternative ways to accommodate plastic deformation.

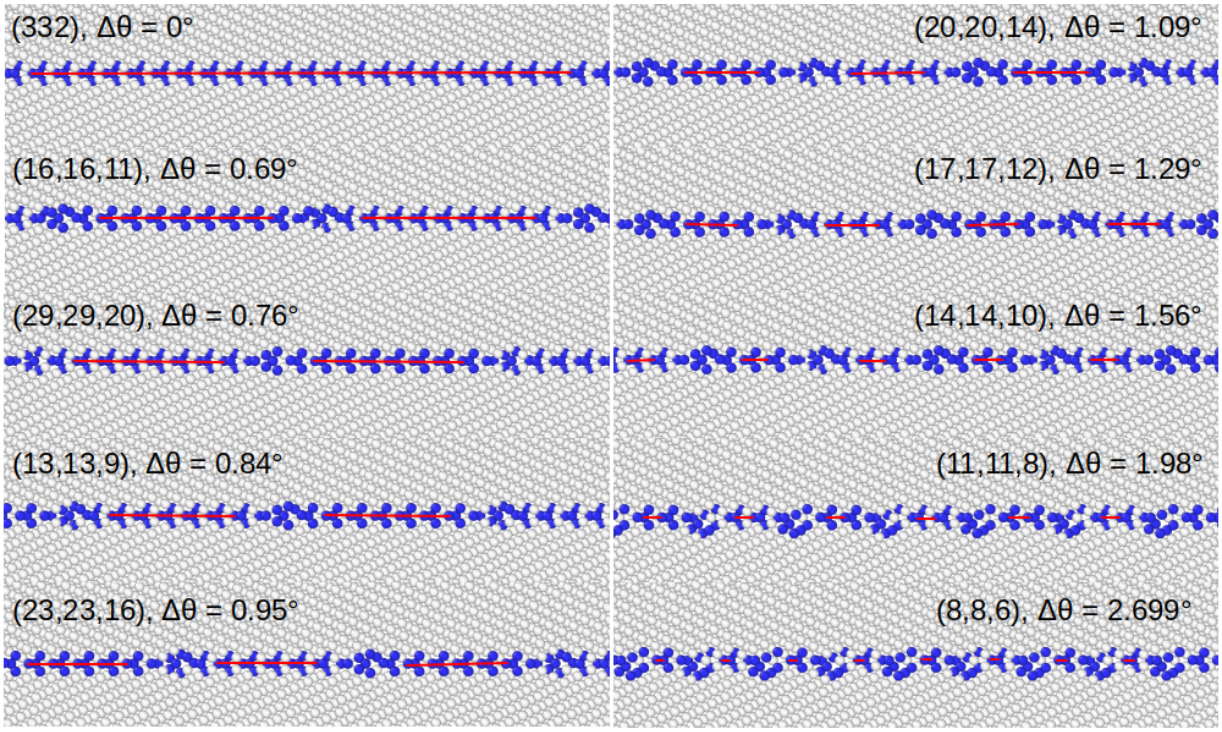

Figure 3.8: Snapshots showing the atomic structure of the investigated GBs vicinal to the {332} GB. The red lines indicate the location of the pristine {332} segments between the $\mathbf{b}_{1/-1}$ GBDs.

The {112} interface and its vicinal GBs always perform SCGBM because the Burgers vectors of the EDisc and GBD are perpendicular and the sum is a crystal dislocation. The reaction does not need atomic diffusion and the GBD, acting as a source of EDisc, follows the GB. On the contrary, for the {332} vicinal, the EDisc dipoles are generated in the pristine interface segments between GBDs, therefore bigger number of GBDs implies more dipoles to be created and therefore higher total stress to produce them. At $T < 50$ K, the EDisc cannot overcome the barrier created by the GBDs, which leads to the creation of twins (Fig. 3.9b). However, when the temperature is high enough to overcome the energy barrier the EDisc of opposite sign annihilate allowing SCGBM in a conservative way (Fig. 3.9d).

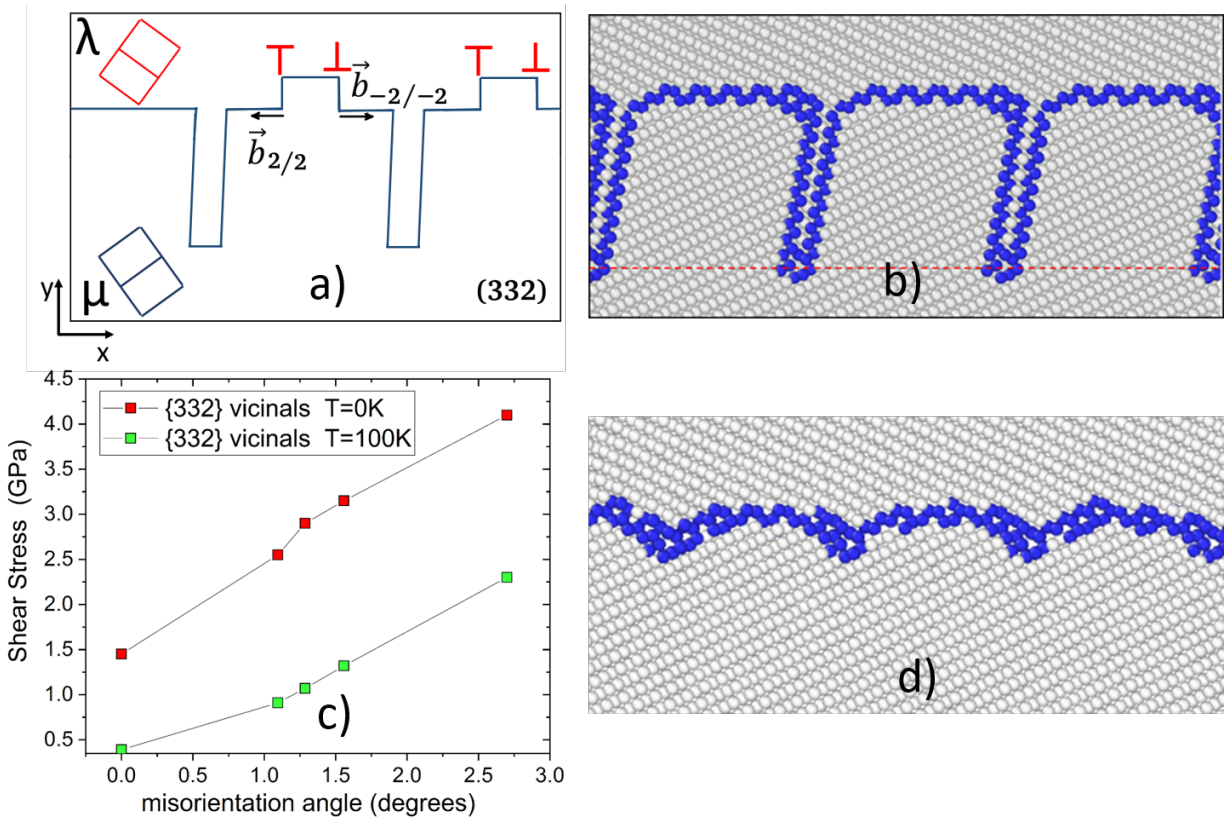

Figure 3.9: a) Schematic showing the SCGBM process by creation of EDisc dipoles at the pristine segments of the interface. b) & d) Snapshots of the (17,17,12) vicinal of the {332} GB, showing the creation of {112} twins at the $\mathbf{b}_{1/-1}$ GBD positions during the GB migration at T = 0 K and conservative migration at T = 100 K. The red line indicates the starting location of the GB. c) Shear stress necessary for the displacement of {332} GBs versus the increment of the misorientation angle.

3.3 Conclusion

The accommodation of plastic deformation by shear-coupled migration of symmetric tilt GBs in bcc metals is efficiently produced by the creation and glide of elementary disconnections, which description is summarized as follows.

The conservative displacement of {112} and {332} symmetric ⟨110⟩ tilt boundaries under shear stress is produced by the motion of EDisc that can be produced either in the pristine GB, as dipole pairs, or by GB dislocations acting as sources of disconnections.

The resolved shear stress of EDisc at the {112} interface is small (about 20 MPa in Fe) and there are no shuffles during glide. This compares with the resolved shear stress of EDisc in {332} interface ($\sim$ 550 - 620 MPa in Fe) that needs shuffling an atom at the core of the disconnection during glide to restore the crystal structure. These properties are applicable to the coherent interfaces of the {112} and {332} conjugate twins and they influence the existence of such twins. Whereas the {112} twin is the most abundant, the {332} twin only appears in some bcc alloys.

These two interfaces form cusps in the curve of the surface energy versus misorientation. Consequently, they can accommodate increments of misorientation up to 11.5 degrees in the {112} GB and 2.7 degrees in the {332} GB by introducing GBDs. The new GBs, named vicinal, are formed by pristine segments separated by GBDs. The {112} vicinal GBs perform shear-coupled GB migration by the glide of the EDisc. The interaction of the EDisc with the GBDs is a conservative climb. The EDisc gliding in {332} vicinal GBs need to overcome an energy barrier when encountering the GBD. To do so the temperature must be above 50 K. At lower temperature the EDisc pileup at the GBD creating {112} twins.

No EDisc are created at the {111} GB. Under local stress the GB reorient into new interfaces by the creation of pure steps through the shuffling of two atoms of the CSL unit cell. This GB is a strong barrier for the glide of crystal dislocations and does not perform shear-coupled GB migration.

Finally, the Σ19{116} GB presents more than one EDisc although only one of them is stable and contribute to the displacement of the GB. The level of stress needed to create the EDisc in this GB is much higher than in the {112} and {332} GBs. The other EDiscs are produced during the interaction of the GB with crystal dislocations. Although they show a very short lifetime, they seem to play the role of facilitators, allowing a more efficient way to couple plastic deformations by creating new interfacial defects and EDisc capable to sustain the displacement of the GB.

Now let us take a closer look to the interactions between each GB studied and both single crystal dislocations and dislocation pileups.

CHAPTER 4

INTERACTION OF ⟨110⟩ TILT GB WITH SINGLE ½⟨111⟩ DISLOCATIONS

As it has been stated in the Introduction Chapter, slip transfer plays an influential role in plastic deformation in polycrystalline materials. A full understanding of the phenomena related to slip transfer requires a detailed analysis at the atomic scale on the interactions between GBs and dislocations. For that reason, the first case considered for each GB has been the interaction of the interface with a single dislocation. The work presented here has been published in [57, 74, 113, 114].

4.1 {112} GB

As it is detailed in Section 3.1.1 the {112} GB shows many singular features among the ⟨110⟩ tilt GBs. One of these distinctive features is that only a very reduced set of GBDs appears to be involved in the reactions related to the slip transfer. In this Section we describe, in terms of dislocation reactions based in the theory of interfacial defects [37, 38, 40] a GBD acting as a source of disconnections. We also describe the role of this GBD on the interaction of a crystal dislocation with the {112} GB.

The interactions of the family of ½⟨111⟩ crystal dislocations with the {112} tilt GB in Fe are described in detail showing that they are related to the source of disconnections. In this Section we prove that the mechanism previously described for hcp and fcc metals occurs in bcc metals indicating that it is essentially controlled by the existence of the appropriate dislocation reactions at the GB expressed in terms of their Burgers vectors.

The admissible GBD for the {112} tilt GB can be identified easily using the dichromatic pattern associated to the interface, as shown in Fig. 4.1. Lattice sites of the two crystals are drawn as yellow (λ) and black (μ) in their tilt related orientations, with the sites of the {112} plane of the two crystals in coincidence. The unit cells of each crystal are superimposed in red (λ) and blue (μ) respectively. The unit cell of the λ crystal contains the two Bv of bulk dislocations ($\mathbf{b}_{2/0} = \frac{1}{2}[111]_\lambda$ and $\mathbf{b}_{1/0} = \frac{1}{2}[1\bar{1}1]_\lambda$), with edge and mixed character respectively, that interact with the GB. Fig. 4.1 shows five examples of possible Bv of disconnections ($\mathbf{b}_{1/1}$, $\mathbf{b}_{-1/-1}$, $\mathbf{b}^{\alpha}_{2/2}$, $\mathbf{b}^{\beta}_{2/2}$, $-\mathbf{b}^{\beta}_{2/2}$). In our simulations, only disconnections denoted $\mathbf{b}_{1/1}$ and $\mathbf{b}_{-1/-1}$ have been observed; $\mid \mathbf{b}_{\pm 1/\pm 1} \mid = \frac{\sqrt{3}}{6}a_0 =$ 0.827 Å. Thus, $\mathbf{b}_{1/1}$ disconnections are glissile, they have small Bv (1/3 of the Bv of the ½⟨111⟩ bulk dislocation) and a step high of one {112} interplanar distance, which means that no shuffles are required during glide [111].The resolved shear stress is around 20 MPa [64]. In terms of the topological theory of interfaces, the Bvs of the disconnections are related to the translations vectors of the λ and μ crystals as: $\mathbf{b}_{1/1} = \frac{1}{2}[1\bar{1}1]_\lambda - [010]_\mu$ and $\mathbf{b}_{-1/-1} = [010]_\lambda - \frac{1}{2}[1\bar{1}1]_\mu$. The disconnection denoted as $\mathbf{b}^{\alpha}_{2/2}$ is unstable and decomposes into two $\mathbf{b}_{1/1}$ that move apart. The disconnection denoted $\mathbf{b}^{\beta}_{2/2}$ is sessile. The GBD denoted as $\mathbf{b}_{1/-1}$ (encircled by blue dashed line in Fig. 4.1) is the outcome of the

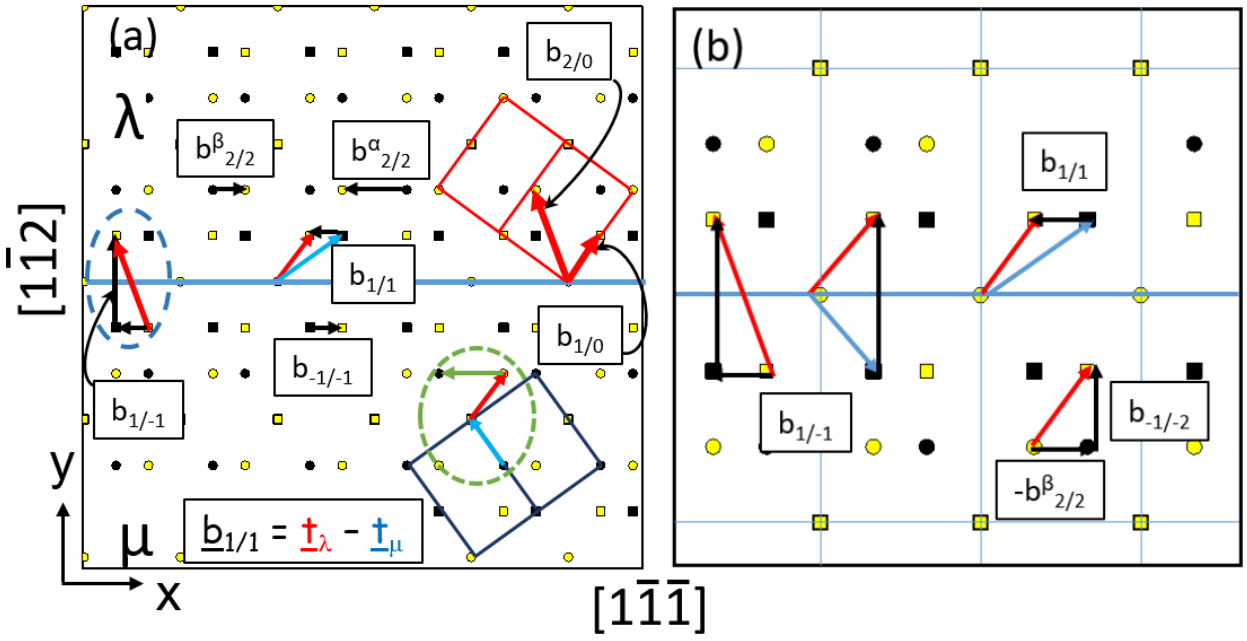

Figure 4.1: a) [110] projection of the dichromatic pattern associated with the {112} GB in Fe showing the Burgers vectors of the GB dislocations (black) and crystal dislocations (red and blue).b) From left to right: decomposition of the edge dislocation($\mathbf{b}_{2/0}$) into GBD and disconnection; GBD and disconnection expressed as difference of translation vectors of λ and μ crystals. Possible decomposition of the mixed dislocation ($\mathbf{b}_{1/0}$) into two GBDs

interaction with a single crystal edge dislocation. Since we describe essentially two GBD, hereafter the one that does not step the GB is denoted as 'GBD' ($\mathbf{b}_{1/-1}$) and the one that steps the GB is denoted as 'disconnection' ($\mathbf{b}_{1/1}$ and $\mathbf{b}_{-1/-1}$).

In the following subsections we are going to describe the atomic mechanisms involved on the interaction between the {112} GB and a single dislocation. We will focus specially on the effect in the GB displacement due to the presence of a GBD acting as a source of disconnections.

4.1.1 Interaction of the {112} GB with a ½⟨111⟩ crystal dislocation

The GB – dislocation interaction depends on the orientation and sense of the Burgers vector of the dislocation. The attraction/repulsion forces acting on the crystal dislocation are image forces ($F = \frac{\Delta E}{d}$) due to the increment of energy (ΔE) of the system when the dislocation is at a distance d of the GB [115]. The origin of ΔE is on the interaction of the stress field of the dislocation with the stress field of the GB. Fig. 4.2a&b show two edge dislocations, denoted as $\mathbf{b}_{-2/0} = \frac{1}{2}[1\bar{1}1]$ and $\mathbf{b}_{2/0} = \frac{1}{2}[\bar{1}1\bar{1}]$, located in the μ and λ crystals respectively, with dislocation lines along the tilt axis [110]. While $\mathbf{b}_{-2/0}$ is attracted and absorbed by the GB, the dislocation $\mathbf{b}_{2/0}$ is repelled by the GB. The shear stresses at Fig. 4.2 push the dislocation $\mathbf{b}_{-2/0}$ towards the GB. Reversing the stress would approach the dislocation $\mathbf{b}_{2/0}$ to the GB against the repulsion exerted by the GB.

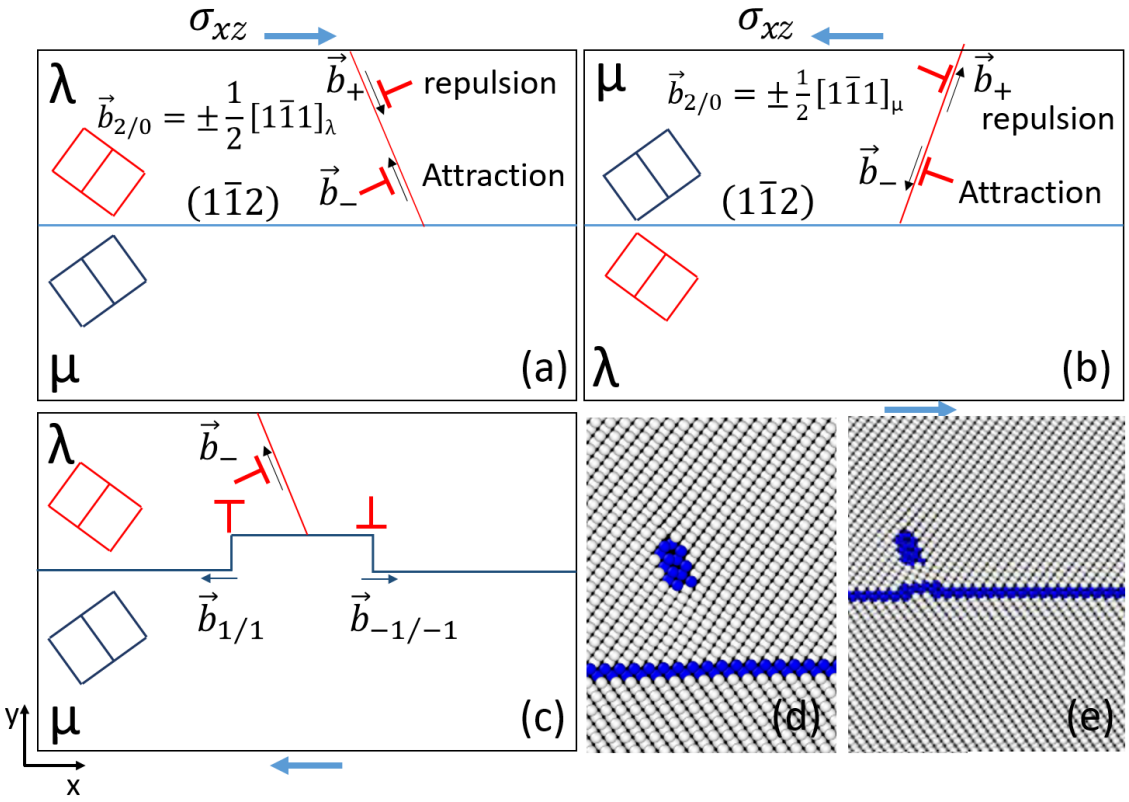

Figure 4.2: a) and b) Bicrystals showing the glide planes of crystal dislocations. The unit cell of each crystal is represented in red and blue respectively. In this work, crystal dislocations are located in the upper crystal. c) Interaction of the {112} GB with a crystal dislocation gliding in the λ crystal: when dislocation is close to the GB a disconnection dipole is created. d) Detail of the pristine GB with the crystal dislocation approaching it. e) Detail of the simulation showing the creation of the disconnection dipole.

4.1.1.1 Edge dislocation $\mathbf{b}_{2/0}$

Let us first consider the edge dislocation, $\mathbf{b}_{2/0}$, that approaches the GB under an applied shear stress (Fig. 4.2c). Initially the system contains a flat GB and a bulk dislocation approaching it. When $\mathbf{b}_{2/0}$ is about 1 nm from the GB, a disconnection dipole is created, as shown in Fig. 4.2c&e, that glides away and moves up the GB by one plane. Simultaneously, the dislocation is absorbed by the GB producing a drop of the shear stress $\Delta\sigma_{xy} = 0.15$ GPa. When the external shear stress reaches the value of $\sigma_{xy} = 2.0$ GPa the reactions described below occur which can be described as a two-steps process:

Step 1: $\mathbf{b}_{2/0}$ decomposes into a GBD that do not step the GB, $\mathbf{b}_{1/-1} = \frac{1}{3}[1\bar{1}2]_\lambda$, and a $\mathbf{b}_{1/1}$ disconnection according to the reaction shown in Fig. 4.3b:

$$\mathbf{b}_{2/0} = \mathbf{b}_{1/1} + \mathbf{b}_{1/-1} \tag{4.1}$$

The Burger circuits shown in Fig. 4.3a allowed identifying in the dichromatic pattern the disconnection $\mathbf{b}_{1/1}$ (red circuit) and $\mathbf{b}_{1/-1}$ (green circuit). This reaction is depicted on the left of Fig. 4.1, enclosed in a blue dashed line. The GBD $\mathbf{b}_{1/-1}$ has a Bv perpendicular to the GB and cannot move along the GB while the disconnection $\mathbf{b}_{1/1}$ glides to the left under the applied shear strain. As shown in Figs. 4.1 and 4.3b, their respective Bv are at 90° and the decomposition is energetically compatible with Frank's rule: $\mathbf{b}^2_{2/0} = \mathbf{b}^2_{1/1} + \mathbf{b}^2_{1/-1}$, which in terms of the magnitudes of Bv in units of lattice parameters reads: $(\frac{\sqrt{3}}{2})^2 = (\frac{\sqrt{6}}{3})^2 + (\frac{\sqrt{3}}{6})^2$. Actually, this reaction is reversible, as shown below.

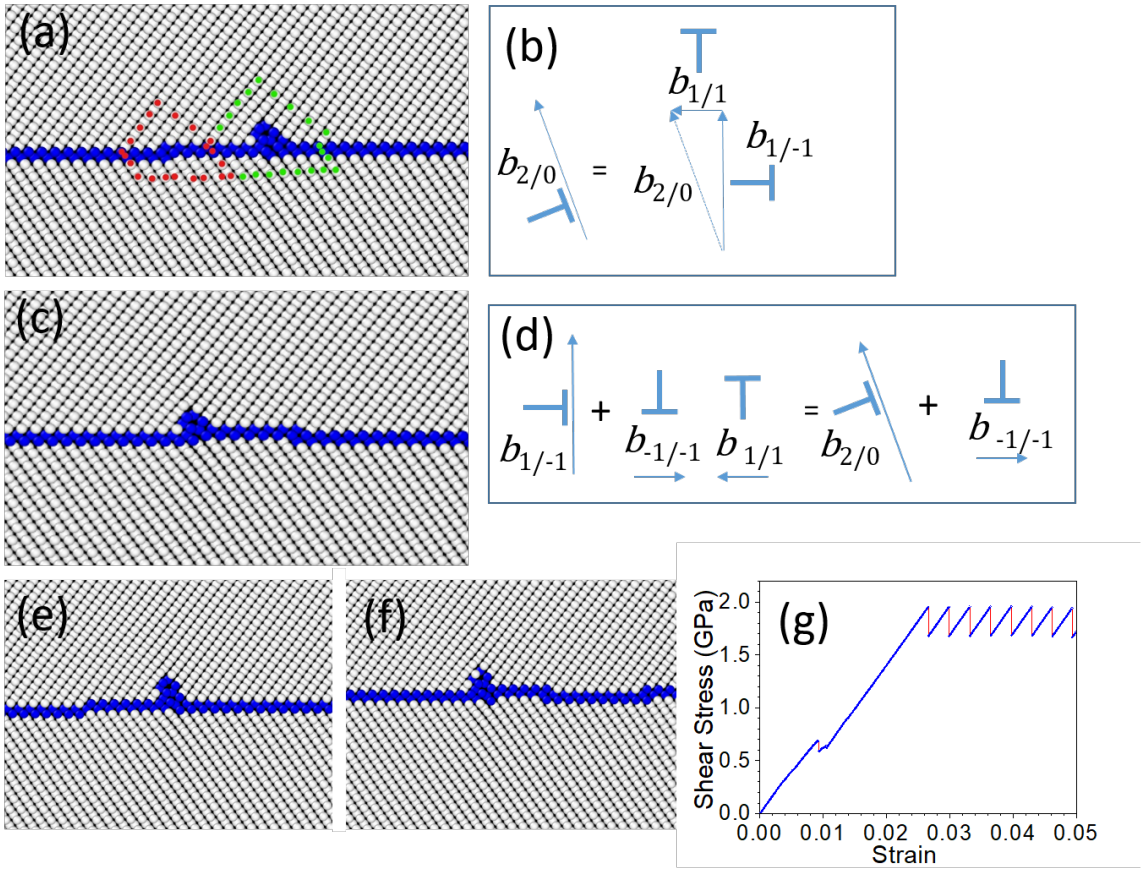

Figure 4.3: a) First decomposition of crystal dislocation into a disconnection (left) and a GB dislocation (right). Burgers circuits are indicated in red and green respectively. b) Analysis of the reaction shown in a. c), e), f) Emission of further disconnections: see steps at the GB. d) Analysis of the reaction shown in c. g) Stress-strain curve of the process.

Step 2: The sessile GBD $\mathbf{b}_{1/-1}$ acts as a stress concentrator that favors the creation of dipoles $\{\mathbf{b}_{1/1}; \mathbf{b}_{-1/-1}\}$ that follow the reaction shown in Fig. 4.3d:

$$(\mathbf{b}_{-1/-1} + \mathbf{b}_{1/1}) + \mathbf{b}_{1/-1} = \mathbf{b}_{2/0} + \mathbf{b}_{-1/-1}, \tag{4.2}$$

where $\mathbf{b}_{2/0}$ is created one plane above and the $\mathbf{b}_{-1/-1}$ runs away towards the right. Due to the length of the X direction, we can see the creation of the dipole before the first disconnection annihilates with one of the disconnections of the dipole, as shown in Fig. 4.3f. Altogether, the GB and the crystal dislocation, $\mathbf{b}_{2/0}$, have moved one plane up and the vicinity of $\mathbf{b}_{2/0}$ is identical as in step 1. In the simulation, due to the periodic boundary conditions, the disconnection dipoles coalesce. Fig. 4.3e shows the emission of a $\mathbf{b}_{1/1}$ (step 1) and Fig. 4.3f shows the emission of $\mathbf{b}_{-1/-1}$ (step 2), which is about to annihilate with the image of $\mathbf{b}_{1/1}$ that has re-entered into the system from the right. The stress strain curve shown in Fig. 4.3g indicates that the creation of disconnection dipoles, and hence the coupled shear-GB motion, is sustained once the threshold stress is reached. A drop of stress of about 0.25 GPa is produced each time a disconnection dipole is created and glides away. The first drop of stress shown in Fig. 4.3g at a strain 0.01 corresponds to the absorption of the crystal dislocation by the GB (reaction described in Eq. (4.1)).

The mechanism was studied by applying strain increments of 5.618×10^{-6} followed by relaxation of the system. A continuous production of disconnection dipoles at the dislocation core allowed the GB to move up along the Y direction and the dislocation itself moved together with the GB along its own glide plane.

4.1.1.2 Edge dislocation $\mathbf{b}_{-2/0}$

If the sense of the shear is reversed, the dislocation that moves towards the GB is $\mathbf{b}_{-2/0}$ and the created dipoles swap positions (see Fig. 3.2), then the displacement of the GB is reversed. When $\mathbf{b}_{-2/0}$ is at a distance of 4 nm from the GB, the repulsion between $\mathbf{b}_{-2/0}$ and the GB provokes a local concentration of stress in the region between the dislocation and the GB of 2.48 GPa and 2.30 GPa before and after the dipole is created, respectively. Thus, the dislocation is not absorbed, even it does not reach the GB, but it facilitates the conservative displacement of the GB downwards. In this case, the necessary external stress to trigger the GB motion is $\sigma_{xy} = 1.66$ GPa.

Therefore, a crystal edge dislocation acts as a source of disconnections that enhances the conservative motion of the GB. When the {112} GB is a coherent twin boundary, this mechanism produces either the growth or shrinkage of the twin.

4.1.1.3 Mixed dislocation $\mathbf{b}_{\pm 1/0}$

To complete our study, we have considered the case of a dislocation containing both edge and screw components, that is, with mixed character, which is denoted $\mathbf{b}_{1/0}$ in Fig. 4.1a. Its Burgers vector $\frac{1}{2}[1\bar{1}1]$ can be described as the sum of: $\frac{\sqrt{2}}{2}a_0$ (screw: along the tilt axis) + $0.5a_0$ (edge). The edge part, in turn, is formed by a component perpendicular to the GB and a component parallel to the GB that has a magnitude $\mid \mathbf{b}_{1/1} \mid$. Since the screw component is common to both crystals, a hypothetical transmission of the dislocation through the GB would need a transformation of the edge part as shown in the diagram of Fig. 4.1a (green dashed circle). This implies adding $2\mathbf{b}_{1/1}$ (green) disconnections. This reaction is not energetically favorable and, in fact, there is no transmission of the mixed dislocation through the GB. We checked it by performing several simulations of the interaction at T = 0 K and T = 600 K; in a pristine GB and in a GB with a source of disconnections. The dichromatic pattern in Fig. 4.1b presents another possible reaction at the GB of the mixed dislocation. This is the decomposition into a disconnection $\mathbf{b}_{-1/-2}$ stepping down the GB and a disconnection $\mathbf{b}^{\beta}_{2/2}$. This reaction does not occur either; this is because both disconnections are sessile and they cannot go apart. The GB attracts the mixed dislocation (of either sense) that is attached to the GB without changing its Bv. When a disconnection sweeps the GB and encounters the mixed dislocation, the lateral motion due to the pass of the disconnection corresponds to the continuous motion of the mixed dislocation in its glide plane [65]. As a result, the mixed dislocation moves along its own glide plane together with the GB in a conservative manner. In other words, the GB drags the dislocation.

4.1.2 Discussion

There is a third crystal dislocation with Burgers vector oriented along the X axis that can be understood as a GBD with modulus exactly 3 $\mid \mathbf{b}_{1/1} \mid$ that could glide along the GB. In fact, such a dislocation does not exist at the GB because it decomposes into three disconnections and a line defect of pure step character of three planes high. The decomposition is consistent with Frank rule and it follows the conservation of Bv and step height.

These results show that only one dislocation is needed to activate and enhance SCGBM which, in the case of TBs, can lead to twin growth or shrinkage. This mechanism, in opposition to the double cross slip proposed in [116] and the coalesce theory proposed in [117], does not require a continuous supply of crystal dislocations to maintain GB displacement or twin growth/shrinkage. The interaction occurs in the pristine interface, no other previous steps or disconnections are needed for the reaction to occur, as shown in Fig. 4.3. The fact that all the process is conservative, no shuffles are needed and it is triggered by a single dislocation, would explain the accommodation of plastic deformation by {112} twinning at high strain rates and low temperatures. This result proves that the most complex reaction presented in [62] is not necessary and would reduce the probability of the reaction. Moreover, the complementary zonal dislocation described as $\frac{1}{3}\langle 111\rangle$ in [62] is, in fact, a disconnection $\mathbf{b}_{2/2}$, therefore a perfect GBD.

4.2 {332} GB

In this Section, based on [74], we present, first, the GBDs created by the interaction of the {332} tilt GB with a crystal dislocation. Then, we describe, in terms of the crystallography involved, the stress-mediated atomic level processes at the GB that accommodates plastic deformation. These processes include the creation of elementary disconnections and their interaction with the existing GBDs that leads to the displacement of the GB and, in some cases, to the nucleation of a {112} twin.

{332}⟨110⟩ GB move conservatively under a shear stress by the creation and glide of disconnections. When crystal dislocations interact with the GB they are absorbed and transformed into GBDs. The behavior of GBDs under shear stress depends on the orientation of the Burgers vector and sense of shear stress. There are two possible scenarios: a) the GBD moves together with the GB in a compensated climb, then plastic deformation is accommodated by shear-coupled GB migration; b) the GBD is sessile because it cannot undergo a compensated climb when interacting with the disconnections. If so, the sessile GBD is the nucleus of a {112} twin. The nucleation of the twin is produced by the pileup of disconnections at both sides of the GBD. Then, plastic deformation is accommodated by the combination of the motion of the {332} GB and the growth of {112} twins inside the grain.

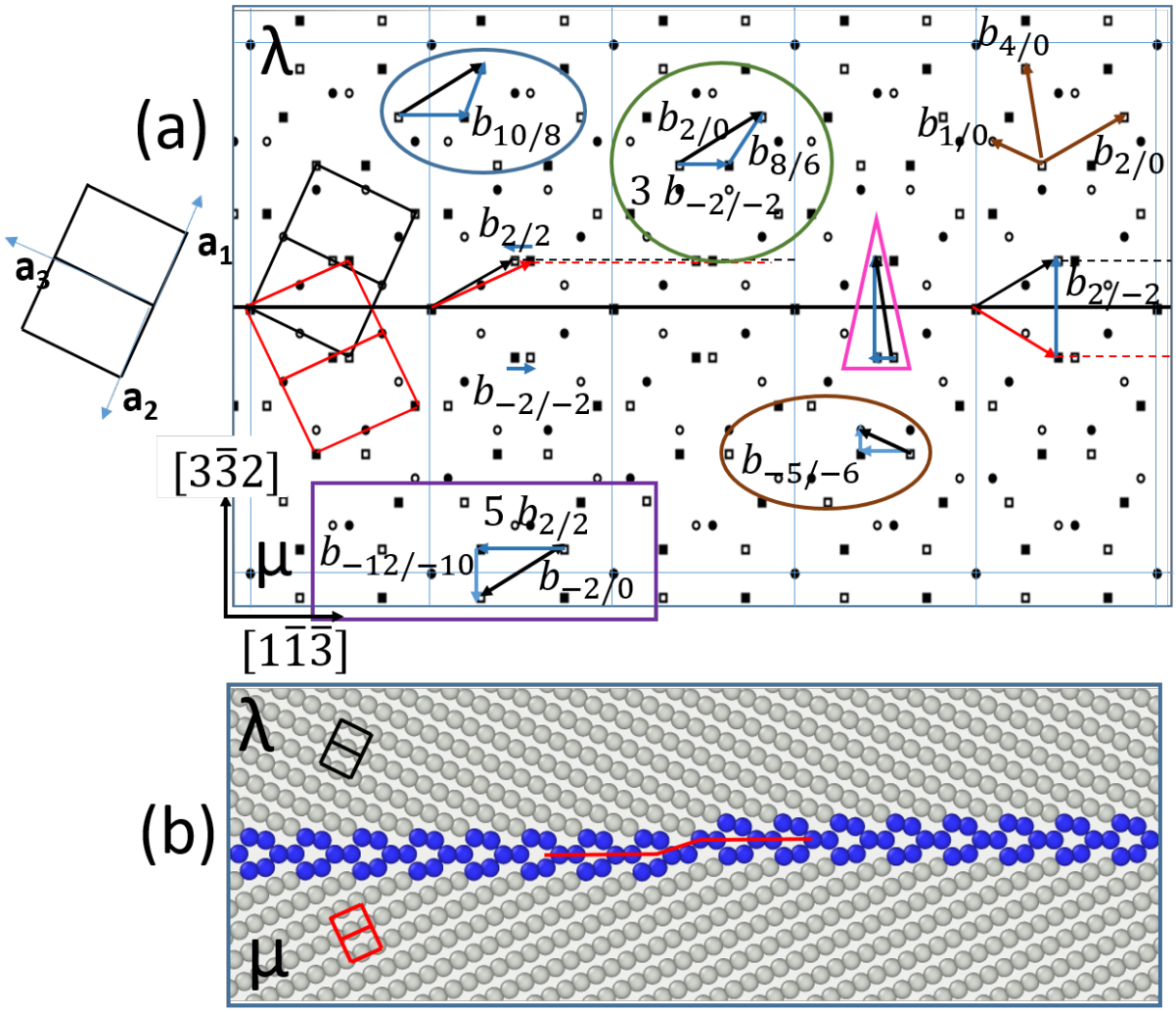

Figure 4.4: a) [110] projection of the dichromatic pattern of the {332} GB showing the Burgers vectors of the EDiscs ($\mathbf{b}_{2/2}$), the crystal dislocations ($\mathbf{b}_{n/0}$) interacting with the GB and few reactions showing GBDs (see text). The CSL is indicated in pale blue. The unit cell of λ crystal shows the principal axes a_i. b) [110] projection of the {332} GB with a $\mathbf{b}_{2/2}$ disconnection stepping up the GB. The unit cells of crystals are represented in black (λ) and red (μ).

Fig. 4.4a shows the dichromatic pattern of the GB in projection along the tilt axis [110]. The dislocations of the λ (white crystal) that interact with the GB (brown vectors on the top right) are named as $\mathbf{b}_{2/0} = \frac{1}{2}[1\bar{1}\bar{1}]$ (edge), $\mathbf{b}_{4/0} = \frac{1}{2}[1\bar{1}1]$ (edge) and $\mathbf{b}_{1/0} = \frac{1}{2}[111]$ (mixed). The EDisc, $\mathbf{b}_{2/2}$, is the difference between the translation vector of the λ crystal (black arrow) and the μ crystal (red arrow) as: $\mathbf{b}_{2/2} = \frac{1}{2}[1\bar{1}\bar{1}]_\lambda - [00\bar{1}]_\mu = \frac{1}{22}[\bar{1}13]_\lambda$ [75]. The dotted lines indicate the position of the GB on the right of the core of the disconnection showing that it steps up the GB by two {332} planes. Thus, when the disconnection glides to the left it transforms λ crystal to μ crystal and the GB moves two planes upwards. Notice that the shear imposed by the Bv of the disconnection moves black squares into white squares but the sites below represented by circles must do an extra displacement (shuffle) to restore the perfect μ lattice [63]. Fig. 4.4b shows the relaxed {332} GB containing a $\mathbf{b}_{2/2}$ disconnection (the red line is a guide for the eye).

In the following, we describe, in subsection 4.2.1, the transformation of crystal dislocations at the GB that are represented in the dichromatic pattern (DP) as sum of vectors within a circle, ellipsoid, rectangle and triangle respectively. For each GBD obtained, the response of the faceted GB to an external shear stress is described in subsection 4.2.2.

4.2.1 Interaction of the {332} GB with a ½⟨111⟩ dislocation

The results of our simulations show that crystal dislocations with Bv ½⟨111⟩ are fully absorbed by the GB. The reaction and final defects at the GB depend on the orientation of the glide plane, the sign of the Bv and the edge or mixed character of the dislocation, considering that in the simulations the dislocation line is always along the [110] tilt axis of the GB. The interaction follows the conservation of Bv and, in all interactions, the dislocation transforms into a GBD with a riser, faceting the GB, and several EDisc that glide away ($\vec{b}_{Xtal} = \vec{b}_{GBD} + n\vec{b}_{EDisc}$). For a given interaction, the number of EDisc has shown to be dependent on the temperature.

4.2.1.1 Edge dislocation $\mathbf{b}_{\pm 2/0}$ (glide plane at 29.5°)

Fig. 4.5 shows the GB after the interaction with edge dislocations inclined 29.5°. Comparing Fig. 4.5a and Figs. 4.5b&c we can observe that the reaction depends on the sign of the entrant dislocation.

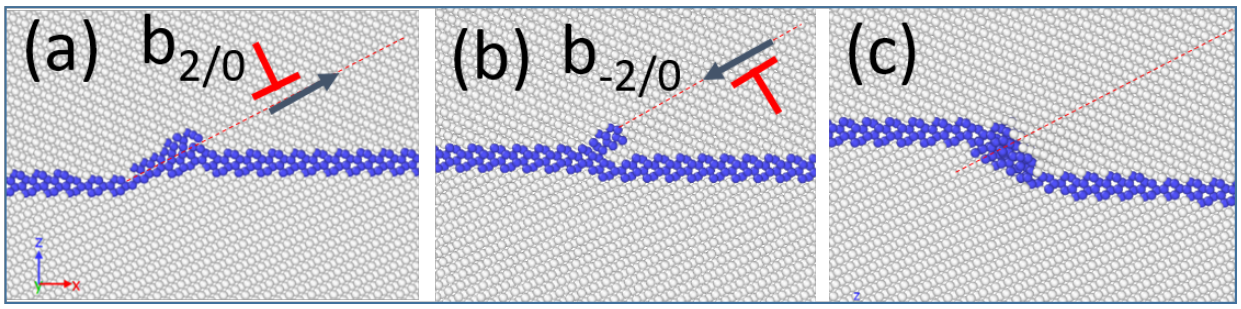

Figure 4.5: Interaction of the {332} GB with an edge dislocation (red symbol) at T = 0 K. a) Dislocation Bv forming an acute angle ($\mathbf{b}_{2/0}$): The riser of the GBD is along the glide plane. b) & c) Dislocation Bv forming an obtuse angle ($\mathbf{b}_{-2/0}$); there is an initial repulsion; the dislocation is absorbed if enough stress is applied: (b) before absorption and (c) after absorption; the riser of the GBD is inclined to the glide plane shown as a dashed red line.

Interaction with $\mathbf{b}_{2/0}$. When the Bv forms an acute angle with the GB (Fig. 4.5a) and the dislocation is at a distance of about three lattice parameters, the GB attracts the dislocation and absorbs it. The dislocation transforms into a GBD with a riser, as shown in Fig. 4.5a, and several EDisc that glide away. The riser of the GBD is along the glide plane of the dislocation forming a facet $\{112\}_\lambda/\{110\}_\mu$.

The Bv of the GBD depends on the number of EDisc emitted, which may be three or four depending on the temperature and the local stress. The reactions are:

$$\mathbf{b}_{2/0} = \frac{1}{2}[1\bar{1}\bar{1}] = \frac{1}{11}[4\bar{4}\bar{1}] + 3\frac{1}{22}[1\bar{1}\bar{3}] = \mathbf{b}_{8/6} + 3\mathbf{b}_{-2/-2}. \tag{4.3}$$

$$\mathbf{b}_{2/0} = \frac{1}{2}[1\bar{1}\bar{1}] = \frac{1}{22}[7\bar{7}1] + 4\frac{1}{22}[1\bar{1}\bar{3}] = \mathbf{b}_{10/8} + 4\mathbf{b}_{-2/-2}. \tag{4.4}$$

The reaction (4.3) occurs in a static simulation (T = 0 K) with relaxation after each strain increment. The reaction (4.4) occurs in a dynamic simulation at T = 300 K reported in [75]. The dependence on the local stress is evidenced when the incident dislocation is the first of a pileup of dislocations, as shown in [75].

The reactions (4.3) and (4.4) are represented in the DP of Fig. 4.4a. In the green circle the Bv of the crystal dislocation $\mathbf{b}_{2/0}$ (black) is decomposed into the Bv of the GBD, $\mathbf{b}_{8/6}$, and three $\mathbf{b}_{-2/-2}$ EDisc (blue). The riser of the GBD (Fig. 4.5a) intersect eight planes of the λ crystal and six planes of the μ crystal. The reaction (4.4) is represented inside the blue ellipsoid at the top-left of the DP. The location in the DP of the Bvs of the GBDs indicates the step height of the riser. These two GBDs have the same behavior under deformation. In fact, one transforms into the other by emitting/adding a $\mathbf{b}_{-2/-2}$ disconnection.

Interaction with $\mathbf{b}_{-2/0}$. When the Bv forms an obtuse angle with the GB (Fig. 4.5b), there is an initial repulsion between the dislocation and the GB. If an external stress is applied, the dislocation overcomes the repulsion and it is linked to the GB but it does not change its Bv. When the shear stress is about 1.3 GPa, then there is absorption of the dislocation. The reaction produces a GBD with riser and several EDisc but there is a main difference with $\mathbf{b}_{2/0}$: the riser of the GBD forms an angle of 126 degrees to the glide plane of the dislocation forming a facet $\{110\}_\lambda/\{112\}_\mu$ (see Fig. 4.5c). The number of EDisc is temperature dependent and varies from five (T ≤ 150 K) to seven (at T = 900 K). The reaction at 150 K is marked in the DP of Fig. 4.4a with a purple rectangle:

$$\mathbf{b}_{-2/0} = \frac{1}{2}[\bar{1}11] = \frac{1}{11}[\bar{3}3\bar{2}] + 5\frac{1}{22}[\bar{1}13] = \mathbf{b}_{-12/-10} + 5\mathbf{b}_{2/2}. \tag{4.5}$$

The Bvs of the GBDs are calculated by Volterra operations, as the difference of two translation vectors from the upper and lower crystals respectively obtained from a Burgers circuit (as detailed in Chapter General Concepts and in [42]). The Bv is double-checked by calculating the Bv as the difference of the initial crystal dislocation and the produced EDiscs.

4.2.1.2 Edge dislocation $\mathbf{b}_{\pm 4/0}$ (glide plane at 100°)

The crystal dislocations gliding on plane at 100° are denoted $\mathbf{b}_{4/0}$ and $\mathbf{b}_{-4/0}$, respectively.

Interaction with $\mathbf{b}_{4/0}$. There is attraction and absorption by the GB of the $\mathbf{b}_{4/0}$ dislocation. The reaction is presented in the DP of Fig. 4.4a inside a pink triangle:

$$\mathbf{b}_{4/0} = \frac{1}{2}[1\bar{1}1] = \frac{2}{11}[3\bar{3}2] + \frac{1}{22}[\bar{1}13] = \mathbf{b}_{2/-2} + \mathbf{b}_{2/2}. \tag{4.6}$$

The Bv of the GBD is presented on the right of the DP as the difference of two translation vectors $t_\lambda = \frac{1}{2}[1\bar{1}\bar{1}]_\lambda$ (black) and $t_\mu = \frac{1}{2}[1\bar{1}\bar{1}]_\mu$ (red). Apart from the $\mathbf{b}_{2/-2}$, another GBD with a Bv perpendicular to the GB interface has been observed, namely $\mathbf{b}_{1/-1}$ related to the GBs vicinal to the {332}. The GBD could be imagined as cutting the λ crystal along the black dotted line and the μ crystal along the red dotted line. After joining the two crystals the generated GBD does not step the GB. Under relaxation, the core of the $\mathbf{b}_{2/-2}$ GBD is decomposed into two GBDs, each of them with a facet, as shown in Fig. 4.6.

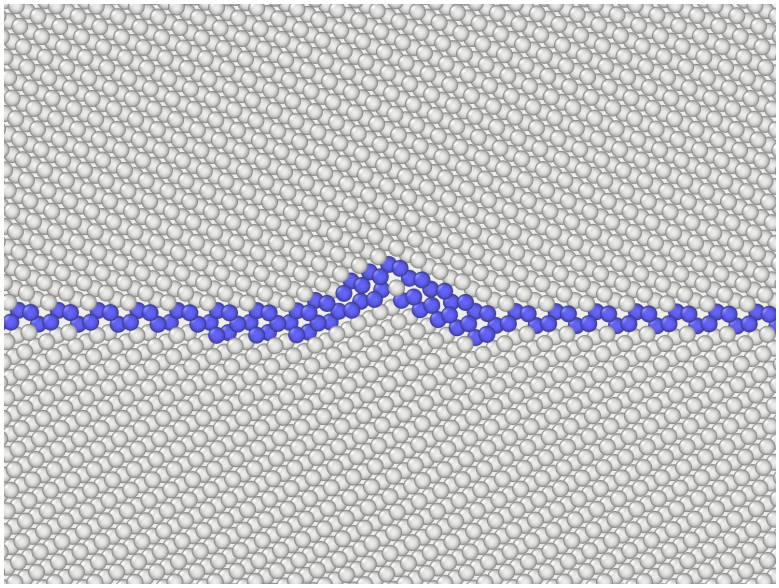

Figure 4.6: Core of the $\mathbf{b}_{2/-2}$ GBD split into $\mathbf{b}_{12/10} + \mathbf{b}_{-10/12}$.

The reaction is as follows:

$$\mathbf{b}_{2/-2} = \mathbf{b}_{12/10} + \mathbf{b}_{-10/12} = \frac{1}{11}[3\bar{3}2] + \frac{1}{11}[3\bar{3}2] = \frac{2}{11}[3\bar{3}2]. \tag{4.7}$$

Interaction with $\mathbf{b}_{-4/0}$. The crystal dislocation with opposite Bv, i.e., $\mathbf{b}_{-4/0} = \frac{1}{2}[\bar{1}1\bar{1}]$, does not transform into the $\mathbf{b}_{-2/2}$ GBD. Indeed, there is repulsion of the $\mathbf{b}_{-4/0}$ dislocation by the GB. The dislocation overcomes the repulsion if a shear stress of 1.3 GPa is applied. Then, the dislocation stays attached to the GB but it keeps its Bv.

4.2.1.3 Mixed dislocations $\mathbf{b}_{\pm 1/0}$ (glide plane at 154.8°)

Interaction with $\mathbf{b}_{1/0}$. The mixed dislocation $\mathbf{b}_{1/0} = \frac{1}{2}[111]$ gliding along the $(1\bar{1}0)$ plane inclined at 154.8° interacts with the GB under a shear stress of about 500 MPa. Since the screw part $(\frac{1}{2}[110]_\lambda)$ is along the tilt axis, it is common to both, the crystal dislocation and the GBD created by the interaction. The reaction produced emits three EDisc $\mathbf{b}_{2/2}$ that run away and a GBD with a riser along the glide plane of the dislocation forming a facet $(1\bar{1}0)_\lambda/(1\bar{1}2)_\mu$. The reaction is plotted in the DP of Fig. 4.4a inside a brown ellipsoid below the interface.

$$\mathbf{b}_{1/0} = \frac{1}{2}[001] + \frac{1}{2}[110] = \frac{1}{22}[3\bar{3}2] + \frac{1}{2}[110] + \frac{3}{22}[\bar{1}13] = \mathbf{b}_{-5/-6} + 3\mathbf{b}_{2/2}. \tag{4.8}$$

Interaction with $\mathbf{b}_{-1/0}$. The reaction with the dislocation of opposite sign $\mathbf{b}_{-1/0}$ occurs at about 600 MPa and the GBD produced has a riser inclined to the glide plane with a facet $(1\bar{1}2)_\lambda/(1\bar{1}0)_\mu$.

$$\mathbf{b}_{-1/0} = \frac{1}{2}[00\bar{1}] + \frac{1}{2}[\bar{1}\bar{1}0] = \frac{1}{22}[\bar{2}2\bar{5}] + \frac{1}{2}[\bar{1}\bar{1}0] + \frac{2}{22}[1\bar{1}\bar{3}] = \mathbf{b}_{3/4} + 2\mathbf{b}_{-2/-2}. \tag{4.9}$$

Notice that the orientation of risers relative to the glide plane (see Fig. 4.11 in Section 4.2.2.3) is comparable to the ones of the GBDs produced by the dislocations $\mathbf{b}_{2/0}$ and $\mathbf{b}_{-2/0}$. The orientation of the risers determines the stress necessary for the accommodation of a pileup of dislocations approaching from the same glide plane [75].

4.2.2 Displacement of the {332} GB under an applied shear stress

Dipoles of disconnections are created at shear stress of $\sigma_{xz} = 1.45$ GPa at T = 0 K in the case of the pristine {332} interface. If a stress concentrator exists in the GB, the stress necessary to create the

dipole of disconnections is smaller [57]. For instance, a GBD may act as a source of disconnections. If the GBD can follow the GB during its displacement, then the source is effective and a sustained SCGBM occurs. This is found in the {112}⟨110⟩ tilt GB [57], but in the {332}⟨110⟩ tilt GB, not all GBD can follow the GB; an example of sustained motion of the GBD $\mathbf{b}_{8/6}$ is shown in Fig. 4.7. As described in Section 4.2.1, there is a variety of GBDs present at the {332} GB depending on the characteristics of the crystal dislocation interacting with the GB. The interaction of a GBD with the glissile EDiscs, when a shear stress is applied, depends on the GBD and the sense of the shear stress.

In the following, we describe the effect of an external shear stress on the displacement of the GB containing different GBDs. Initially, the GBD is created as an outcome of the reaction with the crystal dislocation. Then, a shear stress is applied to the system containing the GB with the stable GBD. To study the displacements upwards and downwards of the GB, two senses of the shear stress are applied for each GBD.

4.2.2.1 GBDs $\mathbf{b}_{8/6}$ and $\mathbf{b}_{10/8}$ (glide plane at 29.5°)

The crystal dislocation $\mathbf{b}_{2/0}$, attracted by the GB, originates a GBD (either $\mathbf{b}_{8/6}$ or $\mathbf{b}_{10/8}$ as described above). When a shear stress is applied, the GBD acts as a source of pairs of $\mathbf{b}_{2/2}$ EDisc of opposite sign that glide along the GB allowing its displacement, as shown in Fig. 4.7. The mechanism, originally described in [53, 65, 66] for the $\{10\bar{1}2\}$ twin in hcp metals, occurs in bcc metals for certain tilt GBs such as the {112} twin [56, 57] and its conjugate, the {332} twin, as described in [75]. The scheme in Fig. 4.7a indicates that, while the GB moves, the riser is displaced along the glide plane of the $\mathbf{b}_{2/0}$ (red dotted line). Fig. 4.7a shows in detail the displacement downwards of the riser due to the creation of $\mathbf{b}_{2/2}$ that expand outwards and allow the boundary to migrate. If the stress is reversed the same mechanism operates (exchanging the sign of the $\mathbf{b}_{2/2}$ disconnections) and the GB is displaced upwards (Fig. 4.7b). Thus, the GBD produced by the $\mathbf{b}_{2/0}$ facilitates the shear-coupled GB migration.

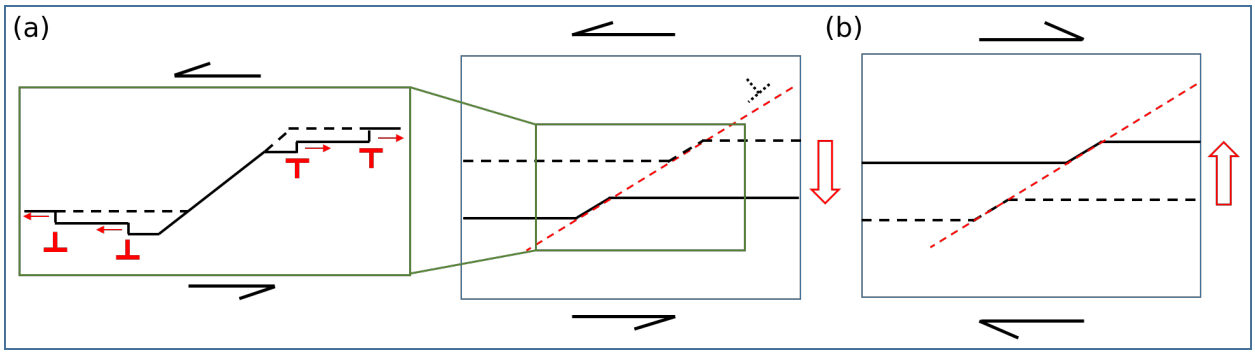

Figure 4.7: Displacement of the GB with the $\mathbf{b}_{8/6}$ GBD. The big red arrows indicate the direction of motion of the GB. Black arrows indicate the sense of shear stress. The red dotted line indicates the glide plane of the $\mathbf{b}_{2/0}$ dislocation; notice that the riser of the GBD is displaced along this plane downwards on a) and upwards on b). (Green rectangle) Detail of the $\mathbf{b}_{8/6}$ defect in the {332} GB acting as source of $\mathbf{b}_{2/2}$ EDisc. A snapshot of $\mathbf{b}_{8/6}$ is shown in Fig. 4.5a.

4.2.2.2 GBD $\mathbf{b}_{-12/-10}$ (glide plane at 29.5°)

The crystal dislocation $\mathbf{b}_{-2/0}$ under stress reacts with the GB forming the GBD $\mathbf{b}_{-12/-10}$; its riser gradually orients along the $[1\bar{1}0]_\lambda$ plane. The interaction of this GBD with the $\mathbf{b}_{2/2}$ EDisc differs from the interaction with the $\mathbf{b}_{-2/-2}$; as a consequence, the displacement of the GB under shear stress depends on the sense of the shear, as shown schematically in Figs. 4.8&4.9.

Under positive shear stress, $\mathbf{b}_{-2/-2}$ glides to the right (at 550 MPa) and $\mathbf{b}_{2/2}$ glides to the left (at 620 MPa). Therefore, $\mathbf{b}_{-2/-2}$ approaches the GBD from its left side and $\mathbf{b}_{2/2}$ approaches the GBD from its right side. In both cases, there is no compensated climb.

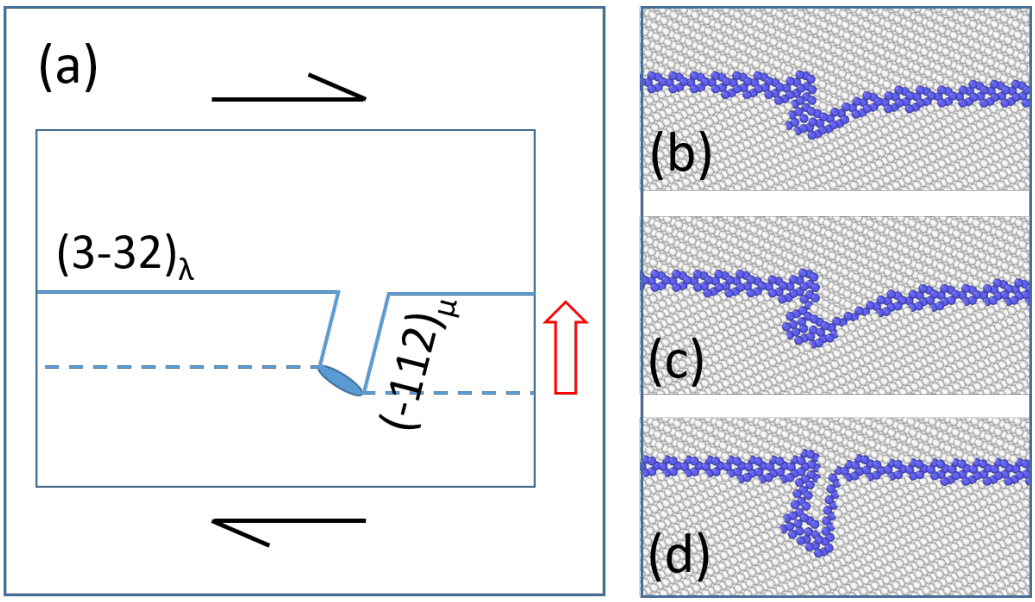

Figure 4.8: a) Displacement of the GB with the $\mathbf{b}_{-12/-10}$ disconnection and nucleation of the {112} twin. The red arrow indicates the direction of motion of the GB under the shear stress. Black arrows indicate the sense of shear stress. b-d) Snapshots showing the formation of the {112} twin from the GBD.

The EDiscs $\mathbf{b}_{-2/-2}$ are stopped by the GBD and pileup at the left side of the GBD whereas $\mathbf{b}_{2/2}$ pileup at the right side forming a facet $\{112\}_\lambda/\{110\}_\mu$, as shown in Fig. 4.8b. When the facet is large enough it becomes unstable and transforms into a symmetric {112} facet forming the embryo of a {112} twin shown in Fig. 4.8c.

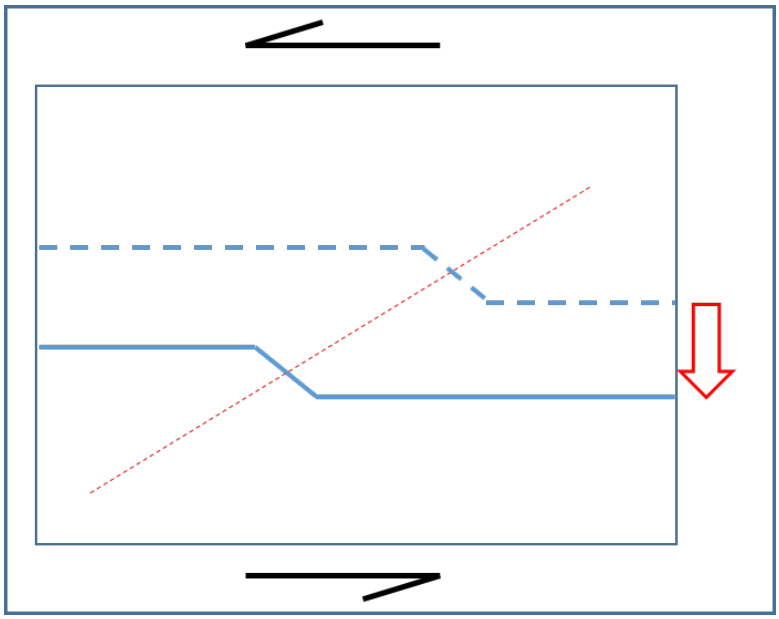

Figure 4.9: Displacement of the GB with the $\mathbf{b}_{-12/-10}$ disconnection under a negative shear. The red dotted line indicates the glide plane of the incident $\mathbf{b}_{-2/0}$ dislocation, notice that the riser of the disconnection is displaced along this plane. A snapshot of $\mathbf{b}_{-12/-10}$ is shown in Fig. 4.5c.

When a negative shear stress is applied to the GB with a $\mathbf{b}_{-12/-10}$ GBD, $\mathbf{b}_{2/2}$ EDiscs glide from the left side; when five of them pileup on the GBD, the reaction (4.5) in Section 4.2.1.1 is produced. Notice that the reaction is energetically feasible in both senses since the Bvs form a right triangle (see

purple rectangle Fig. 4.4). The initial crystal dislocation is recovered and can glide along its own glide plane releasing stress, as shown in Fig. 4.9; when relaxing to the new equilibrium, the reaction (4.5) is repeated and five EDiscs are emitted that continue gliding to the right. The same mechanism is found in the interaction of the {112} GB with a crystal dislocation, as presented in Section 4.1.1, although in that case only one disconnection is needed for the reaction to occur.

4.2.2.3 GBDs $\mathbf{b}_{12/10}$ and $\mathbf{b}_{-12/-10}$ (glide plane at 100°)

In the case of $\mathbf{b}_{4/0}$, the GBD is decomposed into two adjacent GBDs, i.e., $\mathbf{b}_{12/10}$+$\mathbf{b}_{-10/-12}$, with risers differently oriented, as shown in Fig. 4.10a. This fact impedes that these risers can move upwards and determines the behavior of the GB under a positive shear stress.

Thus, under positive shear stress, the interaction of the EDisc with the GBD would be as follows: $\mathbf{b}_{-2/-2}$ can interact with the GBD approaching from its left side and $\mathbf{b}_{2/2}$ can interact approaching the GBD from its right side (Fig. 4.10b). These EDisc move the GB upwards by two planes and return the GBD back to $\mathbf{b}_{2/-2}$. The following process of GB displacement is like for the GBD $\mathbf{b}_{-12/-10}$ described in Section 4.2.2.2 and the same {112} twin embryo is formed as shown in Fig. 4.10c&d, although the dislocation content at the tip of the twin is different in each case. The sustained growth of the twin is produced at a shear stress of 1.15 GPa.

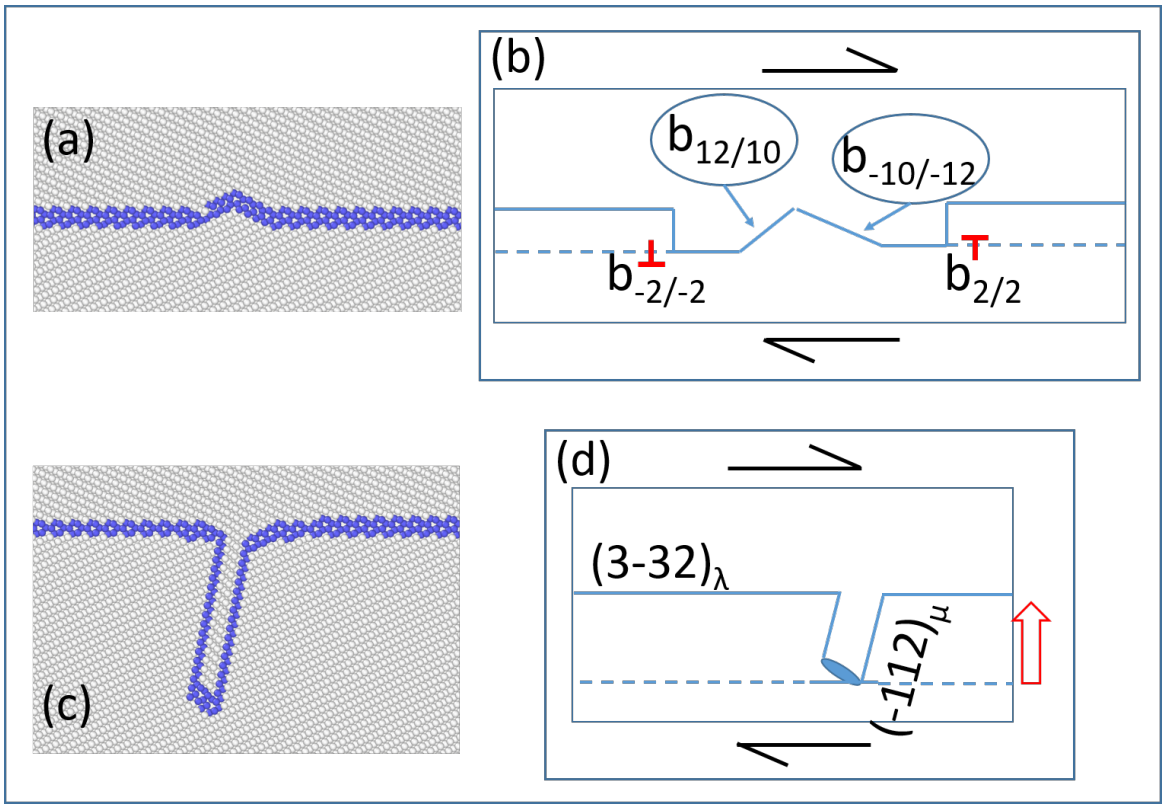

Figure 4.10: a) Core of the $\mathbf{b}_{2/-2}$ GBD that relaxes into $\mathbf{b}_{12/10}$ and $\mathbf{b}_{-10/-12}$ disconnections. b) Under positive shear stress EDiscs approach the GBDs. c&d) {112} twin embryo created by successive glide of EDiscs.

Under negative shear stress, initially a dipole of EDisc is created at the junction of the two facets and creates a plateau in between the facets, as shown in Fig. 4.11. From then on, the mechanism presented in Fig. 4.7b operates on $\mathbf{b}_{12/10}$ GBD and the equivalent mechanism represented in Fig. 4.11b operates on the $\mathbf{b}_{-10/-12}$ GBD. Both GBDs perform a compensated climb and move along their risers (dotted red line), as shown in Fig. 4.11. The process is a conservative SCGBM. The steady state for the displacement downwards of the GB is produced at a stress of 1.35 GPa.

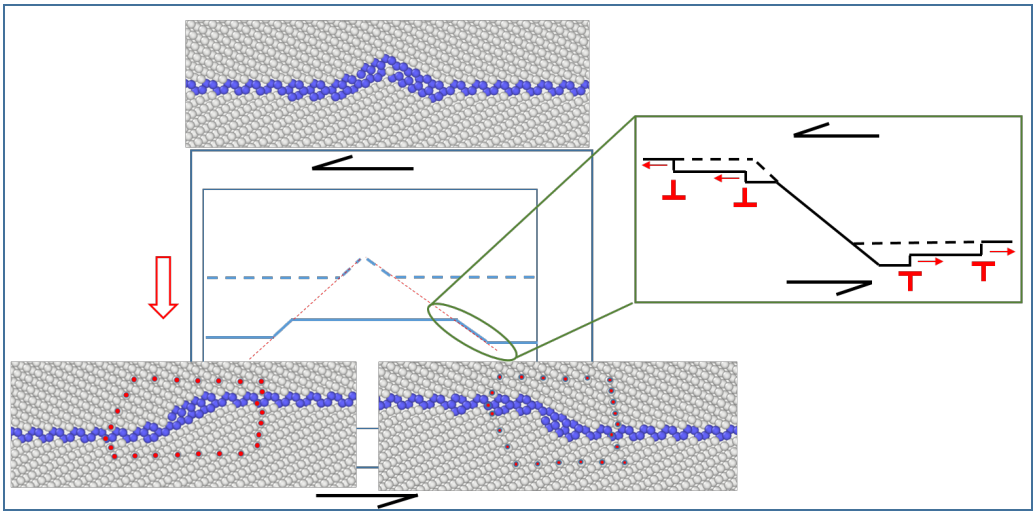

Figure 4.11: Displacement of the GB under a negative shear stress. The GB moves down and the disconnections $\mathbf{b}_{12/10}$ (left) and $\mathbf{b}_{-10/-12}$ (right) move with a compensated climb. The Burgers circuits used to analyze the two disconnections are marked in red. (Green rectangle) Detail of the mechanism of displacement of the riser of the $\mathbf{b}_{-10/-12}$ disconnection.

In the case of $\mathbf{b}_{-4/0}$, the dislocation is attracted but not absorbed by the GB and it keeps its own Bv. Under both, positive and negative shear stress, the dislocation is dragged by the GB while the GB is displaced upwards and downwards, respectively.

4.2.2.4 GBDs $\mathbf{b}_{-5/-6}$ and $\mathbf{b}_{3/4}$ (glide plane at 154.8°)

The screw part of the mixed dislocation is not modified by the reaction. Only the edge part transforms by emitting EDisc during the interaction. The resultant GBDs, $\mathbf{b}_{-5/-6}$ and $\mathbf{b}_{3/4}$, perform a compensated climb when the GB is displaced, as shown in Fig. 4.12, and follow the GB with the mechanism described in Section 4.2.2.1 and Figs. 4.7b and 4.11b. Thus, when the GB interacts with a mixed dislocation it performs a SCGBM.

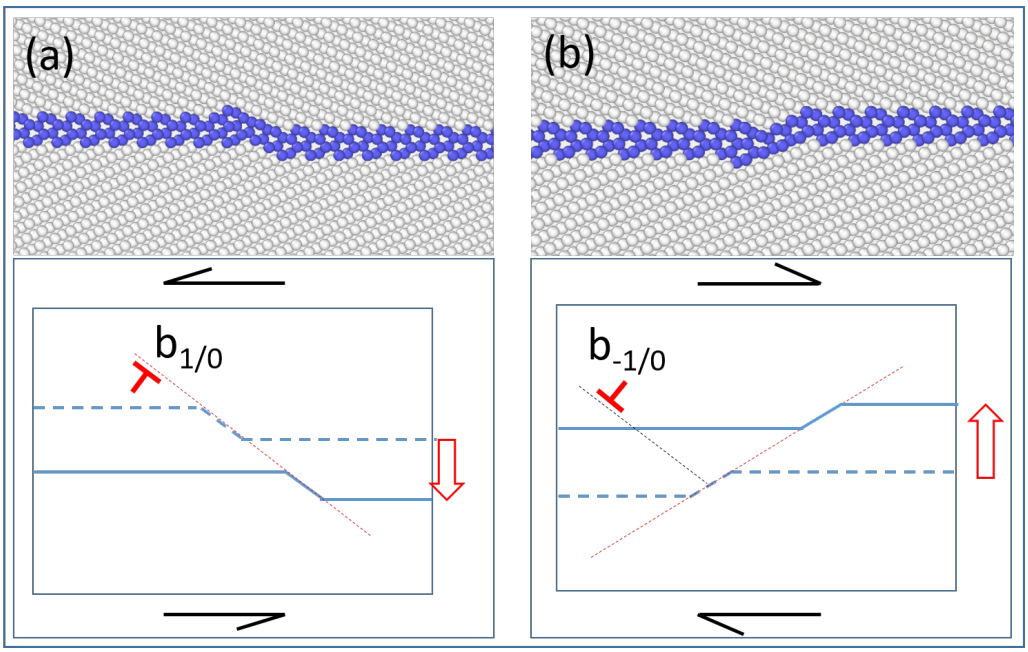

Figure 4.12: Displacement of the GB with the $\mathbf{b}_{-5/-6}$ GBD (a) and GBD $\mathbf{b}_{3/4}$ (b). The initial crystal mixed dislocations (before reaction) with their glide planes are included.

4.2.3 Growth of the {112} twin

The {112} twin is initially nucleated either at the core of the $\mathbf{b}_{-12/-10}$ GBD or the core of the $\mathbf{b}_{2/-2}$ GBD, when the GB is under a positive shear stress, i.e., the μ crystal, containing the twin, grows at expenses of the λ crystal (where the crystal dislocations come from).

The development of the twin is produced in several steps, as follows.

(i) The gliding $\mathbf{b}_{\pm 2/\pm 2}$ disconnections cannot overcome these GBDs and pileup at both sides of the GBD creating a twin embryo of four or six planes thick, depending on the core of the GBD, as shown in Figs. 4.8 and 4.10. The core of the GBD forms the twin tip. In the first stage of growth, the twin, with a constant thickness, increases its length due to the displacement of the {332} GB but the twin tip is not moving.

(ii) The thickening of the twin starts when the EDisc associated to the twin boundary, i.e., $\mathbf{b}_{\pm 1/\pm 1}$, are produced [57]. This may occur at the pristine {112} boundary under a shear stress along the twin boundary of about 2.4 GPa, or at a smaller stress if there are stress concentrators [57].

(iii) The reaction of the intrinsic elementary disconnections of the {112} twin boundary with the dislocation at the tip of the twin creates a glissile dislocation that run into the crystal. An example is shown in Fig. 4.13, which corresponds to the reaction of the GB with the $\mathbf{b}_{4/0}$ crystal dislocation, increasing the length of the twin.

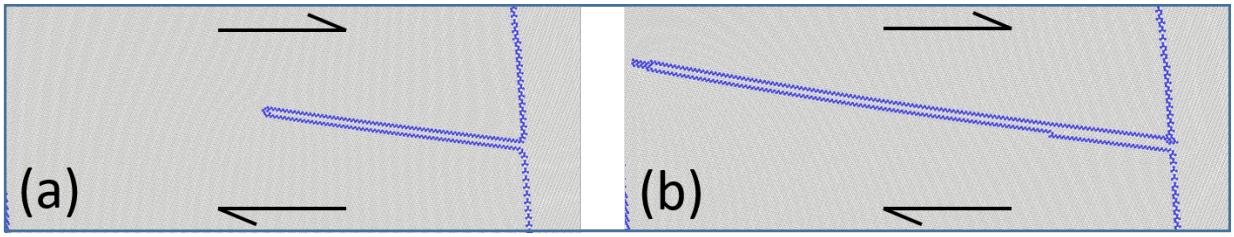

Figure 4.13: {112} twin under an applied shear stress (black arrows). a) The growth of the twin is produced by the motion of {332} GB (vertical in the images). b) The twin thickens by glide of disconnection dipoles created at the twin boundary and increase its length by the transformation and glide of the tip.

Let us describe the process in more detail. The misorientation of the {332} GB is 50.48° and the misorientation of the {112} GB is 70.53° (minimal possible misorientation angle is considered). Note that $\angle(1\bar{1}\bar{2})_\lambda/(1\bar{1}0)_\mu = 4.26°$ and $\angle(1\bar{1}2)_\lambda/(1\bar{1}\bar{2})_\mu = 20.04°$ for the {332} GB. The $\mathbf{b}_{2/2}$ disconnection has $(1\bar{1}\bar{2})_\lambda/(1\bar{1}0)_\mu$ facet in its core (Fig. 4.4) and the pileup of such disconnections gliding on parallel $(3\bar{3}\bar{2})_\lambda$ planes produces the $(1\bar{1}\bar{2})_\lambda/(1\bar{1}0)_\mu$ facet shown in Fig. 4.8. It is interesting that a row of $\mathbf{b}_{2/2}$ disconnections located along the bisection plane of $(1\bar{1}\bar{2})_\lambda$ and $(1\bar{1}0)_\mu$ (such plane is inclined to $(3\bar{3}2)_\lambda$ boundary by 27.4°) is equivalent to a disclination dipole with Frank angle $\omega = 4.26°$, i.e., this disclination dipole exactly compensates the misorientation between $(1\bar{1}\bar{2})_\lambda$ and $(1\bar{1}0)_\mu$ planes. However, the asymmetrical $(1\bar{1}\bar{2})_\lambda/(1\bar{1}0)_\mu$ facet becomes unstable, when it becomes longer. It transforms into the symmetrical {112} twin boundary. Such transformation is possible because a row of $\mathbf{b}_{2/2}$ disconnections located along bisect plane of $(1\bar{1}2)_\lambda$ and $(1\bar{1}\bar{2})_\mu$ planes is equivalent to disclination dipole with Frank angle $\omega = 20.04°$. Such disclinations are settled in facet junctions and exactly compensate the misorientation between $(1\bar{1}2)_\lambda$ and $(1\bar{1}\bar{2})_\mu$ planes.

4.2.4 Discussion

The most significant intrinsic dislocations of the {332}⟨110⟩ tilt GB are, on the one hand, the elementary disconnections, $\mathbf{b}_{\pm 2/\pm 2}$, responsible for the shear-coupled GB migration. The passage of each of them accommodates a shear due to its dislocation character and moves the GB by two planes due to its step. These disconnections may be produced in pairs at the pristine GB or at centers of stress concentration. On the other hand, there are the GB dislocations produced by the interaction of the GB with 1/2⟨111⟩ crystal dislocations. Their reaction with the GB depends on the orientation and

sense of the Burgers vector. Therefore, considering all possible orientations of 1/2⟨111⟩, there are six different reactions producing six GBDs that, in turn, may act as sources of $\mathbf{b}_{\pm 2/\pm 2}$. The final product of each reaction is a GBD and several glissile disconnections that glide away. The Bv of the GBD is, in general, not parallel to the GB; therefore, the GBD cannot glide along the GB.

A GB in a polycrystal subjected to an external shear stress may have several GBDs that will interact with the gliding $\mathbf{b}_{\pm 2/\pm 2}$. Since the sense of the applied shear stress may result in a different reaction between the elementary disconnections and the GBD, we should consider twelve cases. These reactions are reduced to two possible scenarios when viewed at a higher scale: a) In general, with only two exceptions, the two interacting GB defects may climb over each other in a compensated climb and the GBD moves together with the GB in a conservative manner (no atomic diffusion is needed) producing shear-coupled GB migration. b) The two exceptions occur for a positive shear stress when the μ crystal grows at the expenses of the λ crystal (where the crystal dislocations come from). Then, the core of the GBD does not allow a compensated climb. The accumulation of $\mathbf{b}_{\pm 2/\pm 2}$ at each side of the GBD nucleates a {112} twin embryo. In this case, the displacement of the GB is produced by the glide of disconnections that pileup forming the boundaries of the twin. In a second stage, the twin boundary creates disconnection dipoles that thicken the twin and react with the tip that emits dislocations, increasing the length of the twin.

In both scenarios, the motion of the GB due to the glide of disconnections, with or without creation of a twin, accommodates the plastic deformation.

4.3 {111} GB

In this Section, based on [113], we have investigated the interaction of a Σ3{111}⟨110⟩ tilt GB with single crystal dislocations in bcc-Fe. The dichromatic pattern [39] presented in Fig. 4.14 shows the only EDisc that could be related to the SCGBM (identified as #4). As it is detailed in the Results subsection, this EDisc does not appear involved on the reactions observed. This makes the {111} GB a suitable choice to investigate the plasticity mechanisms in absence of EDisc, which will contribute to complete the understanding of the GB – dislocation interaction in bcc materials.

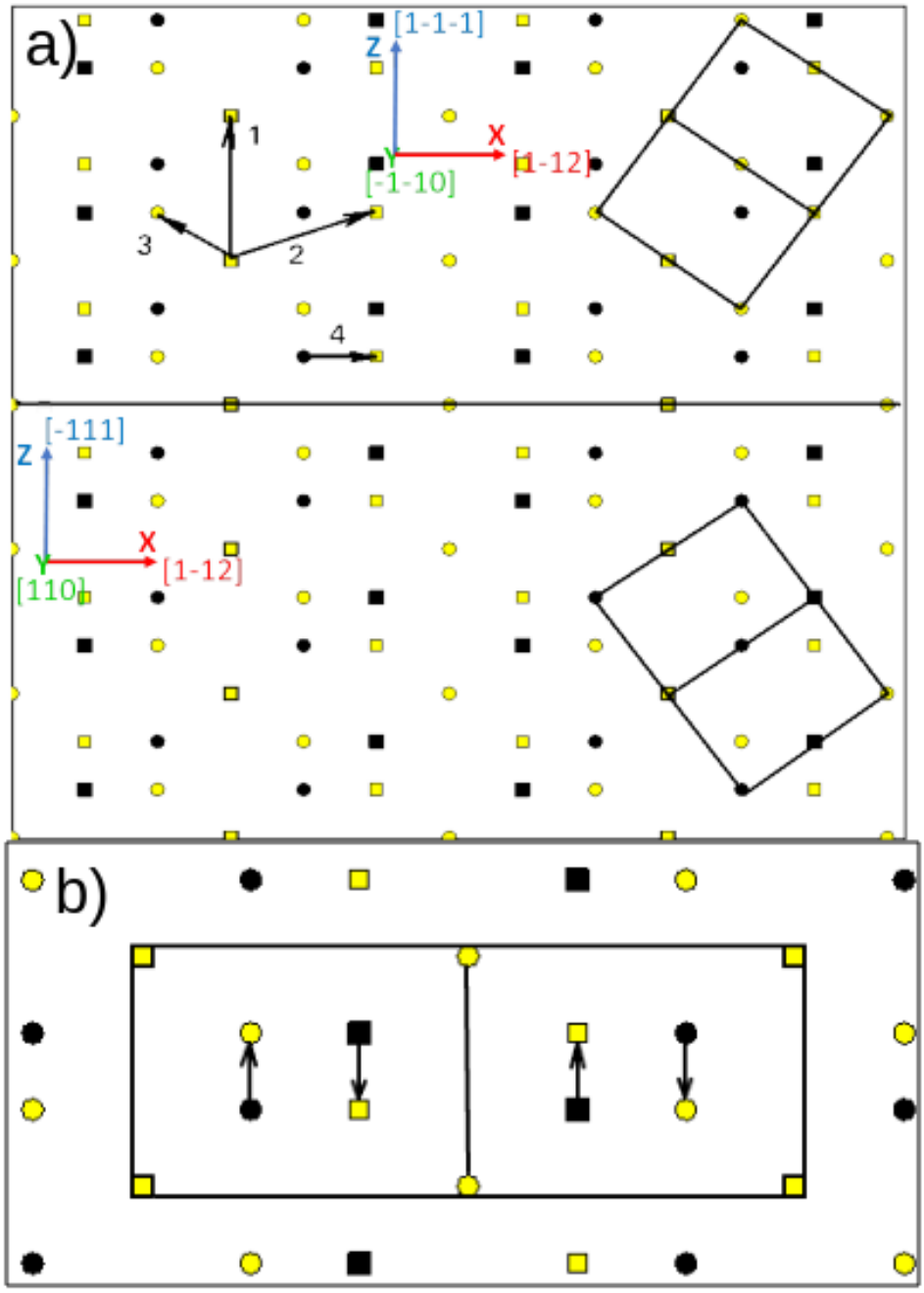

Figure 4.14: a) Dichromatic pattern of {111} GB. Black sites represent the lower grain, yellow sites the upper grain. Burgers vectors marked with numbers "1" and "2" are the Bvs of crystal edge dislocations gliding on two different {112} planes. "3" is the Bv of a mixed dislocation gliding on a {110} plane, "4" is the Bv of a potential EDisc with the lowest possible step. b) Coincident-site Lattice for the {111} GB. The arrows indicate the motion of atoms necessary to create a step in the interface.

There have been considered three different glide plane inclinations with respect to the GB to introduce the dislocations, which are identified in Fig. 4.14. The first corresponds to an edge dislocation tagged as #1, gliding at 90 degrees, named $\mathbf{b}_{3/0} = \frac{1}{2}[1\bar{1}\bar{1}]$. The second one, tagged as #2, is another edge dislocation gliding at 19.47 degrees and named $\mathbf{b}_{1/0} = \frac{1}{2}[1\bar{1}1]$. And the last one, tagged as #3 is a mixed dislocation gliding at 144.74 degrees and named $\mathbf{b}_{1/0} = \frac{1}{2}[11\bar{1}]$. For every glide plane inclination, it has been considered, in turn, two senses of the Bv, pointing away from the interface (denoted $\mathbf{b}_{n/0}$) and pointing towards the interface (denoted $\mathbf{b}_{-n/0}$).

The Section is structured as follows: in subsection 4.3.1 there are presented the most relevant findings on the interaction of the {111} GB with single dislocations, while in subsection 4.3.2 we present the discussion of the results obtained.

4.3.1 Interaction of the {111} GB with a ½⟨111⟩ dislocation

In the present Section, we describe the whole process of transformation undergone by both crystal dislocations and the interface when the former interacts with a {111} GB. The absence of glissile EDisc as a part of the reactions observed leads to a mechanism for coupling plastic deformation very different from the ones observed for other interfaces in bcc metals [57, 74, 75].

The results presented in the previous Sections of this chapter for the {112} and {332} GB show that single ½⟨111⟩ dislocations are spontaneously absorbed by the boundary followed with the formation of a GBD and the emission of one or several EDisc. Conversely, for the {111} GB we noticed that there is no absorption of the incident dislocation, independently of the glide plane, Bv orientation or dislocation character considered. On every possible case investigated the crystal dislocation stays attached to the GB keeping its Bv, the parameters defining each case only affect the final defects at the GB and the stresses at which the transformation takes place. In this Section we present the results obtained for a range of temperatures going from 0 K up to 900 K. However, there are noticeable differences between the mechanisms observed at T = 0 K with those for T > 0 K, for that reason we have presented the results in two different subsections, one for static and another for dynamic calculations.

4.3.1.1 Static simulations

The analysis of the results obtained from Molecular Statics on the interaction between a single dislocation and the GB shows exactly the same pattern irrespectively on the glide plane inclination, Bv orientation or character of the dislocation (edge or mixed) which can be described qualitatively as a three-steps process:

1. Attachment of the crystal dislocation to the GB without changes in its Bv.
2. Transformation of the defect (formation of several non-glissile steps and residual defect).
3. Accumulation of stresses at this region up to an eventual formation of a {112} twin attached to the GB.

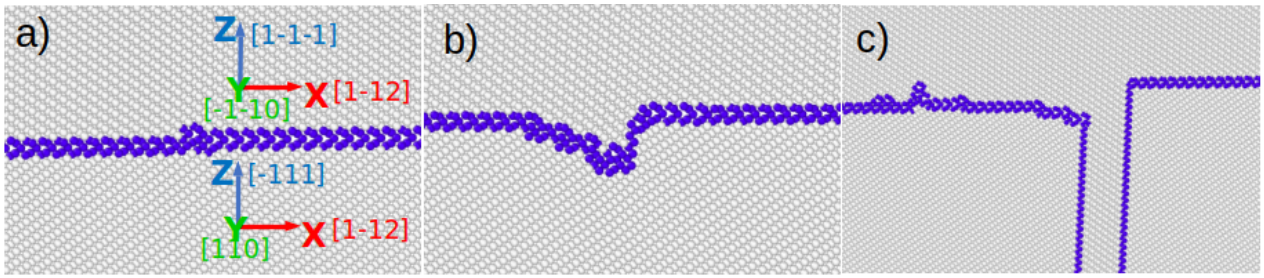

Figure 4.15: Interaction of the {111} GB with $\mathbf{b}_{3/0}$ edge dislocations at 90°. a) Dislocation is attached to the GB; b) start of steps formation; c) formation of a {112} twin.

In the frames of Fig. 4.15 we can see the details on this process for the single dislocations on a glide plane forming an angle of 90 degrees with the GB. It starts moving from the attachment of the incident crystal dislocation to the GB (Fig. 4.15a) to the final formation of the {112} twin in the lower crystal (Fig. 4.15c) including the intermediate configurations where it can be noticed the formation of pure steps without dislocation character, that is, they are sessile. The only change with respect to other cases lies on the number of steps produced and the growth direction of the twin, which can expand towards the upper crystal or the lower crystal, depending on the sense of the Bv, i.e., the direction of the stress to be applied to trigger the reaction.

The creation of these pure steps is shown on Fig. 4.14b. In this frame it is displayed the Coincidence Site Lattice unit cell for this GB. The shuffles of two atoms inside this unit cell, indicated in the figure by the position and direction of the vertical arrows, leads to the appearance of steps on the boundary. The energy barrier of the transformation of the GB is 99 mJ/m^2. Mrovec et al. [61] reported this mechanism of stress accommodation for the {111} GB in tungsten.

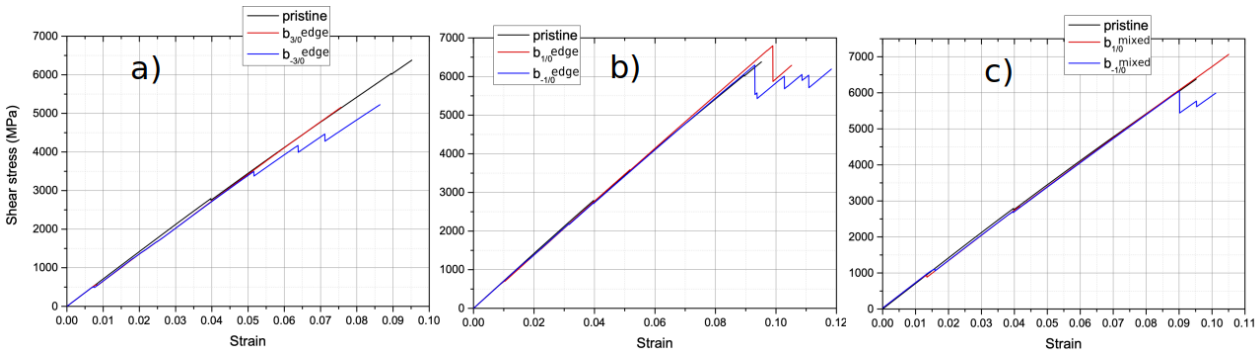

Figure 4.16: Shear stress in the system vs strain applied for different incidence angles. The response of the pristine GB is included as reference. a) 90 degrees, b) 19.47 degrees and c) 144.74 degrees.

Under shear stress loading, the pristine interface remains unchanged up to a very high stress level ($\sim$ 9 GPa at T = 0 K). The shear stresses averaged on all mobile atoms for all the cases considered are shown in Fig. 4.16. The results evidence that the presence of a dislocation attached to the GB allows to decrease the stress needed to initiate a reaction. From the 9 GPa in the pristine interface the values of shear stress are reduced to approximately 4 GPa in $\mathbf{b}_{-3/0}$ case, to 6.3-6.7 GPa in $\mathbf{b}_{1/0}$ (mixed) and 6 GPa in $\mathbf{b}_{-1/0}$ (edge). Therefore, the cases with the glide plane perpendicular to the GB are the most favored ones, although, according to geometrical criteria, the GB should be transparent for the dislocations. All the big drops in the shear stress correspond to the formation of {112} twins.

4.3.1.2 Dynamic simulations

At temperature T > 0 K, the interface allows accommodation of stress by forming steps or irregular structures on the interface, as can be observed in Fig. 4.17. The shape of the GB far from the interaction region is no longer flat while on the local region of the boundary where the dislocation is attached there is no formation of {112} twins and the steps formed are higher (Fig. 4.17c). This total absence of {112} twin formation indicates that stepping the interface is the preferred mechanism on this boundary for accommodation of plastic deformation.

Unlike static simulations, the outcome of MD calculations shows to be sensitive to the glide plane inclination and Bv sense, so the results for each case are presented separately. In Fig. 4.17 it is displayed the evolution of the GB interacting with a $\mathbf{b}_{-3/0}$ crystal dislocation at T = 300 K. Once the dislocation is attached to the interface as the stress increases it is formed a new interface: it grows a {112} interface (Fig. 4.17b) in a reaction quite similar to the initial split of the Bv shown on Fig. 4.15b. Applying temperature allows a better accommodation of the new interfacial structure, so that the formed defect is not a {112} twin, but a pair of two interfaces: a {112} GB, coinciding with the initial glide plane of a dislocation, and an asymmetrical interface formed by steps created on {111}

GB (Fig. 4.17c). For the $\mathbf{b}_{3/0}$ dislocations the process is similar although the change on the interface is less pronounced.

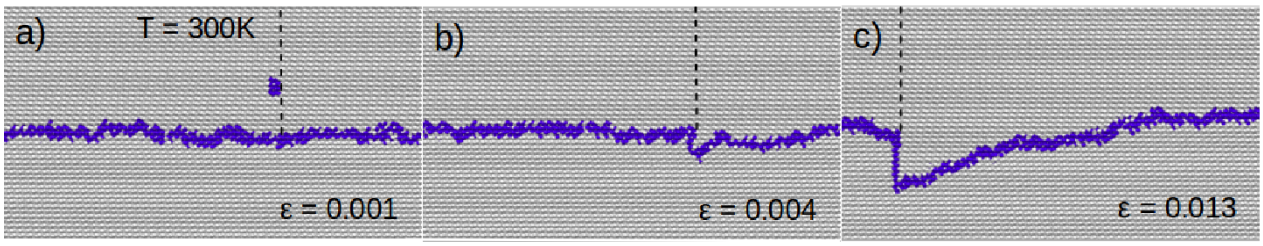

Figure 4.17: Interaction of the {111} GB with an edge dislocation $\mathbf{b}_{-3/0}$ at T = 300 K. The dashed lines are a guide for the eye showing the position of the glide plane.

In the case of edge dislocations gliding at 19.47 degrees applying temperature also leads to a formation of an asymmetrical interface. Once again, there is no formation of twins with re-emission of crystal dislocations and the interface is formed along the initial glide plane of the dislocation. There is a formation of a complementary interface to compensate the step height. As an example, Fig. 4.18 shows the two interfaces formed from the absorption of $\mathbf{b}_{1/0}$ dislocation at T = 300 K.

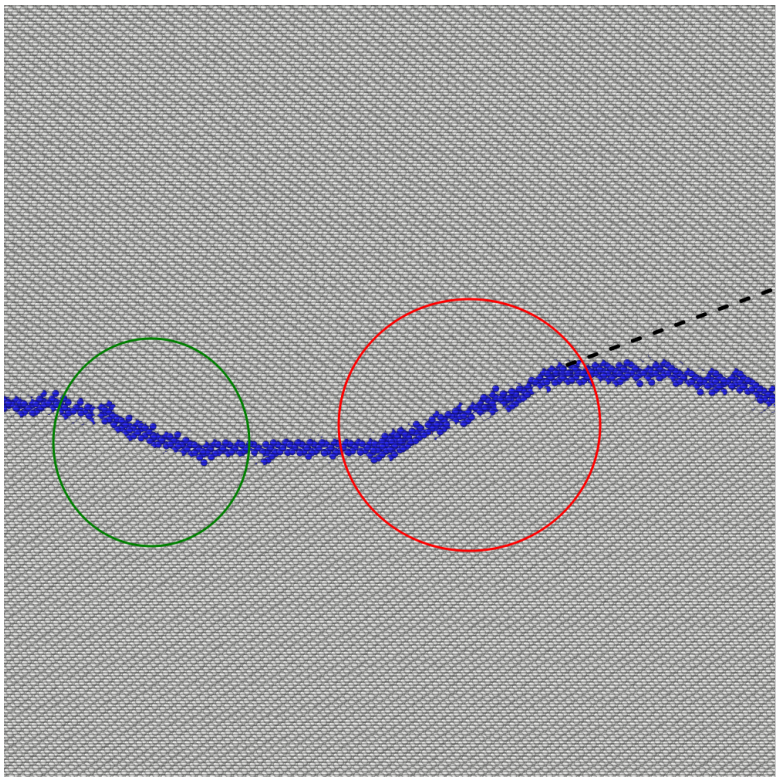

Figure 4.18: A GBD formed by the absorption of an edge $\mathbf{b}_{1/0}$ at T = 300 K in iron. The picture shows two formed risers: one on the right (red circle) containing the absorbed dislocation and another one on the left (green circle) which is a 'complementary' step. The dashed line is a guide for the eye showing the position of the glide plane.

Finally, for the mixed dislocations gliding at 144.74 degrees, we have found that, irrespective to the screw component and Bv sense, the dislocation becomes attached to the interface but no reaction is observed. The main difference with edge dislocations is that no new interface is created as no risers or {112} GB formation takes place. Therefore, we can conclude that this attached mixed dislocation is not as effective as a stress concentrator as its counterparts for pure edge dislocations. The edge part of the Bv of this mixed dislocation is shorter than the Bv of $\mathbf{b}_{3/0}$ and $\mathbf{b}_{1/0}$ edge dislocations ($0.5a_0$ vs. $0.866a_0$).

4.3.2 Discussion

As a general trend, there is no transmission or reflection of crystal dislocations; the GB acts as an impenetrable barrier to incoming dislocations. Instead, in the interaction, there is a significant transformation of the atomic configuration of the interface. This is because the stress field associated to the incident dislocation enhances the local reorientation of the GB into other more stable states of lower energy. It is worth noticing that among the stable Σ3 interfaces associated to the ⟨110⟩ tilt axis, this GB has the highest interfacial energy. The reorientation of the GB under stress allows the process of penetration of one grain into the other along with the growth of asymmetrical interfaces. A distinctive feature of the {111} GB under stress is its ability of changing the orientation by the creation of pure steps, $h_{3/3}$ (without dislocation character) by the shuffle of two atoms per CSL unit cell.

Thus, the GB does not experience shear-coupled GB migration as other studied GBs with ⟨110⟩ tilt axis. This is due to the absence of elementary disconnections that in other GBs are created either as dipoles in the pristine GB or as the reaction with a crystal dislocation. In fact, the smallest disconnection of the GB has a screw component and its magnitude ($0.64a_0$) is high compared to the disconnections at GBs that experience shear-coupled GB migration. Moreover, the reaction of the GB with the edge dislocation cannot supply the screw component of the disconnection. Only the reaction with the mixed dislocation could decompose into a disconnection and a residual defect, but even in this case, the GB would be pinned by the residual defect, and the disconnection, with large magnitude, would not glide at low stresses.

The interaction of a single dislocation with the GB at 0 K is not dependent on the glide plane inclination, Bv orientation or character of the dislocation. In all cases, the process ends up with the creation of a {112} twin that initiates at the core of the dislocation and grows in the adjacent crystal. Under temperature the evolution of the interaction depends on the incident dislocation. No twins are developed in the region where the dislocation is attached. Instead, the stress is released by the reorientation of the GB into facets and this process depends on the glide plane of the dislocation. The dislocation with {112} glide plane at 90° of the GB is not absorbed but penetrates the adjacent grain by forming two facets, one facet along its glide plane and the other facet formed by pure steps ($h_{3/3}$). Dislocations gliding along other glide planes are absorbed by the GB forming a facet along the glide plane resulting on a wavy GB.

The level of stresses for the reactions to occur depends on the metal considered, iron in this study. The value of the external stress at which a specific reaction takes place depends also on the ambient temperature. Even for a fixed temperature, the critical stress varies with the simulation conditions, indicating that the observed event is probabilistic and thermal activation plays a role in it.

4.4 {116} GB

The structure of the Σ19{116}⟨110⟩ GB presents more than one type of mobile disconnection with different step height. This GB has been investigated for completeness, as it can be considered as an intermediate case between the {112} and {332} GBs with only one elementary disconnection, and the {111} GB without any EDisc. However, the {116} GB is of a pure academic interest, as there is no experimental evidence of it in the literature.

The reaction between the single dislocation and the interface is mainly absorption. The outcome of the interaction is a GBD along with the emission of EDisc $\mathbf{b}_{\pm 3/\pm 3}$. When the local stress on the vicinity of the GBD is high enough then it splits into a new GBD and a HS Disc, shown in Fig. 4.19, which in turn ends splitting into $\mathbf{b}_{3/3}$ and $\mathbf{b}_{-3/-3}$ EDisc. Specifically, the crystal dislocation denoted as $\mathbf{b}_{4/0}$ in Fig. 3.1d reacts with the GB as depicted in Fig. 4.19:

(i.a) First step of the reaction: $\mathbf{b}_{4/0} = \mathbf{b}_{7/3} + \mathbf{b}_{-3/-3}$;

(i.b) In Miller indices the reaction is: $\frac{1}{2}[1\bar{1}\bar{1}] = \frac{1}{38}[13\bar{1}\bar{3}2\bar{1}] + \frac{1}{19}[3\bar{3}1]$;

(ii.a) In turn, the disconnection $\mathbf{b}_{7/3}$ decomposes as: $\mathbf{b}_{7/3} = \mathbf{b}_{-3/-3} + \mathbf{b}_{2/-2} + \mathbf{b}_{8/8}$;

(ii.b) In Miller indices the reaction is: $\frac{1}{38}[13\bar{1}\bar{3}2\bar{1}] = \frac{1}{19}[3\bar{3}1] + \frac{2}{19}[1\bar{1}\bar{6}] + \frac{1}{38}[3\bar{3}1]$.

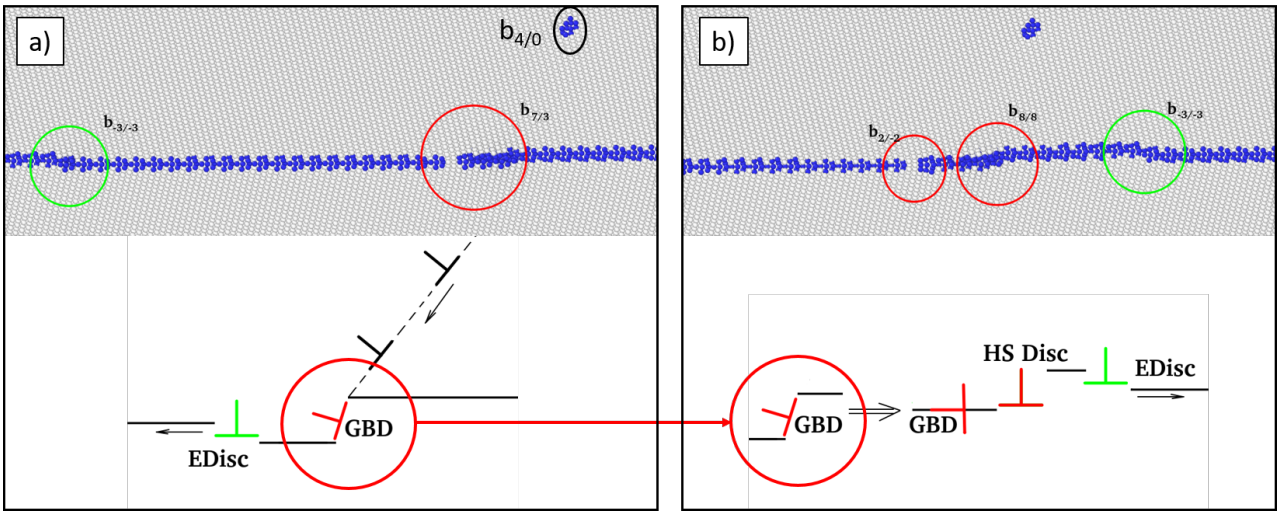

Figure 4.19: Snapshots of MD simulation of a {116} GB interacting with a crystal dislocation $\mathbf{b}_{4/0}$ in Fe at 300 K. A second crystal dislocation is shown in the top of the image. a) First step of the reaction. b) Decomposition of the $\mathbf{b}_{7/3}$ disconnection.

When the crystal dislocation interacts with the {116} GB, a GBD is created that suffers several transformations by reacting with the external EDisc that are gliding along the interface (formerly created during the interaction or emitted by the GBD). The full process consists of initial absorption and split of the crystal dislocation into disconnection and further reactions between the disconnections at the interface, that may lead to transmission.

4.5 Summary and discussion

In this chapter we present the results of a MD study on the interaction of a single ½⟨111⟩ crystal dislocation with a set of ⟨110⟩ symmetric tilt grain boundaries, namely {112}, {332}, {111} and {116}. All the orientations and senses of the crystal dislocation have been considered. The interaction of the symmetric ⟨110⟩ tilt GB with the family of $\frac{1}{2}\langle 111\rangle$ crystal dislocations depends on the orientation of the dislocation.

The way of stress accommodation by the pristine GB interfaces defines the outcomes of the reactions with the crystal dislocations. In case of the {112} GB, upon interaction with an edge dislocation a $\mathbf{b}_{1/-1}$ GBD is created at the at the interface, which is the same GBD appearing at the GBs vicinal to the {112} (see Section 3.2.1). Under stress, these GBD act as sources of disconnections and the vicinal GB is displaced by the same mechanism. The fact that the crystal dislocation decomposes, in a reversible way, into $\mathbf{b}_{1/-1}$ plus the disconnection responsible for the motion of the GB is essential to have a conservative process. Thus, the mechanism described accommodates efficiently plastic deformation since no residual defects are left behind in the displacement of the GBs and no atomic diffusion is needed during the whole process.

While the edge dislocation produces a source of disconnections, the mixed dislocation keeps its own Burgers vector and it is dragged by the GB during its shear-coupled GB migration. Both dislocations are absorbed by the GB and no transmission to the next grain is produced.

The {332} GB has absorbed the dislocations, either due to its mutual attraction or under an applied shear stress. The reaction and final defects at the GB depend on the orientation of the glide plane, the sign of the Burgers vector and the edge or mixed character of the dislocation.

Depending on the glide plane inclination and the sense of the Bv several outcomes of the reaction are possible:

1. For the dislocation with a Burgers vector forming an angle of 29.5° with the GB ($\mathbf{b}_{2/0}$) the reaction is absorption with the following formation of a GBD with a core riser that acts as a source of EDisc dipoles under an applied shear stress. Thus, the GBD facilitates the shear-coupled GB migration.

2. For the dislocation gliding on the glide plane at 29.5° with the reversed sense of Bv ($\mathbf{b}_{-2/0}$) and the dislocation on the glide plane at 100° the $\mathbf{b}_{4/0}$ Bv the GBDs formed by absorption impede the glide of EDisc under positive shear stress. Thus, the GBDs are transformed into symmetric {112} facets leading to a creation of {112} twins. On the one hand, the appearance of these twins accommodates plastic deformation, on the other hand, they interact with crystal dislocations hindering their glide and therefore contributing to hardening of the material. Moreover, such twins act as neutral sinks for point defects [64].

3. For both signs of Bv and direction of stress application for mixed dislocations ($\mathbf{b}_{\pm 1/0}$) the GB with a formed GBD performs a shear-coupled migration. This is also applicable to the $\mathbf{b}_{-2/0}$ and $\mathbf{b}_{4/0}$ dislocations under negative shear stress applied. In case of the $\mathbf{b}_{-4/0}$ dislocation gliding on the glide plane at 100° there is repulsion between the dislocation and the interface. Once the repulsion is overcome the dislocation is attached to the GB keeping its Bv. Under both senses of applied stress, the GB migrates dragging the dislocation. Thus, the interaction with such dislocations slows down the GB migration process and therefore contributes to plastic deformation accommodation.

The interaction of the {111} GB with an individual dislocation studied in static simulations (i.e., T = 0 K) demonstrated that the interaction of an individual dislocation with the GB occurs by the same mechanism irrespective of the orientation of the glide plane. The dislocation was not absorbed but the stress was accommodated by the creation of {112} twins that penetrate the adjacent grain. Interaction in dynamic simulations, i.e., at T = 300 K, realizes via two channels, and the particular path depends on the orientation of the glide plane of the dislocation, namely:

1. If the glide plane is perpendicular to the GB plane, there is a penetration of one grain into the other with the dislocation in the tip of the intrusion bounded at each side by an asymmetric interface formed by pure steps and a {112} symmetric tilt GB segment along the dislocation glide plane. The process is not reversible if the applied stress is reversed in a cyclic deformation.

2. All other orientations of the glide plane of the dislocation facilitate the absorption of the dislocation by the creation of a facet along the glide plane. Another facet formed by pure steps compensates the slope of the dislocation riser. This happens independently of the dislocation character.

Hence, a direct transmission or reflection of the individual dislocation has not been observed in the {111} GB. This behavior noticeably differs from the other types of ⟨110⟩ tilt GBs. The reason for the difference in the behavior of the {111} GB comes from the GB structure (CSL) and its flexibility to convert into another interface (steps and {112} twin) under externally applied shear stress.

Due to the large value of Σ, the planes perpendicular to the {116} GB are situated very close together. So that the crystal dislocations bring in highly stepping character when get absorbed (compare the step height: for example, $\mathbf{b}_{2/0}$ in {112} and {332} and $\mathbf{b}_{4/0}$ in {116}). Hence, the formed GBD also have high stepping character. It is energetically favorable for the highly stepping GBD to split into the new defects with smaller step height. The high stepping disconnections have the Bv smaller than the elementary one and the higher step (see Table 3.2). In order to move such disconnections more shuffles of underlying atoms are needed, so the stress level required to move them is much higher and it is never reached.

4.6 Conclusion

On the basis of the obtained results and their analysis a number of observations regarding the deformation and modification of the atomic structure of the GBs upon the interaction with dislocations or externally applied stress can be summarized.

We describe a mechanism of plastic deformation in bcc metals associated to the shear-coupled grain boundary migration of both {112} and {332} tilt GBs. The mechanism is directly applicable to the {112} twin boundary and governs the growth and shrinkage of the twin.

The shear-coupled GB migration is produced by the creation and glide of disconnections in both {112} and {332} GBs. These disconnections are either created directly at the pristine GB or can be created at a lower stress level by a source of disconnections.

While plastic deformation is efficiently accommodated by SCGBM in both {112} and {332} by production and glide of EDisc, in {111} GB SCGBM does not take place, as there is no production of EDisc. Under externally applied shear stress, at sufficiently high value, the {111} tilt grain boundary reorients by forming pure steps of three {111} atomic planes high, through shuffling of two atoms of the CSL unit cell of the grain boundary. This atomic transformation path plays an important role in the interaction of the GB with crystal dislocations.

To conclude:

- The {112} GB and vicinal GBs accommodate plastic deformation by shear-coupled GB migration. The same mechanism is applied to the growth and shrink of (112) twins.
- The {332} tilt GB performs a shear-coupled migration when the elementary disconnections can climb conservatively along the GBD; otherwise, a twin embryo is created at the place of the GBD. This GB accommodates deformation by combining the shear-coupled GB migration and the formation of (112) twins
- The {111} GB acts as a strong obstacle that does not allow a direct dislocation transmission into the adjacent grain. Correspondingly, upon the interaction of this GB with a crystal dislocation, there is no accumulation (and subsequent rotation) of the Burgers vector of the dislocation, which is required to emit the dislocation into the adjacent grain.
- The {116} GB has many possible disconnections. However, this GB does not experience SCGBM, since the level of stress required to produce and move the disconnection with the lowest step height is high and it is never reached. Instead, plastic deformation upon interaction with crystal dislocations is accommodated by creation higher-stepping disconnections from GBD.

CHAPTER 5

INTERACTION OF ⟨110⟩ TILT GB WITH PILEUPS OF ½⟨111⟩ DISLOCATIONS

The results presented in the previous chapter have allowed us to realize the inherent complexity of the interaction between dislocations and grain boundaries. It has been found that a detailed analysis of every possible case (Bv orientation, glide plane inclination, temperature, etc.) is required with the aim of ascertaining the evolution of the system when a single dislocation contacts a GB. As mentioned in the Introduction (Chapter 1), upon severe plastic deformation dislocation pileups are produced, which subsequently interact with the interfaces between grains. Therefore, the study of these interactions becomes essential in order to have a complete picture of the processes involved in the plastic response of the material. To that purpose, the present Chapter is devoted to investigate the interaction between a dislocation pileup and the same set of ⟨110⟩ tilt GBs used in Chapter 4 with the exception of the {116} GB. The exclusion of the latter is justified by the absence of novel results as the ones obtained are almost identical to those in Section 4.4. For consistency, each subsection of the chapter corresponds to one of the GBs. The results presented here have been published in [75, 110, 113, 114].

All the results presented below have been obtained by applying a hybrid atomistic/discrete-dislocation model which is thoroughly described in the Section 2.2 of the Method Chapter. The glide planes used to introduce each dislocation pileup are exactly the same ones used to introduce single dislocations. Therefore, a direct comparison between these results and the equivalents in Chapter 4 can be established, allowing to evaluate the effects on the dislocation – GB interaction of the stress field generated by the next incident dislocations in the pileup.

5.1 {112} GB. Slip transmission criterion

As detailed in the different subsections of Section 4.1, the interaction of the {112} GB with a single ½⟨111⟩ dislocation can be described in a very simple way because there are only involved one GBD ($\mathbf{b}_{1/-1}$) and one EDisc ($\mathbf{b}_{\pm 1/\pm 1}$) and the interaction process is conservative. These results are also valid for a {112} twin boundary when the width of the twin is large enough to avoid the influence of the other coherent twin boundary.

The study presented in Section 4.1 reports that a single crystal dislocation under stress might be absorbed by the {112} interface but there is no transmission through the interface. However, as we show in this Section, this behavior changes when other dislocations, gliding along the same glide plane, approach the {112} GB. The present Section explores the reaction at the GB if the interaction is produced by a dislocation pileup and apply the results to the analysis of the twin-slip interaction.

The Section is based on [110] and structured as follows: subsections 5.1.1 – 5.1.5 present the results on the interaction of the {112} GB with a DPU, while subsection 5.1.6 presents the results on the slip-twin interaction, finally in subsection 5.1.7 we present the discussion of the obtained results.

Although the study is mainly focused in bcc Fe, in order to understand the effect of the interatomic forces on the different processes studied, we compare the main features found in Fe with the interaction in two other bcc metals, namely Cr and W, which also have wide use as structural materials in nuclear applications.

The standard simulation setup employed to perform this study includes some features that may produce some spurious effects on the results. In order to check the generality of our findings, we have performed two different tests. In the first test, for the sake of favoring the creation and propagation of EDisc, we ran a set of simulations at T = 300 K where a shear stress parallel to the GB has been applied. And the purpose of second test has been to check the effect on the relaxation mechanisms of the box thickness along the tilt axis. To this end we performed several simulations with the thickness increased up to 60 lattice parameters.

To describe the relationship between the crystal dislocations and the GBDs we use the dichromatic pattern shown in Fig. 5.1. Since the local atomic configuration at the GB is different for the two adjacent glide planes (see dashed lines A & B in Fig. 5.1), the study was extended to both glide planes.

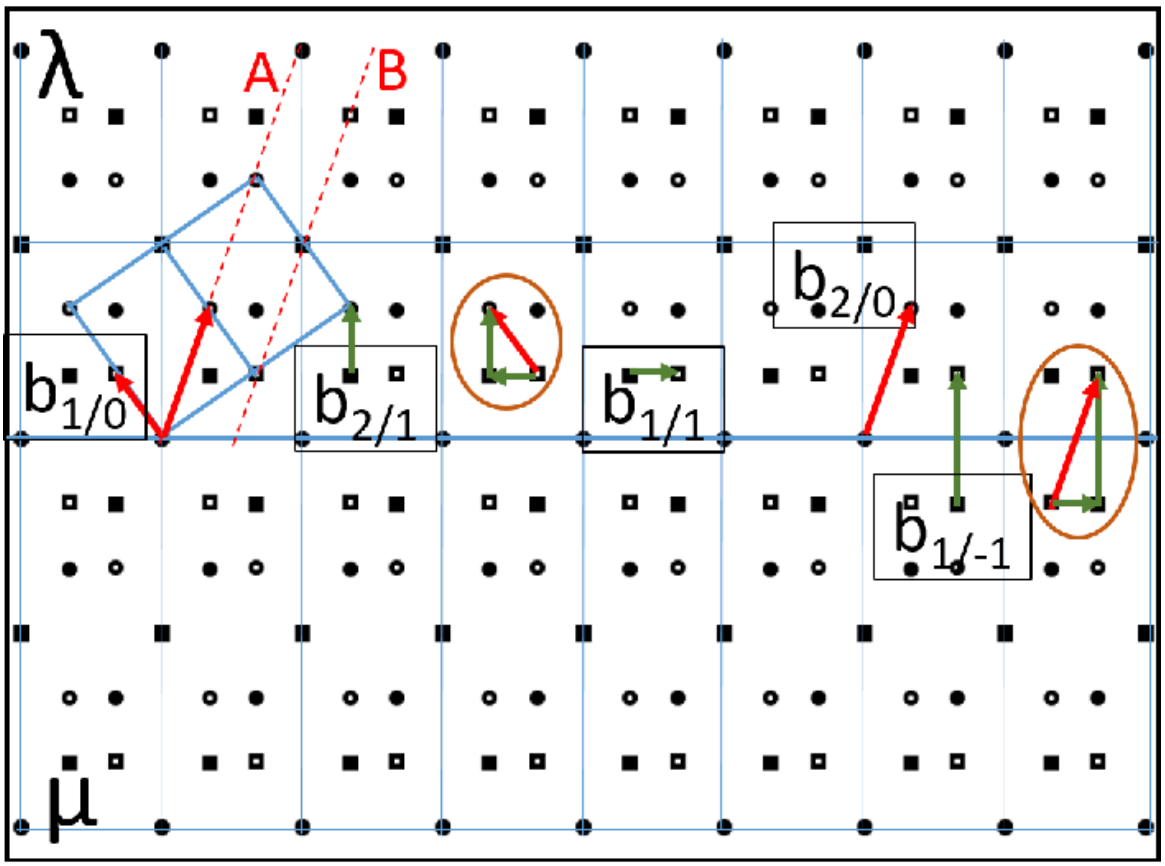

Figure 5.1: Projection along the [110] tilt axis of the dichromatic pattern associated to the $(1\bar{1}2)$ GB showing the Burgers vectors of interfacial defects (green), crystal dislocations of the λ crystal (red) and two adjacent glide planes of edge dislocations (red dotted lines).

The following subsections describe the interaction of a DPU of ½⟨111⟩ dislocations with the {112}⟨110⟩ tilt interface. At the atomic scale, within the delimited volumes of the dislocation interaction, the interface can be understood as a grain boundary as well as a twin boundary. Thus, subsections 5.1.1 – 5.1.5 describe the slip transfer conditions at the {112} GB and the subsection 5.1.6 describes the slip-twin interaction, i.e., the interaction of the DPU with a $(1\bar{1}2)$ twin, which is directly related to the results of the first part.

The pileup of crystal dislocations considered for the interaction with the $(1\bar{1}2)$ GB are: the edge $\mathbf{b}_{\pm 2/0} = \pm\frac{1}{2}[1\bar{1}1]$ gliding along the $(\bar{1}12)$ plane inclined at 70.53° with the GB and the mixed $\mathbf{b}_{\pm 1/0} =$

$\pm\frac{1}{2}[111]$ gliding along the $(1\bar{1}0)$ plane inclined at 125.26° with the GB. They are represented (red arrows) in the dichromatic pattern of Fig. 5.1 together with the interfacial defects: EDisc $\mathbf{b}_{1/1} = \frac{1}{6}[1\bar{1}\bar{1}]$, the disconnection $\mathbf{b}_{2/1} = \frac{1}{3}[121]$ and the GBD $\mathbf{b}_{1/-1} = \frac{1}{3}[1\bar{1}2]$ that does not step the GB (Green arrows). Except in the subsection 5.1.4, the external shear stress was applied along the glide plane of the DPU.

5.1.1 Interaction with a pileup of edge dislocations $\mathbf{b}_{2/0}$

The Burgers vector (upper red arrow in Fig. 5.2a) of the $\mathbf{b}_{2/0}$ dislocations is pointing away from the interface. When the DPU is few lattice parameters away from the GB, the heading dislocation is attracted and absorbed by the GB according to the following reaction: $\frac{1}{2}[1\bar{1}1]_\lambda = \frac{1}{3}[1\bar{1}2]_\lambda + \frac{1}{6}[1\bar{1}\bar{1}]_\lambda$, written in coordinates of the upper crystal (λ). The absorption, not observed for the single dislocation, is mediated by the stress field produced by the trailing dislocations of the DPU.

Under an applied shear stress, a dipole of disconnections is created at the GB at the right side of the GBD (see Fig. 5.2a), which is the tensile region of the trailing dislocations. Then, the EDisc that approaches the GBD is $\mathbf{b}_{-1/-1} = \frac{1}{6}[\bar{1}11]$ and the reaction taking place is:

$$\frac{1}{3}[1\bar{1}2]_\lambda + \frac{1}{6}[\bar{1}11]_\lambda = \frac{1}{6}[1\bar{1}5]_\lambda = \frac{1}{2}[\bar{1}11]_\mu = \mathbf{b}_{0/2}. \tag{5.1}$$

Therefore, the dislocation has changed the orientation of the Bv making it able to glide into the lower crystal (μ), i.e., the dislocation has been transmitted. As the transmitted dislocation moves downwards, the other EDisc of the dipole has glided away along the GB, leaving a pristine interface for the second dislocation of the pileup which, in turn, is absorbed, as it was the first dislocation.

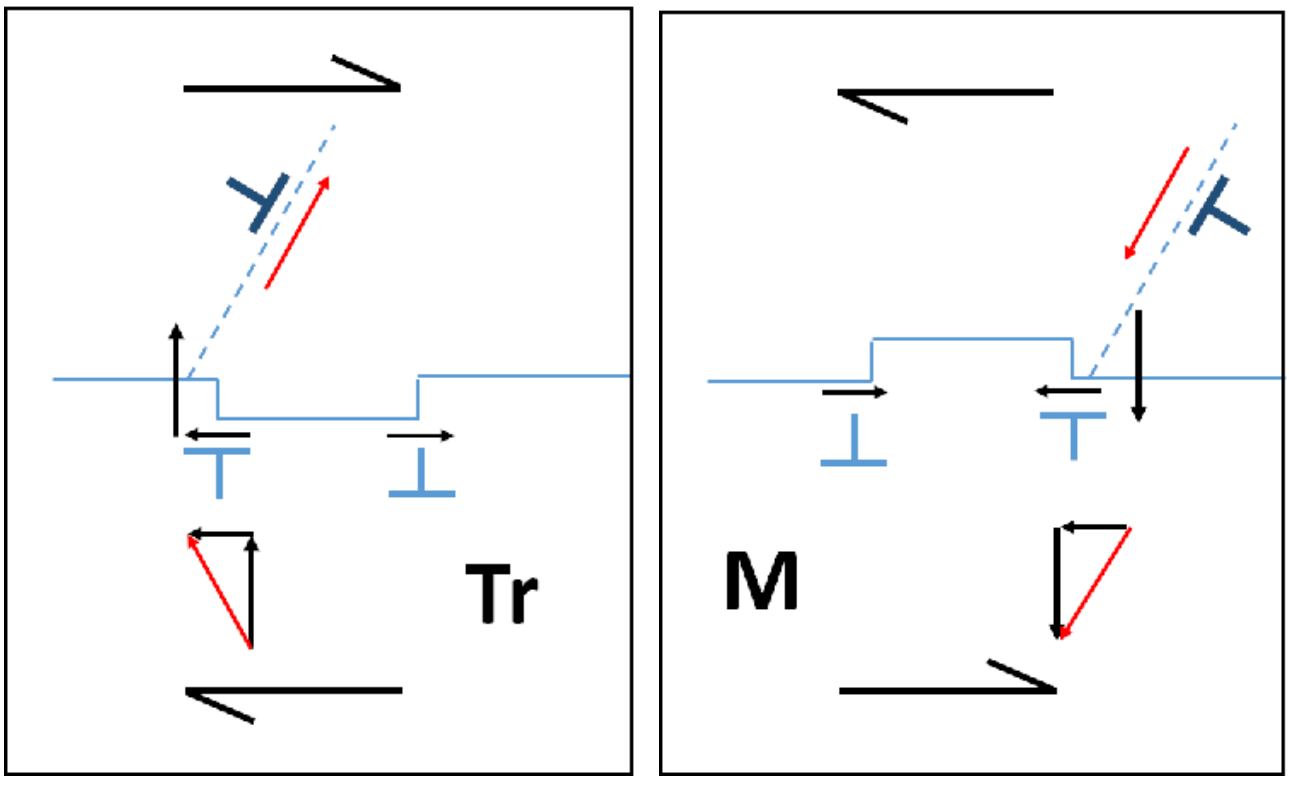

(a) (b)

Figure 5.2: Schematic showing the production of a EDisc dipole under external stress (big black arrows at the top and the bottom show the component parallel to the GB) leading to a transmission reaction (Tr) on a) and migration (M) of the GB on b). Red arrows indicate the Bvs of the incident and transmitted crystal dislocations and black arrows the Bv of EDisc and the GBD.

Although the atomic distribution at the intersection of neighboring glide planes with the GB are not identical (see red dashed lines A & B in Fig. 5.1) the transmission of dislocations occurs in both glide planes. The transmission occurs when the stress field of the DPU can supply the threshold shear stress in the vicinity of the GBD for the dipole to be created, as detailed in Table 5.1.

5.1.2 Interaction with a pileup of edge dislocations $\mathbf{b}_{-2/0}$

The Burgers vector of the $\mathbf{b}_{-2/0}$ dislocations is pointing towards the interface (upper red arrow in Fig. 5.2b). The heading dislocation of the pileup is absorbed by the GB according to the following reaction: $\frac{1}{2}[\bar{1}1\bar{1}]_\lambda = \frac{1}{3}[\bar{1}1\bar{2}]_\lambda + \frac{1}{6}[\bar{1}11]_\lambda$, written in coordinates of the upper crystal (λ). The EDisc ($\frac{1}{6}[\bar{1}11]_\lambda$) glides away and the GBD ($\frac{1}{3}[\bar{1}1\bar{2}]_\lambda$) does not step the GB.

Under the stress field of the trailing dislocations, a dipole of EDisc is created at the GB on the left side of the GBD, which is the tensile region of the trailing dislocations, as shown in Fig. 5.2b. Then, the Bv of the disconnection that approaches the GBD is $\frac{1}{6}[\bar{1}11]_\lambda$, and the reaction in this case is: $\frac{1}{3}[\bar{1}1\bar{2}]_\lambda + \frac{1}{6}[\bar{1}11]_\lambda = \frac{1}{2}[\bar{1}1\bar{1}]_\lambda = \mathbf{b}_{2/0}$. The resulting orientation of the Bv of the formed crystal dislocation is not favorable to the glide on the lower crystal and the result is the migration of the GB into the λ crystal against the DPU.

Fig. 5.2 shows that the reaction is controlled by the location of the created EDisc dipoles, which determines whether the dislocation could be transmitted or not. Since the creation of dipoles is stress dependent, the shear stress at both sites of the interaction region, corresponding to the tension and compression regions of the dislocation core were calculated. Table 5.1 shows the local shear stress parallel to the GB at each side of the interaction region for $\mathbf{b}_{2/0}$ and $\mathbf{b}_{-2/0}$, respectively, as shown in the schemes. Only the tension region experiences enough shear stress for the dipole to be created and the sense of the shear determines whether the dipole displaces the GB upwards or downwards. The local shear stresses for the $\mathbf{b}_{2/0}$ diminish slightly by increasing the temperature. The decreasing of stress is more pronounced for the $\mathbf{b}_{-2/0}$.

Table 5.1: Local shear stress at the reaction site necessary for triggering a reaction at the interface for the edge dislocations in Fe.

$\mathbf{b}_{2/0}$			
Temperature (K)	Compression region (MPa)	Tension region (MPa)	Scheme
300	795	-1385	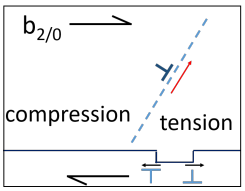
450	794	-1371	
600	789	-1353	
750	771	-1324	
900	730	-1323	
$\mathbf{b}_{-2/0}$			
Temperature (K)	Tension region (MPa)	Compression region (MPa)	Scheme
300	1524	-594	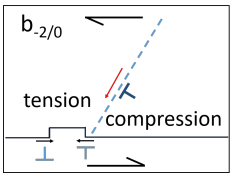
600	1202	-590	
900	1070	-543	

5.1.3 Interaction with a pileup of mixed dislocations $\mathbf{b}_{\pm 1/0}$

The mixed dislocations glide on the $(1\bar{1}0)$ plane that forms an angle of 125.26° with the GB. The Burgers vectors of the dislocations of the pileup are $\mathbf{b}_{-1/0} = \frac{1}{2}[\bar{1}\bar{1}\bar{1}]_\lambda$ and $\mathbf{b}_{1/0} = \frac{1}{2}[111]_\lambda$.

For the mixed dislocation, the phenomenology is much simpler than in the previous cases: there is only absorption of the first dislocation of the DPU. No other reactions were observed at any temperature up to the maximum stress applied. The reactions of the $\mathbf{b}_{1/0}$ and $\mathbf{b}_{-1/0}$, respectively, are described in the following equations and plotted schematically in Fig. 5.1:

$$\begin{aligned} \frac{1}{2}[111]_\lambda &= \frac{1}{3}[211]_\lambda + \frac{1}{6}[\bar{1}11]_\lambda, \\ \frac{1}{2}[\bar{1}\bar{1}\bar{1}]_\lambda &= \frac{1}{3}[\bar{2}\bar{1}\bar{1}]_\lambda + \frac{1}{6}[1\bar{1}\bar{1}]_\lambda \end{aligned} \tag{5.2}$$

where $\frac{1}{3}[211]_\lambda = \mathbf{b}_{2/1}$ and $\frac{1}{3}[\bar{2}\bar{1}\bar{1}]_\lambda = \mathbf{b}_{-2/-1}$ are disconnections that can be described as a sum of edge and screw parts: $\frac{1}{6}[1\bar{1}2]_\lambda + \frac{1}{2}[110]_\lambda$ and $\frac{1}{6}[\bar{1}1\bar{2}]_\lambda + \frac{1}{2}[\bar{1}\bar{1}0]_\lambda$, respectively.

5.1.4 Interaction under a shear stress parallel to the GB at 300 K

Our results show that slip transfer is directly controlled by the creation and propagation of EDisc, therefore, an applied shear stress parallel to the GB would optimize the production of dipoles of EDisc, and subsequently would reduce the applied stress necessary for the transmission reaction at the GB to take place. To check this hypothesis, an external shear stress parallel to the GB has been applied to a bicrystal at T = 300 K. The results prove that both, transmission and interface displacement, are produced at lower stresses ($\sim$ 300 MPa and $\sim$ -250 MPa in the compression region for $\mathbf{b}_{2/0}$ and $\mathbf{b}_{-2/0}$, respectively).

The measured reduction in the stress implies that the transmission of dislocations is more efficient and with the stress applied parallel to the GB for the $\mathbf{b}_{2/0}$ DPU, we observe the consecutive transmissions of every dislocation of the DPU (Fig. 5.3), while when the stress is applied along the glide plane, the level of stresses for the second and further dislocations to be transmitted was not reached within the maximum shear stress applied.

Fig. 5.3 shows the transmission of a pileup of five $\mathbf{b}_{2/0}$ dislocations under a shear parallel to the GB. In Fig. 5.3a, the first dislocation is at the GB and has been transformed first into a GBD ($\mathbf{b}_{1/-1}$) emitting an EDisc (shown in inset). Then, a dipole of EDiscs is created on the right of the GBD; the left EDisc is added to the GBD forming a dislocation of the lower crystal, while the right EDisc glides away (shown in inset). In Fig. 5.3b, the pileup of dislocations, except the last one which remains absorbed, has been transmitted and the remaining EDisc are piling up at the right fixed boundary of the simulated system.

For the mixed dislocation $\mathbf{b}_{1/0}$, the migration of the GB, by creation of EDisc dipoles, occurs before the DPU reaches the GB. As a consequence, the DPU follows the GB on its displacement. Therefore, the accommodation of the plastic deformation is produced by the displacement of the GB and the coordinated glide of the DPU. Since the sense of stress should be reversed if the $\mathbf{b}_{-1/0}$ DPU has to approach the GB, the sense of the displacement of the GB itself is reversed. Therefore, the GB moves against the DPU inducing the absorption of the first dislocation and creating a $\mathbf{b}_{-2/-1}$ disconnection. Increasing the shear stress allows the absorption of the second dislocation. Eventually, the transmission of two mixed dislocations of ⟨100⟩ and ½⟨111⟩ type is favored.

All these results prove that our initial guess was correct, an applied shear stress parallel to the GB enhances the creation of EDisc dipoles and therefore facilitates the interactions of the dislocations at the GB.

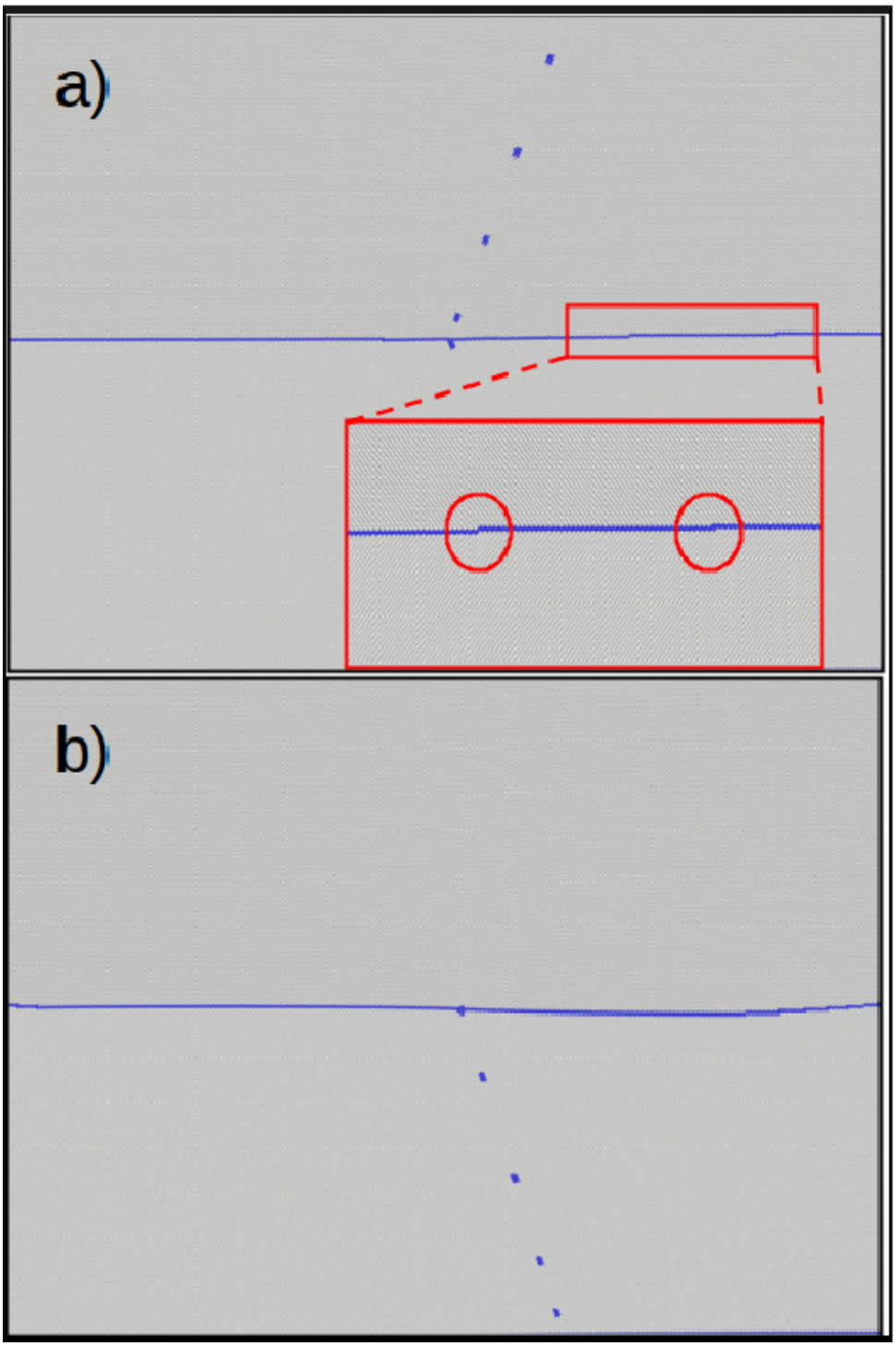

Figure 5.3: Interaction of a pileup of edge dislocations with the $(1\bar{1}2)$ GB. a) Interaction of the first dislocation. Enlarged image: detail of EDisc emitted during the interaction. b) Transmitted pileup of dislocations. The remaining EDisc are piling up at the right fixed boundary of the simulated system.

5.1.5 Interaction in Chromium and Tungsten

As the previous Sections show, a proper description of the GB – DPU interaction requires a careful analysis of the reactions taking place on the interface. The reaction presented above depend on crystallographic parameters such as the atomic structure of the interface and the Bv of the dislocations but, as well, on the stress field that controls the distance between dislocations and the threshold stress necessary to create the dipoles of EDisc. Whereas the former conditions are related to the bcc structure, the latter condition is material dependent.

The interaction of a pileup of $\mathbf{b}_{2/0}$ and $\mathbf{b}_{-2/0}$ dislocations in chromium follows exactly the same pattern as in iron: there is transmission of the dislocations for the $\mathbf{b}_{2/0}$ DPU and shear-coupled GB migration for the $\mathbf{b}_{-2/0}$. Table 5.2 presents the local shear stresses parallel to the GB at each side of the interaction region necessary to initiate the reaction, it shows the same tendency as the stresses in Table 5.1.

Table 5.2: Local shear stress at the reaction site necessary for triggering a reaction at the interface for the edge dislocations in Cr.

$\mathbf{b}_{2/0}$		
Tempe-rature (K)	Compression region (MPa)	Tension region (MPa)
300	693	-1543
600	681	-1502
900	646	-1419
$\mathbf{b}_{-2/0}$		
Tempe-rature (K)	Tension region (MPa)	Compression region (MPa)
300	1399	-549
600	1309	-521
900	825	-426

On the other hand, the features of the interaction in tungsten are noticeably different, becoming a good example on the influence of elastic constants. For this metal, the distance between the first and second dislocation of the DPU is higher than in the other two metals for the same stress applied. This influences the stress field at the interaction region of the GB. For the interaction of the $\mathbf{b}_{2/0}$ DPU, the second dislocation is far from the GBD created by the heading dislocation and the dipole at the tensile site of the DPU is not created; the GBD acts as a source of single EDiscs, which are responsible for the shear-coupled migration of the GB. No transmission occurs and the trailing dislocations follow the GB in the displacement. Table 5.3 presents the shear stress necessary for the initiation of the migration of the GB in tungsten as a function of temperature due to both, $\mathbf{b}_{2/0}$ and $\mathbf{b}_{-2/0}$ DPUs.

Table 5.3: Local shear stress at the reaction site necessary for triggering a reaction at the interface for the edge dislocations in W.

$\mathbf{b}_{2/0}$		
Tempe-rature (K)	Compression region (MPa)	Tension region (MPa)
300	1104	-1733
600	1063	-1575
900	921	-1481
$\mathbf{b}_{-2/0}$		
Tempe-rature (K)	Tension region (MPa)	Compression region (MPa)
300	2371	-896
600	2104	-820
900	1806	-650

In order to change the distance between dislocations, looking for a possible transmission, the applied stress in $\mathbf{b}_{2/0}$ DPU along the glide plane was increased up to 3.7 GPa at 300 K. Then, the second dislocation reacted with the GBD originated by the heading dislocation. The reaction is:

$$\begin{aligned} \mathbf{b}_{1/-1} + \mathbf{b}_{2/0} &= \frac{1}{3}[1\bar{1}2]_\lambda + \frac{1}{2}[1\bar{1}1]_\lambda = ... \\ ... &= 3\frac{1}{6}[1\bar{1}\bar{1}]_\lambda + [001]_\lambda + \frac{1}{3}[1\bar{1}2]_\lambda = ... \\ ... &= 3\mathbf{b}_{1/1} + \mathbf{b}_{2/0} + \mathbf{b}_{-2/-4} \end{aligned} \tag{5.3}$$

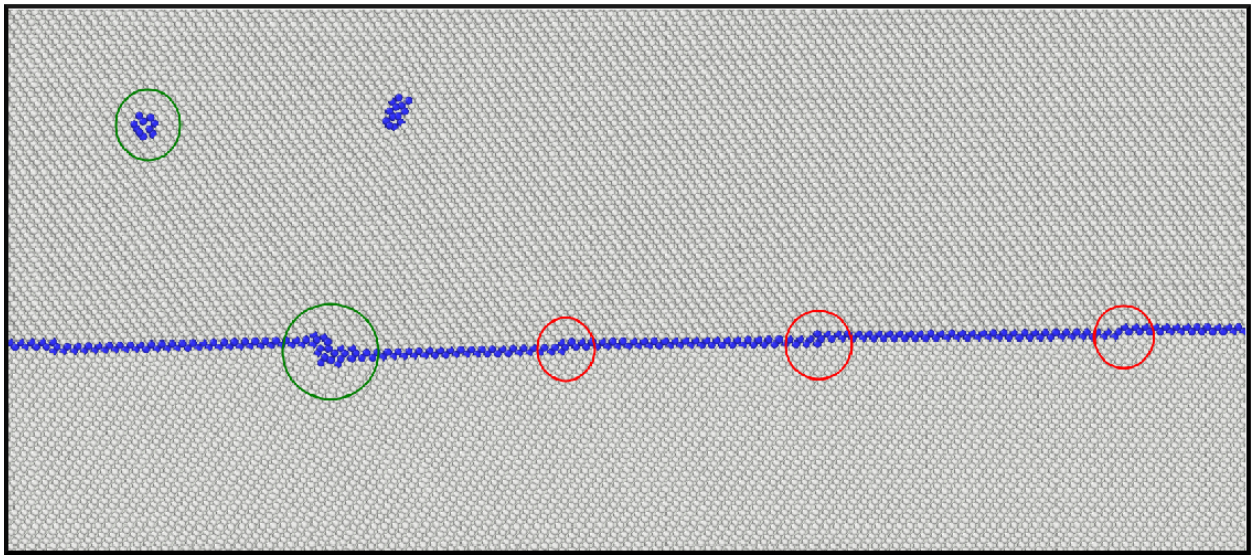

Figure 5.4: Snapshot of the interaction of the $\mathbf{b}_{2/0}$ DPU with the {112} GB in W at T = 300 K. Defects are indicated with circles: red for EDiscs, green for $\mathbf{b}_{-2/-4}$ GBD and $\mathbf{b}_{2/0}$ reflected dislocation.

The result is the reflection of a new crystal dislocation (green circle in Fig. 5.4); no other mechanisms to accommodate the deformation and stress are observed, besides GB migration.

From the comparison of the results obtained on each bcc metal we have reached the conclusion that the final process depends on the balance between two factors: the stress necessary to approach two edge dislocations and the stress necessary to create a dipole of EDisc at the GB, i.e., which distribution and level of stresses occurs first.

5.1.6 Dislocation pileup - twin interaction

The comparison of the results presented in subsections 5.1.1 and 5.1.2 clearly shows that the result of the interaction of a pileup of ½⟨111⟩ dislocations with the {112} interface depends on the orientation and sense of the Burgers vector. This dependency extends, consequently, to the interaction of a pileup of dislocations with a {112} twin. In the following, we consider a twin in Fe consisting of two parallel coherent {112} boundaries with a variable width. By using the same simulation setup of subsection 5.1.4 5.1.4 shear strain increments are applied in a direction parallel to the twin followed by the energy minimization of the system.

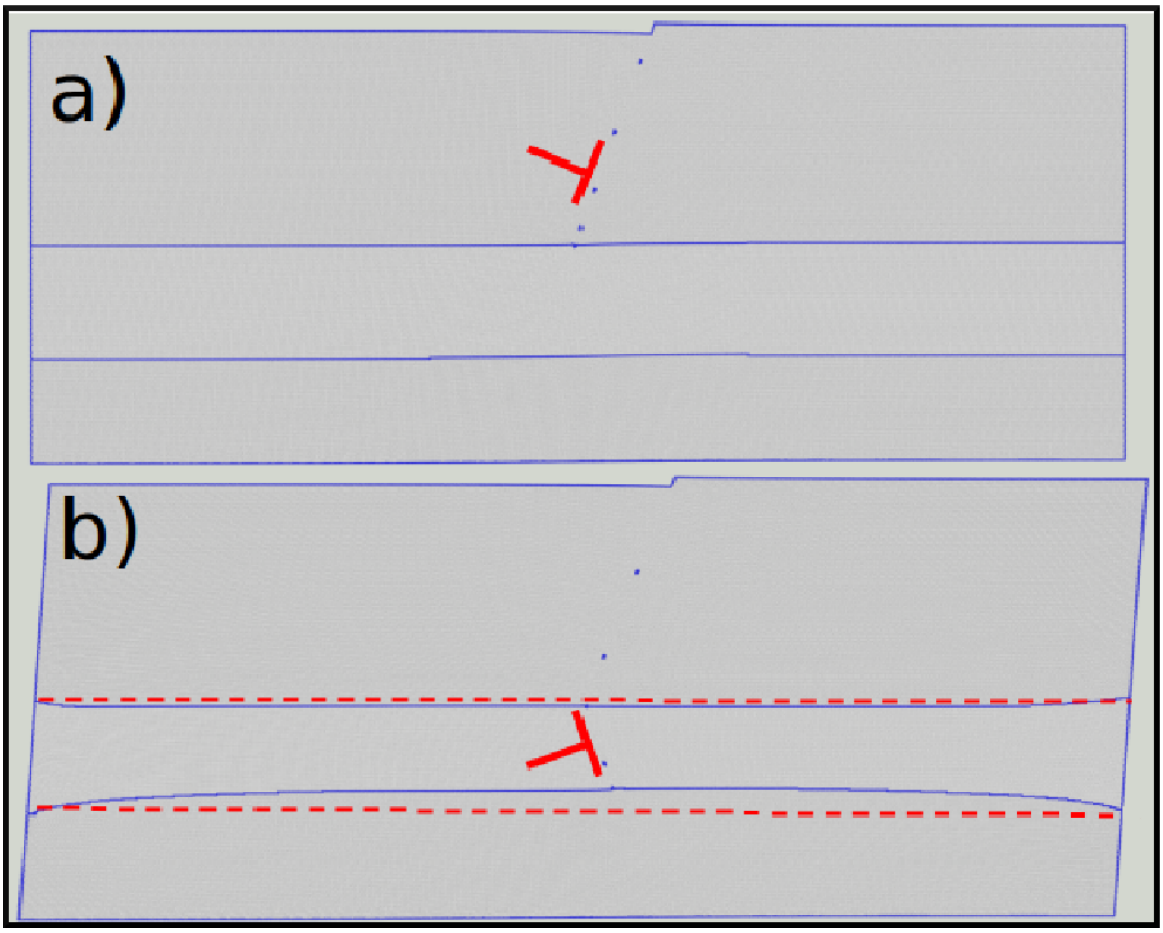

Figure 5.5: Snapshots of the interaction of the $\mathbf{b}_{2/0}$ DPU with the $(1\bar{1}2)$ twin of 14 nm thickness in Fe. a) The first dislocation has been absorbed by the upper twin boundary (TB1) producing a $\mathbf{b}_{1/-1}$ TBD. b) The first and the second dislocations of the DPU have been transmitted inside the twin and the former has already been absorbed by the lower twin boundary (TB2) producing another $\mathbf{b}_{1/-1}$ TBD. Red dashed horizontal lines show the initial thickness of the twin for the sake of comparison.

Fig. 5.5 shows the interaction of a $\mathbf{b}_{2/0}$ DPU with a {112} twin with a thickness of 14 nm, i.e., large enough so that the lower TB (TB2) does not affect the interaction at the upper TB (TB1). Since the tensile region of the dislocations is closer to the TB1, the DPU is transmitted into the twin. However, the transmitted dislocations inside the twin have an orientation as $\mathbf{b}_{-2/0}$ with respect to TB2, i.e., the compression region is closer to the TB and therefore the dislocation is not transmitted. Instead, the heading dislocation is absorbed by the TB2 and it is transformed into a TBD that creates pairs of EDisc that displace the TB upwards. The number of dislocations entering into the twin is a function of the width of the twin. The n dislocations inside the twin are stopped by the repulsion of the TBD in TB2. The $(n+1)$th dislocation of the DPU remains at the TB1 emitting few EDisc that move the TB1 down. Altogether, the interaction slip-twin diminishes the width of the twin and accumulates n dislocations inside the twin. Thus, although there is a favorable case for the DPU be transmitted into the twin, the dislocations cannot come out of it. Therefore, the twin is a barrier for the slip of dislocations.

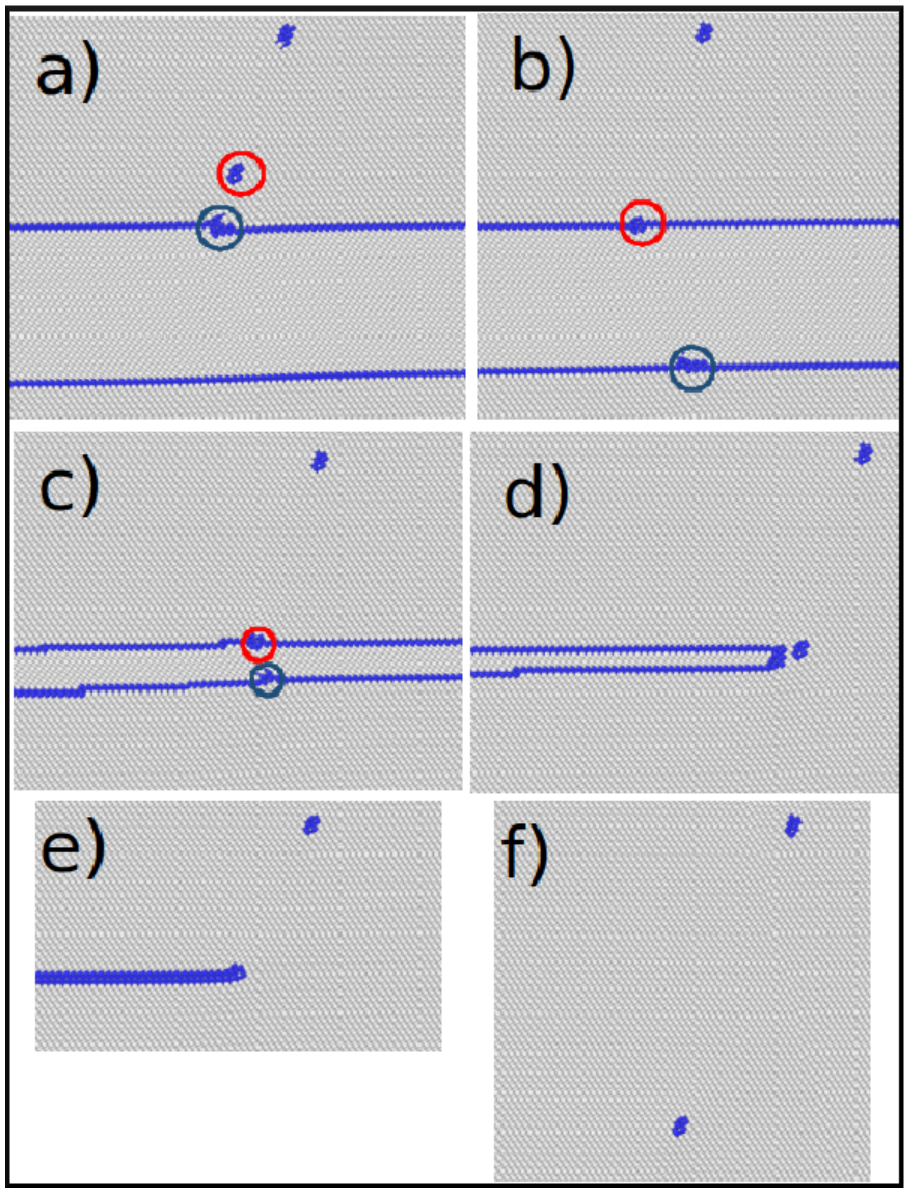

Figure 5.6: Snapshots of the interaction of the pileup of $\mathbf{b}_{2/0}$ edge dislocations with the $(1\bar{1}2)$ twin of 4.2 nm thickness in Fe. a) The absorption of the first dislocation of the DPU by the upper twin boundary (TB1) produces a $\mathbf{b}_{1/-1}$ TBD (green circle) with the second dislocation in close proximity (red circle). b) After the transmission of the first dislocation to the twin it glides up to TB2 where it is absorbed likewise the second dislocation is absorbed by TB1. In both interfaces a $\mathbf{b}_{1/-1}$ TBD is produced as a result. (red and green circles) c), d), e) and f) The emission of EDisc dipoles in TB1 and TB2 by the TBDs leads to a progressive reduction of twin thickness up to the total annihilation of the twin.

By diminishing the thickness of the twin into the interval 36-48 (112) planes, the number of transmitted dislocations is reduced to $n = 1$. Then, there is a TBD in the TB2, a dislocation absorbed by the TB1 and no dislocations inside the twin as shown in Fig. 5.6b. While TB1 emits only few EDisc, the TBD in TB2 is a profuse source of EDisc that displace upwards TB2 up to the total annihilation of the twin.

If the thickness of the twin is smaller than 36 planes, the TB2 influences the interaction of the dislocation with the TB1 and there is no transmission of the heading dislocation, that remains in the TB1. The stress field created by the dislocation triggers the creation of dipoles of EDiscs in the TB2 (as shown in Fig. 4.2e of ref. [57]) that displace the TB2 upwards.

Therefore, for twins with thickness smaller than 48 planes (5.6 nm), the twin is annihilated and

the dislocation pileup glides freely in the matrix. There is softening of the material.

If the pileup of dislocations is of $\mathbf{b}_{-2/0}$ type, for the interaction to occur the sense of the stress is reversed. Then, the leading dislocation approaches the TB1 and it is absorbed and transformed into a TBD. In this case, the generation of disconnections displaces the TB1 upwards against the trailing dislocations, which increases the local stress that, in turn, triggers the creation of EDisc dipoles in the TB2 that displace the TB2 downwards. Thus, the width of the twin increases. All together it represents a strong obstacle for the slip of the pileup, as for the interaction with the {112} GB described above.

Given the interesting results obtained in Fe, we decided to analyze the interaction for Cr and W as well. The conclusion is that the outcome of the DPU – twin interaction is the same for all three metals. Even in the interaction of $\mathbf{b}_{2/0}$ in W, where the dislocations do not penetrate into the twin, they are stopped by the twin boundary that results in a strong obstacle.

5.1.7 Discussion

Under an applied shear stress, a single ½⟨111⟩ dislocation is absorbed by the {112} tilt GB being transformed into a GBD that acts as a source of disconnections mediating the shear-coupled migration of the GB. No transmission of the dislocation to the next grain occurs. This scenario changes when a pileup of dislocations interacts with the GB. The reason behind this change is the local stress field at the interaction region of the heading dislocation with the GB induced by the trailing dislocations. When the tensile region around the dislocations is closer to the GB than the compression region, then transmission takes place ($\mathbf{b}_{2/0}$ dislocation, Fig. 5.2a). Otherwise, the heading dislocation cannot be transmitted and it behaves as the single $\mathbf{b}_{-2/0}$ dislocation, i.e., the absorbed dislocation is transformed into a GBD that mediates the shear-coupled migration. A closer look to this different behavior reveals that the key lies on the location at the GB where the disconnection dipoles are created under the stress field of the trailing dislocations, as shown in Figs. 5.2a and 5.2b. In this way, dislocations with the same orientation of the Burgers vectors but opposite signs perform different interactions. In $\mathbf{b}_{2/0}$ case, the plastic deformation is accommodated by slip transfer through the GB, while for the $\mathbf{b}_{-2/0}$ case by shear-coupled GB migration. This mechanism for accommodation of plastic deformation by slip transfer of the $\mathbf{b}_{2/0}$ and the $\mathbf{b}_{-1/0}$ dislocations is more efficient since it is activated at a lower external shear stress. The shear-coupled migration of the GB, related to the $\mathbf{b}_{-2/0}$ and $\mathbf{b}_{1/0}$, is produced against the motion of the dislocation pileup and therefore the local stresses accumulated at the interaction region are high.

The above-described behavior is the basis for the understanding the slip-twin interaction. The interaction depends on the incident Burgers vector of the pileup but, in any case, there is no transmission across the twin. This is because the dislocations transmitted across the first TB ($\mathbf{b}_{2/0}$), under a shear in the anti-twinning direction, have an orientation like $\mathbf{b}_{-2/0}$ with respect to the second TB, therefore they cannot be transmitted back to the matrix. Huang et al. [118] have reported the same confinement of the dislocations inside a twin in a nanoindentation experiment performed by MD in bcc Tantalum. Reversing the sense of the shear into the twinning direction would approach the $\mathbf{b}_{-2/0}$ dislocation to the twin and it would not be even transmitted into the twin.

The stress field at the TBs generated by the interacting dislocations enhances the creation of gliding disconnection dipoles at the TBs that displace the TBs either towards each other ($\mathbf{b}_{2/0}$) decreasing the width of the twin or apart from each other ($\mathbf{b}_{-2/0}$) increasing the width of the twin. In the former case, if a maximum of one dislocation from the pileup is transmitted into the twin, the two coherent twin boundaries annihilate and release the dislocation. As a result, the pileup of dislocations removes any thin twin encountered along its glide plane contributing to the softening of the material. In any other case, twins block the propagation of dislocations confining them inside the twin, contributing to hardening.

Summarizing all the results obtained we can conclude that twins represent a strong obstacle for the glide of a pileup of ½⟨111⟩ dislocations in two cases: i) when the applied shear is in the twinning direction; ii) when the applied shear is in the anti-twinning direction and the thickness of the twin is larger than about 48 (112) planes (5.6 nm in Fe).

5.2 {332} GB. Formation of new interfaces

The comparison between the results of Sections 4.1 and 4.2 anticipates a more complex picture to describe the interaction between the {332} GB and a pileup of dislocations than for the {112} GB. For a single dislocation we have found only one type of reaction with this GB: absorption. However, the GBD produced in each reaction is different, depending directly on many factors (glide plane inclination, Bv orientation, edge or mixed character of dislocations). Some of these GBDs are glissile and can move together with the GB in a compensated climb, while others are sessile, acting as stress accumulators and becoming the nuclei of {112} twins. In the present Section, we analyze for the very same set of cases investigated in Section 4.2, the mechanisms involved on the interaction between a pileup and the {332} GB. Once again, we pay special attention to the behavior under shear stress of the GBDs produced during the interactions. All the results presented below have been published in [75].

Analogous to the {112} GB, the study is mainly focused on bcc Fe but to ascertain the influence of the interatomic forces on the different processes studied, we extend it to another two bcc metals, namely Cr and W. As it is shown, qualitatively the mechanisms and processes described are exactly the same for all three metals. For that reason and for the sake of brevity and clearness, we present in detail the results for Fe, compiling the results for Cr and W in Tables 5.4 and 5.5.

In the {332}⟨110⟩ tilt GB, the only reaction observed has been the absorption of pileup dislocations. The absorption resulted in the transformation of crystal dislocations into GBDs with core riser (riser hereafter) and several elementary disconnections, $\mathbf{b}_{\pm 2/\pm 2}$ (vectors #2 and #3 in Fig. 5.7), that step the GB two planes either upwards or downwards, depending on the reaction $\mathbf{b}_{Xtal} = \mathbf{b}_{riser} + N\mathbf{b}_{\pm 2/\pm 2}$. The reaction is not unique and it is only restricted by the two conditions applicable to any GB – dislocation interaction. On the one hand, the reaction follows the conservation of Bv and, on the other hand, the GB defects are defined by the difference of broken symmetries of the crystals that form the interface [81, 119]. These two conditions can be visualized in the dichromatic pattern presented in Figs. 5.7, 5.9 & 5.12. The position of the Bv of GBDs relative to the common {332} plane indicates the step height of the GBDs. In the DP of Fig. 5.7 the λ crystal (white) includes the Bvs of the crystal dislocations that are studied. They are numbered as follows: 1 and 4 are edge dislocations and 5 and 6 are mixed dislocations (notice they link lattice sites of the white crystal). The vectors 2 and 3 are elementary disconnections. The figure shows only one direction of the Bv for convenience. Following the notation introduced in [42], we denote them as: 1 = $\mathbf{b}_{-2/0}$ ($\mathbf{b}_{2/0}$ for the reversed Bv); 2 = $\mathbf{b}_{2/2}$; 3 = $\mathbf{b}_{-2/-2}$; 4 = $\mathbf{b}_{-4/0}$ ($\mathbf{b}_{4/0}$ for the reversed Bv); 5 = 6 = $\mathbf{b}_{-1/0}$ ($\mathbf{b}_{1/0}$ for the reversed Bv). The Bvs of the mixed dislocations 5&6 differ in the sign of the screw part, which does not contribute to step the GB. The vectors $\mathbf{b}_{2/2} = \frac{1}{22}[\bar{1}\,1\,\bar{3}]$ and $\mathbf{b}_{-2/-2} = \frac{1}{22}[1\bar{1}3]$ are the shortest in the DP and correspond to the elementary disconnections responsible for the displacement of the GB by gliding along it [51].

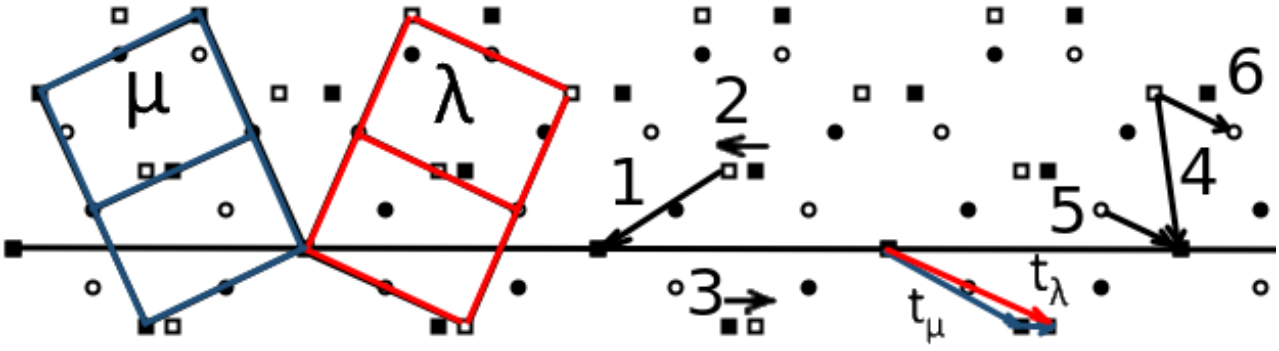

Figure 5.7: Dichromatic pattern of {332} GB. White sites (upper grain), black sites (lower grain). Bv of crystal dislocations: edge = 1 and 4; mixed = 5 and 6. Elementary disconnections: 2 and 3 stepping the interface up and down, respectively. Red and blue vectors are translation vectors of λ and μ crystals: their difference is $\mathbf{b}_{-2/-2}$. The unit cells of both crystals are included.

Considering the pileup of edge dislocations gliding along {112} planes, there are two possible glide plane inclinations, namely, inclined to the GB at 29.5 degrees ($\mathbf{b}_{-2/0}$; $\mathbf{b}_{2/0}$) and inclined at 100.02 degrees ($\mathbf{b}_{-4/0}$; $\mathbf{b}_{4/0}$). The third dislocation has mixed character and approaches the GB along a {110} glide plane inclined 154.76 degrees ($\mathbf{b}_{-1/0}$; $\mathbf{b}_{1/0}$). For each glide plane inclination, two dislocations with opposite sense of the Burgers vectors are considered because the interaction of the GB with the first dislocation of the pileup is a function of the sense of the Bv.

Like GBDs at the {112} interface, the GBDs at the {332} interface can act as a source of disconnections [57] under certain conditions, as detailed below. The evolution of the Bv of the risers depends on the number of dislocations of the pileup that are absorbed.

We describe the observed interaction mechanisms, as they were visualized using OVITO software [103]. The reaction mechanism was studied by inspecting atomic configurations at each strain increment. The following subsections detail the specificities of the interaction between the DPU and the interface for the possible senses of the Burgers vector. It is shown how the outcome of the reactions involved is strongly dependent on the sense of Bv.

5.2.1 Interaction with a pileup of edge dislocations $\mathbf{b}_{2/0}$

The Burgers vector of the edge dislocations of the pileup is $\mathbf{b}_{2/0} = \frac{1}{2}[1\bar{1}1]$. Fig. 5.8 shows the interaction of the GB with three dislocations of a pileup at 300 K in Fe. The first dislocation is attracted by the GB and is absorbed as shown in Fig. 5.8a (notice the second dislocation of the pileup at the upper right corner of the figure).

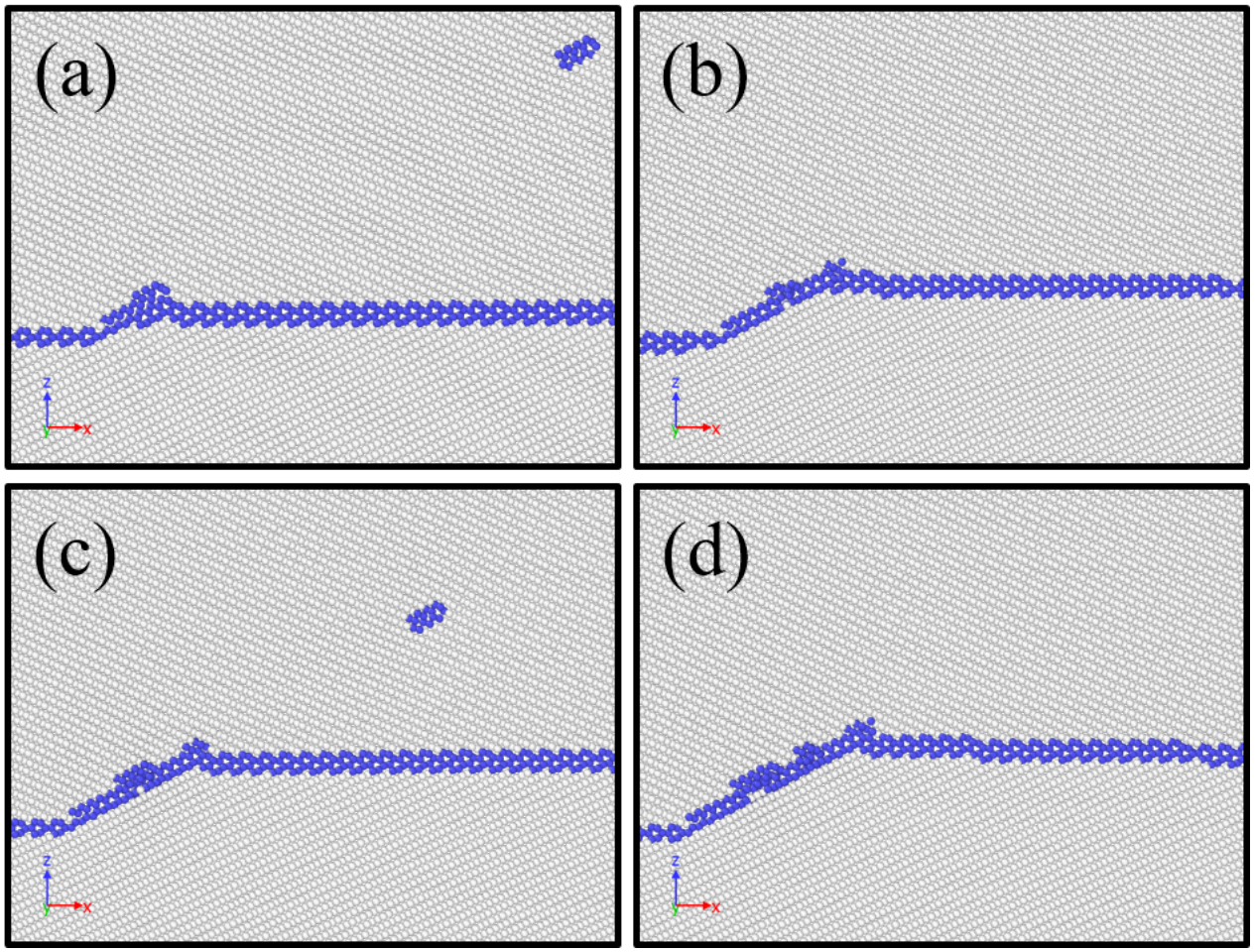

Figure 5.8: Snapshots of the interaction of the DPU with the {332} GB in Fe at T = 300 K: a) after the absorption of the first dislocation of the pileup; b) after the absorption of the second dislocation; c) before the absorption of the third dislocation; d) after the absorption of the third dislocation.

In the reaction it is formed a GBD with a stepping up riser along the $(\bar{1}12)_\lambda$ (glide plane of the pileup) in the upper grain and the $(1\bar{1}0)_\mu$ plane in the lower grain. In this reaction, four $\mathbf{b}_{-2/-2}$ are emitted stepping down the GB and run away under the local stress. This reaction can be described as:

$$\mathbf{b}_{2/0} = \mathbf{b}_{10/8} + 4\mathbf{b}_{-2/-2} \tag{5.4}$$

where $\mathbf{b}_{10/8}$ is the Bv of the riser shown in the DP of Fig. 5.9a as #2; this vector goes from the 8th plane of the black crystal to the 10th plane of the white crystal. The sum of vectors is marked by a green circle.

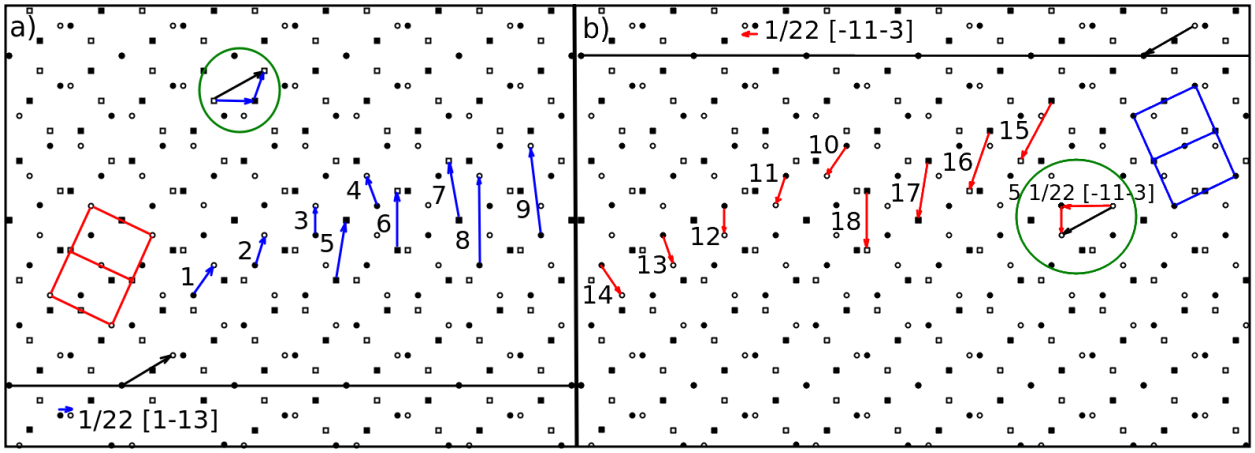

Figure 5.9: Dichromatic pattern with possible Bvs of GBDs with core riser for a different number of absorbed dislocations $\mathbf{b}_{2/0}$ (a) and $\mathbf{b}_{-2/0}$ (b). Black horizontal lines indicate the GB. Black arrows are Bvs of pileup dislocations. Arrows from black to white sites are Bvs of GB defects. Examples of reactions (green circles) are shown for #2 (a) and #12 (b).

Then, under an increase of the applied stress, the second and third dislocations are absorbed. The Bvs of the risers for each absorption are depicted and numbered in the DP of Fig. 5.9a. The reactions observed on the three metals are detailed in Table 5.4, where the Bv of the reaction, the accumulated number of disconnections emitted after each reaction and the number assigned in the DP are presented together with the local shear stress necessary for the absorption of the dislocation.

Some remarks: The Bv number 7 in Table 5.4, corresponding to tungsten, is $\frac{1}{2}[1\bar{1}\,\bar{1}]$. Although it is a lattice vector, it is not the Bv of a crystal dislocation, because it is attached to the GB, it is the Bv of a GBD and is restricted to stay at the GB. The balance of Bv is indicated in the equation:

$$2\mathbf{b}_{2/0} = \mathbf{b}_{26/22} + 11\mathbf{b}_{-2/-2} \tag{5.5}$$

The indexes indicate that this riser is 26 planes of λ above the GB. In order to reduce the dimensions of Fig. 5.9, vectors 5, 6 and 7 have been shifted down by 11 planes (notice they are linked to square symbols) and vectors 8 and 9 have been shifted down by 22 planes (the periodicity of the coincident site lattice (CSL) along the z direction).

The calculation of the Bv of the riser is performed in the standard way (Burgers circuit) and is double-checked by calculating it as the difference of the initial crystal dislocation and the produced elementary disconnections. The decomposition of the Bv of the bulk dislocation is not unique; the reactions numbered from 1 to 4 in the DP of Fig. 5.9a are possible decompositions of the crystal dislocation that differ in the number of disconnections emitted. This is evidenced in Table 5.4 where the decomposition of the same Bv results in different number of elementary disconnections depending on the temperature and material.

As the reaction progresses and more dislocations get absorbed, the Bv of the riser evolves and its length increases. The labels from “5” to “7” indicated in the DP of Fig. 5.9a correspond to two

absorbed crystal dislocations and labels "8" and "9" correspond to three absorbed crystal dislocations.

The maximum strain applied in all simulations has been the same for all materials and temperatures considered in this study, even though, the total number of absorbed dislocations varies from two (in W) to three (in Fe and Cr).

Comparing the results of the absorption of each dislocation for the three temperatures studied we conclude that the mechanism of absorption of the pileup of dislocations by the {332} GB is independent of the temperature and material. For instance, the length of the riser after the absorption of the third dislocation in Fe is the same for all temperatures. This is because the total number of disconnections emitted is the same and consequently the Bv of the GBD associated to this riser is the same at the end of the full process, i.e., $\mathbf{b}_{38/32} = \frac{1}{22}[17\bar{1}7\,1\bar{5}]$

Although there is a unique mechanism for all materials and temperatures, the stress needed for the absorption of each dislocation is temperature dependent. Fig. 5.10 shows the shear stress, measured locally within the interaction region (#2 in Fig. 2.3), necessary for the absorption of the dislocations for Fe (Fig. 5.10a) and Cr (Fig. 5.10b). In the case of $\mathbf{b}_{2/0}$, only the stress necessary for the reaction with the second and third dislocations are plotted because the first dislocation is attracted and spontaneously absorbed by the GB. As expected, the stress increases with the number of dislocations absorbed but for a given dislocation of the pileup there is a decrease of stress with increasing temperature, common for the three metals studied. This indicates that the process is thermally enhanced. For $\mathbf{b}_{-2/0}$, described below, the stress necessary for the first dislocation of the pileup to overcome the repulsion of the GB is included in Fig. 5.10 and Table 5.5.

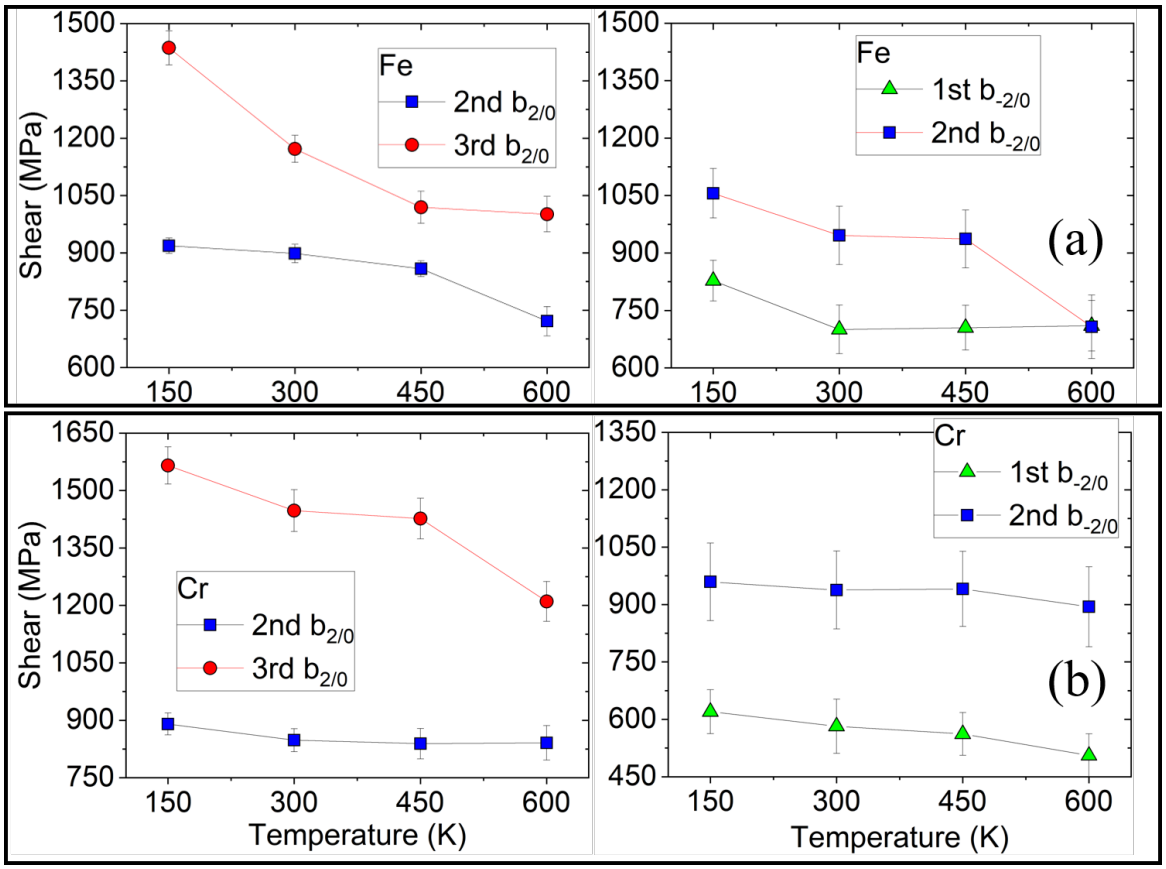

Figure 5.10: Shear stress, measured in the interaction region #2, for the absorption of the pileup dislocations $\mathbf{b}_{2/0}$ and $\mathbf{b}_{-2/0}$ vs temperature for Fe (a) and Cr (b).

5.2.2 Interaction with a pileup of edge dislocations $\mathbf{b}_{-2/0}$

In this subsection we consider the complementary case, when the Bv of the dislocations points towards the GB ($\mathbf{b}_{-2/0} = \frac{1}{2}[\bar{1}\,1\,\bar{1}]$); in this case the Bv of the elementary disconnections formed is $\mathbf{b}_{2/2} =$

Table 5.4: Products of the reactions of $\mathbf{b}_{2/0}$ at 29.5 degrees. N absorbed is number of absorbed crystal dislocations; T is the temperature (K); Bv is the Burgers vector of formed GBD with core riser; el. disc: number of accumulated $\mathbf{b}_{-2/-2}$; ID React.: Identification of GBDs Bv in Fig. 5.9a and Shear is the local shear stress necessary for the absorption (MPa).

N absorbed		1				2				3			
Mater.	T	Bv	EDisc	ID React.	Shear	Bv	EDisc	ID React.	Shear	Bv	EDisc	ID React.	Shear
Fe	150	$^1/_{11}[4\bar{4}\,1]$	3	1	-	$^2/_{11}[3\bar{3}\,\bar{2}]$	3+7=10	6	919	$^1/_{22}[17\bar{1}\,\bar{7}\,\bar{1}\,\bar{5}]$	3+7+6=16	9	1436
	300	$^1/_{22}[7\bar{7}\,\bar{1}]$	4	2	-	$^1/_{22}[13\bar{1}\,\bar{3}\,\bar{5}]$	4+5=9	5	898	$^1/_{22}[17\bar{1}\,\bar{7}\,\bar{1}\,\bar{5}]$	4+5+7=16	9	1172
	450	$^1/_{11}[4\bar{4}1]$	3	1	-	$^1/_{22}[13\bar{1}\,\bar{3}\,\bar{5}]$	3+6=9	5	858	$^1/_{22}[17\bar{1}\,\bar{7}\,\bar{1}\,\bar{5}]$	3+6+7=16	9	1019
	600	$^1/_{22}[7\bar{7}\,\bar{1}]$	4	2	-	$^1/_{22}[13\bar{1}\,\bar{3}\,\bar{5}]$	4+5=9	5	721	$^1/_{22}[17\bar{1}\,\bar{7}\,\bar{1}\,\bar{5}]$	4+5+7=16	9	1001
Cr	150	$^1/_{11}[3\bar{3}\,\bar{2}]$	5	3	-	$^2/_{11}[3\bar{3}\,\bar{2}]$	5+5=10	6	890	$^1/_{22}[17\bar{1}\,\bar{7}\,\bar{1}\,\bar{5}]$	5+5+6=16	9	1565
	300	$^1/_{11}[3\bar{3}\,\bar{2}]$	5	3	-	$^2/_{11}[3\bar{3}\,\bar{2}]$	5+5=10	6	848	$^1/_{22}[17\bar{1}\,\bar{7}\,\bar{1}\,\bar{5}]$	5+5+6=16	9	1447
	450	$^1/_{11}[3\bar{3}\,\bar{2}]$	5	3	-	$^2/_{11}[3\bar{3}\,\bar{2}]$	5+5=10	6	839	$^3/_{11}[3\bar{3}\,\bar{2}]$	5+5+5=15	8	1427
	600	$^1/_{11}[3\bar{3}\,\bar{2}]$	5	3	-	$^2/_{11}[3\bar{3}\,\bar{2}]$	5+5=10	6	841	$^3/_{11}[3\bar{3}\,\bar{2}]$	5+5+5=15	8	1210
W	150	$^1/_{11}[3\bar{3}\,\bar{2}]$	5	3	-	$^1/_2[1\bar{1}\,\bar{1}]$	5+6=11	7	2026	-	-	-	-
	300	$^1/_{22}[7\bar{7}\,\bar{1}]$	4	2	-	$^1/_2[1\bar{1}\,\bar{1}]$	4+7=11	7	1918	-	-	-	-
	450	$^1/_{22}[5\bar{5}\,\bar{7}]$	6	4	-	$^1/_2[1\bar{1}\,\bar{1}]$	6+5=11	7	1276	-	-	-	-
	600	$^1/_{11}[3\bar{3}\,\bar{2}]$	5	3	-	$^1/_2[1\bar{1}\,\bar{1}]$	5+6=11	7	1352	-	-	-	-

$\frac{1}{22}[\bar{1}\,1\bar{3}]$. The first relevant difference with the previous result is that there is no spontaneous absorption of the first dislocation because its interaction with the GB is repulsive.

Fig. 5.11 shows the detail of the interaction of the GB with the first two dislocations of a pileup at 300 K in Fe. For the same total shear stress that was applied to the system for $\mathbf{b}_{2/0}$, the GB absorbs only two dislocations of the pileup. The essential difference with the $\mathbf{b}_{2/0}$ interaction is the orientation of the riser of the formed GBD; it is formed by the $(1\bar{1}\,0)_\lambda$ plane in the upper grain and $(\bar{1}\,12)_\mu$ plane in the lower grain. Now, the angle between the riser and the glide plane of pileup dislocations is bigger than 90 degrees impeding any possible glide of the pileup along it. So, after the absorption of two dislocations, the maximum external stress cannot overcome the repulsion between the third pileup dislocation and the GBD.

Table 5.5: Products of the reactions of $\mathbf{b}_{-2/0}$ at 29.5 degrees. N absorbed is number of absorbed crystal dislocations; T is the temperature (K); Bv is the Burgers vector of formed GBD with core riser; EDisc: number of accumulated $\mathbf{b}_{2/2}$; ID React.: Identification of GBDs Bv in Fig. 5.9a and Shear is the local shear stress necessary for the absorption (MPa).

N absorbed		1				2			
Material	T	Bv	EDisc	ID React.	Shear	Bv	EDisc	ID React.	Shear
Fe	150	$^1/_{11}[\bar{3}32]$	5	12	828	$^1/_{11}[\bar{7}71]$	5+3=8	16	1056
	300	$^1/_{22}[\bar{2}25]$	7	14	700	$^2/_{11}[\bar{3}32]$	7+3=10	18	946
	450	$^1/_{22}[\bar{5}57]$	6	13	705	$^1/_{11}[\bar{7}71]$	6+2=8	16	937
	600	$^1/_{22}[\bar{5}57]$	6	13	710	$^2/_{11}[\bar{3}32]$	6+4=10	18	707
Cr	150	$^1/_{11}[\bar{3}32]$	5	12	620	$^1/_{11}[\bar{7}71]$	5+3=8	16	959
	300	$^1/_{11}[\bar{3}32]$	5	12	582	$^1/_{22}[\bar{1}313\,5]$	5+4=9	17	938
	450	$^1/_{11}[\bar{3}32]$	5	12	562	$^1/_{22}[\bar{1}515\bar{1}]$	5+2=7	15	941
	600	$^1/_{11}[\bar{4}4\bar{1}]$	3	10	505	$^1/_{22}[\bar{1}313\,5]$	3+6=9	17	894
W	150	$^1/_{22}[\bar{7}71]$	4	11	1735	$^1/_{22}[\bar{1}515\bar{1}]$	4+3=7	15	2299
	300	$^1/_{22}[\bar{7}71]$	4	11	1767	$^1/_{11}[\bar{7}71]$	4+4=8	16	2215
	450	$^1/_{22}[\bar{7}71]$	4	11	1607	$^1/_{11}[\bar{7}71]$	4+4=8	16	2149
	600	$^1/_{22}[\bar{7}71]$	4	11	1587	$^1/_{11}[\bar{7}71]$	4+4=8	16	2128

The sequence of events is as follows: the first dislocation has been pushed by the pileup towards the GB against the initial repulsion of the GB. Fig 5.11a shows the equilibrium position of the first dislocation that is not absorbed by the GB and keeps its Bv. By increasing the shear stress (see the values in Fig. 5.10), the first dislocation is absorbed by the GB producing a GBD with the riser; it is shown in Fig. 5.11b for Fe. Table 5.5 indicates the Bvs of the GBDs as a function of temperature and material (from #10 to #14) that are shown in Fig. 5.9b; accordingly, the number of $\mathbf{b}_{2/2}$ varies from 4 to 7. By increasing the shear strain, the second dislocation is absorbed with emission of $\mathbf{b}_{2/2}$'s. The Bv of the GBD and the number of disconnections is presented in Table 5.5 and the DP of Fig. 5.9b. Bvs from #15 to #18 represent absorption of two crystal dislocations. Fig. 5.10 shows the local shear stress necessary for the first and second dislocations to be absorbed.

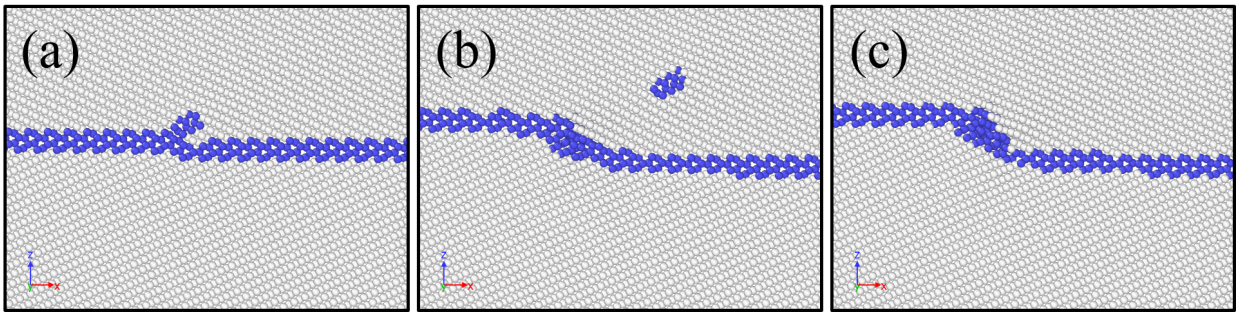

Figure 5.11: Absorption of the first two $\mathbf{b}_{-2/0}$ dislocations of the pileup in Fe at T = 300 K. a) 1st dislocation of pileup after relaxation (no absorption). b) 1st dislocation is absorbed under the stress of the 2nd dislocation. c) 2nd dislocation absorbed under the stress of the 3rd dislocation.

By comparing Tables 5.4 and 5.5, namely comparing the reactions of $\mathbf{b}_{2/0}$ and $\mathbf{b}_{-2/0}$, we observe a slightly higher dependence on the material in the reaction with the latter. In this case, in Fe there is an emission of a higher number of disconnections, especially after the absorption of the first dislocation, indicating a better accommodation of the strain applied, compared to Cr and W.

5.2.3 Interaction with a pileup of edge dislocations $\mathbf{b}_{\pm 4/0}$

For the second glide plane inclination considered, the Burgers vectors of the dislocations of the pileup are $\mathbf{b}_{4/0} = \frac{1}{2}[1\,\bar{1}\,\bar{1}]$ and $\mathbf{b}_{-4/0} = \frac{1}{2}[\bar{1}\,1\,1]$. For the $\mathbf{b}_{4/0}$ Bv the interaction with the GB requires a much higher stress. There is attraction and absorption of the first dislocation $\mathbf{b}_{4/0}$ of the pileup but after an increase of the shear along the glide plane of the dislocations of about 9.5 GPa, the second dislocation is not absorbed. The Bv of the GBD produced is shown in the DP of Fig. 5.12 (#19 inside a green circle). On the other hand, for the $\mathbf{b}_{-4/0}$ Bv there is no attraction between the first dislocation and the GB. If the dislocation of the pileup is pushed to the GB by increasing the shear stress, it reaches an equilibrium position and remains attached to the GB but it keeps its own Bv. The conclusion derived from these results is that the GB acts as a strong barrier for the glide of the pileup with this high incident angle.

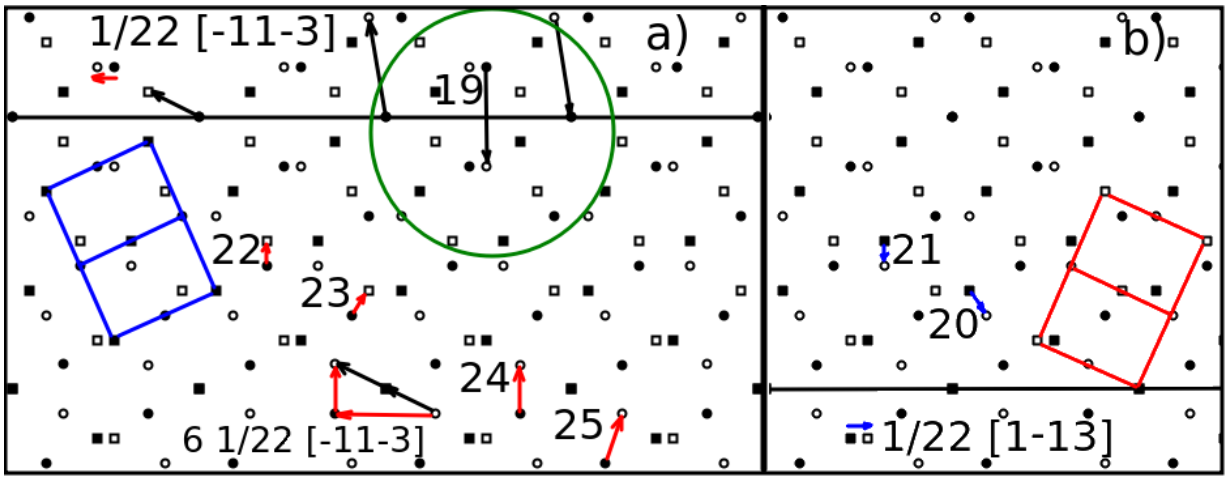

Figure 5.12: Dichromatic pattern with possible Bvs of GBDs with core riser for a different number of absorbed mixed dislocations. a) $\mathbf{b}_{1/0}$ dislocation and the GBD associated (from #22 to #25). In the top in a green circle, it includes the dislocations $\mathbf{b}_{4/0}$ and $\mathbf{b}_{-4/0}$ with the only GBD associated (#19); b) $\mathbf{b}_{-1/0}$ dislocation and the GBD associated (#20 and #21). Black horizontal lines indicate the GB. Arrows from black to white sites are Bvs of GB defects. An example of reaction is shown on a): $2\mathbf{b}_{1/0} = \frac{1}{11}[3\,\bar{3}\,\bar{2}] + [110] + 6\frac{1}{22}[\bar{1}\,1\,\bar{3}]$.

5.2.4 Interaction with a pileup of mixed dislocations $\mathbf{b}_{\pm 1/0}$

The mixed dislocations interacting with the GB glide on a {110} plane. The Burgers vectors of the dislocations of the pileup are $\mathbf{b}_{-1/0} = \frac{1}{2}[\bar{1}\,\bar{1}\,1]$ and $\mathbf{b}_{1/0} = \frac{1}{2}[1\,1\,\bar{1}]$, respectively.

For completeness, in our study of the mixed dislocation we have considered the four vectors obtained by changing the sign of the edge part and the screw part, as indicated in Tables 5.6 and 5.7 that correspond to Fe. In these simulations, the decomposition of the incident dislocation may change in plus or minus a disconnection as with the edge dislocation. Although the most frequent decomposition is related to the minimum magnitude of the Bv of the GBD, the thermal fluctuation or the local stresses may result in a different decomposition.

Table 5.6: Products of reactions for the mixed ($\mathbf{b}_{1/0}$) in Fe. N absorbed is number of absorbed crystal dislocations; T is the temperature (K); Edge and Screw are the edge and screw parts of the Burgers vector of formed GBD with core riser; EDisc: number of accumulated $\mathbf{b}_{2/2}$; ID: Identification of GBDs Bv in Fig. 5.12 and Shear is the local shear stress necessary for the absorption (MPa) plotted in Fig. 5.14.

N absorbed		1					2				
Mater.	T	Edge	Screw	EDisc	ID	Shear	Edge	Screw	EDisc	ID	Shear
Fe	150	$1/22[3\bar{3}\,\bar{2}]$	$1/2[110]$	3	22	504	$1/11[3\bar{3}\,\bar{2}]$	$[110]$	3+3=6	24	483
	300	$1/22[3\bar{3}\,\bar{2}]$	$1/2[110]$	3	22	510	$1/22[7\bar{7}\,\bar{1}]$	$[110]$	3+4=7	25	471
	450	$1/22[3\bar{3}\,\bar{2}]$	$1/2[110]$	3	22	506	$1/11[3\bar{3}\,\bar{2}]$	$[110]$	3+3=6	24	352
	600	$1/22[3\bar{3}\,\bar{2}]$	$1/2[110]$	3	22	506	$1/11[3\bar{3}\,\bar{2}]$	$[110]$	3+3=6	24	375
	150	$1/22[4\bar{4}1]$	$1/2[\bar{1}\,\bar{1}0]$	4	23	509	$1/22[7\bar{7}\,\bar{1}]$	$[\bar{1}\,\bar{1}0]$	4+3=7	25	469
	300	$1/22[3\bar{3}\,\bar{2}]$	$1/2[\bar{1}\,\bar{1}0]$	3	22	508	$1/22[7\bar{7}\,\bar{1}]$	$[\bar{1}\,\bar{1}0]$	3+4=7	25	412
	450	$1/22[3\bar{3}\,\bar{2}]$	$1/2[\bar{1}\,\bar{1}0]$	3	22	507	$1/22[7\bar{7}\,\bar{1}]$	$[\bar{1}\,\bar{1}0]$	3+4=7	25	377
	600	$1/22[3\bar{3}\,\bar{2}]$	$1/2[\bar{1}\,\bar{1}0]$	3	22	507	$1/11[3\bar{3}\,\bar{2}]$	$[\bar{1}\,\bar{1}0]$	3+3=6	24	327

When the edge part of the Burgers vector is pointing away from the interface ($\mathbf{b}_{1/0}$, Table 5.6, lower frame in Fig. 5.13), two dislocations can be absorbed and the riser is along the glide plane, as for the edge $\mathbf{b}_{2/0}$.

Reversing the sign of the edge part ($\mathbf{b}_{-1/0}$, Table 5.7, upper frame in Fig. 5.13) only one dislocation can be absorbed. The angle between the glide plane and the riser is bigger than 90 degrees, it is the same one observed for the edge $\mathbf{b}_{-2/0}$ pointing towards the interface. The injection of a second dislocation only occurs at 900 K for a total shear stress of 5.7 GPa, indicating that the process is thermally activated.

Table 5.7: Products of reactions for the mixed ($\mathbf{b}_{-1/0}$) in Fe. N absorbed is number of absorbed crystal dislocations; T is the temperature (K); Edge and Screw are the edge and screw parts of the Burgers vector of formed GBD with core riser; EDisc: number of accumulated $\mathbf{b}_{2/2}$; ID: Identification of GBDs Bv in Fig. 5.12 and Shear is the local shear stress necessary for the absorption (MPa) plotted in Fig. 5.14.

N absorbed		1				
Mater.	T	Edge	Screw	EDisc	ID	Shear
Fe	150	$1/22[\bar{2}25]$	$1/2[110]$	2	20	602
	300	$1/22[\bar{3}32]$	$1/2[110]$	3	21	589
	450	$1/22[\bar{3}32]$	$1/2[110]$	3	21	601
	600	$1/22[\bar{2}25]$	$1/2[110]$	2	20	586
	150	$1/22[\bar{2}25]$	$1/2[\bar{1}\,\bar{1}0]$	2	20	587
	300	$1/22[\bar{2}25]$	$1/2[\bar{1}\,\bar{1}0]$	2	20	587
	450	$1/22[\bar{2}25]$	$1/2[\bar{1}\,\bar{1}0]$	2	20	583
	600	$1/22[\bar{2}25]$	$1/2[\bar{1}\,\bar{1}0]$	2	20	581

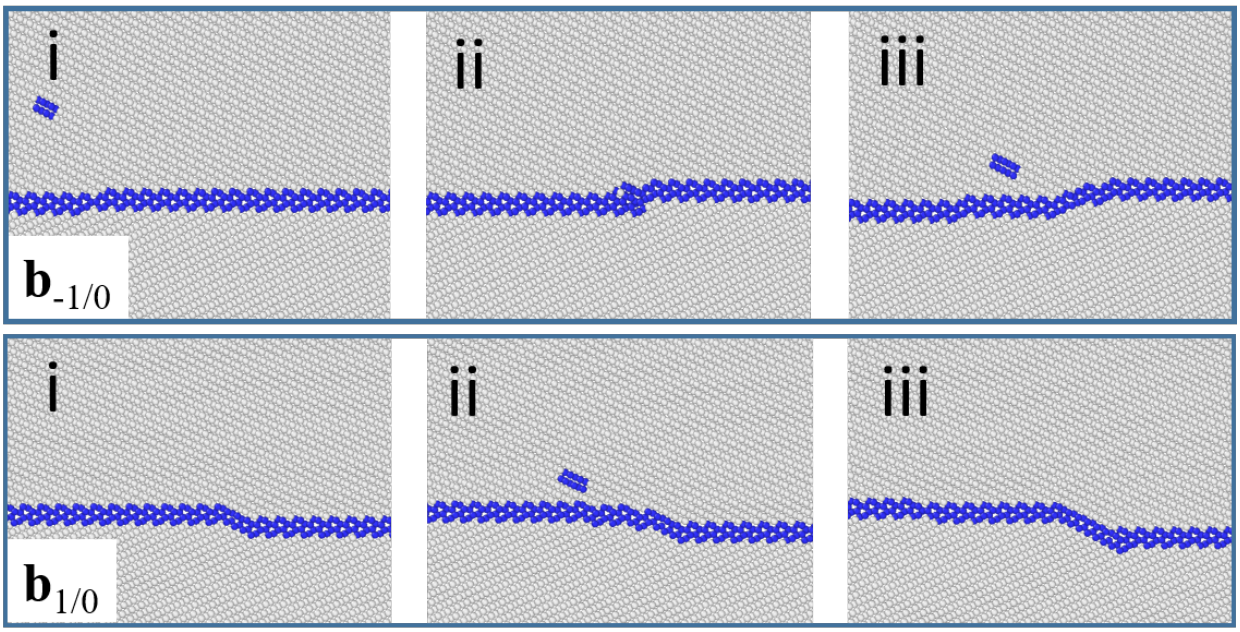

Figure 5.13: Snapshots of the interaction of the mixed dislocation DPU with the GB. $\mathbf{b}_{-1/0}$: before (i) during (ii) and after (iii) interaction. $\mathbf{b}_{1/0}$: first dislocation is absorbed (i) before absorption of second dislocation (ii) and after absorption of second dislocation (iii): notice the riser is parallel to the glide plane.

Fig. 5.14 plots the stresses presented in Tables 5.6 and 5.7. It is shown that stress depends on the edge part of the dislocation, namely the orientation of the riser, but is almost independent on the temperature. Thus, the dislocation $\mathbf{b}_{1/0} = \frac{1}{2}[1\,1\,\bar{1}]$ is attracted by the GB, it creates a riser along the glide plane and needs smaller local shear stress to be absorbed by the GB, allowing a second dislocation to be absorbed. The shear stress for the absorption of the second dislocation is smaller and it is dependent on the temperature, as shown in Fig. 5.14b. It seems to indicate that the accommodation of two mixed dislocations leads to a better faceting of the GB because the screw component is a lattice vector; the GBD separates two identical interfaces.

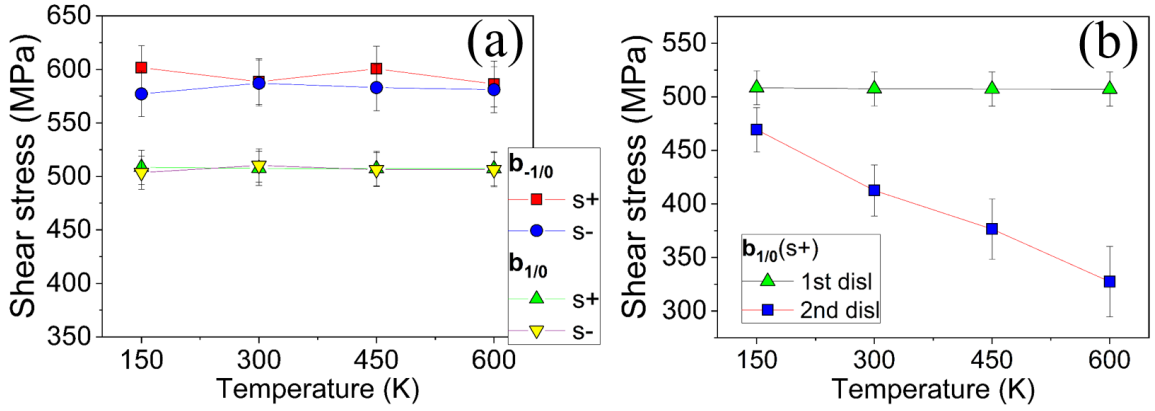

Figure 5.14: a) Local shear stress along the glide plane for the absorption of the first mixed dislocation as a function of the temperature and the orientation of the Bv; b) Shear stress for absorption of first and second $\mathbf{b}_{1/0}$ dislocations.

Once analyzed the results for all dislocations, we conclude that the same crystallographic processes occur for the three bcc metals studied. The differences in the number of disconnections resulting in each absorption may be related to the core energy and Peierls stress of $\mathbf{b}_{2/2}$ that differ from one metal

to the other. Occasionally, reactions with plus or minus $\mathbf{b}_{2/2}$ may occur because, as shown in the DP of Figs. 5.9 and 5.12, the change of the Bv of the GBD, for a given number of dislocations absorbed, is mainly in orientation but small in magnitude.

Thus, the mechanism of the interaction of the {332} GB with the pileup of ½⟨111⟩ dislocations is essentially ruled by the crystallography with almost no influence of the temperature or material. Even though, for a given metal, the absorption is, in general, thermally activated and, especially in Fe, the threshold stress for absorption diminishes by increasing the temperature.

5.2.5 Dynamic behavior of GBDs under an applied shear stress

The creation of GBDs has a crucial effect on the GB dynamic as the mobility of the interface can be enhanced or reduced with the subsequent effects on the plasticity. The GBDs created by absorption of dislocations described along the previous Sections are stable GB defects (the absorption is not a reversible process) that cannot glide along the GB because their Bv is not parallel to the GB. Even though, these GBDs can move under certain conditions together with the GB.

Let us consider first the case when the GBD is far from the influence of the pileup. Under an external shear stress parallel to the GB, the GBD created by the absorption of $\mathbf{b}_{2/0}$ moves along its own riser accompanying the GB on its displacement in a shear-coupled GB migration. The process, generated by the glide of $\mathbf{b}_{2/2}$ disconnections along the GB, is the same as for the (10-12) twin boundary in the hcp metals [53]. Thus, the GBD acts as a source of disconnection dipoles that move in opposite directions under the same shear stress. Under the applied stress, while one partner of the dipole glides along the GB, the other moves along the riser of the GBD in a conservative climb [65]. As a result, the whole GB moves by two planes for every dipole pair created. The same result is produced if a single disconnection sweeps the GB and climb conservatively along the riser. Thus, the displacement of the GBD is conservative (no atomic diffusion is needed) and it is reversed if the shear stress is reversed.

Let us consider the GBD that is the result of the interaction with a pileup of $\mathbf{b}_{2/0}$ dislocations. When the sense of the shear stress favors the absorption of the pileup, it favors, as well, the glide of disconnections that move the GB down. If the sense of the shear is reversed after the absorption of few dislocations, the remaining dislocations of the pileup run away from the GB and the glide of disconnections, created at the GBD (or elsewhere) produces the displacement of the GB upwards, as described above.

The displacement of the GBDs created by the interaction with the other dislocations is not always conservative. For instance, the GBDs obtained from the interaction with $\mathbf{b}_{-2/0}$ and $\mathbf{b}_{4/0}$ dislocations pin the GB under a positive shear stress, whereas they perform a conservative climb for a negative shear stress. A detailed study of the behavior of the GBDs under stress is provided in Section 4.2.2 and contained in [74].

5.2.6 Discussion

Irrespective of the conditions considered (stress, temperature, glide plane inclination, Bv orientation, material) the interaction process between a dislocation pileup and the {332} GB starts with the absorption of the first incoming dislocation jointly with the formation of a GBD at the interface and the emission of several elementary disconnections, analogously to the single dislocation case (Section 4.2). The aforementioned conditions only affect the GBD produced as an outcome of the absorption reaction as well as the number of elementary disconnections formed. The stress needed to create one elementary disconnection depends on the intrinsic properties of the material (combination of elastic constants, stacking fault energy and the resolved shear stress to move it). This leads to the formation of a different number of elementary disconnections after the absorption of the first dislocation of the pileup and, consequently, different Bv of the riser (determined by the crystallography). The result of the absorption of the second and further dislocations of the pileup, i.e., the Bv of riser and number of elementary disconnections, depends on the material. The interaction mechanisms related to crystallography are the same for the three metals considered.

In this work, the maximum external stress is fixed for all simulations (5.5 GPa). This controls the maximum number of dislocations to be absorbed by the GB, which depends on the material but, for a given material is not dependent on temperature. Through the performed MD simulations, we have observed that the same crystal dislocation acts differently depending on the sense of the Bv, which determines the reaction, in particular the riser of the GBD, either stepping up or down the GB. The same property has been reported for hcp boundaries, for instance, in the interaction of the (10-12) twin with crystal dislocations [81]. The reaction with the edge dislocation $\mathbf{b}_{2/0}$ steps the GB up, i.e., the riser of the GBD is along the glide plane of the incident crystal dislocation $(\bar{1}\,12)_\lambda/(1\,\bar{1}\,0)_\mu$ which favors the absorption of the following dislocations. The continuous absorption of dislocations leads to the formation of a new asymmetric GB interface of {112}/{110} type which continuously grows as more bulk dislocations are supplied. Thus, the GB becomes faceted due to the interaction with the dislocation pileups created inside the grain. The scenario changes by changing the sign of the Bv of the pileup ($\mathbf{b}_{-2/0}$). In the latter case, the riser is almost perpendicular to the glide plane of the pileup, preventing the accommodation of the pileup along the riser. Even though, a smaller facet {110}/{112} is produced in the GB. If the edge dislocation forms an angle with the GB of 100 degrees, the absorption is not favorable and the GB is a strong obstacle for the glide of the dislocation. When the pileup is formed by mixed dislocations, the orientation of the riser of the produced GBD depends on the sign of the edge part of the dislocation. The riser is $(1\,\bar{1}\,0)_\lambda/(1\,\bar{1}\,2)_\mu$, parallel to the glide plane, for the $\mathbf{b}_{1/0}$ but its orientation is not parallel to the glide plane for $\mathbf{b}_{-1/0}$. Again, the observation of the resistance against the absorption for the mixed dislocation is consistent with the orientation of the riser, being the dislocation $\mathbf{b}_{1/0}$ absorbed with a smaller shear stress; in this case, a second dislocation is absorbed.

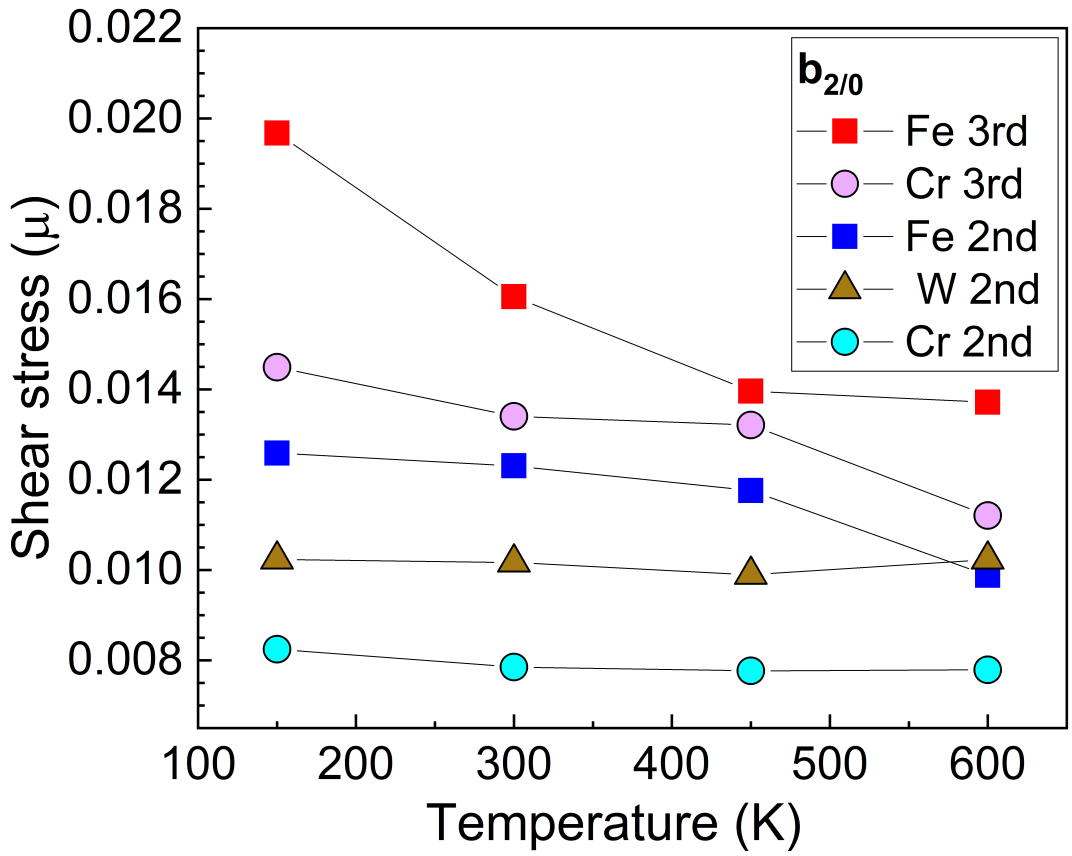

Figure 5.15: Shear stress (normalized with the shear modulus) necessary for the absorption of a pileup with glide plane at 29.5 degrees of the GB.

The effectiveness of the GB to accommodate plastic deformation depends on the activated slip system. Thus, the mixed dislocation is absorbed at the lowest shear stress, as shown in Fig. 5.14, followed by the edge dislocation at 29.5 degrees ($\mathbf{b}_{2/0}$) and, finally, the GB is a strong obstacle for the glide of the edge dislocation with glide plane almost perpendicular to the GB.

The three metals studied keep the same behavior. Fig. 5.10 and Tables 5.4 and 5.5, allow a comparison of the shear stress of each metal. Fig. 5.10 shows quite similar stress values for Fe and Cr, but plotting the shear stress normalized by the shear modulus (μ(Fe,Cr,W)=(73,108,179) GPa, [92, 120]), we can discern the differences. Thus, Fig. 5.15 presents the values in units of the shear modulus to absorb the second and third dislocations of the $\mathbf{b}_{2/0}$ pileup (the first is spontaneously absorbed) versus temperature. The stress to absorb the second dislocation is almost independent of the temperature for Cr and W but it decreases by increasing the temperature for Fe. The injection of the third dislocation requires a higher stress that significantly decreases by increasing the temperature in both, Cr and Fe. The same tendency occurs with the absorption of the second dislocation of the pileup of mixed dislocations, as shown in Fig. 5.14. Therefore, the strength of the {332} GB is highest in Fe followed by W and the weakest is Cr. If the resolved shear stress is measured in shear modulus units, voids also, as well as {332} GB, act as significantly stronger obstacles in Fe than in W, as reported by Osetsky in a recent paper [120].

5.3 {111} GB. Impenetrable barrier

The interaction of the {111} GB with a single dislocation shows no transmission or reflection of the latter and it presents two distinctive features: (i) the atomic configuration on the interaction region shows significant transformation and (ii) there is a total absence of elementary disconnections. When the interaction involves a dislocation pileup, the same features are present, however, as the level of stress on the interaction region is increased by the trailing dislocations, the aforementioned transformation mechanism of the interface is enhanced. When the glide plane is perpendicular to the GB it leads to a penetration of one grain into the other with the dislocation in the tip of the intrusion bounded by the symmetric {112} and asymmetric stepped segment respectively. For the other glide planes, the second dislocation is absorbed increasing the length of the facet.

The Section is structured as follows: in subsections 5.3.1, 5.3.2 and 5.3.3 there are presented the most relevant findings on the interaction of the {111} GB with DPU, while in subsection 5.3.4 we present the discussion of the results obtained.

Similarly to the study of interaction with single dislocations, there have been considered three different glide plane inclinations with respect to the GB to introduce the dislocation pileup. These dislocations are identified in Fig. 4.14. Finally, to assess the local evolution of stress state as a consequence of the GB – dislocation interactions, we have allocated several groups of atoms to record the forces and displacements during the simulation runs. These groups are located where they can provide relevant information on the reactions with the GB. They are indicated in Figs. 5.17, 5.19b & 5.20c (see also Fig. 2.3).

The analysis of the results from the interaction between the {111}[110] tilt grain boundary and a single dislocation has shown a mechanism leading to a local modification of the interface on the interaction region, based on the formation of steps. This mechanism is enhanced when T > 0 K and the final outcome depends on the initial parameters of the simulation: temperature, glide plane inclination and Bv sense. In the following subsection we present the results of our investigation on the interaction of the {111} GB with a pileup of dislocations, considering the same set of cases described in part 4.3.1.2.

There is a common element in all the simulations: the behavior of the first dislocation of the pileup is exactly the same as described for a single dislocation. The discrepancies between the different cases come from the influence of the remaining dislocations of the pileup on the newly formed interface. Apart from the results obtained for each case investigated as a function of the temperature, we have included a subsection where it has been evaluated the stability of the new interfacial structures generated by the GB – pileup interaction.

5.3.1 Interaction with a pileup of edge dislocations $\mathbf{b}_{\pm 3/0}$

The Burgers vectors of the edge dislocations of the pileup are $\mathbf{b}_{3/0} = \frac{1}{2}[1\bar{1}\bar{1}]$ and $\mathbf{b}_{-3/0} = \frac{1}{2}[\bar{1}11]$. In the same way observed for single dislocations, the outcome of the reactions involved with each dislocation is related by a mirror symmetry with respect to the glide plane of the dislocation, as shown in Fig. 5.16. The first dislocation is attached to the interface during all its transformation process. We have checked by using a Burgers circuit that the Bv stays the same as the initial crystal dislocation. As for the 2nd and subsequent dislocations, they are unable to reach the boundary, therefore this GB acts as a strong obstacle. The role played by these dislocations is to increase the local stress on the interaction region, triggering the reactions which modify progressively the shape of the boundary as it is displayed from Fig. 5.16a to Fig. 5.16d.

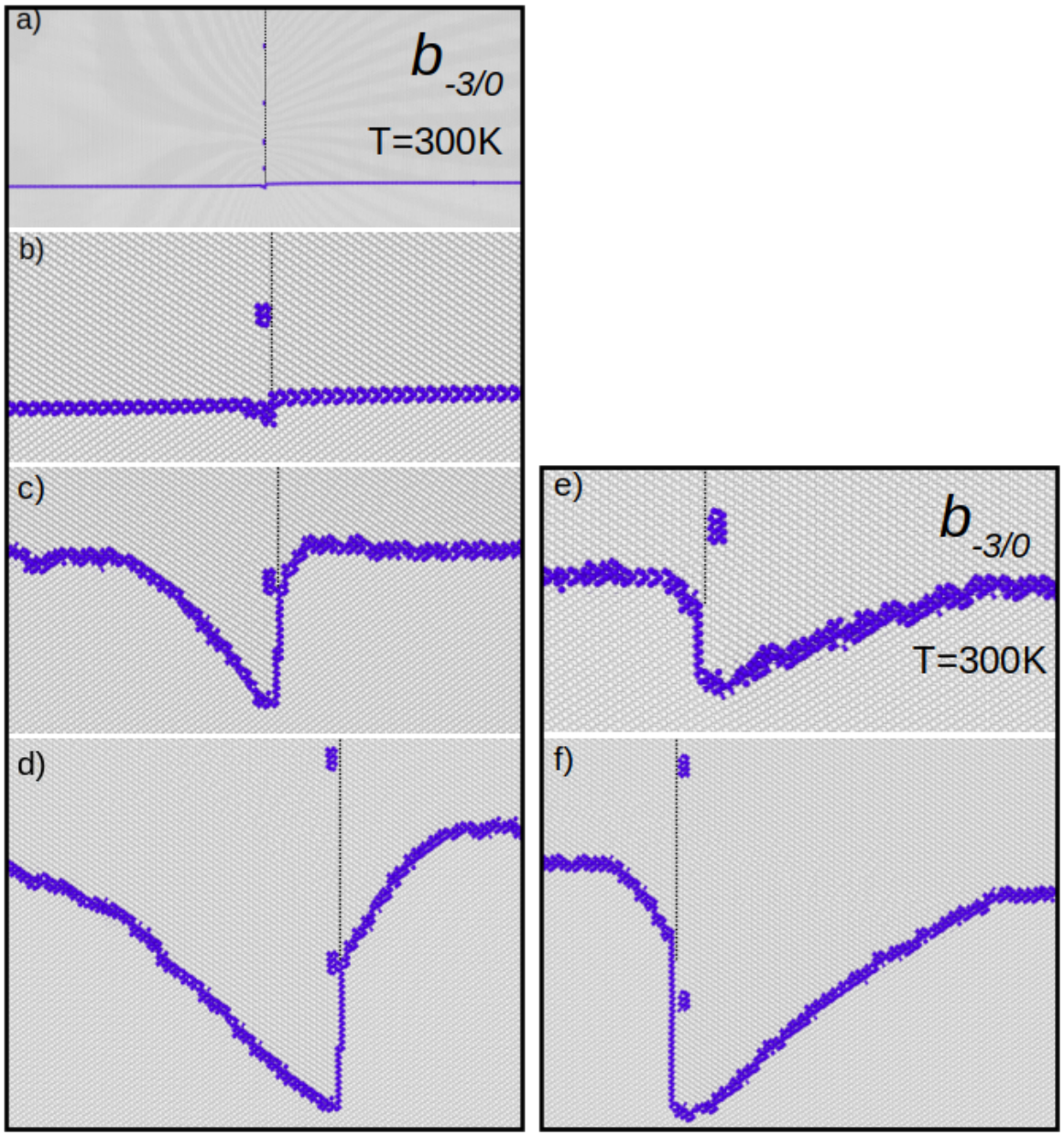

Figure 5.16: a), b), c) and d) Snapshots of MD simulation of a {111} GB interacting with a pileup of $\mathbf{b}_{3/0}$ dislocations at T = 300 K in Fe; e) and f) Idem for a pileup of $\mathbf{b}_{-3/0}$ dislocations.

Fig. 5.16a shows the full box and the region of the reaction after the first $\mathbf{b}_{3/0}$ dislocation absorption while Fig. 5.16b shows in detail the interaction region with the second dislocation in the vicinity of the interface. The dislocation at the interface concentrates stresses coming from other dislocations leading to the formation of a new interface propagating into the lower grain. This new interface is the combination of a {112} GB parallel to the initial glide plane with a {110}/{001} facet, where the planes in the upper grain represent the sectors of {110} planes divided by steps along ⟨110⟩ direction. Figs. 5.16e & 5.16f show the formation of the equivalent structure for the pileup of $\mathbf{b}_{-3/0}$ dislocations which is approximately the mirror image of the formerly described $\mathbf{b}_{3/0}$. In Fig. 5.16d we can observe how the stress field of the second dislocation affects the {112} GB by inducing the creation of a glissile disconnection on this interface. As the applied stress increases up to 4.5 GPa no further reaction between the following pileup dislocation and the interface was observed. The second dislocation continues its glide along with the propagation of the {112} interface, that does not increase in length. Instead, the upper grain extends into the lower by means of the formation of the new stepped facet.

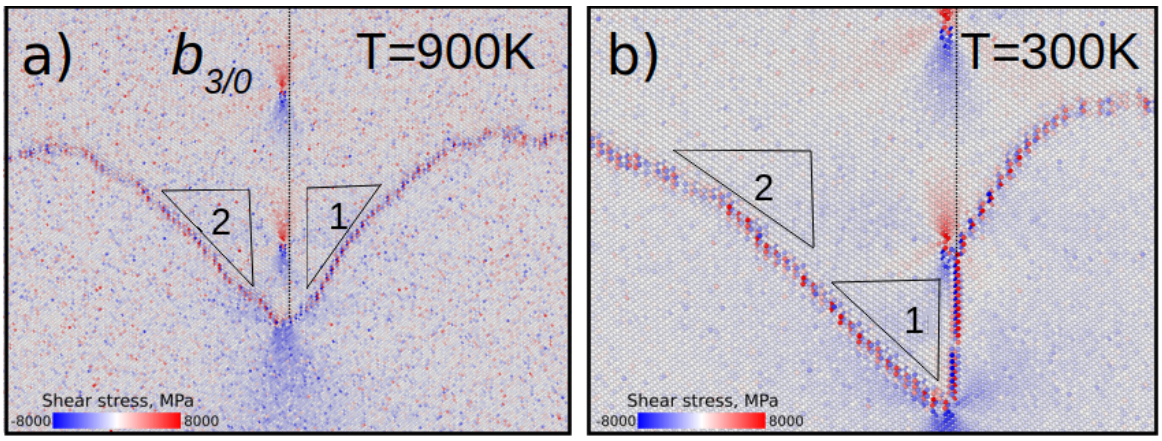

Figure 5.17: a) Snapshot of MD simulation of a {111} GB interacting with a pileup of $\mathbf{b}_{3/0}$ dislocations in Fe at T = 900 K. The figure shows the configuration with two interfaces created along with the propagation of crystal dislocations. b) Idem at T = 300 K. The dashed lines are guides for the eye indicating the glide plane.

In order to investigate the effects of temperature on the interaction mechanism, we have studied the $\mathbf{b}_{3/0}$ case in Fe considering T = 900 K. The equivalent case at T = 300 K shows that the {112} GB of the new interface appears in the tensile region of the dislocations (right) while the {110}/{001} facet is on the compression region (left) as shown in Figs. 5.16d and 5.17b. However, at a higher temperature, even though the reaction is the same, we can observe a different outcome from the interaction indicating that the stress is accommodated differently. The new interface created (Fig. 5.17a) has a more symmetric shape: the {112} GB present at T = 300 K transforms into a {001}/{110} facet.

We have analyzed the stresses at the reaction site region: (1) close to the {112} GB and (2) close to the formed facet on the at T = 300 K and, similarly, close to two different facets at T = 900 K. The regions are shown on Fig. 5.17. The results are given in Table 5.8. There is also the formation of the {112} disconnection for $\mathbf{b}_{3/0}$ dislocations case at T = 300 K. The shear stress before the reaction is in the (1) region - 350 MPa, in the (2) region - 340 MPa. The values obtained for the stresses close to two different interfaces do not differ much, as can be seen on Fig. 5.17.

Table 5.8: Local stresses at the formation of the facets for the edge ($\mathbf{b}_{\pm 3/0}$) in Fe. Shear is the local shear stress.

Region		(1)	(2)
Bv	T (K)	Shear (MPa)	
$\mathbf{b}_{3/0}$	300	570	570
	900	1190	860
$\mathbf{b}_{-3/0}$	300	520	490
	900	870	1000

We can summarize the interaction of a pileup of $\mathbf{b}_{\pm 3/0}$ describing the reactions observed and the effect of temperature on their outcome. The first dislocation of the pileup contacts the interface and remains attached without changing its Bv. As the {111} GB do not experience shear-coupled GB migration, there is another type of accommodation of applied stress – the formation of new interfaces where the upper crystal grows at the expenses of the lower crystal. The stress induced by the subsequent dislocations leads to the creation of a {112} GB on the tensile region and {110}/{001} type facets on the compression region. The {111} GB acts as a strong obstacle for this type of edge dislocations as no transmission is observed, even for a high level of stress ($\sim$ 10 GPa). The temperature affects the final shape of the interface, the higher it is, the more favored is the stepping mechanism

responsible for the {110}/{001} type facets in front of the creation of the {112} GB along the former glide plane of the pileup.

Reversibility of the new interfaces. One question raised from the results presented in Figs. 5.16 and 5.17 is the stability of the new {110}/{001} interfacial structures created from the interaction with the $\mathbf{b}_{\pm 3/0}$ dislocation pileup. To evaluate it, we have applied a reversed stress, as in a cyclic deformation. We have observed that dislocations of the DPU move back, but the facet keeps unchanged. The first dislocation is not detached from the interface and when moving back it leads to the creation of a (112) twin that penetrates either the upper (λ) crystal if it is $\mathbf{b}_{3/0}$ or the lower crystal (μ) if it is $\mathbf{b}_{-3/0}$. The creation of the EDisc responsible for the thickening of the twin are compensated by the creation of crystal dislocations that glide in the opposite direction of the twin. Inside the red circles in Fig. 5.18 there are two of the crystal dislocations created during the thickening of the twin. Notice that their glide planes are parallel but not coincident with the DPU. There is a balance in Bv and planes since three disconnections of the {112} twin boundary are equivalent to one ½⟨111⟩ crystal dislocation and step the twin boundary one plane.

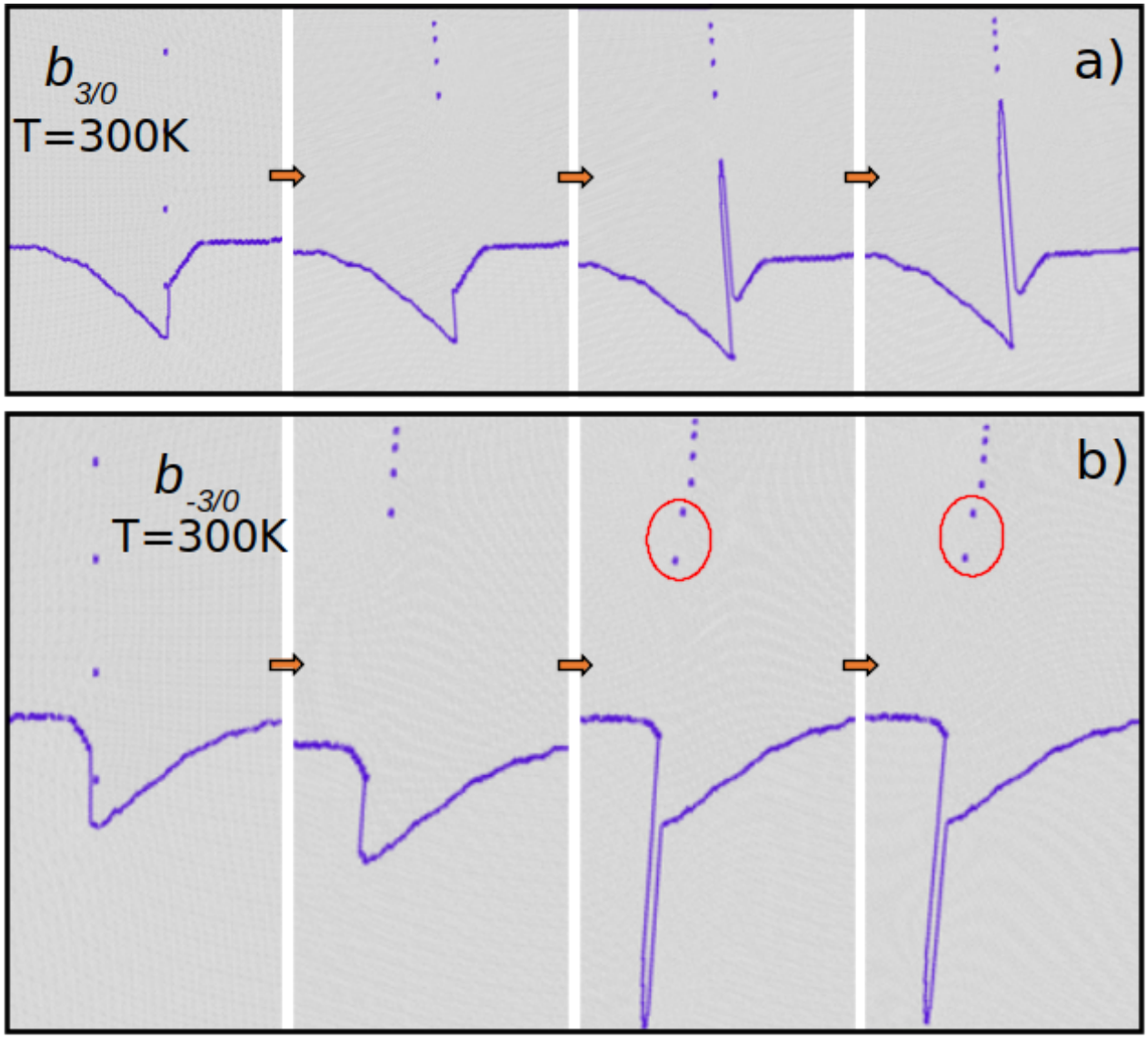

Figure 5.18: Snapshots of MD simulation of a {111} GB interacting with pileups of the $\mathbf{b}_{3/0}$ (a) and $\mathbf{b}_{-3/0}$ (b) dislocations. The reversed sense strain is applied to the box with a newly formed interface. The figures show the evolution (left to right) of the interface along with the dislocations. Enclosed in a red circle there are the crystal dislocations emitted jointly with the creation of the {112} twin.

The full cycle of MD simulations has been performed at T = 300 K and can be divided in two parts: (1) A shear strain has been applied until reaching a level of 4 GPa of shear stress accumulated in the system. (2) The shear strain is then reversed up to the point where there is created a {112} twin on the interface, then the simulation is ended.

In Fig. 5.18 there are displayed several snapshots showing the described evolution of the boundary along with the dislocations of the pileup during the second part of the simulations for both Bv sense. The first configuration shown in Fig. 5.18a & 5.18b corresponds to the precise moment where the strain applied is reversed. On the remaining frames we can track the second and subsequent dislocations being gradually pulled away from the boundary until a {112} twin is created jointly with the emission of one or two crystal dislocations. For the $\mathbf{b}_{3/0}$ dislocations, the twin is created towards the upper crystal while the extra dislocation is emitted into the lower crystal (is out of frame). And for the $\mathbf{b}_{-3/0}$ dislocations the process is essentially mirrored: the twin is created towards the lower crystal and the emitted dislocations appear on the upper crystal (enclosed in red circle), following the ones from the pileup. The main conclusion from these results is that the process of growth of the new interfaces created during the accommodation of plastic deformation is irreversible.

5.3.2 Interaction with a pileup of edge dislocations $\mathbf{b}_{\pm 1/0}$

For this glide plane inclination, the Burgers vectors of the incident edge dislocations of the pileup are $\mathbf{b}_{1/0} = \frac{1}{2}[1\bar{1}1]$ and $\mathbf{b}_{-1/0} = \frac{1}{2}[\bar{1}1\bar{1}]$.

In the same manner as observed for the $\mathbf{b}_{\pm 3/0}$ cases, no transmission takes place and the second and subsequent dislocations of the pileup increase the local stress on the interaction region triggering the transformation of the interface. However, the low incidence angle leads to a very different interaction process with a substantial change in the final outcome, as it is reflected by comparing the frames of Fig. 5.19 (5.19e and 5.19h) with the equivalents in Fig. 5.16 (5.16d and 5.16f).

The interaction process follows the same initial steps: the first dislocation of the pileup reaches the GB and is not absorbed; it remains attached to the interface keeping its Bv. As the applied stress increases, this dislocation eventually gets absorbed forming a GBD with a Bv parallel to the interface. Figs. 5.19a and 5.19b show the configuration of the system once this first absorption has taken place for the $\mathbf{b}_{1/0}$ case. As the stress continues increasing, several steps appear on the interface modifying its shape (Figs. 5.19c, 5.19d and 5.19e for $\mathbf{b}_{1/0}$) around the interaction region. Simultaneously, the second dislocation of the pileup approaches to the GB and is finally absorbed, forming a riser (Fig. 5.19d). As the external stress keeps increasing, the evolution of the interface on the interaction region is different depending on the Bv direction, so let us detail it separately:

(i) For the pileup of $\mathbf{b}_{1/0}$ we observe the formation and subsequent growth of a facet of {112}/{110} (+segments of {001}). Simultaneously, a second facet appears on the left of the interaction region (Fig. 5.19e) described as a facet of {110}/{112} (+segments of {110}). The length of the first formed facet ranges between 40 Å when its formed and 350 Å at the 6.5 GPa of stress applied. We noticed that during this process the mentioned GBD stays sessile and keeps the interface on the compression region of its vicinity flat as can be seen in Fig. 5.19c (red line).

(ii) For the pileup of $\mathbf{b}_{-1/0}$ the GBD formed after the first absorption (green circle in Fig. 5.19f) has opposite sign and this conditions the ensuing interaction with the 2nd dislocation. The riser formed as a result of the second absorption (Fig. 5.19g) spreads and it splits into two risers with the same configuration as in $\mathbf{b}_{1/0}$ case. The final configuration of the interface on the interaction region (Fig. 5.19h) is qualitatively a mirror image of the image in Fig. 5.19e, with a segment of pristine {111} GB between two facets, the main one being {112}/{110} (+segments of {001}), and the 'complementary' one being {110}/{001} + {112} (irregular).

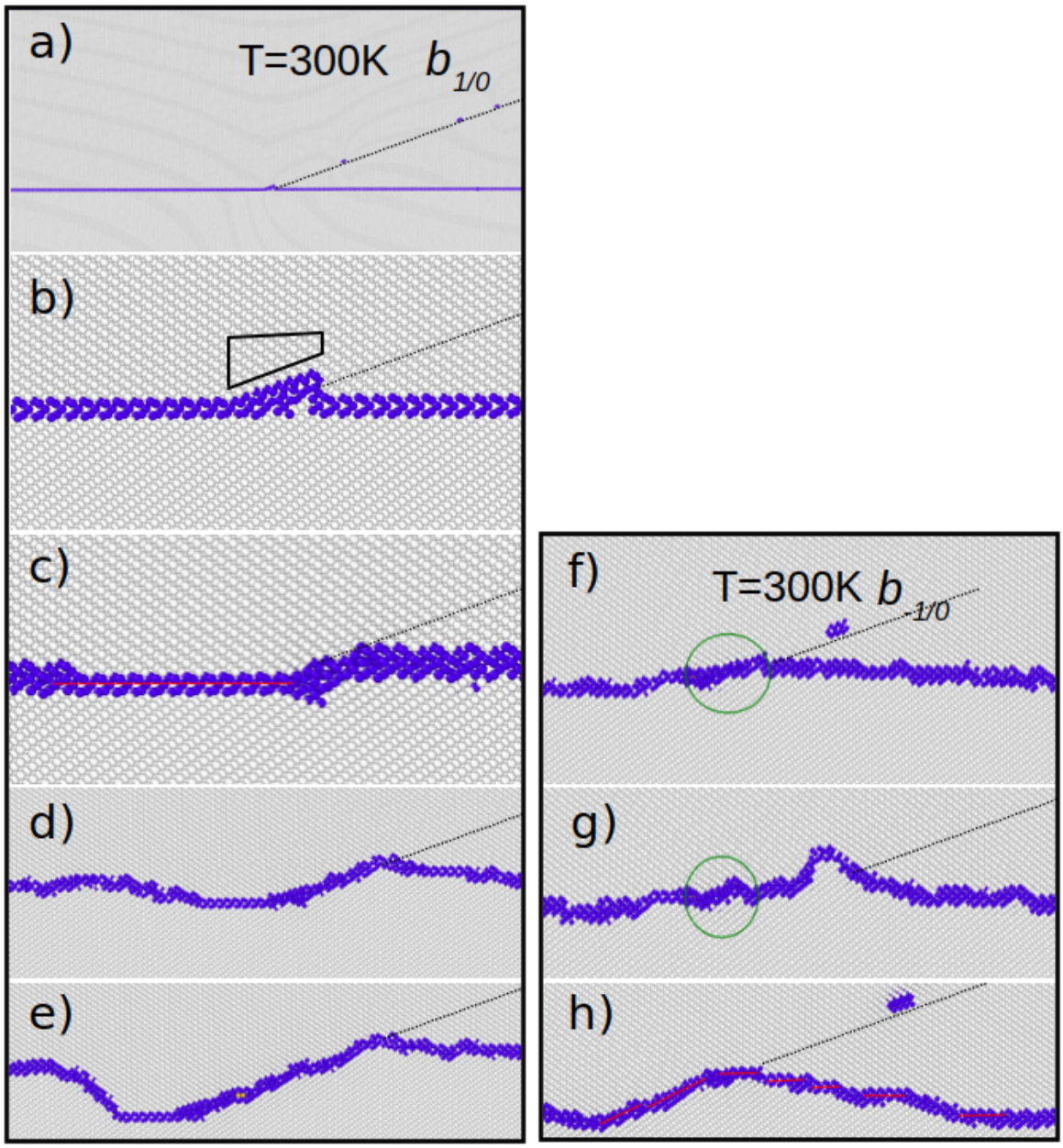

Figure 5.19: a), b), c), d) and e) Snapshots of MD simulation of a {111} GB interacting with a pileup of edge $\mathbf{b}_{1/0}$ dislocations at T = 300 K in Fe; f), g) and h) Idem for a pileup of edge $\mathbf{b}_{-1/0}$ dislocations. The green circles indicate the position of the first absorbed dislocation. The dashed lines are guides for the eye indicating the glide plane.

We have investigated again the effect of temperature on the interaction mechanism comparing the displayed results with ones obtained applying a higher temperature (T = 900 K). For both Bv orientations we noticed that the main effect of temperature is on the way the deformation is accommodated and an additional dislocation is absorbed. The final structure of the interface is not as regular as observed at low temperatures and no flat regions can be found.

In the same manner presented in subsection 5.3.1, we have measured the stresses at the reaction region when significant reactions take place (Fig. 5.19b). At T = 300 K the events are: initial absorption (I) second absorption (II) and formation of one step (III). At T = 900 K the events are the same, except for the (III) reaction, that is the third absorption. The results are given in Table 5.9. The difference between the values for $\mathbf{b}_{1/0}$ and for $\mathbf{b}_{-1/0}$ can be explained by the fact that for the former, stresses are accommodated mainly by the growth of the main riser, i.e., further propagation of initial dislocations, while for the latter, stresses are accommodated by formation of irregularities

(steps) along the whole interface. Comparing the values at different temperature, we can say that the higher the temperature the lower the stresses needed to trigger the reaction.

Table 5.9: Local stresses at the reaction region before the reactions for the edge ($\mathbf{b}_{\pm 1/0}$) in Fe. Shear is the local shear stress.

Reaction		(I)	(II)	(III)
Bv	T (K)	Shear (MPa)		
$\mathbf{b}_{1/0}$	300	830	1170	1320
	900	820	980	1170
$\mathbf{b}_{-1/0}$	300	930	1550	1620
	900	840	1160	980

As a summary of the results presented, we can describe the interaction of a pileup of $\mathbf{b}_{\pm 1/0}$ in a very different way than for $\mathbf{b}_{\pm 3/0}$. Now, we observe the absorption of two or three dislocations of the pileup, depending on the temperature. These absorption reactions lead to the formation of a riser (facet) modifying the shape of the interface. The effect of temperature changes the number of absorptions and the value of the stresses required to trigger the reactions, however, qualitatively the final outcome is very similar.

5.3.3 Interaction with a pileup of mixed dislocations $\mathbf{b}_{\pm 1/0}$

As it is detailed in Fig. 4.14, the mixed dislocations (identified as #3) interacting with the GB glide on a {110} plane. The Burgers vectors of the dislocations of the pileup are $\mathbf{b}_{1/0} = \frac{1}{2}[11\bar{1}]$ and $\mathbf{b}_{-1/0} = \frac{1}{2}[\bar{1}\bar{1}1]$.

As we observed for the single dislocation case, the screw component does not affect the interaction process and there is a noticeable similarity with the results obtained for $\mathbf{b}_{\pm 1/0}$ edge dislocations, although the smaller edge part ($0.5a_0$ vs. $0.866a_0$) of the Bv affects the number and the outcome of the reactions taking place. Once again, the sense of the Bv is relevant as the number of dislocations absorbed by the GB changes.

In Fig. 5.20a it is shown the interaction region once the first $\mathbf{b}_{1/0}$ dislocation of the pileup has been absorbed by the interface. As in the previous cases, initially this dislocation is attached and is absorbed only when the local stress increases by the approaching of the second dislocation. Several steps appear in the interface along with a riser. However, this riser is smaller than for pure edge dislocation as can be seen indicated with a red line. As the stress increases the riser remains in the same position and does not grow while more steps appear on the interface to accommodate it. It seems that there is a repulsion between this riser and the second dislocation causing that no more dislocations are absorbed.

Conversely, for the $\mathbf{b}_{-1/0}$ case there is no repulsion between the GBD created on the first absorption and the second dislocation of the pileup (Fig. 5.20b). Along with the motion of this dislocation towards the GB, as the external stress increases steps appear in the interface. Once the second dislocation is absorbed, it is formed a riser represented as a facet in Fig. 5.20c, equivalent to the one observed for edge dislocations: {110}/{112} (parts of {001}). After this absorption we observed the formation of several pure steps without dislocation character along the interface which interact with each other forming a step with $h_{12/12}$ height on the right of the main riser (Fig. 5.21) leading to a better stress accommodation as can be seen from the comparison of the stress distributions in Fig. 5.20c (right frame) with the one in Fig. 5.21 (right frame).

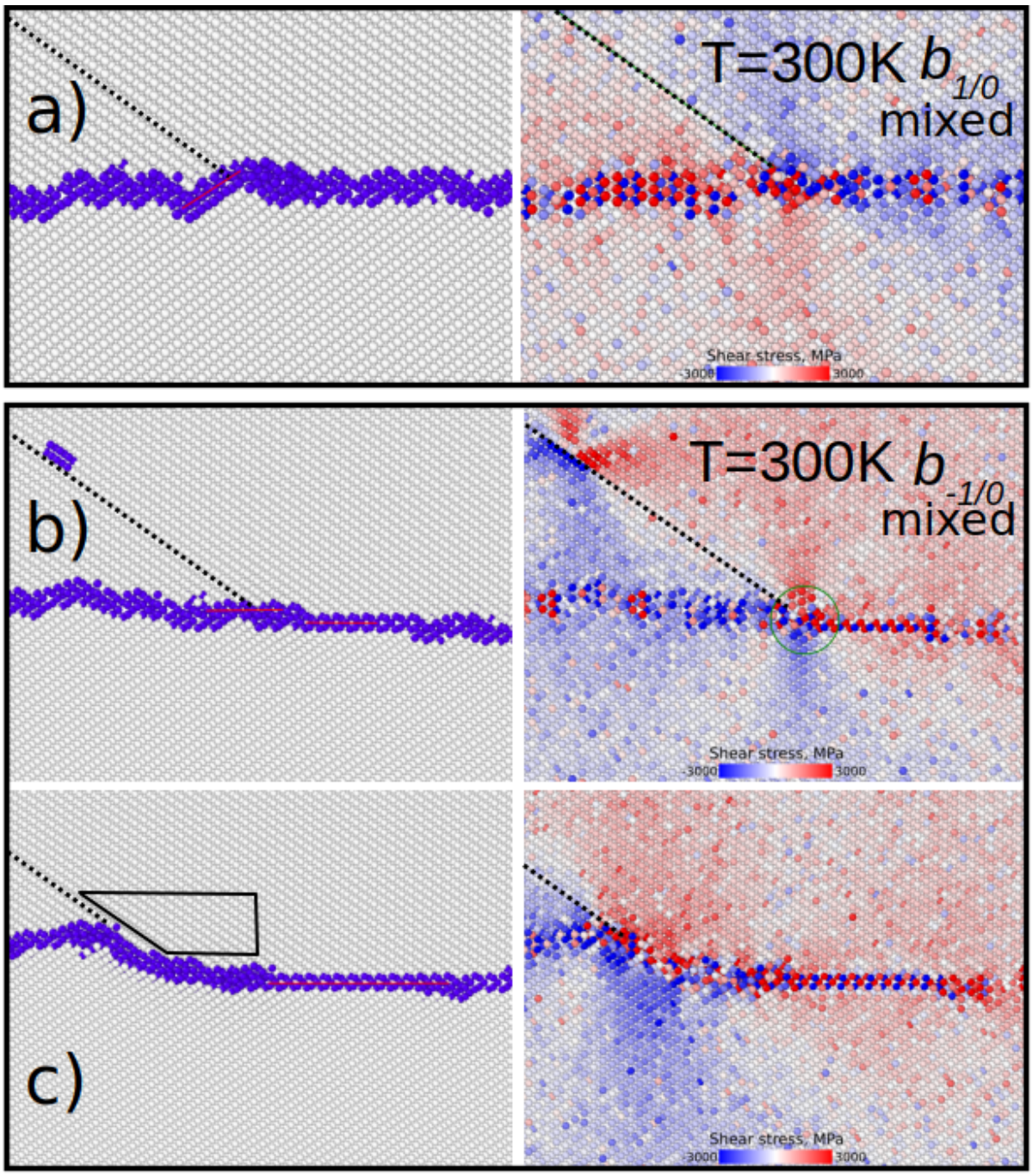

Figure 5.20: Snapshots of MD simulation of a {111} GB interacting with a pileup of mixed dislocations in Fe at T = 300 K. The configurations in a) and b) show the system after the absorption of the first dislocation in $\mathbf{b}_{1/0}$ and $\mathbf{b}_{-1/0}$. Red line on a) indicates the facet of the formed riser. c) Configuration of the system after the absorption of the second dislocation for $\mathbf{b}_{-1/0}$. Dashed lines are guides for the eye indicating the glide plane.

To complete the study we have measured the stresses at the interaction region where the relevant reactions take place (Fig. 5.20c). For the interaction with mixed dislocations we emphasize the following reactions: (I) the creation of the GBD after the first absorption; (II) the second absorption; (III) the creation of a 'complementary' riser; (IV) the end of stress application. The results are given in Table 5.10. There is only one absorption for the $\mathbf{b}_{1/0}$, we can only see how the shear stress in that region increases with the increase of external stress. And for $\mathbf{b}_{-1/0}$ the values obtained are slightly lower. It seems that this extra dislocation absorption allows the system to accommodate the stress better.

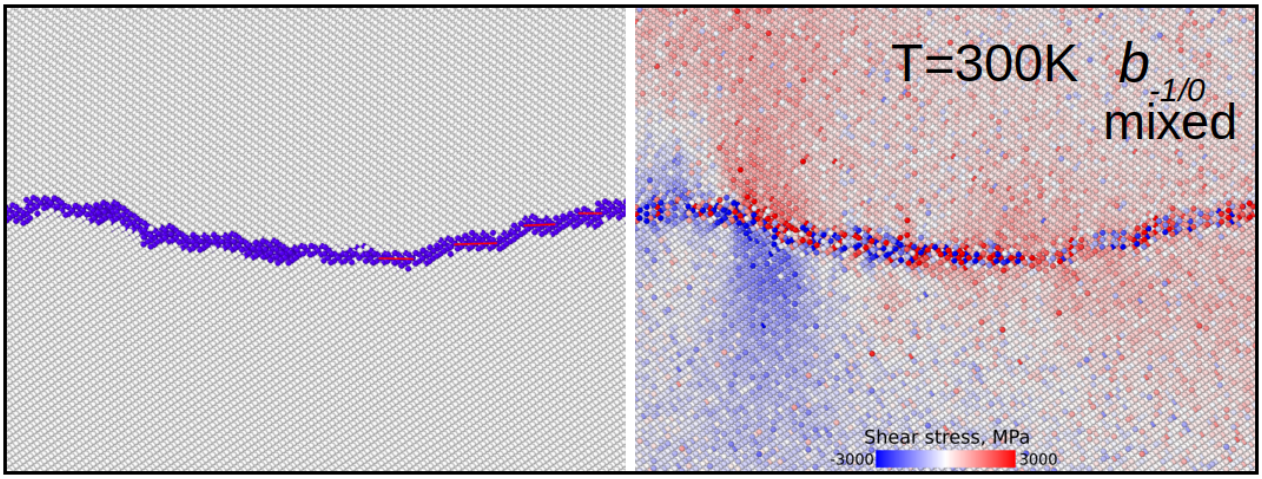

Figure 5.21: Snapshot of MD simulation of a {111} GB interacting with a pileup of $\mathbf{b}_{-1/0}$ mixed dislocations in Fe at 300 K. The figures show the final configuration of the system at the end of stress application.

Table 5.10: Local stresses at the reaction region before the reactions for the mixed ($\mathbf{b}_{\pm 1/0}$) in Fe at T = 300 K. Shear is the local shear stress.

Reaction	(I)	(II)	(III)	(IV)
Bv	Shear (MPa)			
$\mathbf{b}_{1/0}$	390	-	-	770
$\mathbf{b}_{-1/0}$	300	630	600	600

5.3.4 Discussion

The interaction of the {111} GB with a dislocation pileup is defined essentially by the absence of elementary disconnections. As we have seen in the previous Sections of this chapter, these interfacial defects play a pivotal role on the evolution of the GBs and are involved on the reactions with dislocations. The leading role now falls to the stepping mechanism already described in Section 4.3 (Fig. 4.14c). As this mechanism is stress-activated, the presence of many dislocations in the vicinity of the interaction region enhances the transformation of the interface, which is substantially more marked than for a single dislocation.

When the glide plane is at 90 degrees of the GB the changes on the interface are more relevant, the first dislocation is not transmitted but together with the subsequent dislocations it moves deeper into the adjacent grain creating either a combination of {112} GB + {110}/{001} asymmetric facet (T = 300 K) or two {110}/{001} facets (T = 900 K). When the glide plane is at 19.47 or 144.74 degrees with the GB, up to two dislocations can be absorbed, forming an asymmetric facet along the glide plane.

The level of stresses for the reactions to occur depends on the metal considered, iron in this study. The value of the external stress at which a specific reaction takes place depends also on the ambient temperature. Even for a fixed temperature, the critical stress varies with the simulation conditions, hinting that the observed event is probabilistic and thermal activation plays a role in it. Based on the obtained results, one can conclude that {111} GB acts as a strong obstacle for gliding dislocations, does not allow a direct dislocation transmission.

5.4 Summary and discussion

After completing the analysis of the interaction between a DPU and the chosen GBs we summarize the most relevant findings obtained. The role played by different factors (glide plane orientation, temperature, disconnections, material, etc.) is discussed.

Role of elementary disconnections. The final outcome of the interaction is defined and controlled by EDisc. A clear example of this is shown in the results for the {112} GB (Fig. 5.2). Depending on the relative position where the EDisc are produced with respect to the interaction region we can observe two different reactions, either transmission or shear-coupled GB migration. The outcome of the reaction is defined by the Bv of the EDisc which interacts with the GBD.

The behavior upon interaction between the {112} GB and DPU is reflected on the slip-twin interaction. {112} twins thicker than 6 nm act as strong obstacles for the slip of the pileup. Dislocations are blocked with the subsequent hardening of the material. When the thickness of the twin is small (< 5.6 nm), the dislocations provoke the annihilation of the twin.

EDisc in {332} are created at higher stresses than in {112}. Interaction with the DPU creates a riser, and the high level of stresses at either side of the riser produces EDiscs that compensate the step height. The Bv sense of the created EDiscs is the same. There is no interaction between the created GBDs and EDisc. The only reaction at the interface is sequential absorptions. Essentially, if EDisc can perform conservative climb the following reaction is SCGBM, otherwise EDisc pile at the riser leading to formation of {112} twin.

The total absence of EDisc in {111} GB defines the completely different outcome of the reaction with the DPU. This GB does not experience SCGBM and the Bv of the initial dislocation cannot be redistributed into the GB defects. So that none of the reactions shown in scheme of Fig. 1.1 occur in the {111} GB. Instead, motion of the GB is produced by a shuffling mechanism, so that there is a penetration of one grain into another.

Role of dislocations Burgers vector. The glide plane inclination and the Bv sense also affects the reaction products as well as the outcome. For instance, in {112} GB the interaction of a pileup of dislocations with the {112} tilt grain boundary results in either the transmission of the dislocations or the shear-coupled grain boundary migration. (i) If the tension region of the dislocation core is close to the boundary, namely edge $\mathbf{b}_{2/0}$ and mixed $\mathbf{b}_{-1/0}$, the reaction is transmission. (ii) If the compression region of the dislocation core is close to the boundary, namely edge $\mathbf{b}_{-2/0}$ and mixed $\mathbf{b}_{1/0}$, the reaction is shear-coupled grain boundary migration. Note that the migration process is possible because the created GBDs are glissile. Upon initial absorption each crystal dislocation creates a unique GBD with a certain Bv.

The results for the {332} GB also show the influence of dislocation Bv sense and its glide plane. For instance, the riser of the GBD may be either oriented along the glide plane of the pileup, developing a new asymmetrical {112}/{110} GB (case of $\mathbf{b}_{2/0}$ edge dislocations) or may be almost perpendicular to the said glide plane (case of $\mathbf{b}_{-2/0}$ edge dislocations). For the latter case the dislocations suffer repulsion and, for a fixed external stress, the GB absorbs a smaller number of dislocations, therefore the activated slip system defines how efficient the GB accommodates plastic deformation. The formation of the facets is enabled thanks to the specific dislocation – GB interaction. The formation and growth of new GBs, as a result of the extensive plastic deformation is well known to occur experimentally – the phenomenon is called grain refinement

The {111} GB is another example where the creation of new interfaces is the mechanism to accommodate plastic deformation. However, as we have explained above, given the absence of EDisc the formation of new interfaces is based on the creation of pure steps. The higher the angle of glide plane inclination, i.e., the more step height the dislocation brings in, the more steps are created in order to accommodate the step height introduced along with the glide of the dislocations attached to the GB. Thus, the largest deformation of the interface is observed upon interaction with edge $\mathbf{b}_{\pm 3/0}$

dislocations gliding at 90 degrees with respect to the GB (Figs. 5.16 & 5.17). Whereas for edge and mixed $\mathbf{b}_{\pm 1/0}$ the steps are not as high, so as the created risers. The sign of the dislocation Bv defines the orientation of the created step.

Single dislocation vs. dislocation pileup: effect of the local shear stress. The comparison between the results of the single dislocation case (Chapter 4) and the DPU case (Chapter 5) allows us to evaluate at a practical level, the role of the local shear stress on the GB – slip interaction. When the first dislocation of a DPU is on the vicinity of the GB the reactions observed are the same ones than for a single dislocation. The novelty is related to the trailing dislocations which increase the level of stress on the interaction region as a result of which some new processes can be activated leading to a completely different interaction.

The {112} GB represents the most noticeable example of the aforementioned change on the interaction: when a DPU of $\mathbf{b}_{2/0}$ edge dislocations interacts with the interface, the first one is absorbed forming a $\mathbf{b}_{1/-1}$ GBD. While in case of single dislocation there is repulsion between edge $\mathbf{b}_{2/0}$ and the interface, so that the $\mathbf{b}_{1/-1}$ GBD is never created. Subsequently, when the second one approaches, the stress field of the following dislocations allows to vary the location where the EDisc dipole is created. One of these EDisc reacts with the GBD resulting on the effective transmission to the neighboring grain of the first dislocation.

This relevant change also extends to the {112} twin – slip interaction. When a single $\mathbf{b}_{2/0}$ dislocation contacts a twin boundary there is always absorption. But upon interaction with a DPU, depending on the size of the twin and the direction of the stress applied, one or more dislocations can be transmitted into the twin and if the thickness of the twin is small enough, it can be annihilated with the subsequent softening of the material.

The effect of increasing the local shear stress for the other GBs is not as prominent as it is for the {112} GB, given that the reactions observed are similar to the ones with single dislocations. However, the comparison of the final outcome of the interaction for both cases shows remarkable differences. In the {332} GB the only reaction observed is the absorption of the dislocations, like for single dislocation case. The crystal dislocations decompose into a GBD with core riser and mobile EDisc. These EDisc formed during the interaction glide away and displace the GB. The Bv of the GBD is not parallel to the GB and therefore cannot glide along it but, under the appropriate conditions of shear stress and orientation of the dislocation pileup, the GBD may perform a conservative climb and could follow the GB in a shear-coupled GB migration.

In the case of the {111} GB, the interaction with a single dislocation leads to a minor and short-ranged modifications on the interface by the stepping mechanism described above. However, the action of this mechanism under the increased local stress tied to the trailing dislocations of the DPU produces significant changes in the interface which are more evident for the pileup of edge dislocations $\mathbf{b}_{\pm 3/0}$. Under the stress arising from the trailing dislocations the interaction proceeds as: (i) The heading dislocation attached to the interface moves increasing the intrusion; the formed along with the reaction {112} segment is displaced together with the dislocation and it keeps the same length while the asymmetric facets grow. The second dislocation follows the heading. (ii) The second dislocation is absorbed and it increases the length of the facet created by the header dislocation.

Effect of temperature on the interaction. For all three GBs studied the main effect of the temperature is a reduction on the local stress threshold required to initiate the reactions. In the {112} GB, for both migration and transmission reactions, the stress threshold linearly decreases with the increasing temperature. For the {332} GB the relation is slightly more difficult, because for the absorption reactions following the initial formation of the GBD it is required a higher stress that significantly decreases by increasing the temperature. And for the {111} GB, the effect of increasing the temperature has been evaluated for the pileups of edge dislocations $\mathbf{b}_{\pm 3/0}$. We have noticed a transformation of the new interfaces created: while at room temperature we have a combination of one {112} GB with a {110}/{001} facet produced by the stepping mechanism, at T = 900 K the

{112} GB is transformed into another {110}/{001} facet. This indicates that temperature enhances the shuffling mechanism necessary for creation of pure steps responsible for the asymmetric facets, but does not affect the number of absorbed dislocations.

Influence of the material. Our study has been performed using iron as the reference material, nevertheless, in order to assess the influence of the material on the properties and processes investigated we have extended it to other materials sharing the same bcc structure, namely chromium and tungsten.

The comparison of the results for the three materials, which were obtained in equivalent loading conditions, indicates that the differences between metals are related to the interatomic interactions that determine the distribution and magnitude of the stresses required at the interaction region to activate the aforementioned processes. Some particular atomic-level aspects specific of each metal, such as dislocation core structure, stacking fault energy and GB core structure, determines the threshold in the local shear stress needed for the process to occur.

For the {112} GB the stresses at which the dislocations are transmitted or SCGBM takes place are different for each metal and this can lead in some cases to a different interaction. As an example, in the interaction of a pileup of $\mathbf{b}_{2/0}$ in W with a {112} twin the dislocations do not penetrate into the twin, because the Peierls stress for a dislocation is higher than that for the creation of EDisc dipole. As for the {332} GB, the influence of the material is reflected on the maximum number of dislocations absorbed.

5.5 Conclusion

The interaction of a pileup of dislocations with a GB is based on two different aspects, namely: i) the geometrical aspect, i.e., the crystallographic structure of the dislocation and the GB, which is common to all materials of the same structure (bcc, in our study); ii) the atomic interaction features, which are material dependent and which affect the energy balance i.e., the external stress needed to inject dislocations into the interface, the local stresses needed to trigger the reactions, Peierls stress to move elementary disconnections. An ambient simulation temperature also plays a role when thermal action assists in overcoming the energy/stress barrier for a reaction to proceed. On the basis of the obtained results and their analysis a number of observations regarding the deformation and modification of the atomic structure of the studied GBs upon the interaction with DPUs under externally applied stress are listed below.

1. The general conclusions related to the atomic processes of the slip – grain boundary interactions are common to the three bcc metals studied, namely Fe, Cr and W.

2. The differences between metals are related to the interatomic interactions that determine the distribution and magnitude of stresses required at the interaction region to activate the processes.

In conclusion:

- The {112} GB upon interaction with DPUs accommodate plastic deformation either by transmission or by SCGBM. The final outcome is defined by crystallography of the incoming dislocations in relation to the interface.

- The {332} tilt GB upon interaction with DPUs experiences consecutive absorptions of the incoming dislocations forming new asymmetric interfaces. No twins are formed as in case of interaction with a single dislocation.

- The {111} GB upon interaction with DPUs behaves similarly as in the case of interaction with a single dislocation. It acts as a strong obstacle that does not allow a direct dislocation transmission into the adjacent grain or reflection back into the initial grain. There is as well no absorption in terms of decomposition of the heading dislocation Bv.

CHAPTER 6

INTERACTION OF MOBILE GB DEFECTS WITH IRRADIATION DEFECTS

A global vision of the interaction between GBs and dislocations shows, as we already exposed in Section 5.4, that EDisc play a decisive role in these processes. The reasons are essentially two: on the one hand, EDisc appear as an outcome of the observed reactions and on the other hand, they are responsible for SCGBM. Therefore, the evolution of the GBs is closely linked to these defects. With the exception of the {111} GB, EDisc are always present in all the other GBs studied and we have been able to ascertain, given the conditions considered (glide plane inclination, Bv orientation, temperature, etc.), what is the contribution of these interfacial defects on the evolution of the GB structure, ranging from SCGBM to the creation of new interfaces.

From this starting point, now a question arises, which is what would happen with the processes involving EDisc if there are obstacles hindering their motion? Answering this question has been the motivation for the study presented in this chapter. Among the set of GBs, the {112} GB exhibits many features which make it especially relevant in bcc materials, as we have been pointing out throughout the previous chapters. Summarizing our findings, there is only one type of EDisc present ($\mathbf{b}_{1/1}$ and $\mathbf{b}_{-1/-1}$) which can only be produced in two possible ways, either as a dipole at the pristine interface or at a GBD ($\mathbf{b}_{1/-1}$) acting as a source of disconnections. Said GBD appears as an outcome of the GB – dislocation interaction or in the vicinal GBs. Given the relevance of the {112} GB we have chosen it to perform this study, analyzing the interaction of the EDisc with a set of obstacles. The objects chosen to perform as obstacles are several irradiation defects, as they are present in nuclear structural materials when they are under operation conditions.

The study of dislocation interaction with obstacles has been a subject of interest for a long time. Interactions between irradiation defects and dislocations in the bulk have been fully characterized for Fe-based alloys in many studies [121–125]. The nature of dislocation – precipitate interactions is well described by the Orowan mechanism [126]. In contrast, interactions between such defects and GBs are more complex and less understood. Applicability of the Orowan precipitate hardening equation to twin propagation was studied in [127] by two-dimensional dislocation dynamics simulations of a twin tip interacting with a line of obstacles. As for other defects, both voids and He bubbles are considered in a similar way in the literature, despite the fact that the latter shows a slight difference in strength depending on the He amount [128]. Atomic simulations show high shear resistance of such defects leading to strong local interaction [123, 129].

According to the previous studies, spherical irradiation defects can be classified depending on the type of interaction existing between the inner atoms and the incoming linear defects: i) soft defects, also known as shearable defects, when the dislocation interacts effectively with their atoms; ii) hard defects, when the dislocation is not able to interact with the inner atoms because it cannot penetrate the defect. Impenetrable defects cannot be sheared by dislocations or disconnections in case

of interaction with them.

Interaction with hard defects is consistent with the findings of Richman [130], who suggested that twins in bcc metals could bypass the defects forming a torus shape at the interaction. The hard defect in that case is situated in the inner cavity, and it can be described in terms of disconnection loops. These disconnection loops are equivalent to Orowan dislocation loops that are left behind after the interaction of a bulk dislocation with a non-shearable obstacle [126]. The stress increment due to the defects in the case of interactions with dislocations is given by the modified formula for Orowan stress:

$$\Delta\tau_{Orowan} \sim (Gb/l)\left[ln(d^{-1}+l^{-1})^{-1}+B\right] \tag{6.1}$$

where G is the shear modulus, b is the magnitude of the Burgers vector, l is the defect spacing, d is the diameter of the defect, and B is a constant of order 1 [131].

Crystal screw dislocations are able to bypass the defects at high temperatures without direct interaction by shearing. On the other hand, edge dislocations are constrained to their own glide plane, in the same way that disconnections are constrained to the GB interface plane. This is the reason why disconnections are forced to bow around the hard defects leaving a loop on the GB behind the interaction, or to shear them in case of shearable defects. These interesting features of the GB – defect interaction have attracted significant attention of material research at the present time in bcc [64] and hcp [132, 133] metals. In this work we study in detail the interaction of the {112} GB and its glissile defects with irradiation defects placed on or near the GB, such as Cr precipitates, voids and He bubbles. All the simulations have been carried out according to the methodology provided in section 2.3.

For modeling interactions between irradiation defects and GB standard MD has been used. Two different approaches have been used in this task. First approach serves to study the interaction between an irradiation defect placed on a GB with a single disconnection introduced manually. To create the disconnection on the interface, a dislocation is introduced at the step along the translation vector between the two grains as described in [64]. Second approach is used to study the interaction with the successive disconnections supplied by a source of disconnections. To obtain this source, a $\frac{1}{2}\langle 111\rangle$ crystal dislocation is introduced along a {112} glide plane, an external shear strain is applied in order to induce an interaction between the dislocation and the GB and the GBD is produced as an outcome of the reaction. The reactions are described in [57, 110]. These bicrystals were then relaxed again in order to introduce irradiation defects. All the crystal defects are introduced manually with the help of Atomsk software [101].

Due to the limitation of the software, for the first approach fixed boundary conditions were used along the GB plane. This allows to study only single interaction between the disconnection and a certain irradiation defect. Defects present in the simulation box can act as stress concentrators, or obstacles to disconnections glide. In order to study the different effects, two different positions of the defects were chosen. The first one is directly on the interface with the center of the defect at the GB, and the second is 5 Å above the interface. The distance covered by the GB each time the disconnection passes along the interface is equal to the height of the step of the disconnection, which is $\frac{1}{6}\langle 112\rangle a_0$, or around 1.2 Å. The size of the defects has been chosen to be the same for voids, precipitates and bubbles and varies from 2.5 Å to 5 nm in diameter.

As for the irradiation defects introduction, voids are created by simply taking out atoms located in a spherical region with a given position and size. Helium bubbles are introduced by inserting a He sphere in place of void with the ratio of two He atoms per one Fe atom deleted. As for precipitates, three different cases have been studied. Since chromium is a bcc metal as iron, Cr atoms belonging to a precipitate are also oriented in a certain way. Three cases are: 1) atomic planes in the precipitate are oriented the same way as deleted iron atoms (substitution of Fe atoms by Cr atoms considering the difference in lattice parameters) – named 'subst' in the following or referred simply as precipitates; 2) atomic planes in the precipitate oriented the same way as the Fe planes in the λ grain – named '112' in the following; 3) atomic planes in the precipitate are oriented as [100], [010] and [001] for Cartesian axes – named '100' in the following. Both '112' and '110' cases present an extreme case to study the

effect of interaction at the edge of the defect. Periodic boundary conditions along the tilt axis allow to approach the problem as an interaction between the disconnections and row of defects, rather than a single defect, as it was considered in the previous works on dislocation – defects interactions.

In addition to the used for the other tasks potentials we use potentials by D. Terentyev et al. [134] and by G. Bonny et al. [92] for modeling of the interactions of bulk iron atoms with He atoms and Cr atoms, respectively. Two types of simulations have been performed: Molecular Static, to study the interactions in detail removing any influence of thermal agitation and Molecular Dynamics at 300 K to study the effects of the temperature on the reaction and stresses needed to trigger it. In both cases the incremental shear strain was applied in order to move the disconnection to initiate an interaction between two defects.

The chapter is based on [135] and structured as follows: in Section 6.1 there are presented the results obtained for the interaction between the single elementary disconnection and irradiation defects of various sizes, Section 6.2 presents the results on effect of a row of EDisc interacting with the irradiation defects. Initially, we describe the interaction of a single disconnection with irradiation defects of different size placed on the interface via molecular static simulations. In the following we investigate the effect of several factors on this interaction: temperature, relative position of the defect and number of disconnections. Finally, in Sections 6.3 and 6.4 the discussion and the main conclusions reached from the results obtained are presented.

6.1 Size effect on interaction with a single disconnection

In the present Section we focus on the static interaction (T = 0 K) between an irradiation defect and a single disconnection previously inserted on the GB.

Fig. 6.1 shows cases of shear stress versus strain curves for voids and bubbles of different diameters. We can notice that all the curves share the same trends: in the linear elastic region there are small drops of 3 MPa (inset in Fig. 6.1a) which happens when the disconnection glides a distance equivalent to its Bv ($\sim 0.29a_0$). The disconnection motion cannot accommodate all the stress supplied, which leads to an increase of the total stress in the system. When the disconnection interacts with the defects at around 0.005 applied strain, there is a release of around 90–120 MPa.

The full process of interaction between a spherical irradiation defect and a disconnection is qualitatively similar to the interaction between these defects and a crystal dislocation. It can be divided into four stages shown in Fig. 6.1 as follows: (1) the disconnection glides freely towards the defect; (2) the disconnection reaches the defect and gets attached to it; (3) as the stress increases, the shape of the disconnection changes in two possible ways: for hard defects it remains attached to their edge, while for soft defects the disconnection interacts with their inner atoms changing the shape of the defect; and (4) the disconnection totally overcomes the defect and breaks away.

Let us now present each stage of the interaction in full detail. Before the attachment of the disconnection to the defect there is a linear part of the curve corresponding to the glide of the disconnection (region marked as '1' in Fig. 6.1). Although the presence of the defect does not does not affect significantly the elastic properties of the material, increasing the size of the defect causes a slight reduction in the shear modulus.

When a certain size threshold is exceeded, the defects act as strong obstacles for the glide of disconnections. For the smallest sizes, defects are transparent for the motion of the disconnection, i.e., there is no attachment to the defect (compare the black curve in Fig. 6.1a with purple curves in Fig. 6.1a, 6.1b). Indeed, the smallest void consists only of five vacancies. For the bigger defects, once reached the required stress level, it attaches to the defects bending its line (see drop of stress marked as '2' in Fig. 6.1). The attachment allows further concentration of stresses at the defects interaction site, while bowing the disconnection line (region marked as '3' in Fig. 6.1).

The type of the precipitates used in the study of the size effect is the 'subst' one, i.e., without incoherent boundary at the edge. Such precipitates act as transparent obstacles, i.e., the disconnection is not pinned at the edge. In order to investigate the interaction process when the disconnection is attached to the precipitate, additional cases were modeled – 'subst', '112' and '100' with a 5 nm diameter. In doing so, we obtain the configuration with pinned disconnections as shown in Fig. 6.2a.

The final stage takes place when the system accommodates enough stress for the disconnection to break away, reflected as drops of 20–30 MPa in the stress-strain curve (marked as '4' in Fig. 6.1). Note that for the smallest transparent defects there is no such release of stress, it is included in the drop at 0.005 of applied strain. Fig. 6.2b shows the critical line shapes for disconnections passing a certain defect right before the break away of the disconnection. Comparing it with the Fig. 6.2a we can see how the defects interaction changes shape of the line accommodating stress along with it. Disconnections interacting with '100' and '112' precipitates have similar shapes before detachments. The disconnections pass almost the same distance for both cases, as the critical stresses before detachment for these precipitates are similar. Disconnection is detached from 'subst' precipitate at the lowest strain applied since the precipitate keeps the same orientation as the bicrystal. There are only interactions involving the interface between two metals. All three types of precipitates, together with voids, can be considered as soft obstacles, as no residual defects are left on the interface, and the inner atoms of the defects are found to be sheared (see Fig. 6.6).

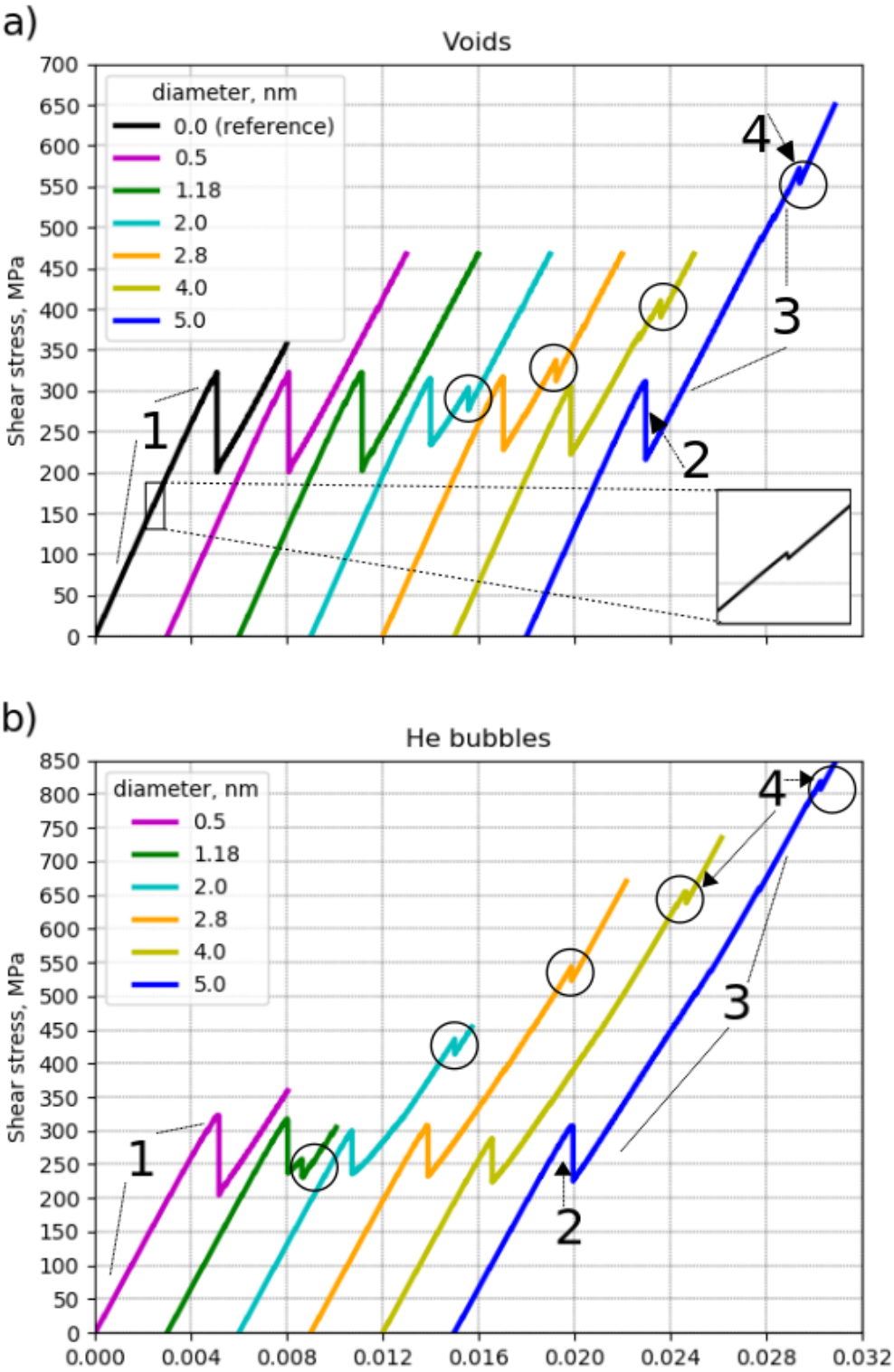

Figure 6.1: Shear stress vs strain applied in static simulations with voids and bubbles of different sizes placed on the interface. The colors correspond to different diameters in nm. Interactions with rows of a) voids; b) He bubbles. Marked with '1' and '3' are the parts with linear increase of stress in the system, while drops at '2' and '4' correspond to the interaction between the disconnection and the defect and the breakaway of the disconnection, respectively. The critical stresses marked as '4', highlighted with circles, are plotted in Fig. 6.3. For the readability purpose the curves are offset from each other along x axis by 0.003.

.

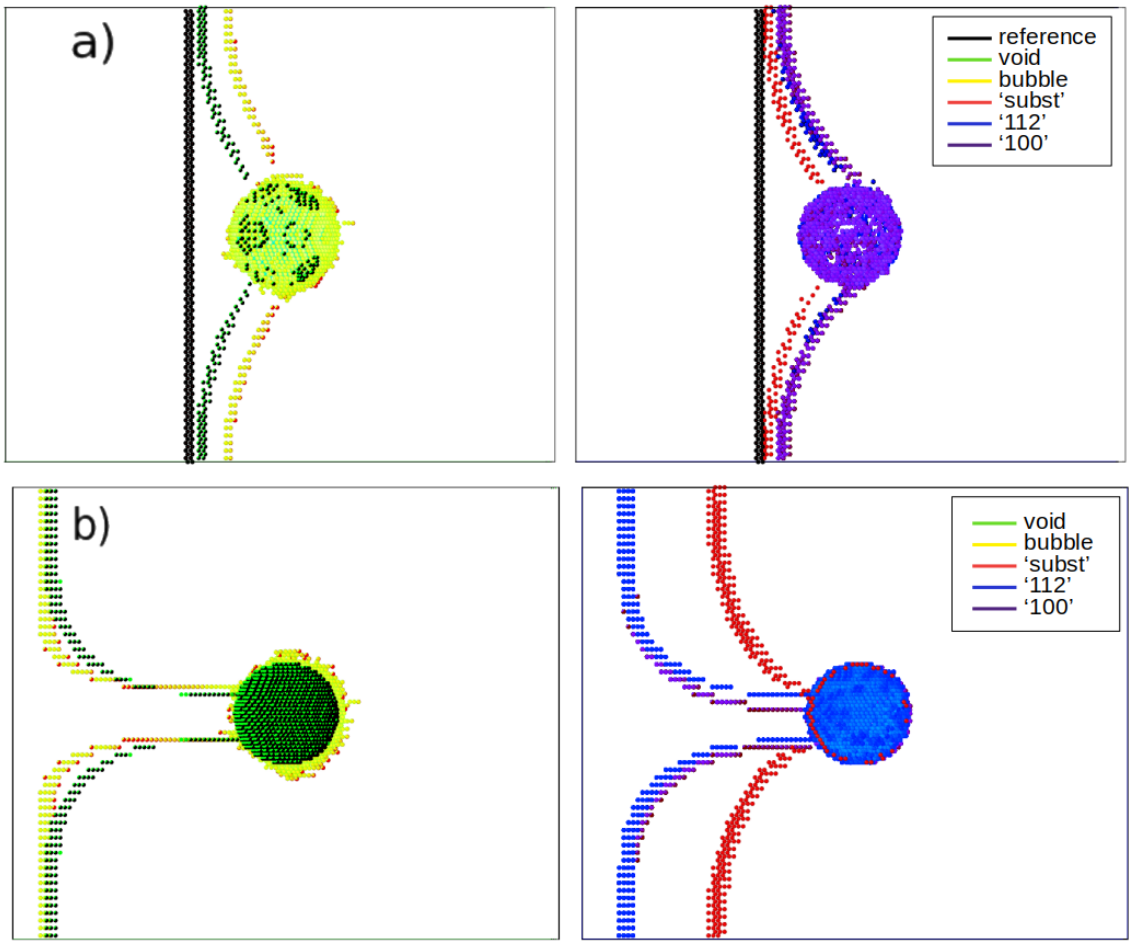

Figure 6.2: Snapshots from the simulations of the 5 nm diameter defects on the interface interacting with the single disconnection. a) Top projections showing the shapes of the disconnection attached to the defect. Reference case is shown in black. b) Snapshots from the same simulations at the critical stress, i.e., critical line shapes.

As for Helium bubbles, the He-He and He-Fe interactions are repulsive [134], leading to an increase of the value of the critical stress and subsequently, to an extension of the critical shape. The disconnection line encircles the bubble without affecting the inner atoms, therefore, bubble act as a hard obstacle.

Comparing the results of the present study with the ones presented in [122, 123] on the interaction between edge dislocations and voids we notice a qualitative agreement between both. This similarity can be explained by the fact that both, dislocations of [122, 123] and disconnections, share the same edge character differing only on the Bv magnitude ($0.87a_0$ vs $0.29a_0$). And it allows to perform an estimation of the critical stress of void strengthening in the same way described in eq. (6.1). In our study $b = 0.87a_0$ is the Bv magnitude of the shortest possible edge dislocation. The dependence of the critical stress as a function of the harmonic diameter for the different defects is plotted in Fig. 6.3 along with the value predicted from eq. (6.1) with values of B taken from [122, 123].

Atomic simulations of dislocation – void interaction showed that the possibility of a dislocation climb reduces the strength of the void, as the size of the void is decreased. However, in the case of disconnections, their glide is strictly limited to a single {112} plane, showing a good agreement between the theoretical values and simulation data on voids.

He bubbles affect not only the elastic properties, but the crystallographic interaction between the defects, increasing the critical stress. The disconnection interacts with the bubble forming a screw dipole, which contributes to distribution, yet the values predicted from eq. (6.1) fit the simulation results. The extra resistance for the largest bubbles, with the size exceeding 3 nm, likely comes from

the large spacing of the dipole arms, because the disconnection is not absorbed inside the bubble unlike inside the void. According to the best fit, $B = 1.52$ provides good agreement for the breakaway stress between MD and eq. (6.1).

Precipitates act as transparent obstacles if the disconnection is not pinned to the defect. This pinning only happens when the size of the precipitate is the highest considered (diameter of 5 nm). For the latter, once the disconnection is attached to the defect, there is a stress threshold that must be reached for the disconnection to be able to overcome the incoherencies at the edges of the defect. At this, the resistance of the coherent ('subst') precipitate is essentially smaller as compared to the precipitate with the core structure different from the interface orientation. The extra resistance can naturally be explained by the additional work required to shear the precipitate in the non-favorable plane. The reason for low and negligible resistance of small precipitates needs to be studied further.

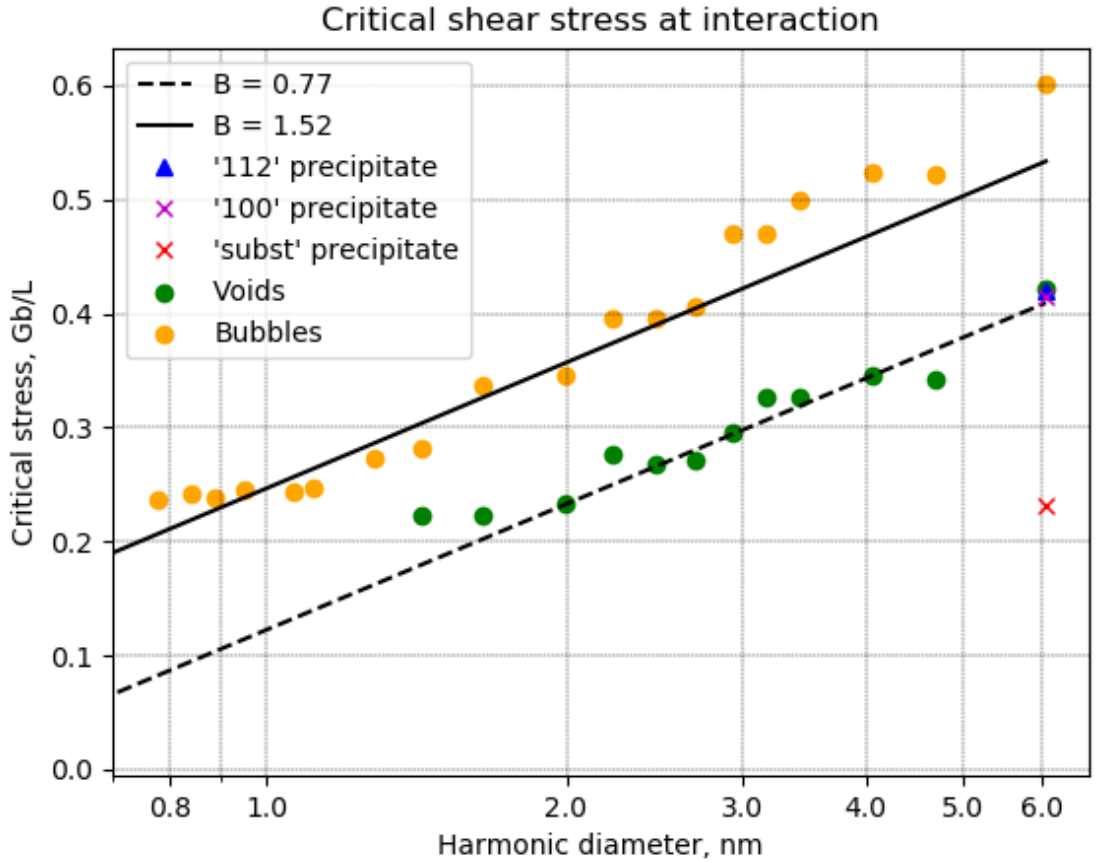

Figure 6.3: Critical stress for the detachment of the disconnections from different defects as function of harmonic diameter of an obstacle.

In the next Section we introduce a new element in the simulations: a source of disconnections. As it has been explained in the previous Chapters, this source is capable to produce continuously a flow of disconnections which interact with the irradiation defects. One of the relevant differences with respect to the single disconnection case is the level of stress in the system. The GBD acting as a source in our simulations can produce a dipole of disconnections when the stress level is around 2.2 GPa, while the stress needed for a single disconnection to glide is around 20 MPa [57, 64]. At the stress level required for the source of disconnections in our simulations, the behavior of the defect does not affect the stress distribution and the reaction outcome. The results show a very different behavior that the one described in this Section, evidencing that the interaction of each disconnection with a given defect is heavily influenced by the next incoming disconnections.

6.2 Effect of disconnection number interacting with different types of irradiation defects

In the present Section we show the details of the interaction between the same set of irradiation defects introduced in Section 6.1 and disconnections supplied continuously by a source. Both, static and dynamic cases, are studied for each defect and initial relative position, namely on and above the GB interface. For the sake of interest, we have only considered defects of extreme sizes, i.e., 5 nm in diameter.

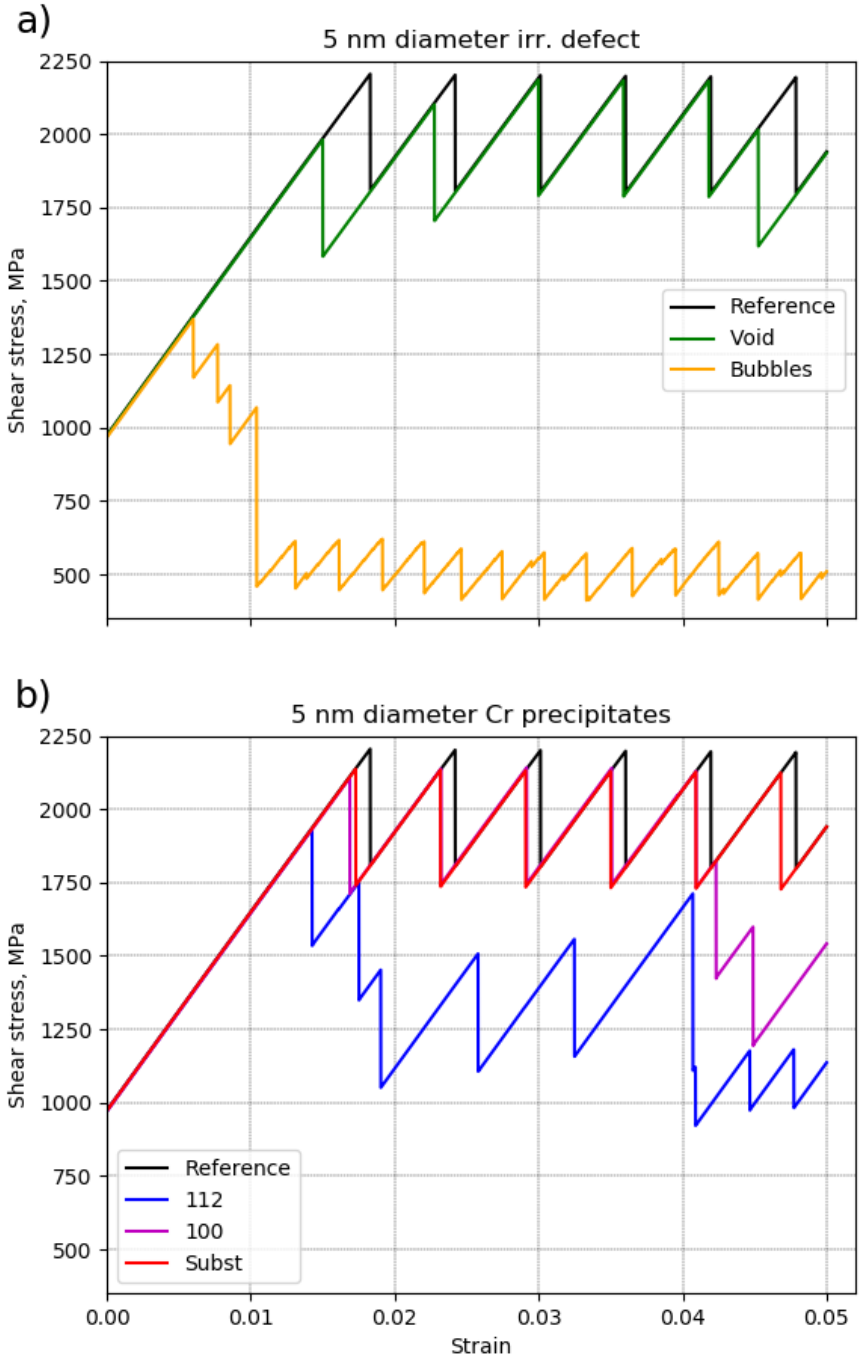

Figure 6.4: Shear stress vs strain applied in static simulations with defects of extreme size placed on the interface. a) Curves for void and bubble; b) curves for precipitates. The colors' meaning is the same as before.

6.2.1 Static interactions with several disconnections

A GBD formed at the interface as a result of the absorption of a crystal edge dislocation acts as a stress concentrator. Once the critical stress is reached, a dipole of disconnections is emitted. When the emission of disconnections takes place, there is a release of stress around 400 MPa and the interface is displaced one {112} atomic plane, i.e., $0.408a_0 \sim 1.2$Å.

Fig. 6.4 shows the shear stress averaged over all mobile atoms versus the strain applied for all defects studied in static simulations, when the defects are placed on the interface. The result for voids seems to indicate that these defects have little to none effect on the gliding of disconnections (green line in Fig. 6.4a), therefore voids act as soft defects. The difference between the shear stress needed for creation of a disconnection dipole (2.2 GPa, see black curve in Fig. 6.4) and the critical shear stress for the void of the extreme size (0.57 GPa, see blue curve in Fig. 6.1a) explains the observed transparency of the void to the glide of disconnections.

On the contrary, helium bubbles have a significant effect on the shear stress (yellow line in Fig. 6.4a) and the propagation of disconnections along the interface. After the initial emission of four disconnections, a steady state is reached at around 0.6 GPa. This level of stress is about 0.2 GPa lower than the critical stress for the interaction between the bubble of extreme size with a single disconnection (0.82 GPa, see blue curve in Fig. 6.1b). In our simulations we have established a ratio of 2 to 1 between He atoms and vacancies in the bubbles, which are considered as over-pressurized according to [128] and consequently, should behave as weaker obstacles than bubbles with a smaller ratio.

The interaction of the first disconnection with the bubble shows remarkable differences with the process described in Section 6.1: in order to minimize the intersection between both defects (accompanied by a reduction of the maximum shear stress) an interstitial cluster is emitted. Simultaneously, it takes place a pile-up of the subsequent disconnections, leading to the formation of residual disconnection loops around the bubble prior to closing of screw disconnection segments followed by detachment (see Fig. 6.5).

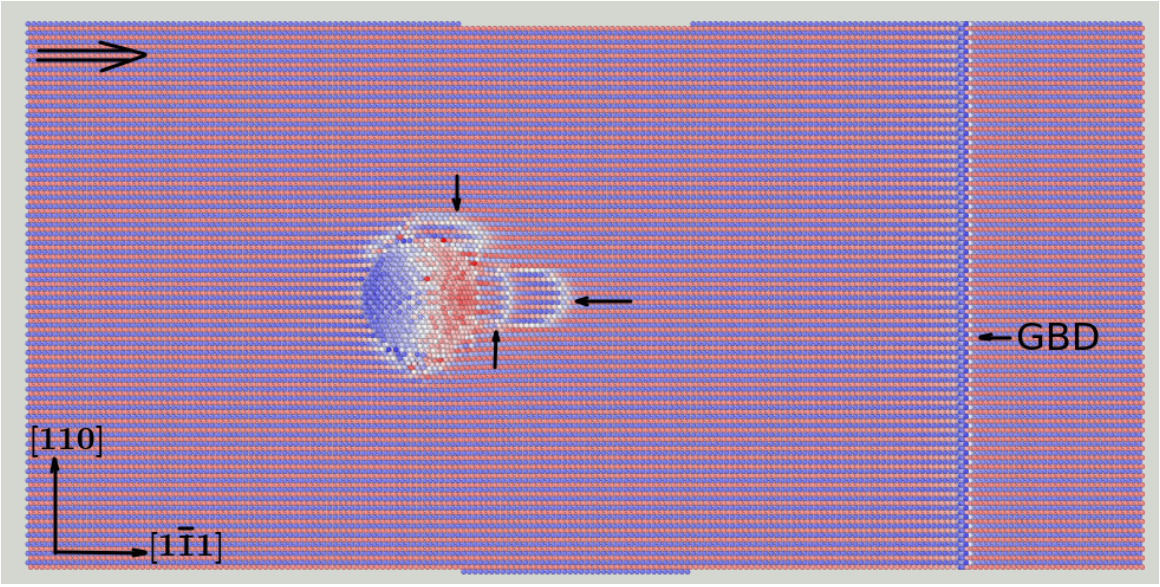

Figure 6.5: Snapshots from the simulations showing the top projection of the He bubble case after a drop of 0.61 MPa at 0.01 applied strain shown in Fig. 6.4a – disconnection is detached and absorbed by the GBD, leaving residual loops, shown by small black arrows. Big arrow in the top left corner shows the direction of the disconnection motion.

As for the Cr precipitates, our results for the 'subst' and '100' configurations prove that propagation of the disconnections seems to be unaffected by the internal structure of the defect, as the level of the critical stress measured for both cases is the same, around 2.2 GPa, which is significantly higher

than the measured values for the single disconnection case ($0.75Gb/l$ = 0.32 GPa for 'subst' and $1.31Gb/l$ = 0.56 GPa for '100' from the Fig. 6.3). At such level of stress the inner structure of the precipitate does not affect the reaction, as the disconnections cross through the precipitates as if they were transparent obstacles. As the GB moves up, the effective size of the defect is progressively reduced, up to the point that disconnections interact only with the tip of the defect. For '100' precipitates we observed that Cr atoms are sheared by the disconnections.

The behavior observed for '112' precipitates indicates that disconnections interact with the inner atoms of the defect, changing the orientation of its atomic planes. The stress state for the '112' case is different as it is sheared by the disconnections. The first disconnection crossing through leaves a stacking fault inside the precipitate, shown on Fig. 6.6a. When the subsequent disconnections cross the defect, the interface moves up, inducing the creation and growth of a 'twin-like' structure inside the precipitate. The lower part of the precipitate keeps the initial orientation and the form, while the upper part is reoriented as the lower grain. Fig. 6.6b shows the configuration after 10 disconnections have crossed through the defect.

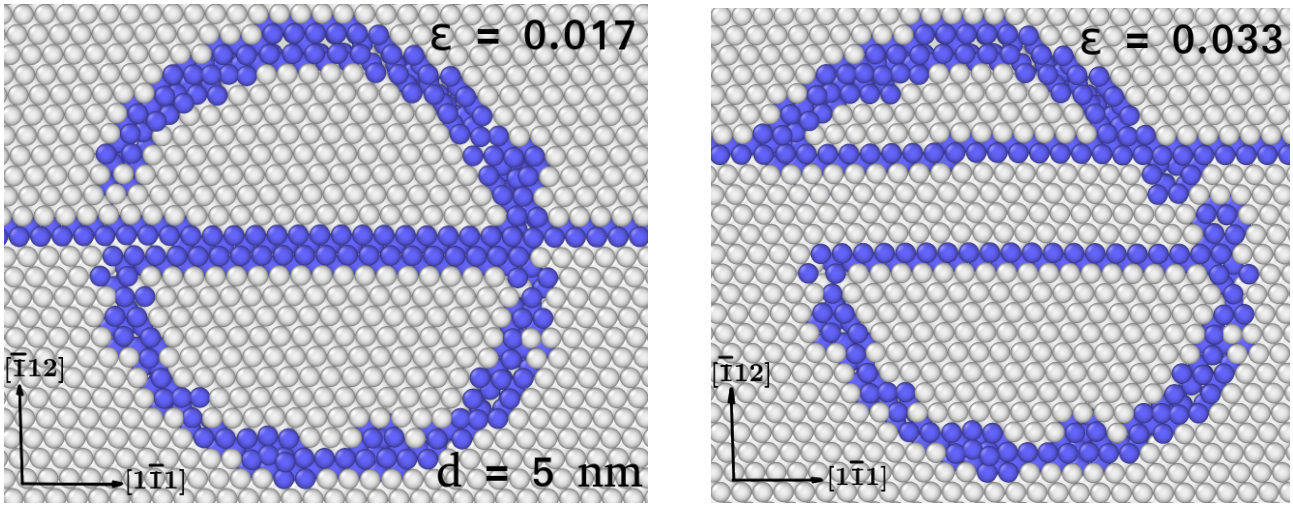

(a) (b)

Figure 6.6: Snapshots from the simulations showing side projections of the '112' Cr precipitate at different strains applied. White atoms correspond to atoms in perfect bcc positions, while blue atoms correspond to disturbed crystal structure.

With the purpose of analyzing the effect of the GB – defect relative position on the interaction, we have carried out a new set of simulations placing the defects three atomic planes above the interface. The main difference with respect to the previous experimental setup is the effective size of the interaction. For all the defects considered, once the interface reaches the edge of the defect, the disconnections interact with it as a hard obstacle. At higher strains applied, when the effective size increases, the defects behave the same way as in the former case of defects placed on the interface.

Static simulations allow us to see the mechanisms of interactions. Depending on the defect type, disconnections can either interact with internal atoms of the defects or pass along the defect surface. The relative position of the defect is immaterial, as it does not affect the outcome of the interaction.

6.2.2 Dynamic interactions with several disconnections

For the simulations at a finite temperature the system was relaxed after the introduction of the defects, thermalized for 25 ps, then a deformation with a constant strain rate $\dot{\varepsilon} = 5 \times 10^7 s^{-1}$ was applied. Emission and glide of disconnections release more stress than in static simulations. For instance, in the reference case emission of disconnections starts at the very beginning of strain application. Because of the presence of the source of disconnections on the interface, the initial stress state is different from zero, but it is around 0.8 GPa. This stress level is enough to trigger an emission of a disconnection

dipole (black line in Fig. 6.7a). This state is steady, i.e., every time the system reaches this level of shear stress, there is an emission of a dipole, which releases around 0.65 GPa.

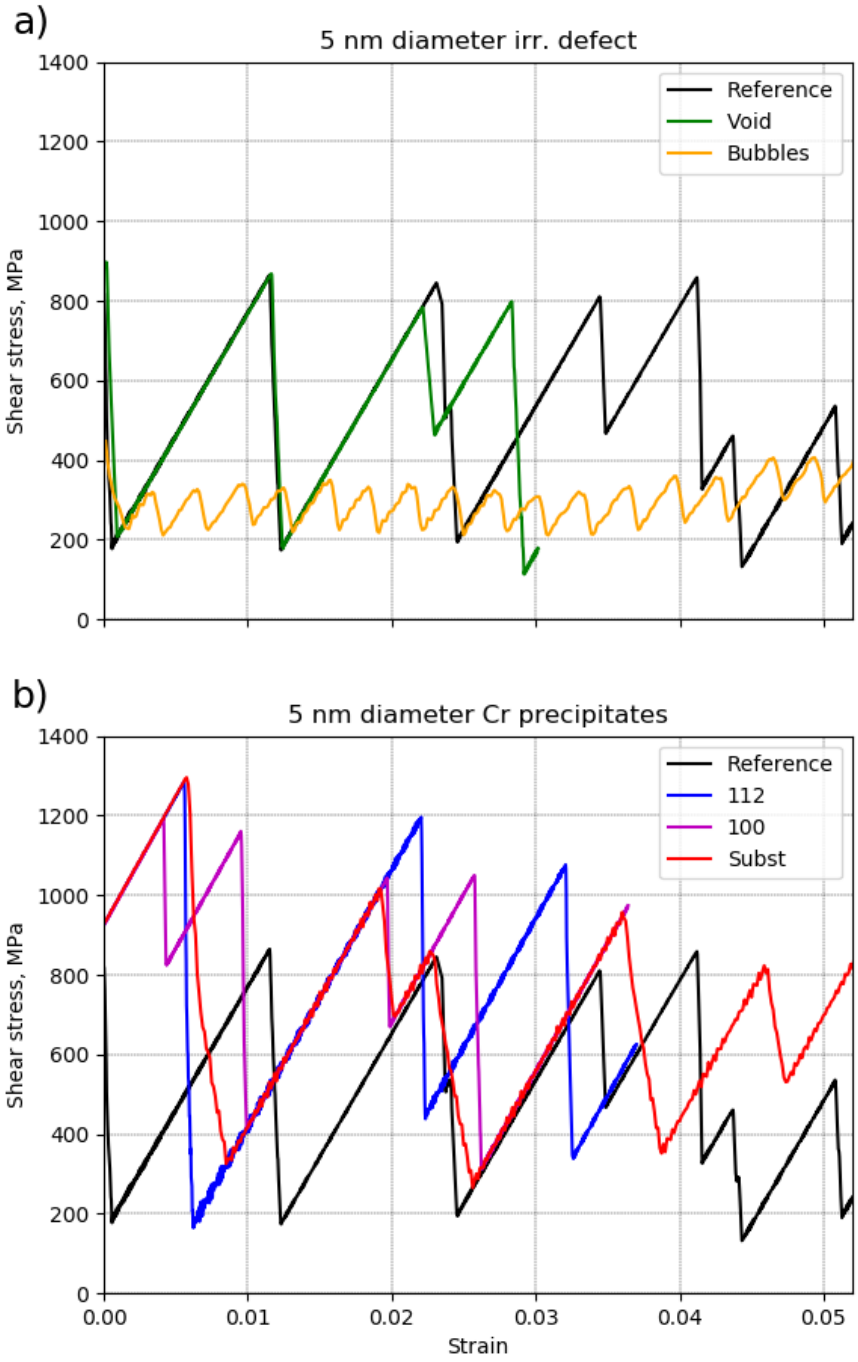

Figure 6.7: Shear stress vs strain applied in dynamic simulations at 300 K with defects of extreme size placed on the interface. a) Curves for void and bubble; b) curves for precipitates. The colors' meaning is the same as before.

In the case of voids, there are few differences between the static and dynamic cases (green line in Fig. 6.7a). The shear stress curves are similar to the reference case curves. Local stress concentrations affect the shape of the disconnection line and the actual stress in the system, but not the reaction and the final outcome. There are no residual defects left attached to the void after the interaction.

As for the Cr precipitates, dynamic simulations show a similar interaction process, irrespective of the GB – defect relative position. The shear stress needed to trigger the first reaction for the precipitates on the GB is around 1.3 GPa for 'subst' and '112' cases and around 1.2 GPa for '100'

case. These values are two times lower than the equivalents from the static simulations (compare Fig. 6.4b and Fig. 6.7b). Once this stress level is reached, the GBD emits sequentially six disconnections. After that the disconnections interact with precipitates as soft transparent obstacles.

Once again, Helium bubbles present the most complex interaction mechanism of all defects considered in this study. Once the first disconnection crosses through the bubble, which acts as a hard obstacle, an interfacial loop is created. The shear stress level when detachment of the disconnection takes place is the lowest among all the measurements. Once at least three disconnections interact with the bubble, a creation of a dislocation loop attached to the interface is possible. Its Bv is the sum of the Bv of the three disconnection loops: $^1/_2\langle 111\rangle = 3^1/_6\langle 111\rangle$, and the height of the step allows the motion of the loop outside the GB plane. This happens for both positions of the bubble. The system reaches steady state at around 0.33 GPa (Fig. 6.7a), at which single disconnections are detached from the bubble releasing around 0.1 GPa. Along with every interaction, the length of the dislocation loop growing in the lower grain increases. After the interaction with the first two disconnections, the length is 94.7 Å (marked as '1' in Fig. 6.8a,c), and 190 Å at the end of strain application (marked as '1' in Fig. 6.8b,d).

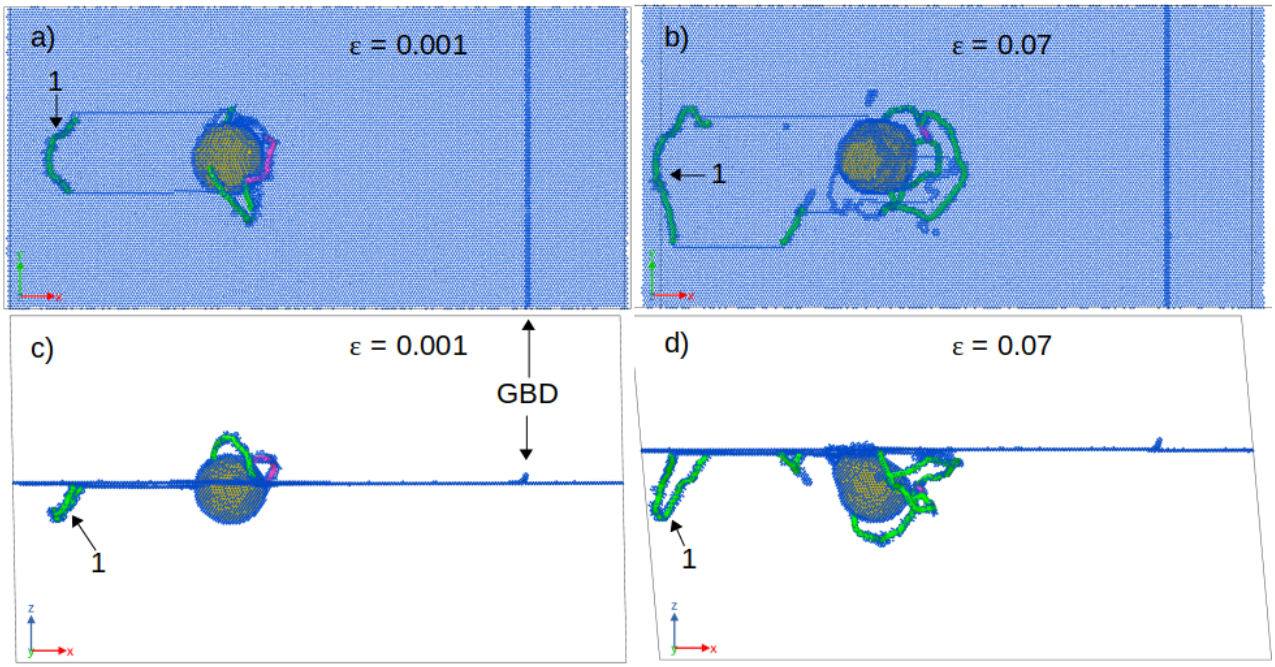

Figure 6.8: Snapshots from the simulations of He bubble on the interface. Top projections at a) 0.001 strain applied and at b) 0.07 of strain applied. Side projections at c) 0.001 strain applied and at d) 0.07 of strain applied. Marked as '1' is the dislocation loop growing into the lower grain. Blue atoms correspond to Fe, yellow atoms correspond to He. Dislocation loops are indicated with colored lines according to their Bv: green is $^1/_2\langle 111\rangle$, while pink is $\langle 100\rangle$.

An overview of the dynamic results shows that applying temperature lowers the stress accumulated in the system, as the stress threshold to initiate the emission of disconnections is significantly lower than for T = 0 K. However, the level of stress is high enough for the disconnection to not interact with the defects as strong obstacles. Changing the GB – defect relative position seems to have a negligible effect on the interaction process, as it only implies a change in the effective size of the defect interacting with the disconnections. This size increases for the defects placed above the interface after the attachment of the defect to the GB, and decreases for the defects placed on the interface, as the GB moves up.

6.3 Summary and discussion

The elementary disconnections of the {112} GB are highly mobile, producing the displacement of the GB along a direction normal to its interface. The step height of the elementary disconnection is just one atomic plane, which means that no shuffles occur and these disconnections glide easily under a relatively low critical resolved shear stress (around 20 MPa in pure Fe). This property is in the basis of the motion of the {112} GB. One particular feature of this interface is that when a single edge dislocation interacts with the {112} GB a GBD is created, which acts as a source of elementary disconnections. This source plays a relevant role on the evolution of the {112} GB because the level of stress it requires for the emission of a disconnection dipole is significantly lower than for the pristine interface, therefore it becomes the preferred mechanism for SCGBM. Since this GB is highly mobile, it can interact with sessile irradiation defects found on the interface or on its vicinity, as GBs are natural sinks for irradiation point defects and mobile defect clusters.

In static simulations of the interaction between a single disconnection with different defects the stress level is not affected by the presence of the other defect regardless of its type. All the irradiation defects studied act as strong obstacles to the motion of a single disconnection. The size of the defect defines the critical value for the disconnection detachment, as well as the defect behavior. Both, the inner structure of the defect and the matrix-defect interface, affect the propagation of the disconnections and the critical stress required to cross through the defect. Table 6.1 presents the details on shear stresses for all studied defects with a 5 nm diameter (extreme size) upon interaction with a row of disconnections. Comparing these results with the ones for interaction with a single disconnection, we can notice that the values of the normalized stress appear to be rather larger compared to the values from the curves in the Fig. 6.3. This difference can be understood as a consequence of the higher stress needed to activate the emission of a disconnection dipole by the GBD. As for the discrepancies observed with respect to the stress level on the interaction with crystal dislocations [121–125, 128], these can be determined by the inability of the disconnections to climb.

Table 6.1: Critical stresses (Gb/l) for the extreme size defects.

Defect type	On GB, 0 K	On GB, 300 K	Above GB, 0 K	Above GB, 300 K
Reference	1.89	0.73	-	-
Void	1.72	0.75	1.89	0.64
He Bubble	0.51	0.28	0.39	0.17
'100' Prec	1.80	1.03	1.85	1.12
'112' Prec	1.63	1.12	1.85	1.12
'Subst' Prec	1.85	1.12	1.84	1.12

When the disconnections are supplied by the GBD, the stresses in the system are substantially higher, so that disconnections cross through the defects as if these were transparent obstacles. In this case the defects interact with several consecutive disconnections, and the influence of each defect is noticeable: i) voids do not contribute to the stress redistribution, as the level of stresses is similar to the reference cases; ii) Cr precipitates increase the total stress content in the system, thanks to the chromium admixture, therefore the chromium potential contributes to the stress; iii) Helium bubbles are the only defects that act as Orowan-like obstacles, inhibiting the initial motion of the disconnections supplied by the source. Despite that they reduce the stress needed to displace the GB one plane.

Applying temperature allows the reduction of the stress needed to trigger the reaction (Table 6.1). When a high strain rate is used, the system is not allowed to accommodate the deformation uniformly as it happens on a relaxation process, leading to the formation of residual disconnection loops and dislocation loops attached to the GB and irradiation defects.

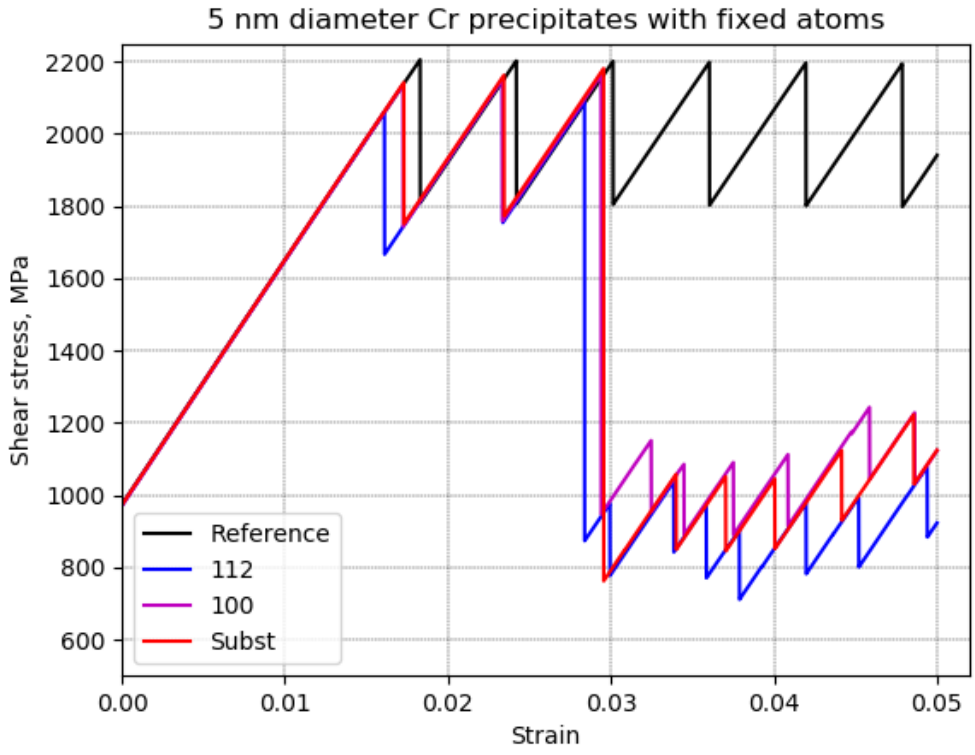

Figure 6.9: Shear stress vs strain applied in static simulations with precipitates of fixed Cr atoms placed on the interface. Colors meaning is the same as before.

In order to exclude the effects of the interaction between two metals for the precipitates case, one can study the configuration with the precipitates atoms held fixed during the whole loading process. This constraint forbids the crystallographic interactions between the disconnections and the atoms inside the precipitates. Instead, the disconnections pass along the surfaces of the defects, as in He bubble case, i.e., precipitates can be considered as hard defects in this case.

Fig. 6.9 shows the shear stress – strain curves for the precipitates placed on the interface. The saw-tooth region of the curve after the linear part corresponds to the interaction of the disconnections emitted by the GBD with the tips of the precipitates without any residual defects outside the GB interface, similarly to the previously described cases. The steady state part is followed by a huge drop of stress of around 1.2 – 1.4 GPa. This drop corresponds to the formation of residual defects – dislocation loops – at the Cr-Fe interface similar to the case of the interaction with bubbles (see Fig. 6.10). These loops stay attached to the GB interface. While the part released into the bulk is able to move under external load, the parts attached to the precipitate increase in length only along with the interaction between the precipitate and a disconnection.

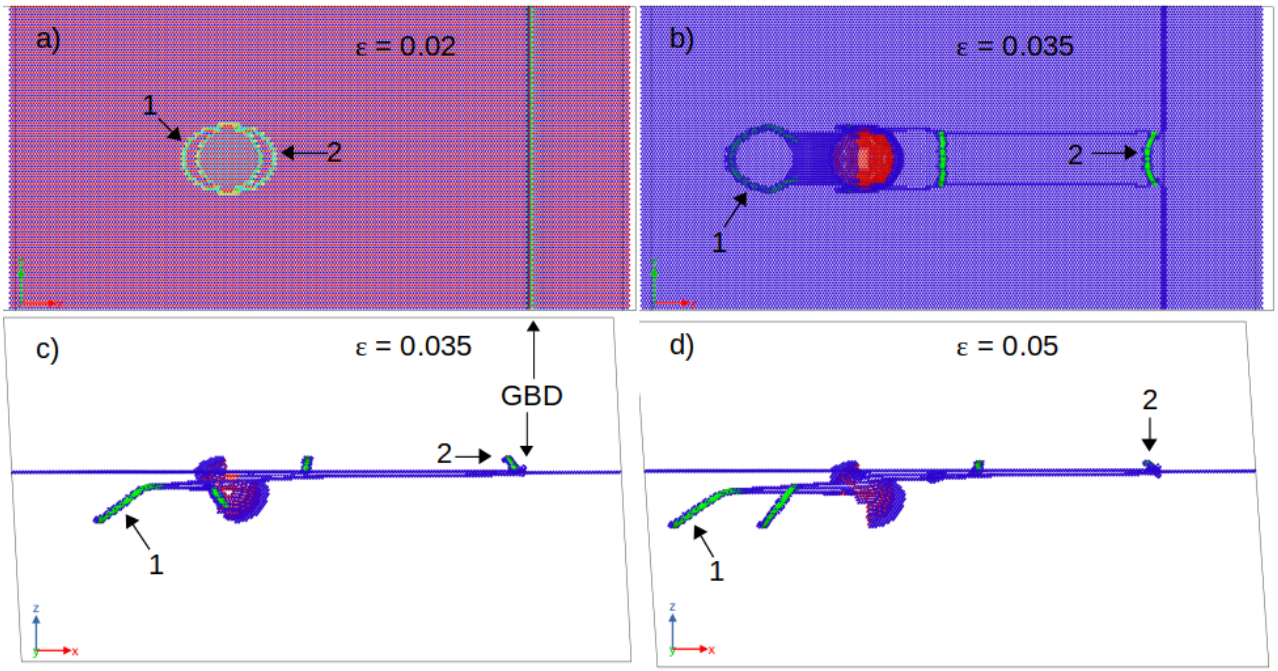

Figure 6.10: Snapshots from the simulations of Cr 'subst' precipitate with fixed atoms on the interface. Top projections on a) at 0.02 strain applied and on b) at 0.035 of strain applied. Side projections on c) at 0.035 strain applied and on d) at 0.05 strain applied. On a) disconnection loops attached to the precipitate are shown (atoms are colored to distinguish the defects); on b), c) and d) several dislocation loops attached to the GB and the precipitate are shown (blue atoms correspond to Fe, while red atoms correspond to Cr). Marked as '1' and '2' are the initial disconnection loops on a) that grow into dislocation loops in the lower grain on b), c) and d).

6.4 Conclusion

The existence of highly mobile disconnections specific to the {112} GB, which are responsible for shear-coupled GB migration allows the interaction between such GB and radiation induced defects segregated at the interface or in its vicinity. The interaction of the GB with a crystal dislocation produces a GBD, which is a source of such disconnections, lowering the critical level of stresses needed to start the motion of the GB.

The purpose of the present work is to investigate the interaction between the mobile disconnections of the {112} GB and irradiation defects. The main objectives of the work can be summarized as follows:

- The description of the interaction mechanisms in terms of changes in the Bv and the final outcome of the reaction.
- The calculation of the stress required to detach the disconnections from the irradiation defects.
- The description and comparison of the results obtained using the formalism developed in earlier works for crystal dislocations.

Depending on their type, irradiation defects can be considered either as hard obstacles – their inner structure is not affected by the glide of disconnections, i.e., impenetrable obstacles (He bubbles), or soft obstacles – their atoms interact with the disconnections changing the shape/structure of the defect, i.e., being sheared (Cr precipitates, voids). The behavior of the defect is directly reflected in both, the critical stress required to overcome the defect and the reaction mechanism involved. For example, the interaction with He bubbles may lead to the generation of disconnection loops (analogy of shear loops in the case of bulk dislocation interaction with impenetrable obstacles).

The response of the voids shows a good agreement with the theoretical prediction of the modified Orowan relation for void-crystal dislocation interactions.

For the studied defects, no drag by the moving GB is found. When the GB interface passes through the soft defect, its shape is transformed according to the orientation of the grain where it is situated.

The main effect of temperature is the reduction of the stress needed to trigger the reaction, as expected.

The reactions between the disconnections and the irradiation defects obey two scenarios. At low stresses in the system, the disconnection is attached to the defect independently of its type; with the increase of strain applied it is detached once the critical level of stress is reached. At higher stresses the disconnections pass the defect almost as a transparent obstacle implying that the friction stress is already so high that the additional contribution coming from the defects is negligible.

Altogether the studied defects do affect the propagation of the disconnections and the corresponding plastic slip of the GB. Hence, the presence of the irradiation defects at GBs should lead to the overall hardening of the material. Such hardening should in turn translate into the suppression of the plastic deformation near the grain boundaries and accumulation of stress concentration eventually causing intergranular fracture. This study reveals a lot of similarities between the interaction mechanisms observed for GB disconnections and observed for standard bulk dislocations [122, 123, 128]. Although further studies are required to investigate other types of GBs, the applicability of the currently established dislocation theory at least extends for the studied {112} GB interface.

CHAPTER 7

CONCLUSIONS AND FUTURE WORK

7.1 Summary and conclusions

In this dissertation are presented the results obtained by atomistic computer simulation on the interaction between dislocations and a number of grain boundaries, displaying a remarkable diversity of behaviors. Any study carried out by simulation has the drawback that it is difficult to extract general conclusions since it is only possible to study particular cases. However, the chosen $\langle 110 \rangle$ tilt GBs cover a wide range of values for the misorientation angle and low Σ, allowing us to consider a significant amount of different structural units. This variety should ensure achieving the objective of a set of interaction rules describing in the most general way possible, the interaction of a GB with a single dislocation or a dislocation pileup. The main purpose of this set of rules is to be used in models at higher scales of space and time providing a more accurate description of the long-term evolution of the microstructure.

Achieving the aforementioned objective is not simple because one of the main findings of this work is the strong dependence observed of reactions on a combination of factors:

- GB type
- Glide plane inclination with respect to the GB
- Dislocation character (edge or mixed)
- Sense of the Burgers vector (towards or away from the interface)
- Temperature
- Absence or presence of GBDs involved in the reactions
- Number of dislocation involved in the interaction
- Local stress level at the interaction region

Considering all possible combinations feasible from this list of factors we obtain a very high number of cases. In order to make such number of cases understandable and with the aim of extracting general conclusions on the dislocation – GB interactions, the outcome of the reactions have been summarized in the Table 7.1. Initially we considered only three possible events: absorption, reflection or transmission, as it is indicated in the Introduction chapter (Section 1.3). However, our results show a higher complexity than expected, therefore it is necessary to provide a higher descriptive level, which in fact is equivalent to consider more events. This allows us to fully capture the complexity of the reactions and their products. As it can be seen in Table 7.1, after the symbols used for absorption (A), reflection (R) and transmission (T) there are three new items, SCGBM, TW and IF, described as:

- SCGBM: After the reaction, it takes place shear-coupled GB migration
- TW: Formation of {112} twin embryos at the reaction site which in turn become twins when stress is applied
- IF: Formation of new interfaces at the reaction site

Table 7.1: Summary of the reactions observed on the interaction between the different ⟨110⟩ tilt axis GBs considered and single dislocations and DPUs. A – absorption; TW – {112} twin formation; T – transmission; R – reflection; IF – creation of the new interfaces.

GB	Glide plane inclination (character)	Reaction, single dislocation	Reaction, DPU
{112}	70.53° (Edge)	A+SCGBM	T/R+SCGBM
	125.26° (Mixed)	A+SCGBM	A/T+SCGBM
{332}	29.50° (Edge)	A+SCGBM/TW	A+IF
	100.03° (Edge)	A+SCGBM/TW	A+SCGBM
	154.76° (Mixed)	A+SCGBM	A+IF
{111}	19.47° (Edge)	IF	IF
	90.00° (Edge)	TW/IF	TW/IF
	144.74° (Mixed)	IF	IF
{116}	48.53° (Edge)	A+SCGBM	A+SCGBM
	158.00° (Edge)	A/T+SCGBM	A+SCGBM
	103.26° (Mixed)	A+SCGBM	A+SCGBM

At a glance, it becomes evident that for all the GBs studied the most probable reaction is the absorption of the dislocations, however, as we have stated, to learn the evolution of the interface after or during the interaction it is essential to know additional information. There are three possible cases involving absorption, identified as A+SCGBM, A+TW and A+IF. Let us proceed with the description of each of these three possible cases.

Absorption + Shear-coupled GB migration. Our results indicate that for a single dislocation this is the most probable event. The general description of the interaction process is as it follows: once the dislocation reaches the vicinity of the GB it is absorbed followed by the formation of a GBD ($\mathbf{b}_{1/-1}$ for the {112} and $\mathbf{b}_{2/-2}$ (under negative shear stress) for the {332}), which has a special feature: it acts as a source of disconnections at a stress level lower than the required for the creation of dipoles at the pristine interface. As we have emphasized along the previous chapters, elementary disconnections are the key element on the shear-coupled GB migration, therefore these sources of disconnections contribute to enhance the mobility of these GBs.

This event can also take place with a dislocation pileup ({112}, {332} ($\mathbf{b}_{2/-2}$) GBs) and the description is quite similar. However, in that case the GBDs do not act as sources of disconnections. Instead the dipoles of disconnections are created under the influence of the stress field of the DPU. These disconnections interact with the GBD conservatively, allowing the migration of the interface along with the GBD. Depending on the conditions considered, one or two dislocations of the pileup can be absorbed and the outcome of the reactions involve the emission of several elementary disconnections, therefore contributing to SCGBM.

{112} twin formation. The formation of twins is an efficient mechanism to accommodate plastic deformation in metals under low temperature and high strain rate conditions. The results found in this work show that {112} twins can also be produced as the outcome of the interaction of {332} and {111} GBs with single dislocations when specific conditions are met. Among the aforementioned conditions the most relevant is the temperature, as we only observe the appearance of twins when $T \leq 50\,K$.

The key element on the twin formation at the {332} GB is the interaction between EDisc and sessile GBDs present at the interface. If a GBD acts as an obstacle and the EDisc cannot perform a conservative climb over the GBDs (for instance, $\mathbf{b}_{2/-2}$ (under positive shear stress), $\mathbf{b}_{-12/-10}$ GBDs at the {332} GB), EDiscs pile at the GBD leading to formation of a {112} twin at the reaction site. This same twinning mechanism is also present at the migration of the vicinal GBs of the {332} at low temperature. Therefore, this process is fully controlled by creation and propagation of EDisc.

For the {111} GB the mechanism is slightly different since EDisc are absent. However, the cause behind twinning is pure shuffles that allow creation of steps oriented along ⟨111⟩ direction perpendicular to the GB interface. In this case twins are created when the crystal dislocation is attached to the GB, that in turn is transformed into several non-glissile steps, in order to accommodate the step height introduced with the glide of the dislocations attached to the GB (Fig. 4.15).

New interfaces creation. The formation of new interfaces is another mechanism observed in our results, mostly on DPU-GB interactions, although it is also present for some cases involving a single dislocation. In order to initiate creation of a new interface, a high step need to be introduced into the GB interface. Such type of reaction has been observed in {332} and {111} GBs. However the mechanism is different for each case due to the presence/absence of EDisc. In the case of the {332} GB interacting with a DPU of $\mathbf{b}_{\pm 2/0}$ edge dislocations and $\mathbf{b}_{\pm 1/0}$ mixed dislocations we observe that several dislocations are absorbed consecutively leading to a progressive increase of the formed GBD with a riser that represents a new asymmetrical interface. Whereas in case of the {111} GB the step is introduced by the glide of initial dislocations. The pure steps without dislocation character formed at the GB allow accommodation of the step height forming either {112} twin boundary or {110}/{001} asymmetrical interfaces, depending on the glide plane and temperature.

Now we have provided the main details on the interactions where there is absorption of dislocations. In order to complete the description of the dislocation – GB interaction, we include the analysis of the other two reactions present in our results, mostly during DPU – GB interaction: transmission and reflection. Below are the main features of the processes where said reactions are observed.

Transmission + Shear-coupled GB migration. The transmission reaction has mainly been observed in {112} GB, which is the most abundant GB according to experimental evidence. The conditions for this reaction to occur are very specific. These conditions are only met in the interaction of a DPU of $\mathbf{b}_{2/0}$ edge dislocations with a {112} GB. The first dislocation of the pileup is absorbed producing a GBD and the stress field of the second dislocation allows the creation of an EDisc dipole at the pristine interface placed in the tensile region next to the GBD. This leads to the reaction between the EDisc and the GBD that results in transmission followed by migration.

The said conditions can explain the behavior of {112} twins as strong obstacles blocking the propagation of DPU. Depending on the size of the twin, one or more $\mathbf{b}_{2/0}$ edge dislocations can be transmitted through the first TB into the twin. Then the first one glides until it meets the second TB, but in this case the dislocation is considered $\mathbf{b}_{-2/0}$ with respect to the second TB and the conditions for transmission are not met, therefore the DPU motion is effectively blocked. However, for thin twins (thickness < 5.6 nm) the situation changes entirely because only one dislocation is transmitted through the first TB inside the twin. GBD created in the second TB produces EDisc that displace the interface of the second TB upwards up to the interaction with the first TB and the twin is annihilated allowing the DPU to glide freely with the subsequent softening of the material.

Another case with possible transmission is observed in the interaction between the {116} GB and a single $\mathbf{b}_{4/0}$ edge dislocation. The existence of several disconnections with Bv parallel to the GB allows {116} GB to accommodate the deformation by splitting the GBD into new disconnections. This enables interaction between the GBD and EDisc, leading to a possible transmission of a crystal dislocation to the adjacent grain. The difference with the transmission process described for the $\mathbf{b}_{2/0}$ crossing trough the {112} GB is that the orientation and Bv of the transmitted dislocation differ from the initial one. As well as the stress level, which is higher for the {116} GB, as the stresses needed to produce and move disconnections in this GB are much higher than those for the {112} GB.

Reflection. The last possible observed reaction is reflection that occurs when the stress needed to move crystal dislocations is higher than that for creation of EDisc dipoles. The probability of such reaction is low and depends on material properties, in fact it has been observed only in tungsten for interaction with $\mathbf{b}_{2/0}$.

In order to complete this Section, the main conclusions obtained are listed below:

- The crystallography drives the interaction processes between GBs and dislocations. For that reason, the use of DP is useful, as a tool capable of providing all necessary information on the possible line defects at the GB.
- The comparison with the results for different materials sharing the same bcc structure of F/M steels (W, Cr) shows that the reactions are the same, with slight changes in the outcome.
- The effect of temperature on the GB – DPU interaction is measured by the stress required for the GB to absorb the first dislocation. In general, the higher the temperature the lower the stress required; therefore the temperature facilitates the absorption process.
- The GBDs, both sessile and glissile, have proven to be imperative to understand the mechanisms behind the evolution of the GB under stress conditions.
- The main mechanism of plastic deformation accommodation in studied GBs is production and glide of elementary disconnections. Their interaction with other interfacial defects leads to different possible reactions.
- Absorption is the predominant reaction observed; however it is necessary complementary information on the reaction mechanisms in order to complete the description of the interaction. Only in this way it is possible to predict the long-term evolution of the interface under plastic deformation.
- Transmission and reflection are possible for both single dislocations and DPUs. For both cases the reaction are the results of the interaction between the formed GBD and EDisc formed on the interface. For the DPU case, these reactions take place when the second dislocation of the DPU reaches the GB: that leads to an increase of the local stress triggering the emission of the first absorbed dislocation towards the upper grain (reflection) or the lower grain (transmission).
- Interactions between mobile interfacial defects and irradiation defects at the GB interface agrees with the description for crystal dislocations interacting with irradiation defects. The defects can be described as either hard or soft, in any case affecting the motion of EDisc and propagation of the corresponding plastic slip of the GB.

The studies developed in the framework of the present PhD work have provided a set of new valuable data, giving a new insight in the atomic scale processes involved on the interaction between GBs and dislocations in F/M steels. The appropriate choice of GBs has allowed to reach conclusions general enough to be useful in the design of high scale models which are imperative tools to investigate the long-term evolution of these materials.

7.2 Future work

The research work contained in this dissertation has produced a considerable amount of results covering many cases of interest, allowing us to reach interesting conclusions. However, there are several possible ways to extend this work that we intend to explore in the near future which are listed below:

- The interaction processes and outcomes of the reaction in other GBs should be investigated. To expand the studied matrix we should consider other tilt axes ($\langle 100 \rangle$, $\langle 112 \rangle$, $\langle 123 \rangle$), varying the misorientation angle, crystal dislocation type, temperature, stress and stain rates.
- As the next step in addition to symmetric tilt GBs, interactions with asymmetrical tilt, twist and general GBs can be studied. It is worth investigating such GBs, as the possible absence of glissile interfacial defects may lead to new mechanisms of deformation accommodation.
- The results obtained in modeling of the interfaces between dissimilar materials, such as the interface between bcc tungsten and fcc copper, can be used to provide elastic and plastic properties for the input for the Finite Element Method simulations.
- Considering the interaction with the irradiation defects, the study can be extended to the other mobile GBs with EDisc, as well as to the interaction with other irradiation defects, for example dislocation loops.
- Finally, the obtained results on reaction outcomes and local stresses at the reaction site might be used as an input for the higher scale simulations, for instance in Dislocation Dynamics or Kinetic Monte Carlo methods. Knowing the behavior of the GB upon interaction with crystal dislocation allows to set the initial conditions for such simulations.

BIBLIOGRAPHY

[1] A. Sutton and R. Balluffi. *Interfaces in crystalline materials*. Oxford Classic Texts in the Physical Sciences, Oxford, 3rd edition, 2006.

[2] I. J. Beyerlein, X. Zhang, and A. Misra. Growth twins and deformation twins in metals. *Annual Review of Materials Research*, 44:329–363, 2014.

[3] P. M. Anderson, J. P. Hirth, and J. Lothe. *Theory of Dislocations*. Cambridge University Press, Cambridge, 3rd edition, 2017.

[4] G. S. Was. *Fundamentals of Radiation Materials Science*. Springer, New York, 2nd edition, 2007.

[5] Yu. N. Osetsky, D. J. Bacon, F. Gao, A. Serra, and B. N. Singh. Study of loop-loop and loop-edge dislocation interactions in bcc iron. *Journal of Nuclear Materials*, 283-287:784–788, 2000.

[6] A. Ostapovets and A. Serra. Slip dislocation and twin nucleation mechanisms in hcp metals. *J Mater. Sci.*, 52:533–540, 2017.

[7] Z. Cheng, H. Zhou, Q. Lu, H. Gao, and L. Lu. Extra strengthening and work hardening in gradient nanotwinned metals. *Science*, 362:1925, 2018.

[8] Y. Shen, L. Lu, Q. Lu, Z. Jin, and K. Lu. Tensile properties of copper with nano-scale twins. *Scripta Materialia*, 52:989–994, 2005.

[9] S. Qu, P. Zhang, S. Wu, Q. Zang, and Z. Zhang. Twin boundaries: Strong or weak? *Scripta Materialia*, 59:1131–1134, 2008.

[10] S. Kim, X. Li, H. Gao, and S. Kumar. In situ observations of crack arrest and bridging by nanoscale twins in copper thin films. *Acta Mater.*, 60:2959–2972, 2012.

[11] J. Wang and X. Zhang. Twinning effects on strength and plasticity of metallic materials. *MRS Bulletin*, 41:274–281, 2016.

[12] X. Li, Y. Wei, L. Lu, K. Lu, and H. Gao. Dislocation nucleation governed softening and maximum strength in nano-twinned metals. *Nature*, 464:877–880, 2010.

[13] T. J. Flanagan, S. Vijayan, S. Galitskiy, J. Davis, B. A. Bedard, C. L. Williams, A. M. Dongare, M. Aindow, and S. W. Lee. Shock-induced deformation twinning and softening in magnesium single crystals. *Mater. & Design*, 194:108884, 2020.

[14] Q. H. Shah. Impact resistance of a rectangular polycarbonate armor plate subjected to single and multiple impacts. *Int. J. Impact Eng.*, 36:1128–1135, 2009.

[15] S. Root, L. Shulenburger, R. W. Lemke, D. H. Dolan, T. R. Mattsson, and M. P. Desjarlais. Shock response and phase transitions of MgO at planetary impact conditions. *Phys. Rev. Lett.*, 115:198501, 2015.

[16] E. Hall. The deformation and ageing of mild steel: III. discussion of results. *Proc. Phys. Soc. B*, 64:747–753, 1951.

[17] N. J. Petch. The cleavage strength of polycrystals. *J. Iron Steel Inst.*, 174:25–31, 1953.

[18] L. Lu, Y. F. Shen, X. H. Chen, L. H. Qian, and K. Lu. Ultrahigh strength and high electrical conductivity in copper. *Science*, 304:422–426, 2004.

[19] M. Dao, L. Lu, Y. F. Shen, and S. Suresh. Strength, strain-rate sensitivity and ductility of copper with nanoscale twins. *Acta Mater.*, 54:5421–5432, 2006.

[20] M. Kapp, O. Renk, T. Leitner, P. Ghosh, B. Yang, and R. Pippan. Cyclically induced grain growth within shear bands investigated in UFG Ni by cyclic high pressure torsion. *J. Mater. Res.*, 32:4317–4326, 2017.

[21] M. Kapp, O. Renk, P. Ghosh, T. Leitner, B. Yang, and R. Pippan. Plastic strain triggers structural instabilities upon cyclic loading in ultrafine-grained nickel. *Acta Mater.*, 200:136–147, 2020.

[22] M. Dewald and W. A. Curtin. Multiscale modelling of dislocation/grain-boundary interactions: I. Edge dislocations impinging on Σ11 (113) tilt boundary in Al. *Modelling and Simulation in Materials Science and Engineering*, 15:S193–S215, 2007.

[23] M. Dewald and W. A. Curtin. Multiscale modelling of dislocation/grain boundary interactions. II. Screw dislocations impinging on tilt boundaries in Al. *Philos. Mag.*, 87:4615–4641, 2007.

[24] M. Dewald and W. A. Curtin. Multiscale modeling of dislocation/grain-boundary interactions: III. 60° dislocations impinging on Σ3, Σ9 and Σ11 tilt boundaries in Al. *Modelling and Simulation in Materials Science and Engineering*, 19:055002, 2011.

[25] W. S. Yu and Z. Q. Wang. Interactions between edge lattice dislocations and Σ11 symmetrical tilt grain boundaries in copper: A quasi-continuum method study. *Acta Mater.*, 60:5010–5021, 2012.

[26] D. Terentyev, A. Bakaev, A. Serra, F. Pavia, K. L. Baker, and N. Anento. Grain boundary mediated plasticity: The role of grain boundary atomic structure and thermal activation. *Scripta Materialia*, 145:1–4, 2018.

[27] Y. Gao and Z. H. Jin. Interactions between lattice dislocation and Lomer-type low-angle grain boundary in nickel. *Computational Materials Science*, 138:225–235, 2017.

[28] S. Chandra, M. K. Samal, V. M. Chavan, and R. J. Patel. Atomistic simulations of interaction of edge dislocation with twist grain boundaries in Al-effect of temperature and boundary misorientation. *Materials Science and Engineering: A*, 646:25–32, 2015.

[29] J. Liu, C. Chen, Q. Feng, X. Fang, H. Wang, F. Liu, J. Lu, and D. Raabe. Dislocation activities at the martensite phase transformation interface in metastable austenitic stainless steel: An in-situ TEM study. *Materials Science and Engineering: A*, 703:236–243, 2017.

[30] W. Z. Abuzaid, M. D. Sangid, J. D. Carroll, H. Sehitoglu, and J. Lambros. Slip transfer and plastic strain accumulation across grain boundaries in Hastelloy X. *J. Mech. Phys. Solids*, 60:1201–1220, 2012.

[31] A. Rajabzadeh, F. Mompiou, S. Lartigue-Korinek, N. Combe, M. Legros, and D. A. Molodov. The role of disconnections in deformation-coupled grain boundary migration. *Acta Mater.*, 77:223–235, 2014.

[32] K. D. Molodov, T. Al-Samman, D. A. Molodov, and S. Korte-Kerzel. On the twinning shear of $\{10\bar{1}2\}$ twins in magnesium - experimental determination and formal description. *Acta Mater.*, 134:267–273, 2017.

[33] D. A. Spearot, K. I. Jacob, and D. L. McDowell. Nucleation of dislocations from [001] bicrystal interfaces in aluminum. *Acta Mater.*, 53:3579–3589, 2005.

[34] A. Serra and D. J. Bacon. Modelling the motion of $\{11\bar{2}2\}$ twinning dislocations in the HCP metals. *Materials Science and Engineering: A*, 400–401:496–498, 2005.

[35] J. Wang, J. P. Hirth, and C. N. Tomé. $(\bar{1}012)$ twinning nucleation mechanisms in hexagonal-close-packed crystals. *Acta Mater.*, 57:5521–5530, 2009.

[36] F. Wang, C. D. Barrett, R. J. McCabe, H. El Kadiri, L. Capolungo, and S. R. Agnew. Dislocation induced twin growth and formation of basal stacking faults in $\{10\bar{1}2\}$ twins in pure Mg. *Acta Mater.*, 165:471–485, 2019.

[37] R. C. Pond. Line defects in interfaces. *Dislocations in Solids Elsevier North-Holland*, 8:1, 1989.

[38] J. P. Hirth. Dislocations, steps and disconnections at interfaces. *Journal of Physics and Chemistry of Solids*, 55:985–989, 1994.

[39] R. C. Pond and D. S. Vlachavas. Bicrystallography. *Proc. The Royal Society of London, Series A: Mathematical and Physical Sciences*, 386:95–143, 1983.

[40] J. P. Hirth and R. C. Pond. Steps, dislocations and disconnections as interface defects relating to structure and phase transformations. *Acta Mater.*, 44:4749–4763, 1996.

[41] J.P. Hirth, R.C. Pond, and J. Lothe. Spacing defects and disconnections in grain boundaries. *Acta Materialia*, 55(16):5428–5437, 2007.

[42] T. Braisaz, P. Ruterana, G. Nouet, A. Serra, T. Karakostas, and T. Kehagias. High-resolution electron microscopy study of the (1012) twin and defects analysis in deformed polycrystalline alpha titanium. *Philosophical Magazine Letters*, 74:331–338, 1996.

[43] A.J. Haslam, D. Moldovan, V. Yamakov, D. Wolf, S.R. Phillpot, and H. Gleiter. Stress-enhanced grain growth in a nanocrystalline material by molecular-dynamics simulation. *Acta Mater.*, 51:2097–2112, 2003.

[44] J. W. Cahn, Y. Mishin, and A. Suzuki. Coupling grain boundary motion to shear deformation. *Acra Mater.*, 54:4953–4975, 2006.

[45] D.S. Gianola, S. Van Petegem, M. Legros, S. Brandstetter, H. Van Swygenhoven, and K.J. Hemker. Stress-assisted discontinuous grain growth and its effect on the deformation behavior of nanocrystalline aluminum thin films. *Acta Mater.*, 54:2253–2263, 2006.

[46] F. Mompiou, D. Caillard, and M. Legros. Grain boundary shear-migration coupling. i. in situ TEM straining experiments in Al polycrystals. *Acta Mater.*, 57:2198–2209, 2009.

[47] T. Gorkaya, D. A. Molodov, and G. Gottstein. Stress-driven migration of symmetrical $\langle 100 \rangle$ tilt grain boundaries in Al bicrystals. *Acta Mater.*, 57:5396–5405, 2009.

[48] D. A. Molodov, T. Gorkaya, and G. Gottstein. Dynamics of grain boundaries under applied mechanical stress. *Journal of Materials Science*, 46:4318–4326, 2011.

[49] A. Rajabzadeh, M. Legros, N. Combe, F. Mompiou, and D. A. Molodov. Evidence of grain boundary dislocation step motion associated to shear-coupled grain boundary migration. *Philos. Mag.*, 93:1299–1316, 2013.

[50] N. Combe, F. Mompiou, and M. Legros. Disconnections kinks and competing modes in shear-coupled grain boundary migration. *Phys. Rev. B*, 93:024109, 2016.

[51] H. Khater, A. Serra, R. C. Pond, and J. P. Hirth. The disconnection mechanism of coupled migration and shear at grain boundaries. *Acta Mater.*, 60:2007–2020, 2012.

[52] A. Rajabzadeh, F. Mompiou, M. Legros, and N. Combe. Elementary mechanisms of shear-coupled grain boundary migration. *Phys. Rev. Lett.*, 110:265507, 2013.

[53] A. Serra and D.J. Bacon. A new model for $\{10\bar{1}2\}$ twin growth in hcp metals. *Phil. Mag. A*, 73:333–343, 1996.

[54] N. Combe, F. Mompiou, and M. Legros. Heterogeneous disconnection nucleation mechanisms during grain boundary migration. *Phys. Rev. Mater.*, 3:060601, 2019.

[55] P. D. Bristowe and A. G. Crocker. A computer simulation study of the structure of twinning dislocations in body centred cubic metals. *Acta Metall.*, 25:1363–1371, 1977.

[56] A. Serra, N. Kvashin, and N. Anento. On the common topological conditions for shear-coupled twin boundary migration in bcc and hcp metals. *Letters on Materials*, 10:537–542, 2020.

[57] N. Kvashin, P. L. García-Müller, N. Anento, and A. Serra. Atomic processes of the shear-coupled migration of {112} twins and vicinal grain boundaries in bcc-Fe. *Phys. Rev. Mater.*, 4:073604, 2020.

[58] J. P. Hirth, R. C. Pond, and J. Lothe. Disconnections in tilt walls. *Acta Mater.*, 54:4237–4245, 2006.

[59] Q. Zhu, G. Cao, J. Wang, C. Deng, J. Li, Z. Zhang, and S. X. Mao. In situ atomistic observation of disconnection-mediated grain boundary migration. *Nature Comm.*, 10:156, 2019.

[60] Y. Cheng, M. Mrovec, and P. Gumbsch. Atomistic simulations of interactions between the 1/2 $\langle 111 \rangle$ edge dislocation and symmetric tilt grain boundaries in tungsten. *Phil. Mag.*, 88:547–560, 2008.

[61] M. Mrovec, C. Elsasser, and P. Gumbsch. Interactions between lattice dislocations and twin boundaries in tungsten: A comparative atomistic simulation study. *Philos. Mag.*, 89:3179–3194, 2009.

[62] B. Jiang, A. Tu, H. Wang, H. Duan, S. He, H. Ye, and K. Du. Direct observation of deformation twinning under stress gradient in body-centered cubic metals. *Acta Mater.*, 155:56–68, 2018.

[63] R. C. Pond, J. P. Hirth, A. Serra, and D. J. Bacon. Atomic displacements accompanying deformation twinning: shears and shuffles. *Materials Research Letters*, 4:185–190, 2016.

[64] N. Anento and A. Serra. Interaction of a mobile {112} grain boundary with radiation induced defects in α-Fe: transformation of defects and impact on the shear-coupled grain boundary migration. *Comput. Mater. Sci.*, 179:109679, 2020.

[65] R.C. Pond, A. Serra, and D.J. Bacon. Dislocations in interfaces in the h.c.p. metals — II. Mechanisms of defect mobility under stress. *Acta Mater.*, 47:1441–1453, 1999.

[66] A. Ostapovets and A. Serra. Characterization of the matrix-twin interface of a $(10\bar{1}2)$ twin during growth. *Philos. Mag.*, 94:2827–2839, 2014.

[67] J. E. Brandenburg, M. Schoof, and D. A. Molodov. Stress induced migration of grain boundaries in Cu-bicrystals. *Philosophical Magazine Letters*, 100:10–22, 2020.

[68] F. Mompiou, M. Legros, and D. Caillard. Direct observation and quantification of grain boundary shear-migration coupling in polycrystalline Al. *Journal of Materials Science*, 46:4308–4313, 2011.

[69] Q. Zhu, S. C. Zhao, C. Deng, X. H. An, K. X. Song, S. X. Mao, and J. W. Wang. In situ atomistic observation of grain boundary migration subjected to defect interaction. *Acta Mater.*, 199:42–52, 2020.

[70] M. Dupraz, S. I. Rao, and H. Van Swygenhoven. Large scale 3-dimensional atomistic simulations of screw dislocations interacting with coherent twin boundaries in Al, Cu and Ni under uniaxial and multiaxial loading conditions. *Acta Mater.*, 174:16–28, 2019.

[71] D. Chen, S. Xu, and Y. Kulkarni. Atomistic mechanism for vacancy-enhanced grain boundary migration. *Phys. Rev. Materials*, 4:033602, 2020.

[72] A. Serra and D. J. Bacon. Computer simulation of screw dislocation interactions with twin boundaries in hcp metals. *Acta Mater.*, 43:4465–4481, 1995.

[73] B. P. Eftink, A. Li, I. Szlufarska, N. A. Mara, and I. M. Robertson. Deformation response of AgCu interfaces investigated by in situ and ex situ TEM straining and md simulations. *Acta Mater.*, 138:212–223, 2017.

[74] N. Kvashin, A. Ostapovets, N. Anento, and A. Serra. On the migration of $\{332\}\langle 110\rangle$ tilt grain boundary in bcc metals and further nucleation of $\{112\}$ twin. *Comput. Mater. Sci.*, 196:110509, 2021.

[75] N. Kvashin, N. Anento, D. Terentyev, A. Bakaev, and A. Serra. Interaction of a dislocation pileup with $\{332\}$ tilt grain boundary in bcc metals studied by MD simulations. *Phys. Rev. Mater.*, 5:013605, 2021.

[76] L. Wang, Y. Wang, P. Eisenlohr, T. R. Bieler, M. A. Crimp, and D. E. Mason. Twin nucleation by slip transfer across grain boundaries in commercial purity titanium. *Metall & Mater. Trans. A*, 41:421–430, 2010.

[77] C. Y. Hung, Y. Bai, T. Shimokawa, N. Tsuji, and M. Murayama. A correlation between grain boundary character and deformation twin nucleation mechanism in coarse-grained high-Mn austenitic steel. *Scientific Reports*, 11:8468, 2021.

[78] L. Jiang, M. Arul Kumar, I. J. Beyerlein, X. Wang, D. Zhang, C. Wu, C. Cooper, T. J. Rupert, S. Mahajan, E. J. Lavernia, and J. M. Schoenung. Twin formation from a twin boundary in Mg during in-situ nano-mechanical testing. *Materials Science & Engineering: A*, 759:142–153, 2019.

[79] E. R. Homer, S. M. Foiles, E. A. Holm, and D. L. Olmsted. Phenomenology of shear-coupled grain boundary motion in symmetric tilt and general grain boundaries. *Acta Mater.*, 61:1048–1060, 2013.

[80] J. S. Weaver, N. Li, N. A. Mara, D. R. Jones, H. Cho, C. A. Bronkhorst, S. J. Fensin, and G. T. Gray. Slip transmission of high angle grain boundaries in bcc metals: micropillar compression of pure Ta single and bi-crystals. *Acta Mater.*, 156:356–368, 2018.

[81] A. Serra, D. J. Bacon, and R. C. Pond. Dislocations in interfaces in the h.c.p. metals – I. Defects formed by absorption of crystal dislocations. *Acta Mater.*, 47:1425–1439, 1999.

[82] M. A. Tschopp, K. N. Solanki, F. Gao, X. Sun, M. A. Khaleel, and M. F. Horstemeyer. Probing grain boundary sink strength at the nanoscale: Energetics and length scales of vacancy and interstitial absorption by grain boundaries in α-Fe. *Phys. Rev. B*, 85:064108, 2012.

[83] Z. Yang, L. Hu, D. Maroudas, and K. D. Hammond. Helium segregation and transport behavior near ⟨100⟩ and ⟨110⟩ symmetric tilt grain boundaries in tungsten. *Journal of Applied Physics*, 123:225104, 2018.

[84] T. Suzudo, H. Kaburaki, and M. Yamaguchi. Modeling of the grain boundary segregation of helium in α-Fe. *Journal of Nuclear Materials*, 417:1102–1105, 2011.

[85] B. J. Alder and T. E. Wainwright. Phase transition for a hard sphere system. *Journal of Chemical Physics*, 27:1208–1209, 1957.

[86] B. J. Alder and T. E. Wainwright. Studies in molecular dynamics. i. general method. *The Journal of Chemical Physics*, 31:459–466, 1959.

[87] R. LeSar. *Introduction to Computational Materials Science: Fundamentals to Applications*. Cambridge University Press, 2013.

[88] J. H. Rose, J. R. Smith, F. Guinea, and J. Ferrante. Universal features of the equation of state of metals. *Phys. Rev. B*, 29:2963–2969, 1984.

[89] Stephen M. Foiles. Embedded-atom and related methods for modeling metallic systems. *MRS Bulletin*, 21:24–28, 1996.

[90] G. Ackland, M. I. Mendelev, D. J. Srolovitz, S. Han, and A. V. Barashev. Development of an interatomic potential for phosphorus impurities in α-iron. *J. Phys.: Condens. Matter*, 16:S2629–S2642, 2004.

[91] D. Terentyev, X. He, A. Serra, and J. Kuriplach. Structure and strength of ⟨110⟩ tilt grain boundaries in bcc Fe: An atomistic study. *Comput. Mater. Sci.*, 49:419–429, 2010.

[92] G. Bonny, R. C. Pasianot, D. Terentyev, and L. Malerba. Iron chromium potential to model high-chromium ferritic alloys. *Philos. Mag.*, 91:1724–1746, 2011.

[93] M. C. Marinica, L. Ventelon, M. R. Gilbert, L. Proville, S. L. Dudarev, J. Marian, G. Bencteux, and F. Willaime. Interatomic potentials for modelling radiation defects and dislocations in tungsten. *J. Phys.: Condens. Matter*, 25:395502, 2013.

[94] S. Plimpton. Fast parallel algorithms for short-range molecular dynamics. *J. Comp. Phys.*, 117:1–19, 1995.

[95] Loup Verlet. Computer "experiments" on classical fluids. i. thermodynamical properties of Lennard-Jones molecules. *Phys. Rev.*, 159:98–103, 1967.

[96] M. P. Allen and D. J. Tildesley. *Computer Simulation of Liquids*. Oxford University Press, Oxford, 2nd edition, 2017.

[97] Loup Verlet. Computer "experiments" on classical fluids. ii. equilibrium correlation functions. *Phys. Rev.*, 165:201–214, 1968.

[98] F. Ercolessi. *A Molecular Dynamics Primer*. Spring College in Computational Physics, Trieste, 1997.

[99] L. E. Shilkrot, R. E. Miller, and W. A. Curtin. Multiscale plasticity modeling: coupled atomistics and discrete dislocation mechanics. *J. Mech. Phys. Solids*, 52:755–787, 2004.

[100] E. Van der Giessen and A. Needleman. Discrete dislocation plasticity: a simple planar model. *Modelling and Simulation in Materials Science and Engineering*, 3:689–735, 1995.

[101] P. Hirel. Atomsk: A tool for manipulating and converting atomic data files. *Comput. Phys. Comm.*, 197:212–219, 2015.

[102] R. Fletcher and C. M. Reeves. Function minimization by conjugate gradients. *The Computer Journal*, 7(2):149–154, 1964.

[103] A. Stukowski. Visualization and analysis of atomistic simulation data with OVITO – the open visualization tool. *Modelling Simul. Mater. Sci. Eng.*, 18:015012, 2010.

[104] H. Beladi and G. S. Rohrer. The relative grain boundary area and energy distributions in a ferritic steel determined from three-dimensional electron backscatter diffraction maps. *Acta Materialia*, 61(4):1404–1412, 2013.

[105] H. Beladi and G. S. Rohrer. The distribution of grain boundary planes in interstitial free steel. *Metallurgical and Materials Transactions A*, 44(1):115–124, 2013.

[106] A. G. Crocker. Twinned martensite. *Acta Metallurgica*, 10(2):113–122, 1962.

[107] H. Tobe, H. Y. Kim, T. Inamura, H. Hosoda, and S. Miyazaki. Origin of {332} twinning in metastable β-Ti alloys. *Acta Materialia*, 64:345–355, 2014.

[108] J. W. Christian and S. Mahajan. Deformation twinning. *Progress in Materials Science*, 39(1):1–157, 1995.

[109] J. Wang, Z. Zeng, C. R. Weinberger, Z. Zhang, T. Zhu, and S. X. Mao. In situ atomic-scale observation of twinning-dominated deformation in nanoscale body-centred cubic tungsten. *Nature Materials*, 14:594–600, 2015.

[110] N. Kvashin, N. Anento, D. Terentyev, and A. Serra. Atomic-level study on the interaction of plastic slip with $\Sigma3\{112\}$ tilt grain boundary and {112} twins in bcc metals. *Phys. Rev. Materials*, 6:033606, 2022.

[111] H. A. Khater, A. Serra, and R. C. Pond. Atomic shearing and shuffling accompanying the motion of twinning disconnections in zirconium. *Philosophical Magazine*, 93(10–12):1279–1298, 2013.

[112] M. Rajagopalan, M. A. Tschopp, and K. N. Solanki. Grain boundary segregation of interstitial and substitutional impurity atoms in alpha-iron. *JOM*, 66:129–138, 2014.

[113] N. Kvashin, N. Anento, D. Terentyev, and A. Serra. {111} tilt grain boundaries as barriers for slip transfer in bcc Fe. *Computational Materials Science*, 203:111044, 2022.

[114] N. Kvashin, N. Anento, and A. Serra. Disconnection-mediated motion of $\langle 110 \rangle$ tilt grain boundaries in α-fe. *Phys. Rev. Materials*, 6:053607, 2022.

[115] O. Khalfallah, M. Condat, and L. Priester. Image force on a lattice dislocation due to a grain boundary in bcc metals. *Philosophical Magazine A*, 67(1):231–250, 1993.

[116] C.Q. Chen, G. Hu, J.N. Florando, M. Kumar, K.J. Hemker, and K.T. Ramesh. Interplay of dislocation slip and deformation twinning in tantalum at high strain rates. *Scripta Materialia*, 69(10):709–712, 2013.

[117] S. Mahajan. Interrelationship between slip and twinning in b.c.c. crystals. *Acta Metallurgica*, 23(6):671–684, 1975.

[118] C. Huang, X. Peng, T. Fu, X. Chen, H. Xiang, Q. Li, and N. Hu. Molecular dynamics simulation of bcc Ta with coherent twin boundaries under nanoindentation. *Mater. Sci. & Eng. A*, 700:609–616, 2017.

[119] R.C. Pond and J.P. Hirth. Defects at surfaces and interfaces. volume 47 of *Solid State Physics*, pages 287–365. Academic Press, 1994.

[120] Y. N. Osetsky. Atomic-scale mechanisms of void strengthening in tungsten. *Tungsten*, 3:65–71, 2021.

[121] D. Terentyev, N. Anento, A. Serra, C. J. Ortiz, and E. E. Zhurkin. Interaction of He and He-V clusters with self-interstitials and dislocations defects in bcc Fe. *Journal of Nuclear Materials*, 458:11–21, 2015.

[122] Yu. N. Osetsky and D. J. Bacon. Atomic-level interaction of an edge dislocation with localized obstacles in fcc and bcc metals. *IUTAM Symposium on Mesoscopic Dynamics of Fracture Process and Materials Strength*, pages 193–202, 2004.

[123] D. J. Bacon and Yu. N. Osetsky. Modelling dislocation-obstacle interactions in metals exposed to an irradiation environment. *Materials Science and Engineering: A*, pages 353–361, 2005.

[124] G. Monnet. Multiscale modeling of precipitation hardening: Application to the Fe-Cr alloys. *Acta Materialia*, 95:302–311, 2015.

[125] G. Monnet. Multiscale modeling of irradiation hardening: Application to important nuclear materials. *Journal of Nuclear Materials*, 508:609–627, 2018.

[126] E. Orowan. Discussion on internal stresses. In *Proc. Symp. Internal Stresses in Metals and Alloys, London: The Institute of Metals*, pages 451–453, 1948.

[127] M. R. Barnett, H. Wang, and T. Guo. An Orowan precipitate strengthening equation for mechanical twinning in Mg. *International Journal of Plasticity*, 112:108–122, 2019.

[128] Y. N. Osetsky and R. E. Stoller. Atomic-scale mechanisms of helium bubble hardening in iron. *Journal of Nuclear Materials*, 465:448–454, 2015.

[129] G. Monnet, Yu. N. Osetsky, and D. J. Bacon. Mesoscale thermodynamic analysis of atomic-scale dislocation-obstacle interactions simulated by molecular dynamics. *Philosophical Magazine*, 90:1001–1018, 2010.

[130] R. H. Richman. The diversity of twinning in body centred cubic structures. Reed-Hill, R.E., Hirth, J.P., Rogers, H.C. (eds.), Deformation Twinning, pages 237–271, New York, 1964. Gordon and Breach Sci. Publ.

[131] D. J. Bacon, U. F. Kocks, and R. O. Scattergood. The effect of dislocation self-interaction on the Orowan stress. *The Philosophical Magazine: A Journal of Theoretical Experimental and Applied Physics*, 28(6):1241–1263, 1973.

[132] A. Ostapovets, K. Kushnir, K. Mathis, and F. Šiška. Interaction of migrating twin boundaries with obstacles in magnesium. *Metals*, 11:154, 2021.

[133] A. Serra and D. J. Bacon. Interaction of a moving $\{10\bar{1}2\}$ twin boundary with perfect dislocations and loops in a hcp metal. *Philosophical Magazine*, 90:845–861, 2010.

[134] D. Terentyev, N. Juslin, K. Nordlund, and N. Sandberg. Fast three dimensional migration of He clusters in bcc Fe and Fe-Cr alloys. *Journal of Applied Physics*, 105:103509, 2009.

[135] N. Kvashin, D. Terentyev, A. Serra, and N. Anento. Effect of irradiation defects on the plastic slip of {112} grain boundary: Atomic scale study. *Computational Materials Science*, 214:111739, 2022.